BODIPY and porphyrin dyes for direct glucose sensing and optical limiting applications

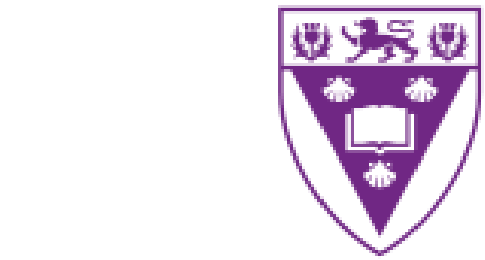

RHODES UNIVERSITY

Where leaders learn

A thesis submitted in fulfilment of the requirements for the degree of

Master of Science

of

Rhodes University

By

NOBUHLE NDEBELE

February 2019

Acknowledgements

Mathew 19 vs 26 “With man this is impossible, but with God all things are possible.” Jeremiah 29 vs 11 “For I know the plan I have for you,” declares the Lord “plans to prosper you and not to harm you, plans to give you hope and a future”. All the glory and honour to the most High, who carried me through this journey. Had it not been for the Lord's mercy, grace and favour this degree would not be obtained.

A big thank you to my supervisor, Dr Mack for guiding me throughout this project. I truly appreciate the great support, encouragement and the opportunities he provided. I would also like to thank my co-supervisor Prof Nyokong. Working under a great black female scientist like her has been so inspiring. Thank you to both my supervisors for bearing with me and allowing me to learn and grow under their wise wings. Prof. Ngoy, thank you for the great scientific and synthetic knowledge that you passed down to me. To Gail Cobus, the real undercover boss, thank you so much for making things run smoothly for us behind the scenes, your work does not go unnoticed. Dr Amuhyu and James Oyim, thank you so much for hosting me during my stay in Kenya. James your hospitality and kindness really made my stay pleasant, and I appreciate it.

To the greatest lab mates ever (S22), thank you all so much for making my masters journey a memorable one. You have all been of great encouragement and support, thank you.

To all my friends, especially Sibusiso, thank you so much for supporting and pushing me I truly appreciate it. 😊 😊 😊

A big, big thank you to my spiritual father Pastor Innocent Dibia, your wise words, encouragement, support and prayers carried me through. Thank you for being a great pillar of strength.

To my parents, my great parents, Thandiwe and Bishop Mbongeni Ndebele where do I even start? Ngiyabonga kakhulu for continuously being selfless and supporting me. Your prayers definitely carried me and did not go unheard degree hence we have a masters degree now, this degree is not mine alone but ours as you worked equally hard for it to be attained. You have both been great, especially mom, umkhozi wam' omuhle, othandekayo, obusisiwe kakhulu, thank you and I love you. To my crazy siblings (Zandile, Bongiwe and Junior) thank you so much, you guys are part of the reason why I pushed hard daily, thank you for tolerating my madness, loving and supporting me.

Thank you to the National Research Fund (NRF) for financial support, I truly appreciate it.

Abstract

A series of BODIPY dyes functionalised with boronic acid in the 3,5-positions were successfully synthesised and characterised by using various analytical techniques. The dyes were prepared through a slight modification of the conventional acid catalysed condensation method. Phenylboronic acid moieties were added as styryl groups at the 3,5-positions of the 1,3,5,7-tetrametylBODIPY cores using a modified Knoevengal condensation method. The addition of the styryls resulted in the main absorption band of the dyes red-shifting to the 630−650 nm region. The photophysical and electrochemical properties of these dyes were studied to determine whether the dyes are suitable for use in the fluorescent, colourimetric and electrochemical detection of glucose. Boronic acid moieties were added as bioreceptor recognition elements because they have an affinity for carbohydrates and therefore would be able to bind and "detect" glucose. The series of BODIPY dyes did not show a "turn-on" fluorescence effect upon addition with glucose at the physiological pH. This was attributed on the basis of molecular modelling to the absence of an MO localised on the boronic-acid-substituted styryl moieties that lie close in energy to the HOMO and LUMO that facilitates the formation of an intramolecular charge transfer state. However, colourimetric changes that are visible to the naked eye are observed at basic pH when glucose was added to the dye solutions. The dyes exhibited favourable electrochemical behaviour and were able to detect glucose directly in this context when glassy carbon electrodes are modified through the drop dry method.

A series of Sn(IV) porphyrins with thienyl and phenyl groups at the *meso*-positions were successfully synthesised and characterised. Pyridine and tetrabutyl axial ligands were added to

the porphyrins to limit aggregation. The optical limiting properties of these porphyrins and three styrylated BODIPY dyes were studied in benzene and dichloromethane. Dyes were also embedded in polystyrene and studied as thin films to further gauge their suitability for use in optical limiting applications. Second-order hyperpolarizability, third-order susceptibly, non-linear absorption with reversible saturable absorption and the optical limiting threshold, were the parameters studied. Three of the four porphyrins and the three styrylated BODIPY dyes showed favourable optical limiting behaviour, which was further enhanced when the dyes are embedded in polymer thin films.

Table of Contents

List of Figures

List of Schemes

List of Tables

List of Symbols

a, **s**, **-a**, and **-s**	MO nomenclature from Michl's perimeter model
α	Linear absorption coefficient
β	Nonlinear absorption coefficient
β_{eff}	Effective nonlinear absorption coefficient
δ	Standard deviation
ε	Molar extinction coefficients
e^-	Electron
f	Oscillator strength
γ	Second-order hyperpolarizability
$\boldsymbol{I}_{lim}$	Optical limiting threshold
$\mathbf{I}m[\chi^{(3)}]$	Third-order susceptibility
λ	Wavelength
M_L	Magnetic quantum number
η	Refractive index
ϕ_F	Fluorescence quantum yield

pK_a	Dissociation constant
S_0	Ground state
S_1	Singlet excited state
σ	Cross-section
T_1	First triplet excited state
τ_F	Fluorescence lifetime

List of Abbreviations

B3LYP	Becke 3-Parameter, Lee, Yang and Parr
BODIPY	4,4'-difluoro-4-bora-3a,4a-diaza-*s*-indacene
CA	Chronoamperometry
CAM-B3LYP	Coulomb-attenuating method — Becke 3-Parameter, Lee, Yang and Parr
CE	Counter electrode
CV	Cyclic voltammetry
DCM	Dichloromethane
DDQ	2,3-Dichloro-5,6-dicyano-1,4-benzoquinone
DFT	Density functional theory
DMF	N,N-Dimethylformamide
DMSO	Dimethyl sulfoxide
DPV	Differential pulse voltammetry
Em	Emission
E_p	Peak potential

ESA	Excited state absorption
EWG	Electron withdrawing group
Exc	Excitation
FT-IR	Fourier transformation Infra-red spectroscopy
GCE	Glassy carbon electrode
GOx	Glucose oxidase
^{1}H-NMR	Proton nuclear magnetic resonance
HF	Hartree-Fock
HOMO	Highest occupied molecular orbital
ICT	Intermolecular charge transfer
ISC	Intersystem crossing
IUPAC	International Union of Pure and Applied Chemistry
LoD	Limit of detection
LUMO	Lowest unoccupied molecular orbital
MALDI-TOF	Matrix-assisted laser desorption/ionisation-time of flight
MO	Molecular orbital
MPA	Multiphoton absorption

MPc	Metallophthalocyanine
MS	Mass spectrometry
Nd:YAG	Neodynium-doped yttrimium aluminium garnet
NIR	Near-infrared region
NLA	Nonlinear absorption
NLO	Nonlinear optics
NLR	Nonlinear refraction
NMR	Nuclear magnetic resonance spectroscopy
OL	Optical limiting
PET	Photoinduced electron transfer
PBS	Phosphate buffer saline
Pc	Phthalocyanine
Redox	Reduction/oxidation
RE	Reference electrode
RSA	Reverse saturable absorption
RSD	Relative standard deviation
SDD	Gaussian09 default basis set

SECM	Scanning electrochemical microscopy
SEM	Scanning electron microscopy
Std	Standard
TCSPC	Time-correlated single photon counting
TD-DFT	Time-dependent density functional theory
TEA	Triethylamine
TFA	Trifluoroacetic acid
TLC	Thin layer chromatography
TPA	Two-photon absorption
UME	Ultramicroelectrode
UV-Vis	Ultraviolet-visible
WE	Working electrode
WHO	World Health Organisation

Chapter 1

Introduction

1.1. Boron dipyrromethene dyes

4,4'-Difluoro-4-bora-3*a*,4*a*-diaza-*s*-indacenes are popularly referred to as BODIPYs. BODIPY dyes are a class of fluorescent organic dyes that have gained great popularity over the past couple of decades for a wide range of applications due to their favourable photochemical and photophysical properties [1-4].

1.1.1. History and structure

In 1968, Treibs and Kreuzer reported the first serendipitous syntheses of BODIPY dyes. The authors noticed that the acylation of 2,4-dipyrromethane with acetic anhydride using boron trifluoride (BF_3) as a Lewis acid catalyst yielded a very fluorescent compound and not the acylated pyrrole they were attempting to synthesise [1]. The fluorescent compound was formed as a result of the acid-catalysed condensation of the two pyrrole units and complexation with a boron fluoride unit [1].

Despite BODIPY dyes being described as highly fluorescent in the late 1960s, it was only in the late 1980s that the dyes were investigated in depth and studied for use in the fluorescence imaging of cells by Monsma *et al.* [5]. Thereafter, the dyes gained considerable popularity. Boyer and Pavlopoulos were the first to report on the potential use of BODIPY dyes as tuneable laser dyes [6]. To date, BODIPY dyes have been used for various applications ranging from biomedical applications, to use in sensors, solar cells and nonlinear optics [2, 3, 7, 8].

BODIPY dyes are favoured in this wide range of applications due to their excellent properties in comparison to other fluorophores. These tuneable properties include [2, 4, 9-11];

i. high molar extinction coefficients (ε) above 80 000M^{-1},

ii. good spectroscopic properties,

iii. narrow absorption and emission bands,

iv. high fluorescent quantum yields,

v. moderate reduction and oxidation properties,

vi. high thermal and photochemical stability,

vii. intense absorption in the visible region,

viii. chemical robustness, and

ix. high lasing efficiency.

These properties can be easily manipulated to favour the application of interest by appropriately modifying the core dye structure.

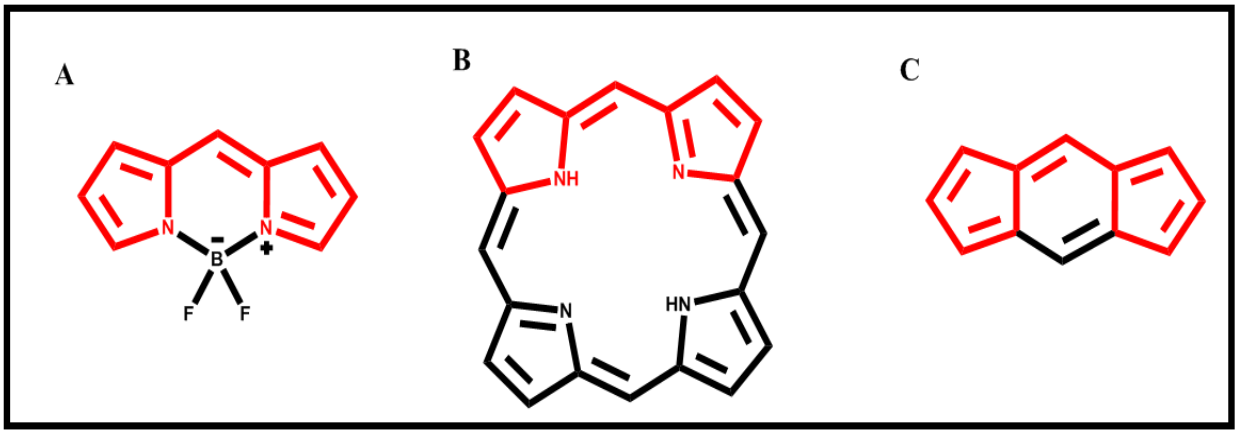

Figure 1.1: Comparison of the structures of (A) BODIPY to (B) porphyrin and (C) *s*-indacene.

BODIPY dyes (**Figure 1.1A**) are heterocyclic molecules. The structure of these dyes is analogous to that of a half porphyrin (**Figure 1.1B**) or *s*-indacene (**Figure 1.1C**), so they are sometimes referred to as "porphyrin's little sister" [1, 3, 11, 12]. The BODIPY structure consists of a dipyrromethene ligand complexed with a boron atom, usually in the form of boron difluoride (BF_2). The dipyrromethene is formed through the condensation of two pyrrole units; the pyrroles are joined via a methine bridge. Complexation with BF_2 results in a rigid structure. The rigidity of the structure prevents isomerisation and "interpyrrolic methine chain-twisting" [2, 9, 13, 14]. **Figure 1.2** illustrates the International Union of Pure and Applied Chemistry (IUPAC) number sequence that is used for naming BODIPY dyes and atom names which stem from porphyrin nomenclature [2, 9, 12, 14]. The central bridging carbon atom is referred to as the *meso*-carbon (8-position), the carbons adjacent (3,5-positions) to the nitrogen atoms are referred to as the α-positions, while the other carbons are referred to as the β-positions (1,2,6,7-positions).

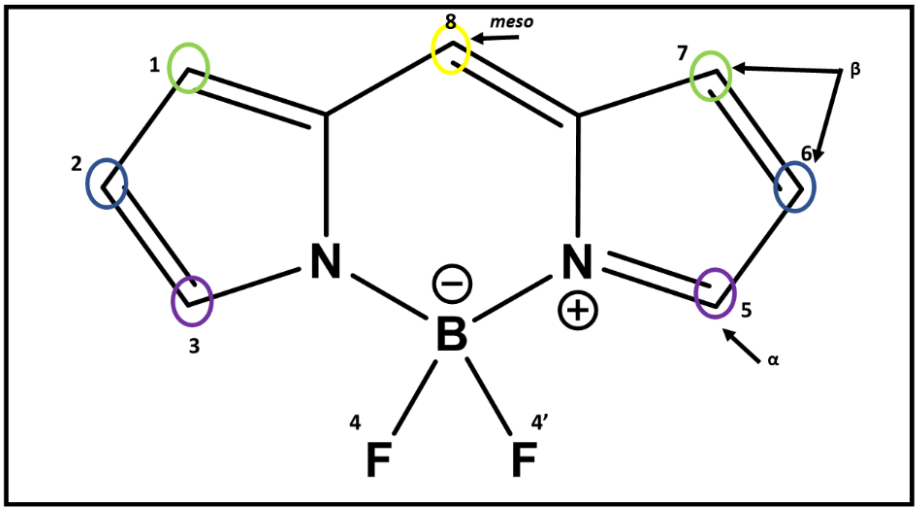

Figure 1.2: BODIPY core structure with the IUPAC numbering system.

1.1.2. Molecular properties of BODIPY dyes

BODIPY dyes do not follow Huckel's rule for aromaticity (4n + 2). However, these highly fluorescent dyes still display properties very similar to those of an aromatic system [9]. This is due to the tetrahedral geometry of the boron centre between the two pyrrole units that forms the rigid planar conformation of the dipyrromethene which is similar to that of an indacene dye [9, 14]. The electronic structures of this class of dyes can be described in a similar manner to heteroaromatic molecules mainly due to the π-molecular orbitals (MO) associated with the indacene plane which are comparable to those of an aromatic $C_{12}H_{12}$ cyclic parameter with MOs arranged as M_L= 0, ±1, ±2, ±3, ±4, ±5, and 6 in ascending energy levels with regards to the magnetic quantum number (M_L) [9, 15, 16]. The quantum number represents the number of nodal planes present in a molecular orbital. Complexation with BF_2 results in the low C_{2V} symmetry, of the molecule. It also disrupts the indacene cyclic perimeter thus lifting all the degeneracies of the MO energies in the π-system [15]. Consequently, the gap between the highest occupied molecular orbital (HOMO) and the lowest unoccupied molecular orbital (LUMO) is narrowed, and they lie well separated from the other MOs in the π-system [15]. Experimentally this leads to the presence of a single dominant absorption band in the visible region. **Figure 1.3** illustrates the HOMO and LUMO nodal patterns of a typical BODIPY core structure.

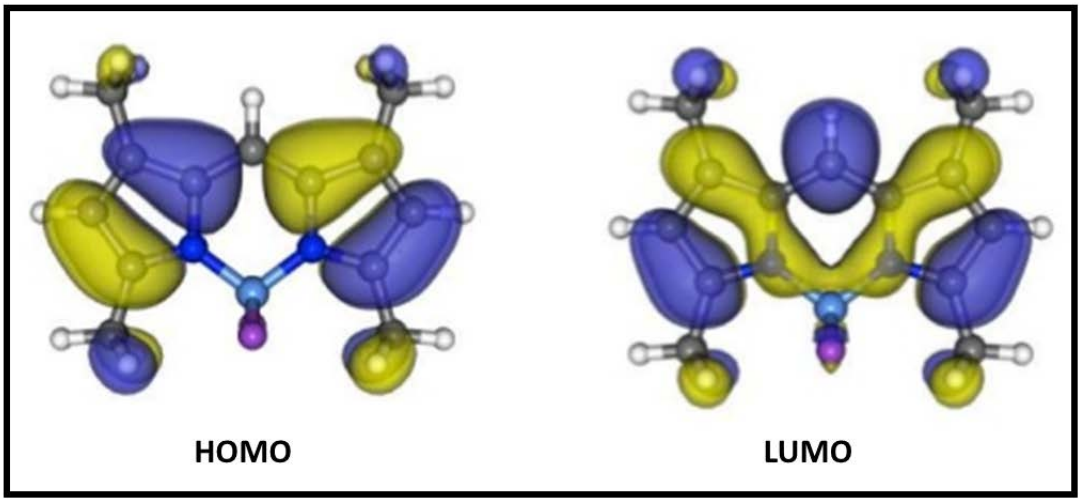

Figure 1.3: BODIPY core LUMO and HOMO molecular orbital structures

1.1.3. Synthesis of BODIPY dyes

BODIPY dyes are synthesised by using well-known condensation reactions that have been extensively employed in porphyrin research [3, 12, 17]. There are various synthetic routes that can be followed to synthesise symmetric and asymmetric BODIPY core dyes (**Figure 1.4**). All of the methods involve the preparation of dipyrromethane ligands from pyrroles and highly electrophilic compounds such as aldehydes, acid anhydrides or acyl chlorides [1, 2, 18]. Dipyrromethane ligands are precursors for various macrocyclic compounds as well as BODIPY dyes [2, 13], so the reaction conditions have to be adjusted to favour the formation of BODIPYs as the main product.

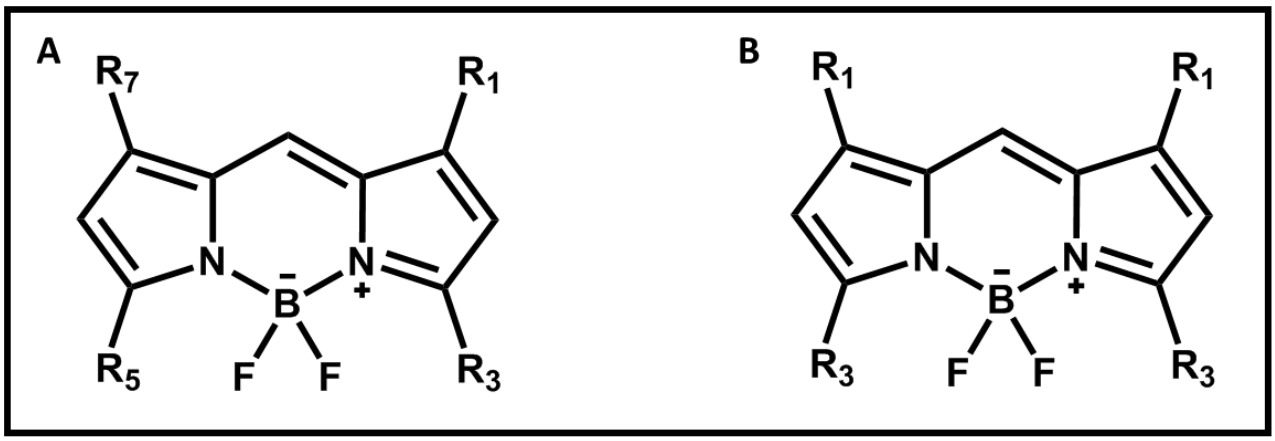

Figure 1.4: Representation of (A) symmetric and (B) asymmetric BODIPY core structures.

There are two distinct synthetic routes employed for the synthesis of BODIPY dyes. One of these was described by Burgess and co-workers in 2008 [13, 19, 20]. This method is only possible when 5-substituted pyrrole aldehydes are used. Instead of undergoing condensation with other pyrroles the phosphorous oxychloride ($POCl_3$) solely condenses the pyrrole (**Scheme 1.1**). This method is used for the synthesis of both symmetric and asymmetric BODIPY core dyes.

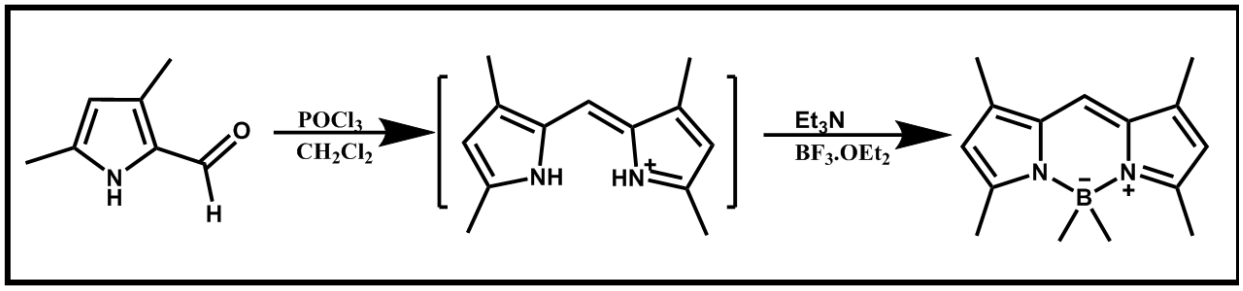

Scheme 1.1: A synthetic route for forming asymmetrical and symmetrical BODIPY dye via decarboxylation by $POCl_3$

The second method, which is the most commonly used BODIPY synthesis route is described in **Scheme 1.2(i)**. This procedure synthesises the BODIPY dyes in "one-pot" although there are several steps that need to be followed. The first step is the MacDonald reaction; an acid-catalysed condensation of a pyrrole (**A**) with an aldehyde (**B**) of choice yielding a dipyrromethane (**C**) ligand. A Lewis acid, usually trifluoracetic acid (TFA), is used as a catalyst. Dipyrromethanes are very unstable molecules that are sensitive to light, air and acid. Therefore, it is recommended that they are used directly after preparation. Hence, once formed they are immediately oxidised in the same reaction vessel. Dipyrromethanes are oxidised with 2,3-dichloro-5,6-dicyano-1,4-benzoquinone (DDQ) or tetrachloro-1,4-benzoquinone (*p*-chloranil) forming a dipyrromethene (**D**) which is relatively stable. The dipyrromethene is further complexed with boron trifluoride diethyl etherate ($BF_3{\cdot}OEt_2$) in the presence of a base. Tertiary amines such as triethylamine (TEA) are usually used to form the BODIPY core dye (**E**).

Scheme 1.2(ii) illustrates another acid-catalysed condensation method that could be used to synthesise BODIPY dyes. The procedure condenses the pyrrole with an acylium equivalent (**F**) such as an acid chloride, anhydride or an *ortho*-ester instead of an aldehyde [21-23]. This approach enables the preparation of asymmetric BODIPY dyes.

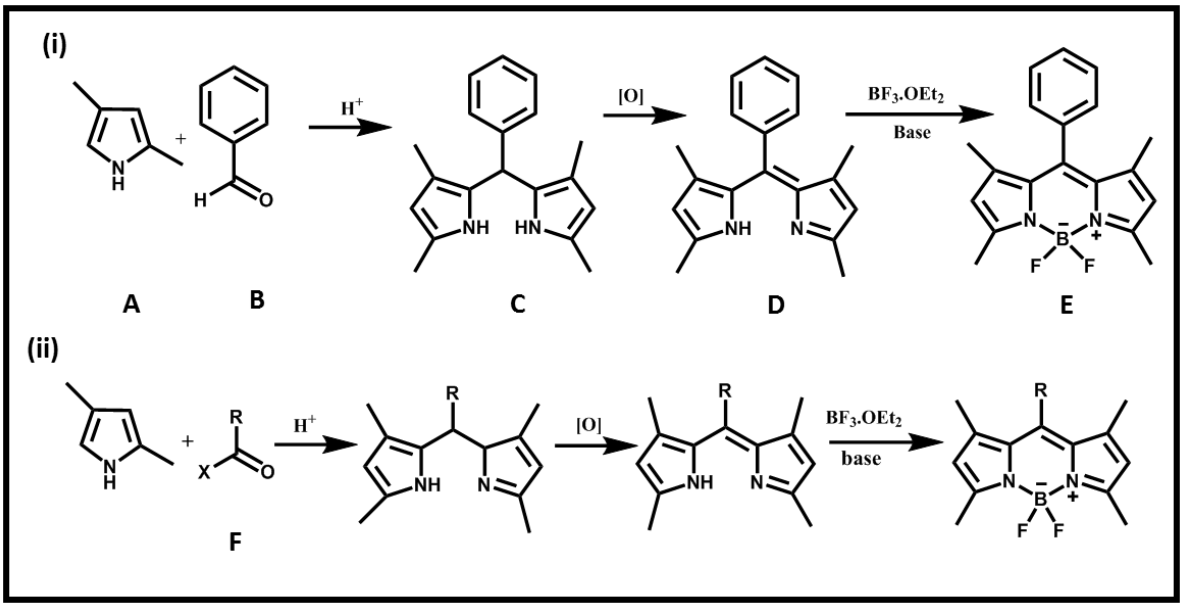

Scheme 1.2: The acid-catalysed condensation of pyrroles with (i) aldehyde and (ii) acylpyrrole to form BODIPY dyes

In this study, the acid-catalysed condensation method described in **Scheme 1.2(i)** was used to prepare the 1,3,5,7-tetramethylBODIPY core dyes by using 2,4-dimethylpyrrole as a starting material. TetramethylBODIPY core dyes tend to be the most commonly synthesised in BODIPY research because the methyl groups block the addition of pyrroles to the dipyrromethane thus preventing the formation of porphyrins.

1.1.4. Functionalisation and modification of 1,3,5,7-tetramethylBODIPY core dyes

BODIPY dyes are used in various applications and are well known for their facile structural modification [11, 24, 25]. The 1,3,5,7-tetramethylBODIPY core dyes prepared in this study can be further functionalised by introducing functional groups at almost all of the positions of the BODIPY core.

1.1.4.1. Functionalisation of the pyrrole building blocks

BODIPY dyes can be functionalised by introducing substituents onto the pyrrole moieties [26, 27]. BODIPY dyes can be easily functionalised by using different pyrrole precursors. During this study, the 2,4-dimethylpyrrole was used because the methyl groups prevent cyclisation and the formation of porphyrins. The methyl groups that occur in the 1,3,5,7-positions of the synthesised tetramethylBODIPY core enable easy functionalisation through the addition of styryls [11, 24].

1.1.4.2. Functionalisation via the meso-substituent

The most common and easiest functionalisation of BODIPY dyes is at the *meso*-position through the use of the appropriate aryl-aldehyde or aryl chloride in the initial synthesis step [28-30]. Certain aldehydes enable further modification post-synthesis [30]. The incorporation of appropriate *meso*-aryl groups facilitates linking with macromolecules or conjugation with nanomaterials and potentially influences the fluorescence emission through photoinduced electron transfer (PET) processes in a manner that can be used to form a sensor [29, 31, 32].

The *meso*-carbon atom can also be replaced with a nitrogen forming another class of BODIPY dyes known as aza-BODIPY dyes (**Figure 1.5**). Aza-BODIPY dyes are usually formed through Michael addition reactions [33, 34]. The nitrogen atom enhances the stability and rigidity of the dye, and stabilises the LUMO, thus red-shifting the main absorption band into the near infrared region (NIR) region [3, 35]. Aza-BODIPY dyes are suitable for a wide variety of applications [4, 36].

1.1.4.3. Electrophilic substitution

The 2,6-positions have the least positively charged carbon atoms in the 1,3,5,7-tetramethylBODIPY core framework, and hence are prone to electrophilic attack and thus can easily undergo electrophilic substitution [2, 3].

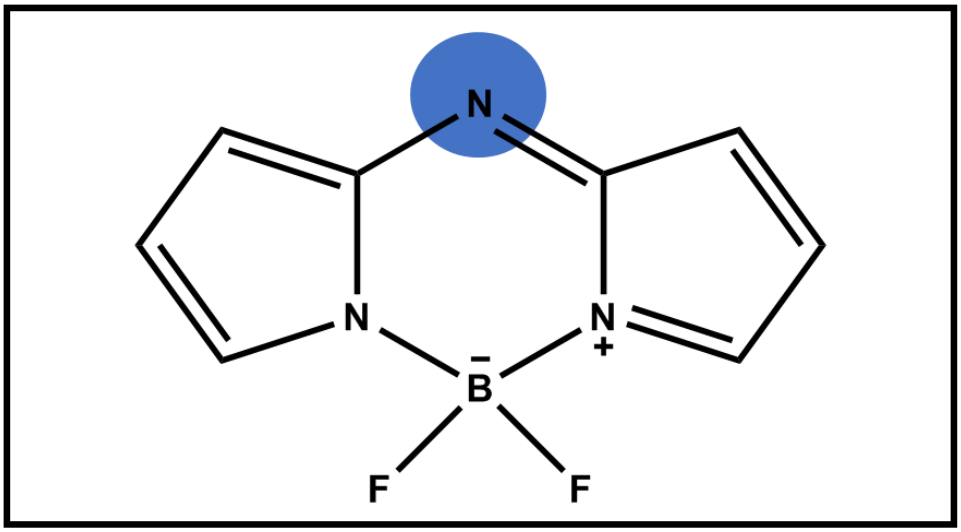

Figure 1.5: Molecular structure of an aza-BODIPY core dye.

Halogen atoms can be readily added to the 2,6-positions. Halogenation at these positions destabilises the HOMO, and this results in a narrowing of the HOMO−LUMO gap and a red-shift of the main absorption band [2, 37]. There is a marked decrease in the fluorescence quantum yields of the dyes due to a heavy atom effect. The latter is highly desirable in biomedical applications such as photoantimicrobial chemotherapy (PACT) and photodynamic therapy (PDT) as it enables the dyes to undergo intersystem crossing (ISC) to the triplet state and thus produces cytotoxic singlet oxygen molecules upon photoexcitation [37, 38].

1.1.4.4. Substitution on the boron centre

The fluorine atoms at the 4,4'-positions attached to the boron atom can be readily substituted through the use of hard nucleophiles. Carbon, oxygen and ethyl nucleophiles can substitute the fluorine atoms under both acidic and basic conditions [2, 39, 40]. Substitution of the fluorine atoms can increase the water solubility, quench the fluorescence and enhance the reduction-oxidation (redox) properties while decreasing the water solubility [2]. Replacement of the boron atom with metal ions also leads to new classes of dyes [2, 40].

1.1.4.5. Substitution through reactive methyl groups

The methyl groups at the 3,5-positions of the 1,3,5,7-tetramethylBODIPY core can readily undergo Knoevenagel condensation reactions. The methyl groups at these positions are acidic and are therefore subject to further condensation with aromatic aldehydes in basic conditions to yield styrylated BODIPY dyes (**Scheme 1.3**) [41, 42]. The reaction is catalysed by a base, and a Dean-Stark apparatus is used to remove water from the reaction mixture. The addition of these styryl groups extends the π-conjugation system of the BODIPY core, and this destabilises the HOMO, narrowing the HOMO−LUMO gap typically red-shifting the main absorption band of the dye to beyond 600 nm [43]. The 1,7-positions can also undergo the base-catalysed condensation reactions and be styrylated as well. However, the structure needs to be very acidic for this to be possible [11, 44].

The synthetic work on BODIPYs in this study focuses initially on the synthesis of a series of 1,3,5,7-tetramethylBODIPY cores from 2,4-dimethylpyrrole, followed by the further modification of the

BODIPY core structures through mechanisms explained above. The 1,3,5,7-position methyl groups of the BODIPY core dyes are highly nucleophilic, so Knoevenagel reactions with aldehydes can be used to form styryl groups [11, 41, 45]. The 3,5-position methyls are known to be more reactive than those at the 1,7-positions in this regard, so the main focus of the synthetic work in this thesis has been on the preparation of 3,5-distyryl-1,7-dimethylBODIPY dyes (**Scheme 1.3**) [11, 24, 45].

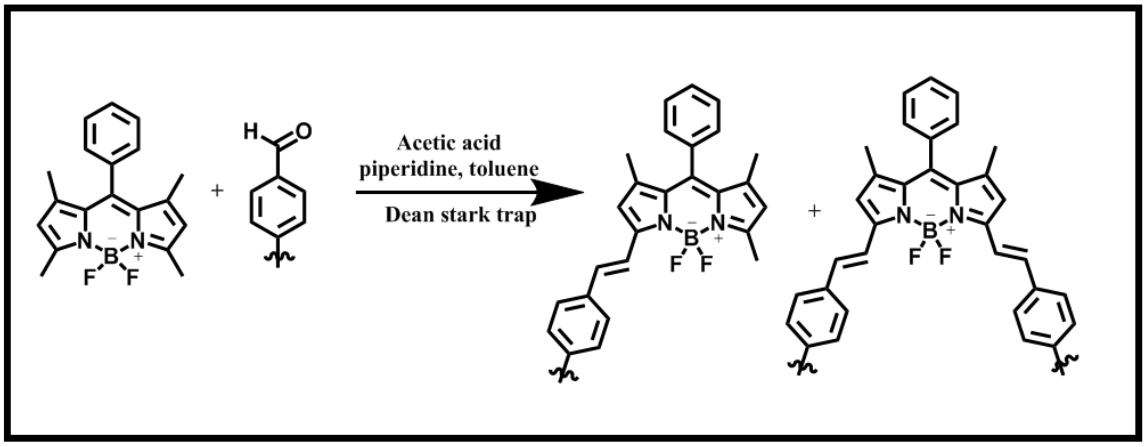

Scheme 1.3: Knoevenagel condensation of the 3,5-position methyl substituents with aryl aldehydes.

1.1.5. Photophysical properties of BODIPY dyes

BODIPY dyes undergo various photophysical processes depending on the structural modifications that are made, and these processes can be visualised with a Jablonski diagram (**Figure 1.6**). When a BODIPY dye at the ground state (S_0) is subject to photoexcitation, the dye absorbs a photon, and an electron is promoted to an unoccupied orbital to form a singlet excited state (S_n). Internal conversion usually converts higher excited states into the first singlet excited state (S_1) within

10^{-12} s. The S_1 state relaxes back to the ground state via fluorescence through the emission of a photon following Kasha's rule, or through non-radiative decay. Since BODIPY dyes have relatively rigid structures, the fluorescence from the singlet excited state back to the ground state results in a spectrum that exhibits mirror symmetry with the lowest energy absorption band [3, 46]. When structural modifications to the BODIPY result in the incorporation of heavy atoms and also in certain other circumstances involving charge transfer, the S_1 state can further undergo a spin-forbidden ISC process into the first triplet excited state (T_1) [47]. The T_1 state relaxes back to the ground state via phosphorescence or non-radiative decay, or during certain applications, energy can be transferred to molecular oxygen producing radical oxygen species.

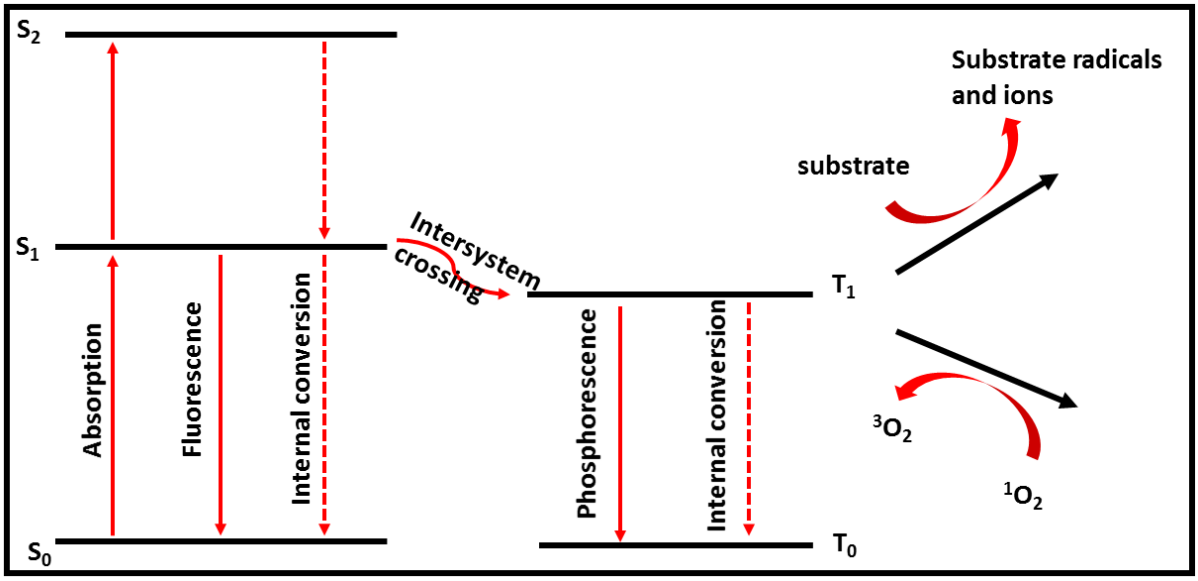

Figure 1.6: A Jablonski diagram applicable to either BODIPY or porphyrin dyes that describes the processes that occur upon photoexcitation.

A key property of BODIPY dyes is their intense fluorescence, which has been used extensively to form colourimetric and fluorescence sensors [2] .

1.1.5.1. Absorption spectra

Figure 1.7 provides typical absorption and emission spectra for a 1,3,5,7-tetramethylBODIPY core dye. The main absorption band lies at ca. 500 nm, while the emission band is observed at ca. 510 nm. The main absorption band arises from the promotion of an electron from the HOMO to the LUMO. A shoulder of absorbance can be observed at ca. 460 nm due to out of plane vibrations [9, 32, 48]. Other less intense bands observed at higher energies in the ultraviolet (UV) region are attributed to transitions to higher singlet excited states [48, 49].

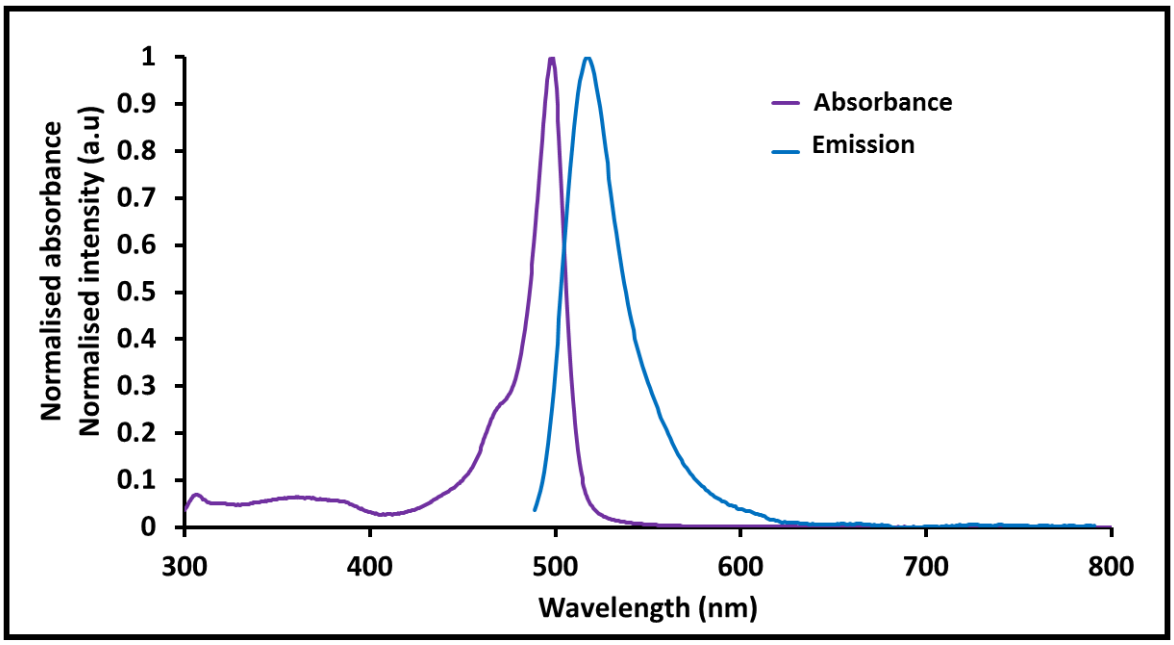

Figure 1.7: The absorption (purple) and emission (blue) spectra of a 1,3,5,7-tetramethylBODIPY core dye.

1.1.5.2. Fluorescence quantum yield (ϕ_F)

As previously discussed, the process of photon emission from the singlet state to the ground state results in a fluorescence spectrum that is a mirror image of the main absorption band (**Figure 1.7)**. BODIPY fluorescence bands typically exhibit a small Stokes shift due to their rigid planar structures. Generally, BODIPY core dyes are highly fluorescent and therefore have relatively high fluorescence quantum yield (Φ_F) values [48, 50]. The fluorescence quantum yield is defined as the ratio of the number of photons emitted relative to the number of photons absorbed (**Equation 1)**.

$$\phi_F = \frac{Number\ of\ photons\ emitted}{Number\ of\ photons\ absorbed} \quad (1)$$

Fluorescence quantum yields are commonly determined with a comparative method (**Equation 2**) [50-52].

$$\phi_F = \phi_F\ (std)\ \frac{F.A_{std}.\eta^2}{F_{std}.\ A.\eta^2_{std}} \quad (2)$$

where F and F_{std} are the integrated fluorescence intensities of the sample (BODIPY dye) and a standard, respectively. The integrated fluorescence intensity is derived from the area beneath a fluorescence emission curve. A and A_{std} are the absorbance values for the sample and the standard at the excitation wavelength. $\phi_F\,(std)$ represents the fluorescence quantum yield of the standard. Rhodamine 6G (Φ_F = 0.94 in ethanol) and zinc phthalocyanine (ZnPc) (Φ_F in dimethylsulfoxide= 0.20, in tetrahydrofuran = 0.23), were used as standards in the determination

of the Φ_F values [53, 54]. The values obtained lie between 0.0 (if the dye is fully non-fluorescent) and 1.0 (when every absorbed photon is re-emitted).

1.1.5.3. Fluorescence lifetime

The fluorescence lifetime (τ_F) is defined as the time that it takes for 1/e of the S_1 excited states to relax back to the ground state through fluorescence (**Equation 3**) [55].

$$\tau_0 = \frac{\tau_F}{\Phi_F} \quad (3)$$

The fluorescence emission profile is typically analysed through monoexponential fluorescence decay curves (**Figure 1.8**) obtained through the use of the time-correlated single photon counting (TCSPC) technique [56]. The technique measures the time-dependent fluorescence intensity profile of the light emitted upon excitation of solutions by a pulsed laser. Repetition of the single photon measurements provides a distribution with respect to time and fitting with exponential curves provides the fluorescence lifetime [48].

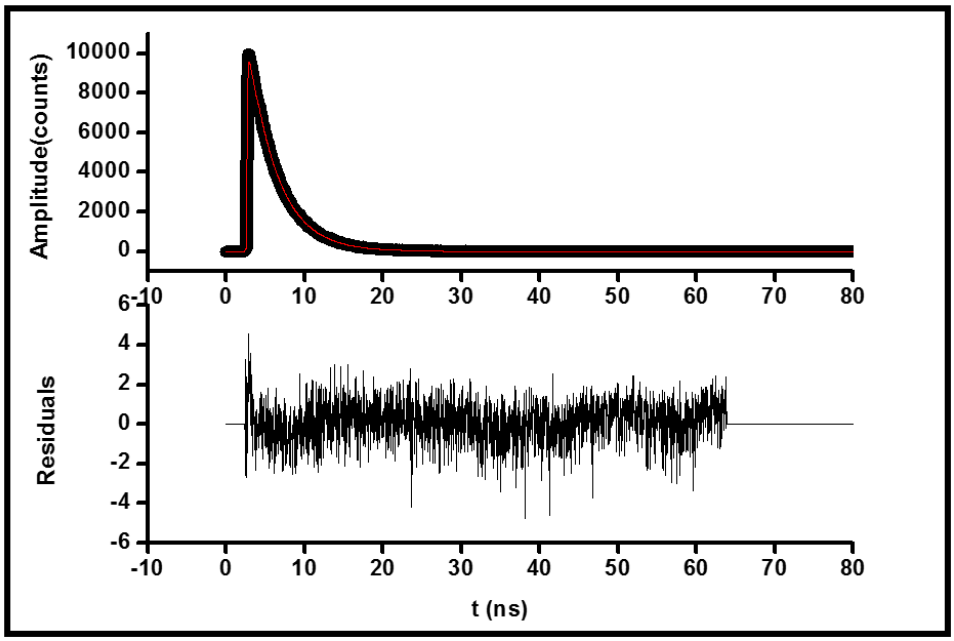

Figure 1.8: A typical fluorescence decay curve for a BODIPY core dye.

1.1.6. Applications of BODIPY dyes

BODIPY dyes have been studied for a wide range of applications, with a particularly strong focus on imaging and biolabeling due to their favourable photophysical properties [11]. In this study, the physicochemical properties of the synthesised BODIPY dyes are analysed along with their potential for use in electrochemical, fluorescence and colourimetric glucose sensing. The optical limiting properties of selected BODIPY dyes were also investigated to evaluate their suitability for use as optical limiters[11].

1.1.7. BODIPY dyes synthesised

Figure 1.9 summarises the BODIPY dye target compounds that were synthesised and studied in this thesis. BODIPY dyes **1-5b** have styryls at the 3,5-positions with phenylboronic acids at the

para-positions of the phenyl rings. This extends the π-conjugation system and results in the main spectral band absorbing in the 600−700 nm region. These dyes were studied for direct glucose fluorescence and colourimetric sensing. BODIPY dyes **1b** and **2b** were further studied for direct electrochemical glucose sensing, and their nonlinear optical properties were also analysed alongside those of dye **6** which has 3,5,7-position styryls that have hydroxyl groups at the *para*-positions of the phenyl rings.

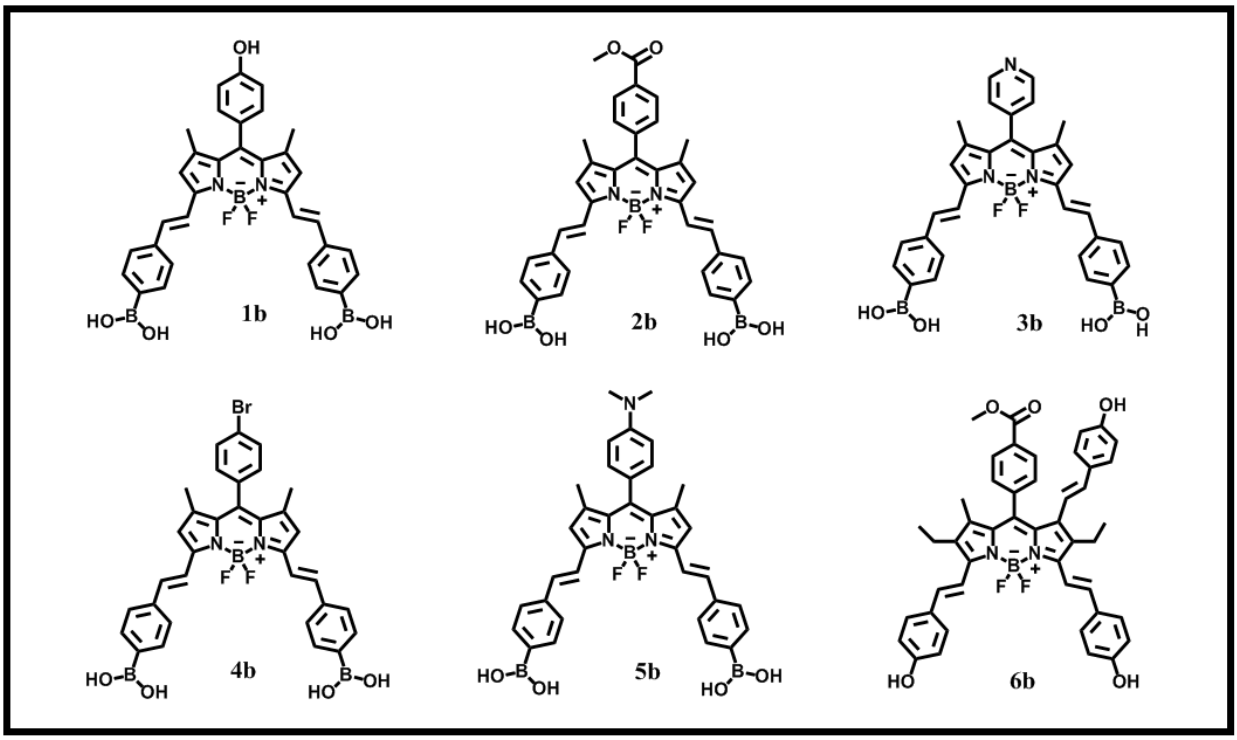

Figure 1.9: BODIPY dyes studied.

1.2. Porphyrins

1.2.1. History and structure

Porphyrins are a class of heterocyclic aromatic organic compounds that are very important in nature due to their role in oxygen transport (haemoglobin and myoglobin), photosynthesis (chlorophyll), and in biological oxidation and reduction reactions. Synthetic porphyrins and their metal complexes have been used for various applications due to their favourable biological, chemical and physical properties [57-59].

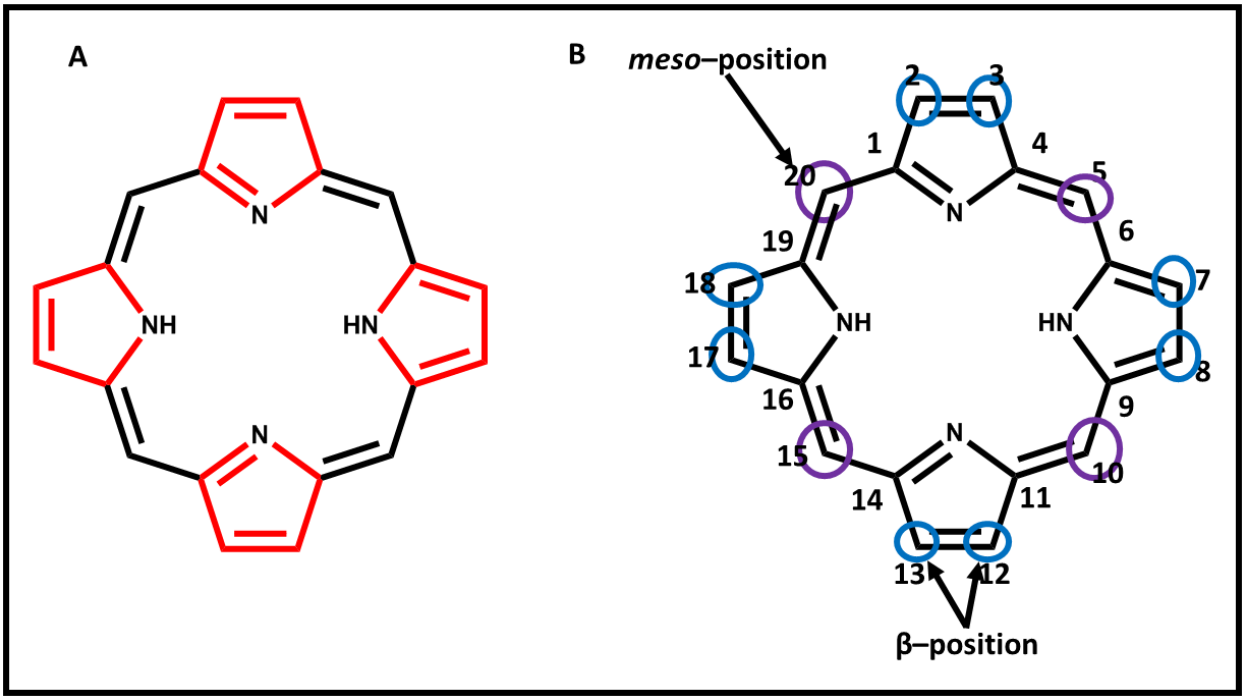

Figure 1.10: The structure of the porphyrin ligand (A) (red = pyrrole ring and black = methene bridges) and (B) porphyrin nomenclature (blue circles = β-positions and purple circles = *meso*-positions).

Küster was the first researcher to propose the correct porphyrin structure in 1912 [60]. However, the structure was only confirmed in 1929 by Fischer and Zeile when they successfully synthesised a haem from pyrrolic starting materials [61]. The typical structure of a porphyrin molecule consists of four pyrrole rings linked together by four methene bridging atoms to form a 16 atom 18-π-electron macrocyclic inner ligand perimeter (**Figure 1.10**). The porphyrin ligand has twenty carbon and four nitrogen atoms on its outer perimeter due to the incorporation of the four pyrrole rings. The carbons on the pyrrole moieties are labelled as the α- and β-positions depending on their relative proximity to the nitrogen atoms, while the bridging carbons are said to lie at the *meso*-positions. The porphyrin structure is easily modified by adding substituents to the β- and *meso*-positions. A key property of the porphyrin ring structure is the ability to bind various metal and metalloid ions in the inner ring cavity to form metal porphyrin complexes.

1.2.2. Molecular properties

Unlike BODIPY dyes, porphyrins follow Huckel's 4N+2 rule for aromaticity. The aromatic nature of these molecules is usually described by the 18 annulene model which was proposed by Vogel [62-64]. **Figure 1.11** illustrates the delocalisation pathway followed by this model. Porphyrins are weak bases, so they can be easily protonated and consequently readily form dictations [65, 66]. A porphyrin ligand with two inner N-H protons is referred to as the "free base", and its two inner protons have the ability to move between the four nitrogen atoms through tautomerism [65-67]. Porphyrins are amongst the most intense light absorbing molecular dyes in Nature, since they absorb strongly in the blue region of the electromagnetic spectra [68, 69]. **Figure 1.12** shows a

typical UV-visible absorption spectra of an unmetalled porphyrin. Porphyrins typically have an intense B (or Soret) band and weaker Q bands that lie between 400–450 and 500–700 nm, respectively. I and III in **Figure 1.12** are electronic bands, whereas II and IV are vibrational bands [66, 70, 71].

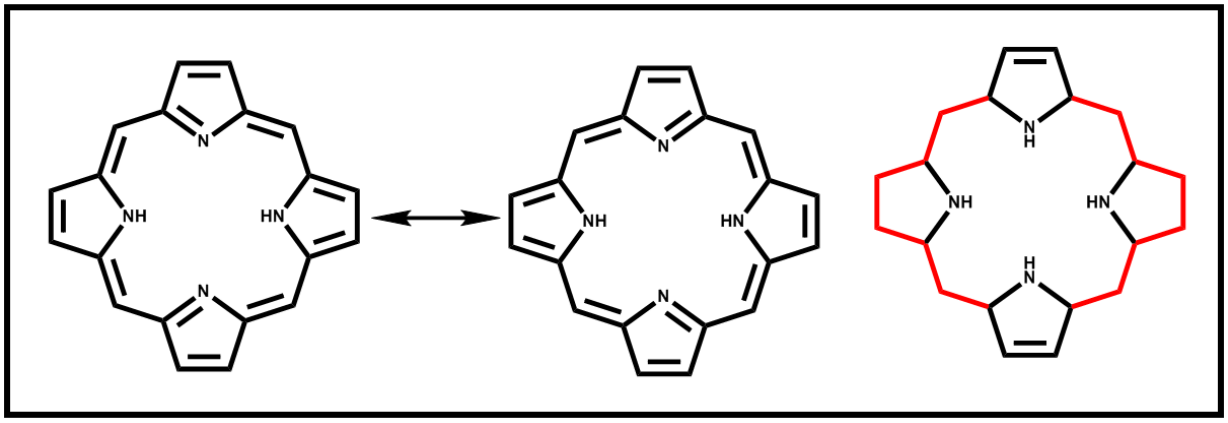

Figure 1.11: The delocalisation of the porphyrin ring.

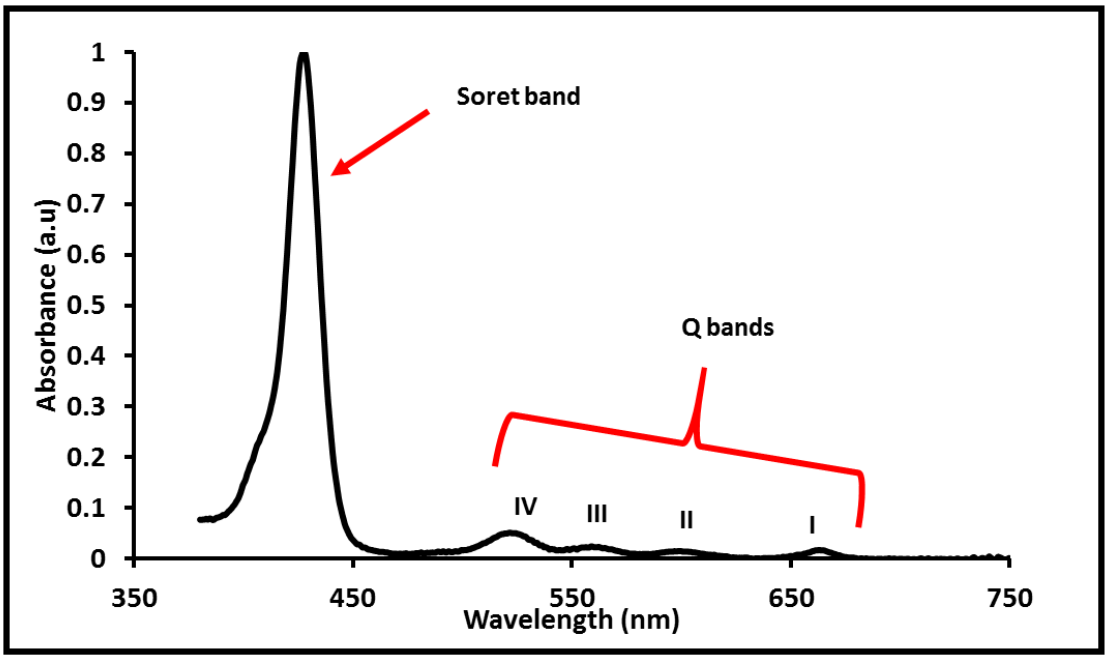

Figure 1.12: The UV-visible absorption spectra of porphyrins.

Gouterman's 4-orbital model (**Figure 1.13**) can be used to describe the electronic absorption properties of porphyrins. The absorption bands arise from transitions between four frontier MOs derived from the HOMO and LUMO of a parent $C_{16}H_{16}^{2-}$ parent hydrocarbon, which have $M_L = \pm 4$ and ± 5 angular nodal properties, respectively [66, 70]. Under the D_{4h} symmetry of metalloporphyrins, the MOs derived from the HOMO transform as nearly degenerate $1a_{1u}$ and $1a_{2u}$ MOs, and the MOs derived from the LUMO transform as $1e_g^*$. Two ^1E_u excited states can be generated for spin-allowed transitions between these MOs, and these states have $\Delta M_L = \pm 1$ and ± 9 orbital angular momentum properties. The higher energy ^1E_u energy state arises from a fully allowed $\Delta M_L = \pm 1$ transition that is associated with the B (or Soret) band, whereas the $\Delta M_L = \pm 9$ transition to the lower energy ^1E_u state is forbidden and is associated with the less intense Q bands [66, 70].

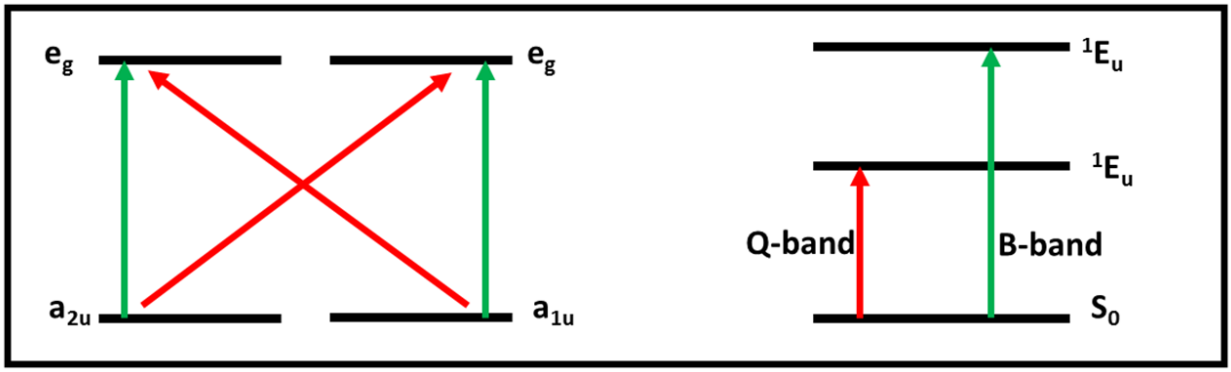

Figure 1.13: Gouterman's four orbital model explaining the origin of the main porphyrin absorption bands.

1.2.3. Synthesis

Porphyrins can be synthesised using various synthetic procedures from a number of different precursors such as aldehydes, pyrroles, dipyrromethanes, dipyrromethenes, tripyrranes and linear tetrapyrroles [72]. In this study, tetraarylporphyrins were synthesised. Two main synthetic routes are generally used in this context [72-75].

1.2.3.1. Synthesis of meso-substituted tetra porphyrins

Rothemund reported the first synthesis of tetraarylporphyrins in 1936 [72, 73, 76]. Various disadvantages associated with Rothemund's method led to the development of other simpler synthetic routes. Adler and Longo's modified Rothemund method provides a one-pot synthesis by refluxing an aromatic aldehyde and pyrrole in the presence of a carboxylic acid to form the target porphyrin structure (**Scheme 1.4**) [72, 74, 76-78]. Alder-Longo's method typically forms porphyrins in relatively low yields of ca. 20% [72, 76]. Asymmetric porphyrins can also be synthesised through the use of two or more aldehydes [77].

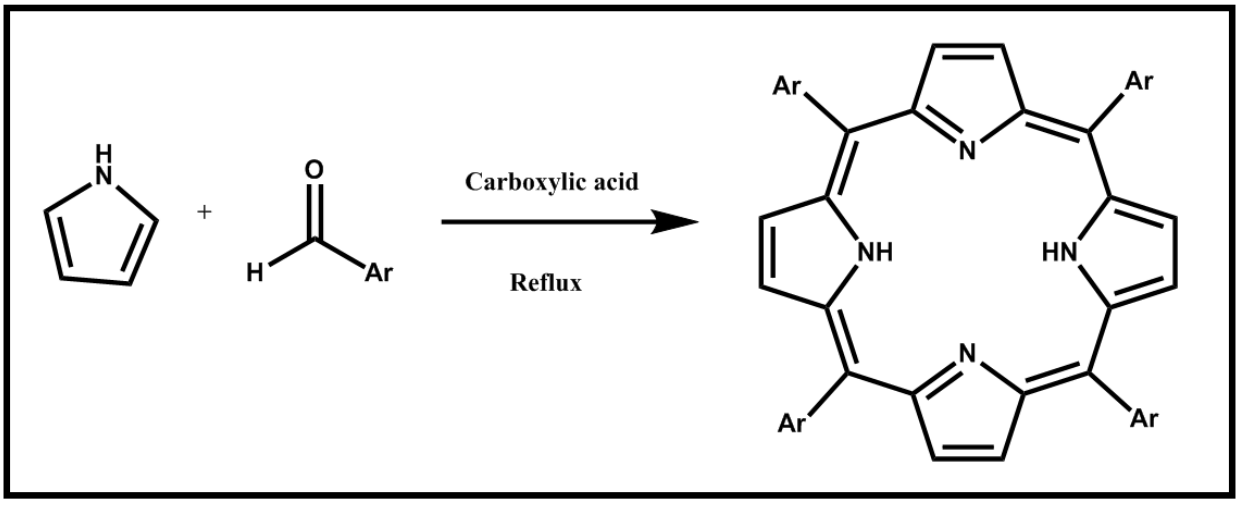

Scheme 1.4: Alder-Longo's porphyrin synthetic route [72, 74].

Lindsay and co-workers subsequently developed another synthetic method that forms tetraarylporphyrins in DCM using $BF_3{\cdot}OEt_2$ as a catalyst and DDQ or *p*-chloranil as an oxidant (**Scheme 1.5**) [72, 76]. This approach also forms the basis of the three-step one-pot method used for BODIPY dyes. This method provides tetraarylporphyrins in relatively high yields and enables the introduction of acid-sensitive functional groups [76].

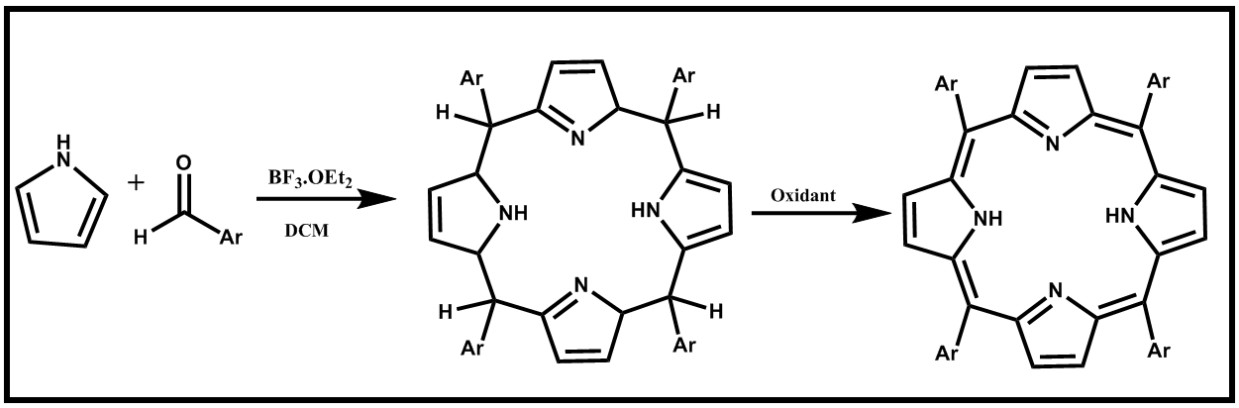

Scheme 1.5: The Lindsey synthetic route [72, 76].

1.2.3.2. Metalation of porphyrins

Porphyrins are tetradentate ligands that can be complexed with metal ions and certain non-metal ions to form complexes that are suitable for the application of choice. Metalloporphyrins are formed when the lone pairs of the nitrogen atoms in the central cavity of the structure are shared with a metal centre acting in a manner similar to a Lewis acid [63, 79, 80]. As illustrated in **Figure 1.11**, the nitrogen atoms are highly acidic and can easily deprotonate to form dianion species in the central cavity in a manner that enables metal and certain metalloid ions to bind [81]. Porphyrins usually complex with divalent metal ions to form an 18-π-electron system, but

more highly charged ions can also be complexed when there are anionic axial ligands present [81]. The metalation of porphyrins involves protonation-deprotonation equilibria, the release of the metal ion from the metal salt, and the completion of the coordination sphere [82]. The stability of metalloporphyrins depends on the size of the metal ion and its compatibility with the cavity of the porphyrin ligand [82].

1.2.4. Porphyrins synthesised

The porphyrin coordinating environment is highly flexible and can easily be modified to provide different oxidation and spin states by varying the peripheral substituents, the central ion and through the addition of different axial ligands. The Sn(IV) porphyrins synthesised in this study are shown in **Figure 1.14**. The effect on the optical limiting behaviour at 532 nm of using different aryl substituents at the *meso*-position and different axial ligands was assessed.

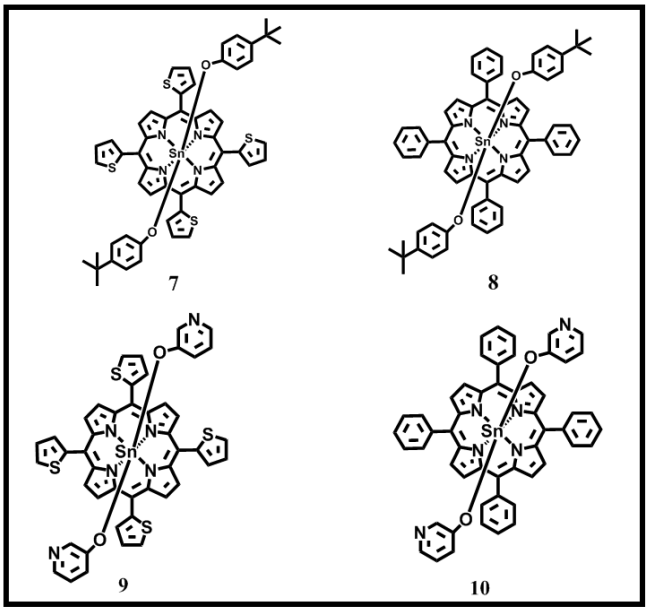

Figure 1.14: The molecular structures of porphyrins **7**-**10**.

1.3. Diabetes and glucose sensing

The main application explored for BODIPY dyes **1-5b** in this study is their glucose sensor properties. *Diabetes mellitus* is an autoimmune class of metabolic diseases in which high blood glucose levels (hyperglycaemia) caused by low and inadequate production of insulin or by the inability of the body to respond appropriately to changes in insulin concentration [83-85]. Diabetes consequently results in various long-term health disorders such as blindness, cancer, cardiovascular diseases, lower limb amputation, and damage to the nerves and organs [85-88]. According to the World Health Organization (WHO), in 2014, 422 million people were reported to have diabetes, while in 2012, 2.2 million deaths were attributed to high blood glucose levels. In 2016, approximately 1.6 million diabetes-related deaths were reported [89]. Unfortunately, diabetes is a chronic disease and therefore cannot be cured. However, the stringent and proper control of glucose concentration in the body can prevent the medical complications caused by diabetes [88, 90, 91]. Blood glucose levels can be controlled through frequent glucose monitoring and administrating corresponding insulin [85, 86, 91].

1.3.1. Background on diabetes and glucose sensing

There have been various efforts made to design, develop, create and improve the performance of glucose sensors. Clarke and Lyons reported the first glucose-enzyme electrode in 1962 [92]. Advances made in the development of glucose sensors are typically categorised into three generations (**Figure 1.15**). During the first-generation (**Figure 1.15A**), molecular oxygen (O_2) was used as an electron (e^-) mediator, passing electrons between the enzyme glucose oxidase (GOx) and the electrode surface. In this process, the oxygen molecule is reduced to produce hydrogen

peroxide [93-96]. The sensor relies on the detection of hydrogen peroxide which is considered to be directly proportional to the concentration of glucose [92, 93, 96, 97]. The main disadvantage of first-generation glucose sensors is that the sensing (detection) occurs in the presence of various interfering redox active species such as ascorbic acid and uric acid, which are readily decomposed in the blood thus reducing the selectivity of the biosensor [93, 96, 98]. These sensors also suffer from oxygen dependence; in the absence of molecular oxygen, glucose cannot be detected, since the presence of excess oxygen results in inaccurate measurements of glucose levels [96, 97].

The second generation (**Figure 1.15B**) of glucose biosensors addressed the latter issue by employing "artificial mediators" in the place of molecular oxygen [99-101]. The "artificial mediators" are chemical species with the ability to transfer electrons from the enzyme's active site to the electrode surface. Ferrocene, ferro/ferricyanide, and methyl blue are the most commonly-used mediators along with various organic dyes [93, 102]. In a similar manner to the first generation, the second generation of biosensors is also vulnerable to interferences by other redox active species that can potentially compete with the mediator and therefore produce inaccurate results [96, 101].

The setbacks experienced by the second-generation of biosensors led to the design and development of the third generation (**Figure 1.15C**), which are based on the direct transfer of electrons and are hence "mediatorless". The electrons are transferred directly from the active

centre of the enzyme to the electrode surface [93, 103, 104]. A highly conductive substrate is usually required for these sensors to be effective [93, 104]. The electrode surface and the enzyme's active centre need to be electronically connected to enable the direct transfer of electrons and to eliminate the detection of other redox active species and co-substrates [103-105]. The use of a few enzymes such as GOx and pyrroloquinoline quinone glucose dehydrogenase (PQQ-GDH) has proven to be successful [103, 104].

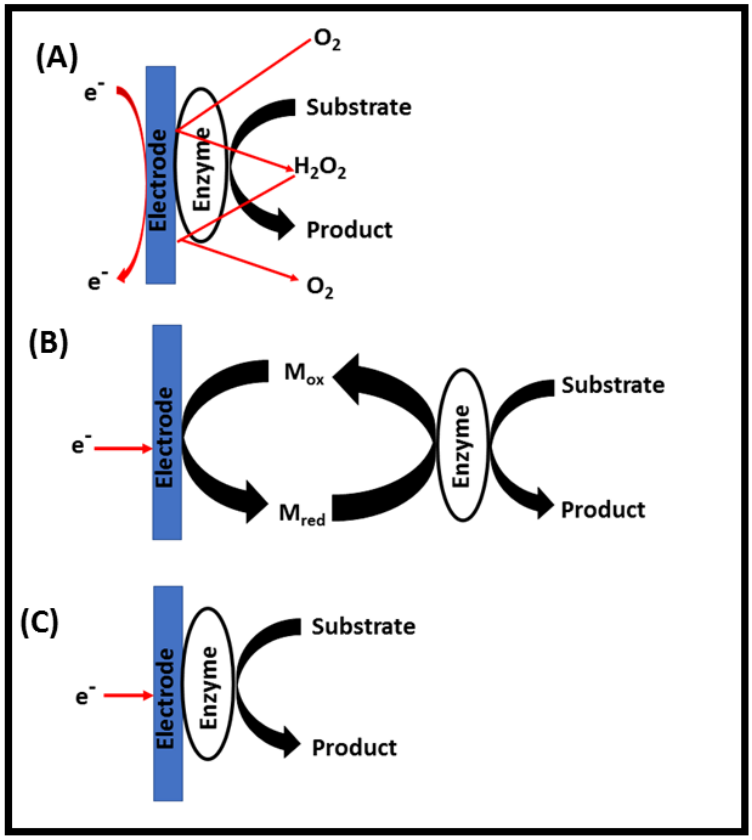

Figure 1.15: Schematic representation of the (A) first generation, (B) second generation and (C) third generation of glucose sensors.

Biosensors that use enzyme functionality for analyte detection are usually unstable because of the inherent instability of the enzyme [93]. GOx is extensively used in glucose biosensors because it is relatively stable [106, 107]. The sensitivity of GOx based sensors is dependent on the activity of GOx, which deteriorates at pH 2 and below as well as at temperatures above 40°C [106, 107]. Exposure to these conditions results in thermal and chemical instability, and damage occurs to the sensor system [106, 107].

Setbacks experienced with the third generation of biosensors have led to the design and development of various non-enzymatic "enzymeless" biosensors, and these are viewed as a fourth generation of biosensors [107]. This approach forms the basis of this study. Non-enzymatic biosensors usually use catalysts to electrooxidise glucose. Initially, precious metals such as copper, gold, platinum and palladium were used to directly electrooxidise glucose in the absence of an enzyme [108-110]. Studies conducted using these precious metals as catalysts reported a number of issues that rendered the metals unsuitable for glucose detection. The biggest issue experienced was the formation of poisonous metal oxides at the electrode surface. This affects the stability and sensitivity of the glucose biosensors [93, 95, 111]. Research towards the use of various catalysts has emerged in which dyes facilitate the direct electrooxidation and detection of glucose. This study aims to create a non-enzymatic glucose sensor through the use of boronic-acid-functionalised BODIPYs to increase the stability, simplicity and reproducibility of glucose biosensors.

1.3.2. Key principles and components of a biosensor

The International Union of Pure and Applied Chemistry defines a biosensor as an analytical transducer device derived for the selective, quantitative or semi-quantitative recognition or measurement of one or more analyte(s) in a sample matrix [112, 113]. “Biosensing” can be classified as a powerful analytical tool used for the detection of biological or chemical molecules using various readout protocols [114]. They are used for a wide variety of applications ranging from medical diagnostics, and environmental and agricultural monitoring to security and warfare defence [115-120].

Selective biosensors are generally comprised of the following components (**Figure 1.16**) [113, 114, 120-122]:

i. The bioreceptor (recognition element): Molecules with the ability to selectively bind to the analyte. Antibodies, enzymes and aptamers are typical examples of bioreceptors. Boronic acid molecules were used in the context of this study.
ii. The reporter moiety: Molecules, usually fluorophores, that enable binding between the analyte and bioreceptor to be recognised. In this study, the possible use of BODIPY dyes as reporter moieties was studied in depth.
iii. The transducer: A device that converts the bioreceptor responses (changes) that occur during the binding into a measurable optical or electrical signal that is transferred to the detector-signal processor.

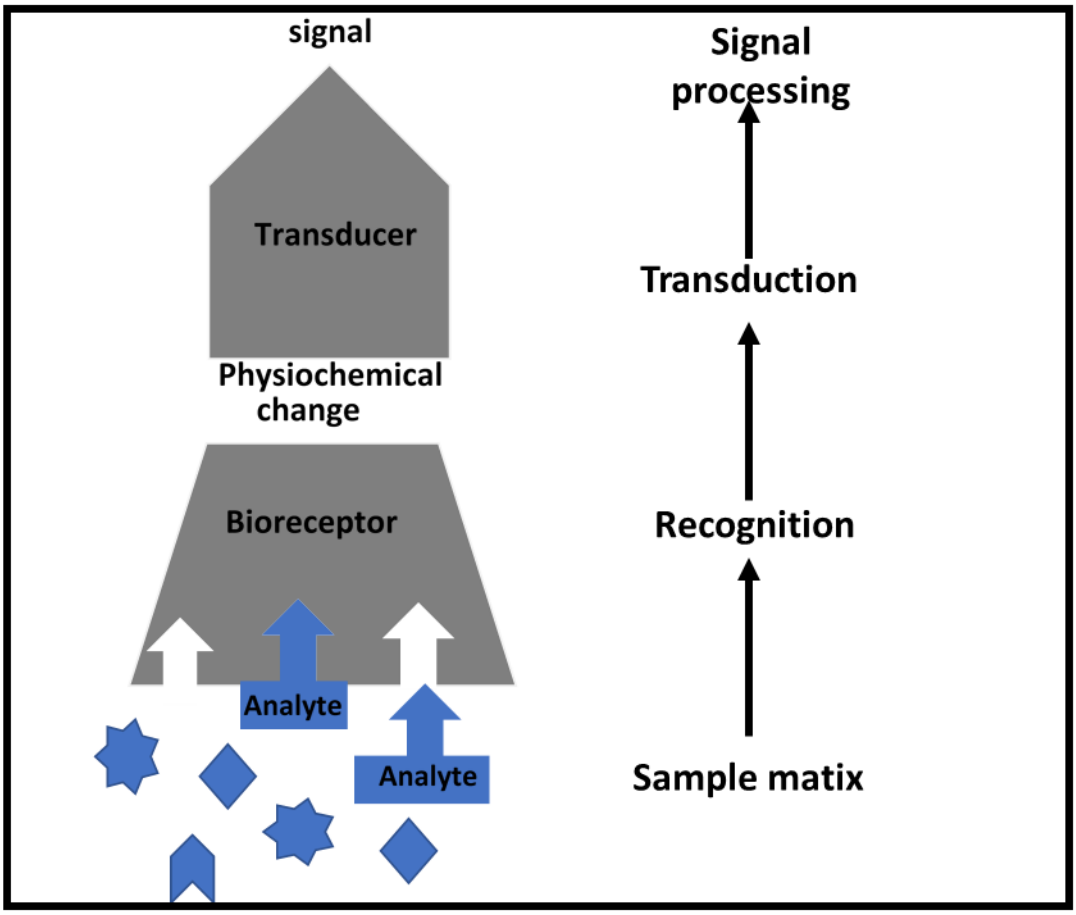

Figure 1.16: Key components of a selective biosensor.

When an analyte binds with the bioreceptor, a change occurs in the system, which can be induced by mass, light, electroactive material and/or pH changes. This is measured by different transducers based on the type of physicochemical change that is involved [120]. This study focuses on fluorescence, colourimetric and electrochemical detection. A considerable majority of the glucose sensors that have been studied previously rely on electrochemical detection, since the technique is highly sensitive, and the instruments are easy to operate and cost-efficient. Very little research has been carried out on electrochemical sensing with BODIPY dyes [123]. Optical

sensors are mainly used in food analysis, drug discovery and medical diagnostics [124-126]. Fluorescence sensors are advantageous in that they are highly sensitive even at low concentrations, and do not require constant calibration and produce accurate results. Colourimetric sensors are also widely used because they are relatively inexpensive, portable, and minimal instrumentation is required that can be easily customised for the detection of specific analytes [127, 128].

1.3.3. Properties of a good sensor

When developing a biosensor, there are several key characteristics that need to be considered [95, 129]. The following is a list of important characteristics that need to be considered when designing an efficient glucose sensor:

i. Accuracy: The sensor needs to be highly accurate and hence produce reliable results.

ii. Sensitivity: Sensitivity is one of the key characteristics in all analytical techniques. Sensitivity provides a measure of the change in observed output relative to a change in glucose concentration. The sensor needs to be highly sensitive and to be able to detect the analyte at low concentrations.

iii. Detection range: The range in which a sensor exhibits a linear response. An ideal glucose sensor should have a wide detection range and thus be able to detect glucose at both very low and very high concentrations.

iv. Response time: Ideal glucose sensors should produce rapid responses to changes in concentration. A steady-state should be reached in the shortest time possible.

v. Selectivity: Sensors need to be highly selective towards the analyte of choice over other interfering species. This is achieved through the careful selection of the bioreceptor.

vi. Calibration provides a measure of the stability of the biosensor response. An ideal glucose sensor should not require frequent calibration.

vii. Testing volume: The biosensor should be able to detect glucose from a small sample size.

This study aims at creating a sensitive enzymeless glucose sensor, by directly detecting glucose through the use of boronic acid groups, since boronic acid has a high affinity for saccharides [130, 131]. The goal was to use BODIPY dyes **1-5b** (**Figure 1.9**) as reporter moieties for fluorescence, and colourimetric sensing, and to use the redox activities of BODIPY dyes **1b** and **2b** to detect glucose molecules in solution at physiological pH.

1.4. Boronic acid molecules

1.4.1. History and application of boronic acid molecules

Boronic acids are small flexible organic molecules (**Figure 1.17**) that have been extensively used in carbohydrate sensing [130-132]. Applications for these molecules have also been studied in the context of enzyme inhibition, cell delivery systems, signalling pathways, chromatographic separation and analysis [131, 133-135].

Boronic acids are useful for carbohydrate sensing because they have a high affinity for carbohydrates particularly those with dicarboxylic acids, α-hydroxycarboxylic acids and diols such as saccharides [136-138]. Boronic acids are used for saccharide sensing in preference to other "carbohydrate binders" because they have the ability to rapidly and reversibly bind covalently to *cis*-1,2 or 1,3-diols in an aqueous environment to form six-membered cyclic esters (boronate esters) [130, 139-143]. The reversibility of the interaction is highly favoured for sensing. The structural flexibility of the molecules also enhances their sensor capabilities [137, 140, 141, 143].

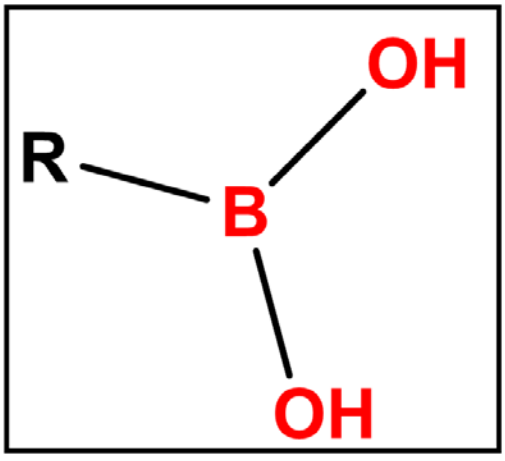

Figure 1.17: The structure of boronic acid molecules.

Boronic acids have been studied extensively for over 100 years. However, their interaction with diols was only recognised in the 1950s. Boronic acids were first used for fluorescent saccharide sensing in the 1990s [137]. Lorand and co-workers were the first to publish a quantitative evaluation of the interaction of phenylboronic acid and various diols by using the pH-depression method, which is primarily based on the concept that binding to/with a boronic acid moiety lowers the pK_a of the system [139]. The diol interactions of boronic acid are known to be highly pH dependent [139, 142].

1.4.2. Interaction of boronic acid with glucose molecules

The interaction between boronic acid molecules and diols is illustrated in **Scheme 1.6**. In their neutral form, boronic acids have a trigonal planar sp^2 hybridised boron atom attached to two hydroxyl groups and either an aryl or alkyl group. These Lewis acids have a high affinity for Lewis bases. It is well known that hydrated metal ions with Lewis acidity exchange bound water in an acid-base reaction [144-146]. The same principle can be applied to the rapid exchange of the Lewis acidic boron atom when it is in a neutral aqueous environment. Under neutral pH conditions, boronic acids complex with two hydroxyl ions and become sp^3 hybridised, by reacting with the water in the buffer system, thus, becoming anionic (with three hydroxyl groups attached to its centre). In their anionic form, boronic acid moieties have the ability to complex with 1,2- and 1,3-*cis*-diols such as glucose to form a boronate ester (**Scheme 1.6**). Upon this complexation with glucose molecules, the *p*K_a value of the system decreases from *ca.* 8.8 in their neutral form to *ca.* 6.8 when interacting with glucose (or *ca.* 4.6 with fructose) [147]. The molecule maintains the anionic form at physiological pH because of the relatively low *p*K_a value. Boronic acids with a

lower pK_a value have a higher affinity for diols. Optimal binding depends on the pK_a values of the boronic acid and the diol. The binding results in a change in ionisation, which results in a measurable change in the electronic properties of the system that can be used to develop an optical, electrochemical or colourimetric sensor. When the pH value of the system becomes higher than the pK_a value of the boronic acid, the boronic acid-glucose complex dissociates as the boronic acid returns to its sp^2 trigonal planar configuration (**Scheme 1.6**).

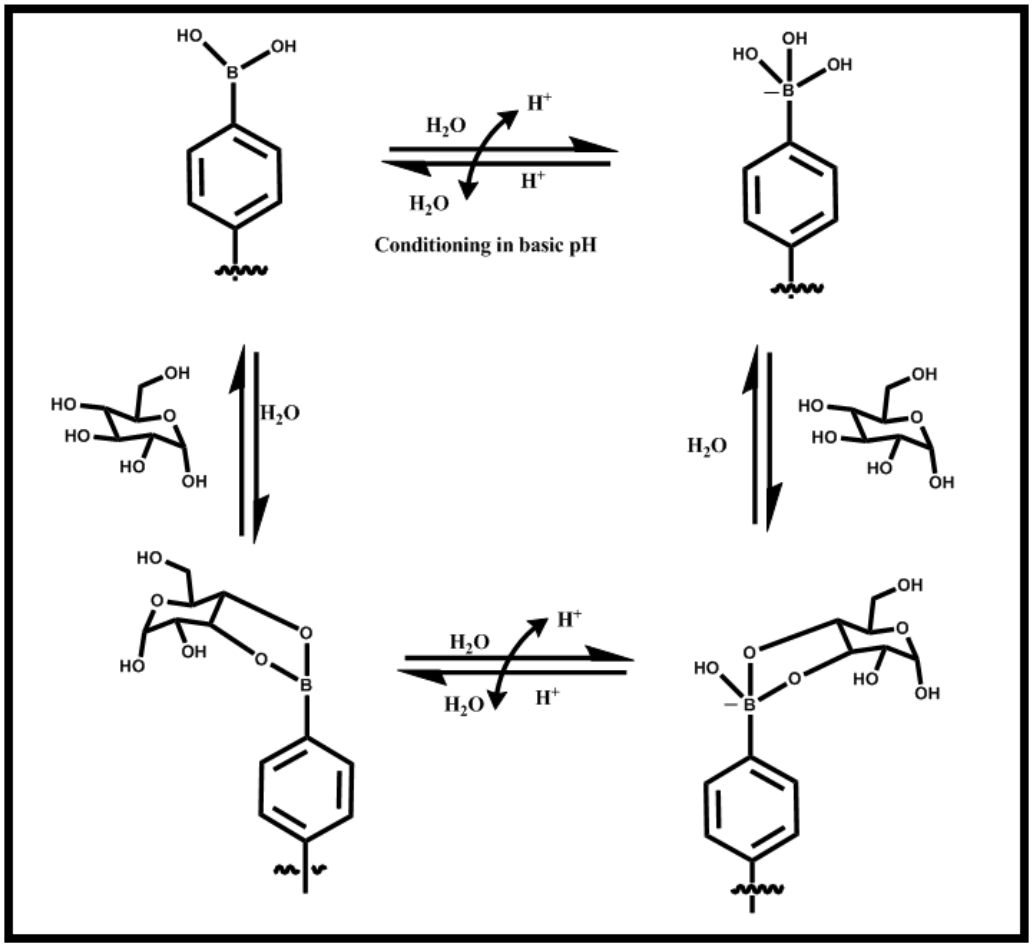

Scheme 1.6: Spontaneous equilibrium interaction between boronic acid and a glucose molecule.

Boronic acid moieties are excellent recognition elements for glucose sensors [131, 147-149]. Boronic acid molecules have different affinities for diols based on their structure. James and Jiang studied the affinity of boronic acid for various monosaccharides [131, 137, 147]. A higher D-glucose affinity was achieved than for D-fructose by making use of the stoichiometry of glucose and fructose binding. Studies have shown that *bis*-boronic systems have higher affinities towards glucose than for fructose or other saccharides [131, 147, 149]. Since one of the key attributes of a good sensor is that it should be selective towards the analyte, 3,5-distyrylBODIPY dyes that have two boronic acid groups were selected for this study (**Figure 1.9**).

Glucose sensing with boronic acid as a recognition element can be studied by using various sensor techniques. This study focuses on colourimetric, fluorescence and electrochemical sensing. A considerable majority of boronic acid sensing reported previously have been conducted by using electrochemical sensing [93, 150]. Very few studies of this nature have been carried out with fluorescence sensing, despite the technique being very popular and well-studied.

1.5. BODIPY dyes in electrochemical glucose sensing

Electrochemistry is a multidisciplinary branch of chemistry that deals with the transfer of electrons so that redox reactions occur in a system through the interrelation of electrical and chemical changes [151]. This phenomenon encompasses analyte detection and quantification, and is used for a wide variety of applications [151-153]. Electrochemistry is extensively used for sensing, since it provides relatively low limits of detection (LoD) and provides rapid measurements [154]. The technique is highly sensitive, reliable, and cost-effective.

The movement of electrons during the redox reactions provides a measurable electrical signal that is related to the electrochemical reactions. Oxidation reactions are characterised by the loss of electrons, which increases the oxidation state of a substance, which becomes “oxidised”. The opposite is true for the reduction reaction, since there is a gain of electrons that results in a decrease in the oxidation state of the “reduced” substance. Electrochemical sensing generally employs electrodes for analyte detection. These electrodes allow the passage of current and/or potential due to the movement of electrons through an aqueous solution.

1.5.1. General setup

Most electrochemical techniques use three electrodes; a working electrode (WE), a reference electrode (RE) and a counter electrode (CE) connected electrically in an electrolytic cell (**Figure 1.18**) [155-158]. The reference electrode, usually a silver/silver chloride (Ag/AgCl) electrode, measures and controls the potential of the working electrode without passing any current [158, 159]. The counter electrode, also known as the auxiliary electrode, is responsible for passing a current [158, 159], which is equal to the current provided by the working electrode [157-159].

The working electrode is the only electrode at which the reaction with the analyte occurs. Current is continuously being passed between the counter and working electrode [159]. The electrochemical system has an external power source that provides the excitation signals to the electrodes and measures the signals obtained. The electrochemical system is connected to a computer with the necessary software installed to analyse and interpret the data received (**Figure 1.18**) [159].

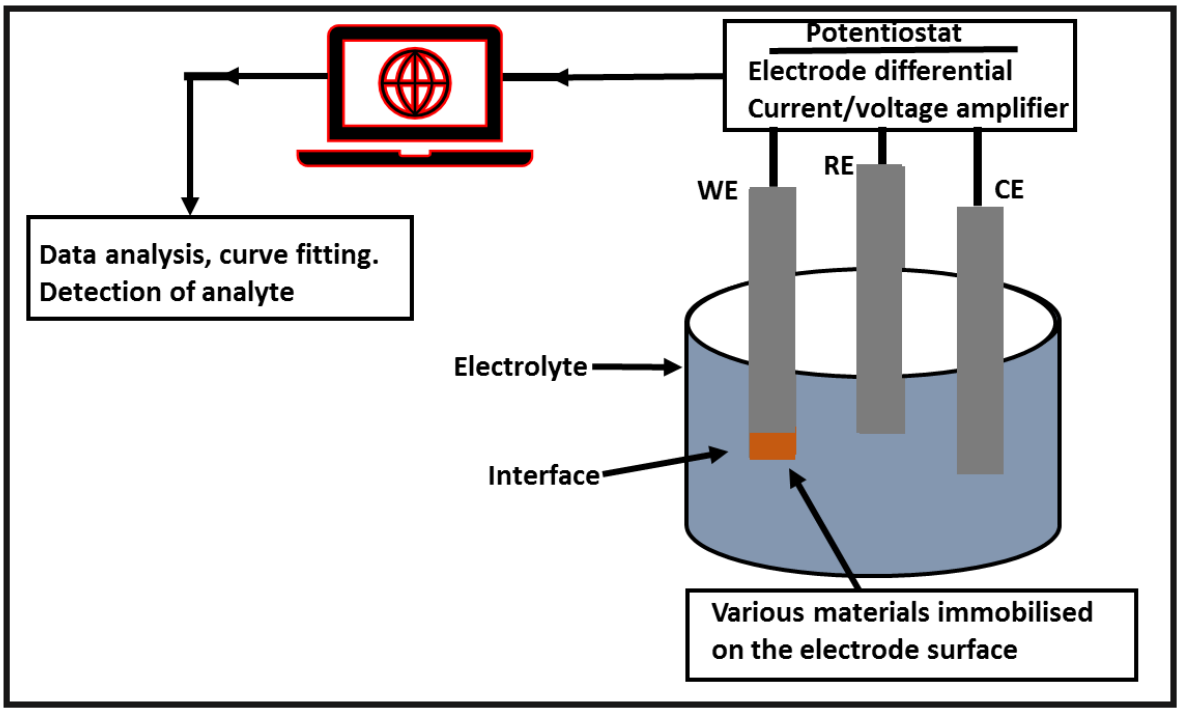

Figure 1.18: The general setup of a three-electrode electrochemical instrumental set up. Image adapted from Bansod *et al.* [158].

1.5.2. Electrode modification

Bare electrodes, such as the glassy carbon electrodes used in this study, suffer from numerous issues such as interferences from surface active and electroactive species, unpredictable surface

reactivity and ill-defined surface processes [160-162]. These issues can be addressed by modifying the electrodes [160-163]. Electrode modification introduces specific catalytic centres onto an otherwise "inactive" electron-conducting electrode surface [164-166]. The working electrode surface can be modified with various interface materials to form electrocatalysts [153, 167, 168]. Electrode modification allows for the control of the chemical and physical properties of the electrode surface in order to enhance the electroanalysis and sensing ability of the device by; i) accelerating the rate of electron transfer, ii) preventing electrode fouling, iii) enhancing selective binding, iv) improving sensitivity, v) improving stability, and vi) providing lower peak potentials [153, 160, 162, 163, 167, 169].

Various electrocatalysts have been used for electrode modification in glucose sensing. The choice of electrocatalyst depends on the application of the electrochemical sensor. In this study, bare glassy carbon electrodes were modified with BODIPY dyes **1b** and **2b** (**Figure 1.9**).

1.5.2.1. Electrode modification techniques

The surface electrode modification techniques used depend on the nature and structure of the electrocatalyst as well as the desired function of the electrocatalyst [164, 170, 171]. There are three main electrode surface modification techniques;

i) Covalent modification: This technique is based on the formation of a covalent bond between the electrocatalyst and the electrode surface. Covalent modification involves creating a covalent bond either via functional groups, or

through an anchor bridge molecule, or by activating the electrode surface [153, 170-173].

ii) Adsorption modification: This technique uses the chemical and physical properties of the electrocatalyst to modify the electrode surface [164, 167].

iii) Polymer film modification: The technique also arguably involves both covalent and adsorption modification since the polymer can be immobilised by using either procedure. While the other two techniques typically result in a monolayer, polymer film modification results in the formation of a multi-layer on the electrode surface [164, 171, 174, 175].

In this study, adsorption modification was carried out by making use of the drop-dry technique (**Figure 1.19**). Adsorption makes use of the chemical (chemisorption) and physical (physisorption) properties of the electrocatalyst to coat the electrode surface [167, 170, 176]. The electrostatic properties of the electron-rich BODIPY dyes used in this study lead to π–π stacking on the electrode surface [177]. The adsorption drop-dry (drop coating) procedure (**Figure 1.19**) was used because most of a substance will spontaneously adsorb onto an electrode surface when an interaction with its outer environment is more favourable energetically than remaining in solution [167, 176]. Physisorption by drop coating and solvent evaporation enables straightforward and effective electrode modification [176]. Several redox mediators have been effectively adsorbed onto glassy carbon electrodes for use in electrocatalysis by making use of this approach [176].

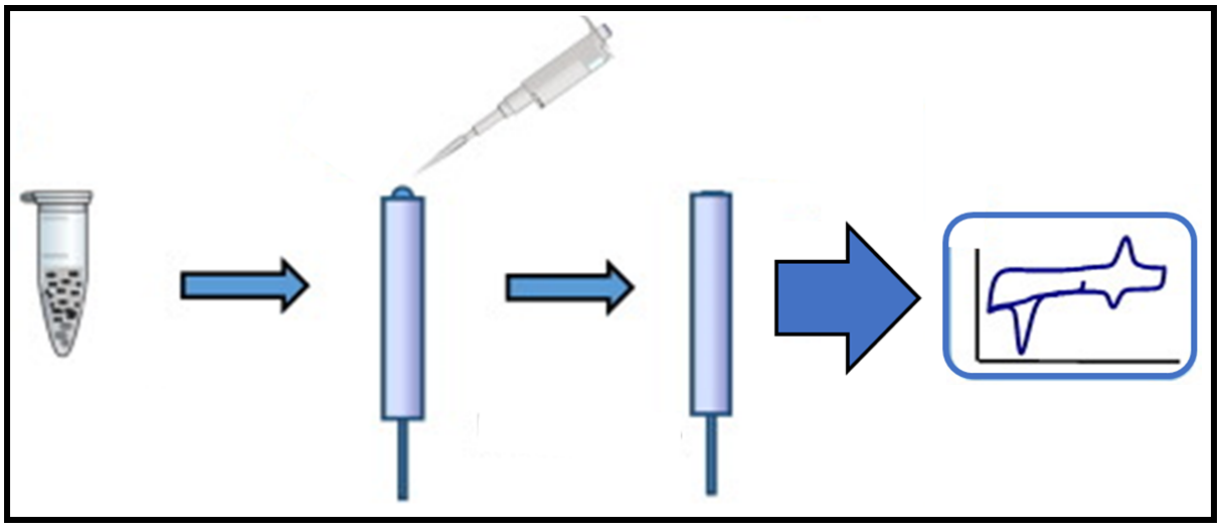

Figure 1.19: Adsorption through the drop-dry coating of the working electrode surface. Image adapted from Moscoso and Carbajo, 2014 [178].

1.5.3. Electrode surface characterisation

In electroanalytical chemistry, it is important to fully characterise the effect of modifications made to the electrode surface. In this study, it is of paramount importance that the electrode surface is characterised before and after modification in order to determine if any modification did in fact occur and the extent of this modification. Various electrochemical and non-electrochemical techniques such as electrochemical impedance spectroscopy, X-ray photoelectron spectroscopy (XPS), cyclic voltammetry (CV), scanning electron microscopy (SEM), scanning electrochemical microscopy (SECM) and Raman spectroscopy can be used in this regard [167, 179-181]. The characterisation techniques do not only determine whether modification occurred but can also be used to explain how the modification affects the electrocatalytic

properties of the electrode surface [153, 167]. SECM and cyclic voltammetry (see section 1.4.4) were used to characterise the electrode surfaces that were prepared in this study.

1.5.3.1. Scanning electrochemical microscopy

SECM can be used to determine and rationalise the surface morphology and catalytic activity of the surface electrode pre- and post-modification [182-184]. The technique has been used in various applications for imaging, and in determining the heterogeneous and homogenous kinetics of electrochemical reactions [182].

An ultramicroelectrode (UME) is used as the probe in this technique [185, 186]. Throughout the analysis a tip current is monitored, which can be affected by; i) the redox probe as there are electroactive species in the probe, ii) the conductivity of the electrocatalyst, and iii) the distance between the tip and the electrode surface [185-187]. The tip current measurement can be used to determine the electrochemical, conductivity and topographic properties of the electrode and electrocatalyst, and is monitored in two stages (**Figure 1.20**). The tip current is initially measured in the bulk solution while the tip is far from the surface [185-187]. During this process, a potential is applied in order to oxidise or reduce the electroactive species in the solution. A steady-state current (**A**) is then observed depending on the radius of the UME, and the concentration and diffusion coefficient of the electroactive species. The tip current is then measured when the tip is close to the surface. The current observed during this stage of the process depends on the nature of the electrode surface. If the surface is conductive, the diffusion of the electroactive

species is enhanced and the current increases (**C**). In contrast, when the electrode surface is insulating, diffusion is blocked, and there is a decrease in the current (**B**) [182, 185, 186, 188].

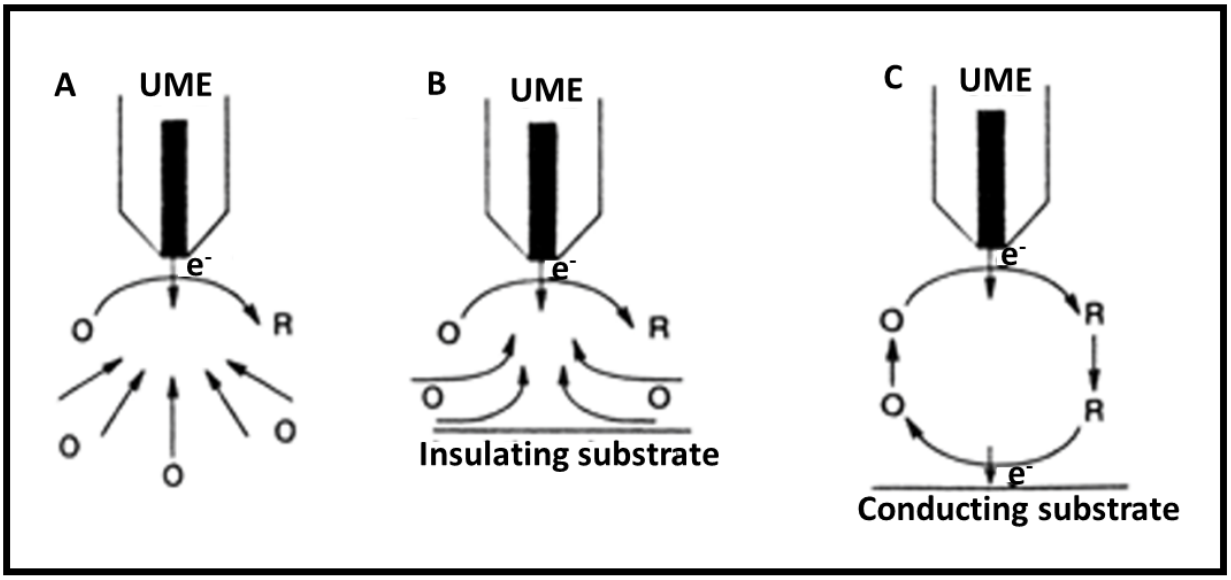

Figure 1.20: Basic principles of SECM.

In this study, SECM approach curves (**Figure 1.21**) and area scans were used to characterise bare and modified glassy carbon electrode surfaces after the drop-dry method was used to introduce BODIPYs **1b** and **2b** as electrocatalysts.

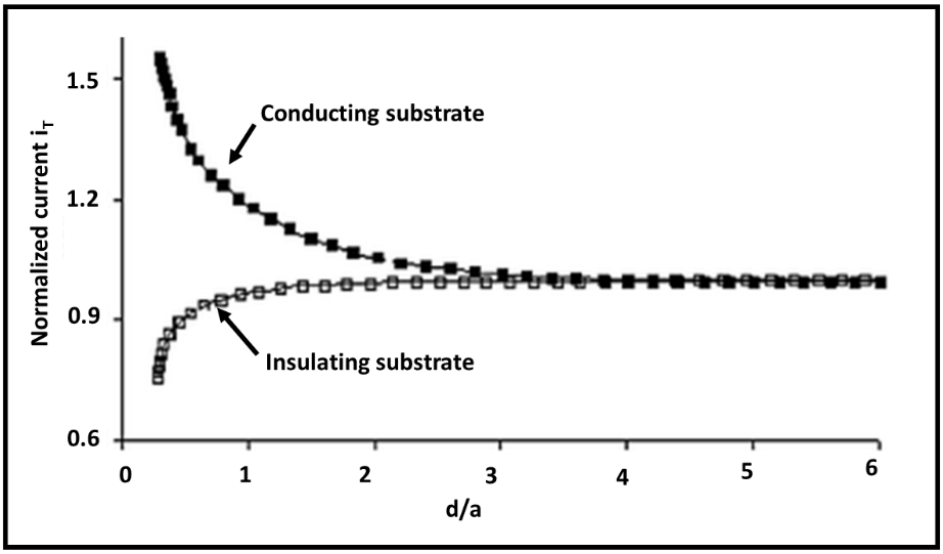

Figure 1.21: Examples of SECM approach curves.

1.5.4. Electroanalytical techniques

Electroanalytical techniques deal with the measurement of electrical quantities, such as potential, charge, and relationships between chemical parameters and current flow [189, 190]. These techniques are important for analysis and sensing. It is of paramount importance in the context of electrocatalysis that these techniques accurately detect analytes at low concentrations. There are various techniques that can be used in this regard, which can be classified into three main categories; i) potentiometry, ii) voltammetry, and iii) conductivity. This study focused primarily on voltammetry.

Voltammetry is concerned with the measurement of the current response at the working electrode as a function of an applied potential with respect to the reference electrode [190]. When a specific potential is applied between the working electrode and the reference electrode,

a current proportional to the concentration of the electroactive species in the bulk solution is produced and passed between the working and counter electrode. This current is measured by a potentiostat providing quantitative information regarding the electroactive species.

There are various voltammetry techniques. This study makes use of cyclic voltammetry, chronoamperometry and differential pulse voltammetry.

1.5.4.1. Cyclic voltammetry

Cyclic voltammetry is by far the most commonly used electroanalytical technique, since it provides a rapid determination of redox potentials and is very convenient to use [189, 190]. The potential of the working electrode is scanned linearly at a particular scan rate in the forward and reverse direction resulting in the current produced being measured as a function of the potential (**Figure 1.22**). CV is used extensively during the quantitative investigation of the redox reaction mechanism. The technique is only rarely used to determine the LoD because it is not very sensitive in this context. When CV is used in characterising modified surface electrodes, the main properties studied are the shift of the detection peak potential towards zero and the increase in the intensity of the current [191, 192], since these properties have a direct relationship with the sensitivity of the electrocatalyst.

1.5.4.2. Chronoamperometry

Chronoamperometry is a more sensitive technique than CV [189, 190]. The potential of the working electrode is stepped from a value where no faradaic reactions occur to a fixed value where either reduction or oxidation of the electroactive species is occurring. The latter potential

is usually obtained from the CV detection peak, since this is the point where the analyte is either reduced or oxidised. The technique is time-dependent, so the current data are plotted as a function of time. Due to the sensitivity of the technique, it is usually used to determine the LoD from a plot of current against analyte concentration.

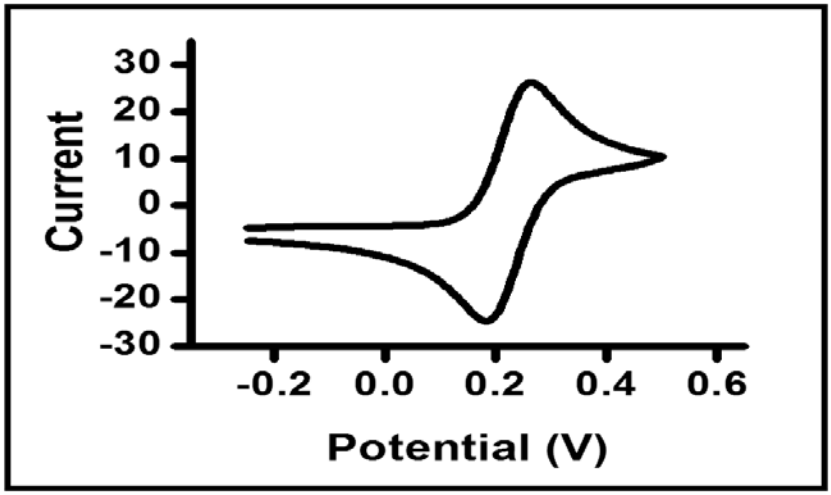

Figure 1.22: An example of a cyclic voltammogram.

1.5.4.3. Differential pulse voltammetry

Differential pulse voltammetry (DPV) is used for quantitative chemical analysis and to study the thermodynamics, kinetics and mechanisms of chemical reactions [189, 190]. The technique is highly sensitive and is therefore very useful in determining trace analyte levels in organic and inorganic media in parts per billion. DPV is also used to enhance the resolution of the voltammograms. The technique is a derivative of linear sweep voltammetry and staircase voltammetry, since it involves a series of short voltage pulses during the linear sweep of potential values and recording the current before each pulse and late in its duration. The current difference

derived from this is plotted against the applied potential. The height of the peak current is usually directly proportional to the concentration of the electroactive species.

1.5.5. BODIPY dyes studied

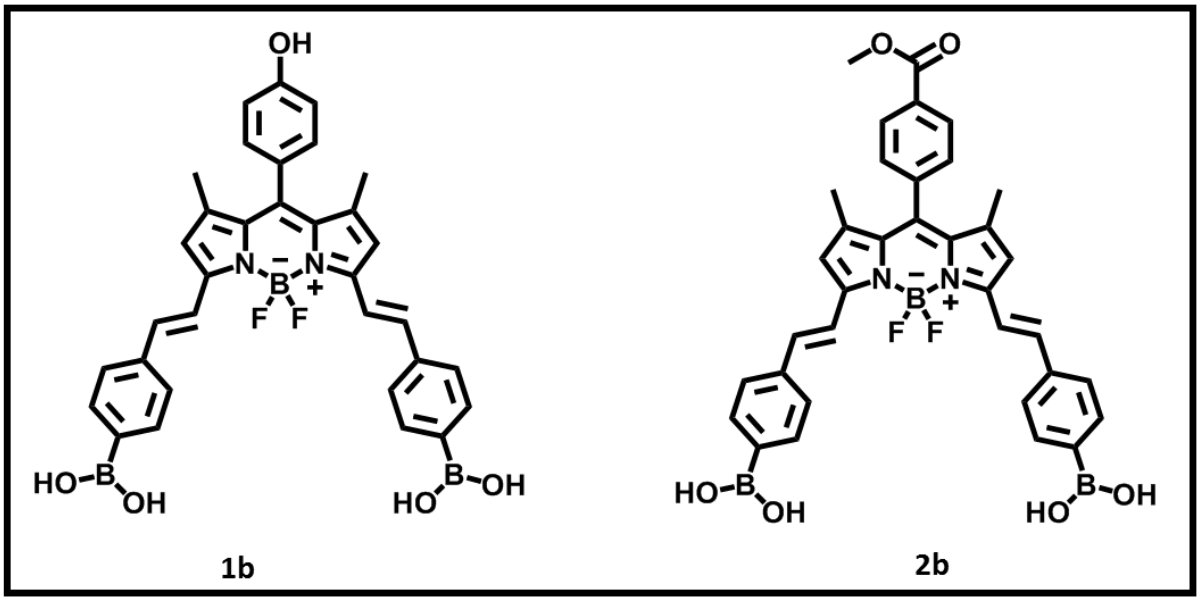

Figure 1.23: BODIPY dyes **1b** and **2b** used to study the direct electrochemical sensing of glucose.

1.6. BODIPY dyes in fluorescence and colourimetric glucose sensing

Fluorescence is among the most widely investigated glucose sensing techniques, because the technique is highly sensitive, and fluorescence measurements typically cause very little or no damage to the host system [193, 194]. When a fluorophore is used that absorbs in the NIR region, the emission can be measured from outside the body thus creating non-invasive sensor systems that are suitable for use as biosensors [195, 196].

Colourimetric techniques have been extensively used during the chemical and biochemical detection of various analytes in different fields, including biomedical, food control and environmental applications [197]. Colourimetric systems are generally favoured in these contexts because of the simplicity of the measurement technique and data analysis, its cost-effectiveness and accuracy. Colourimetric analysis is used for the detection of analytes through a colour change that can be detected visually. The analysis can be performed using light-sensitive elements such as photodiodes, phototransistors, CCD cameras, and more recently by RGB detectors, since several readily available devices now provide this codification for colour description [197, 198].

There are several advantages that make the use of fluorescence and colourimetric biosensors favourable for molecular recognition applications:

i. The techniques enable the simultaneous monitoring of the concentrations of analytes in all regions of a living cell.
ii. The techniques do not require a reference, and hence no calibration is required.
iii. The sensor systems do not consume the analytes.

Despite these favourable properties and the extensive studies that have been conducted on fluorescent and enzymeless sensors for glucose, there are currently no commercially available fluorescent sensors for glucose [199, 200].

1.6.1. Design of fluorescent sensors

A fluorescent sensor typically has two important moieties; a receptor and a fluorophore. The receptor is responsible for the recognition of the analyte, while the fluorophore is responsible for signalling the recognition event upon binding of the analyte and receptor. There are three main fluorescent sensing strategies that have been widely studied, which can be differentiated based on the interaction of the fluorophore and receptor with the analyte [201].

i) Intrinsic fluorescent probes: In this strategy, the signal transduction mechanism involves the interaction of the analyte with part of the π-system of the fluorophore [201, 202].

ii) Chemosensing ensemble: A chemosensing ensemble is a comparative assay in which the receptor and fluorophore dissociate selectively through the addition of an appropriate competitive analyte with the ability to interact with the receptor [201, 203, 204].

iii) Extrinsic fluorescent probe: The receptor and the fluorophore are covalently linked, but electronically independent of each other [201, 205, 206]. Generally, a receptor molecule is synthesised that is attached to the fluorophore at a later stage to enhance the sensitivity of the system. A spacer is used to keep the moieties in close proximity. PET (**Figure 1.24**) is the process that enables the use

of extrinsic fluorescence probe. As it utilises the "fluorophore-spacer-receptor" components and format in its rational design [207]. In PET reactions, the absorption of light activates the donor or acceptor for electron transfer. As illustrated in **Figure 1.24**, when the sensor is in its 'off' state, the excitation of the fluorophore produces an electron transfer from the receptor to the fluorophore [207].

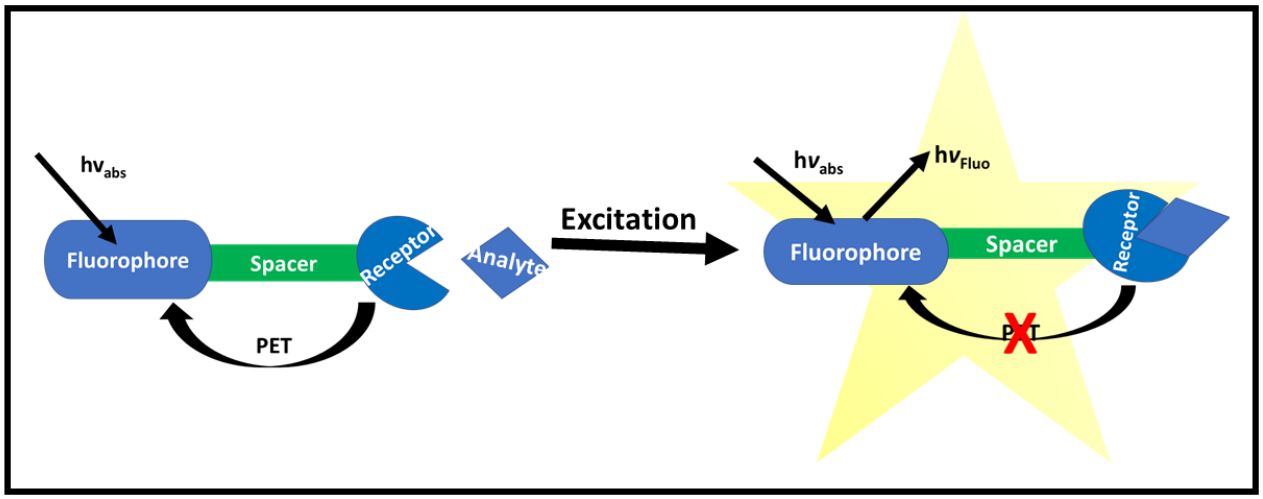

Figure 1.24: Photoinduced electron transfer.

In this study, the goal was to prepare intrinsic rather than extrinsic fluorescent probes by synthesising BODIPY dyes with boronic-acid-functionalised styryl groups that lie co-planar with the BODIPY cores (**Figure 1.9**) that were selected as the fluorophores of choice. As explained previously, boronic acids are known for their selective reactions with saccharides.

1.6.2. Photophysical sensing mechanism

Fluorescence refers to the emission of light by a substance after absorbing light [17]. In this study, the goal was to use intermolecular charge transfer (ICT) as the sensor mechanism for both the

colourimetric and fluorescence detection of glucose at physiological pH (**Figure 1.25**). ICT typically occurs between an electron donor and electron acceptor that are directly π-conjugated, while PET involves a spacer [201, 205]. Upon excitation, electronic charge is transferred from an electron donor to an electron acceptor, increasing the dipole moment in the process. ICT causes noteworthy shifts in the absorption and emission bands, which reflects the strength of the donor-accepter interaction [17], and hence can result in visible colour changes. It can also result in fluorescence quenching.

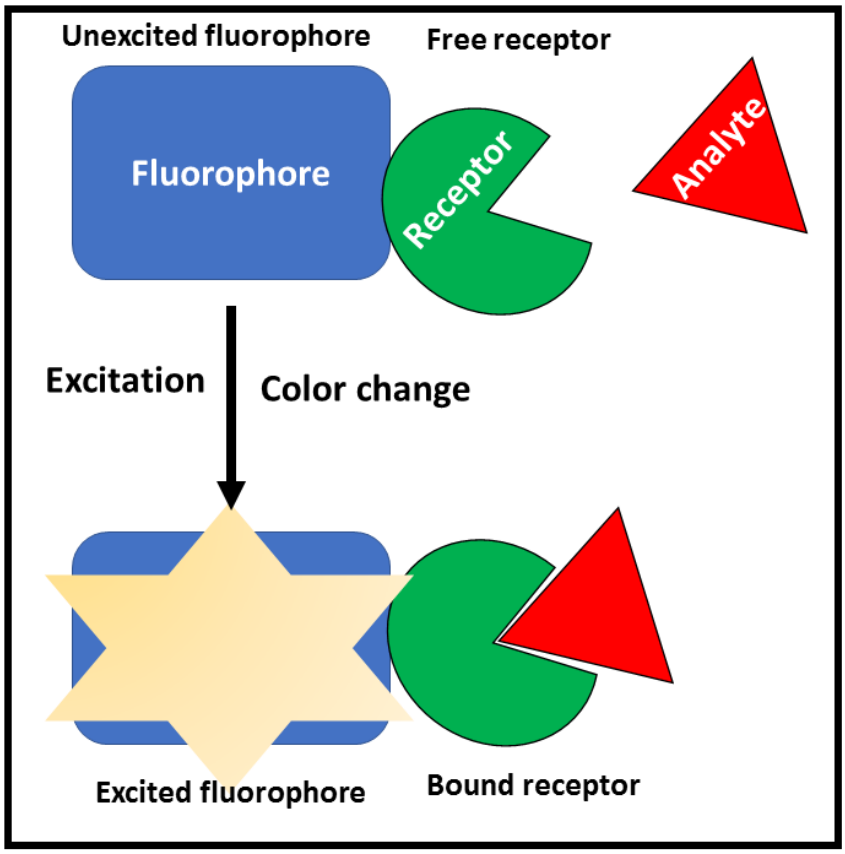

Figure 1.25: Schematic ICT mechanism for fluorescent and colourimetric dyes.

1.7. BODIPY dyes and porphyrins in nonlinear optics

Nonlinear optics (NLO) is a branch of physics that studies how intense light interacts with optically transparent matter [208, 209].

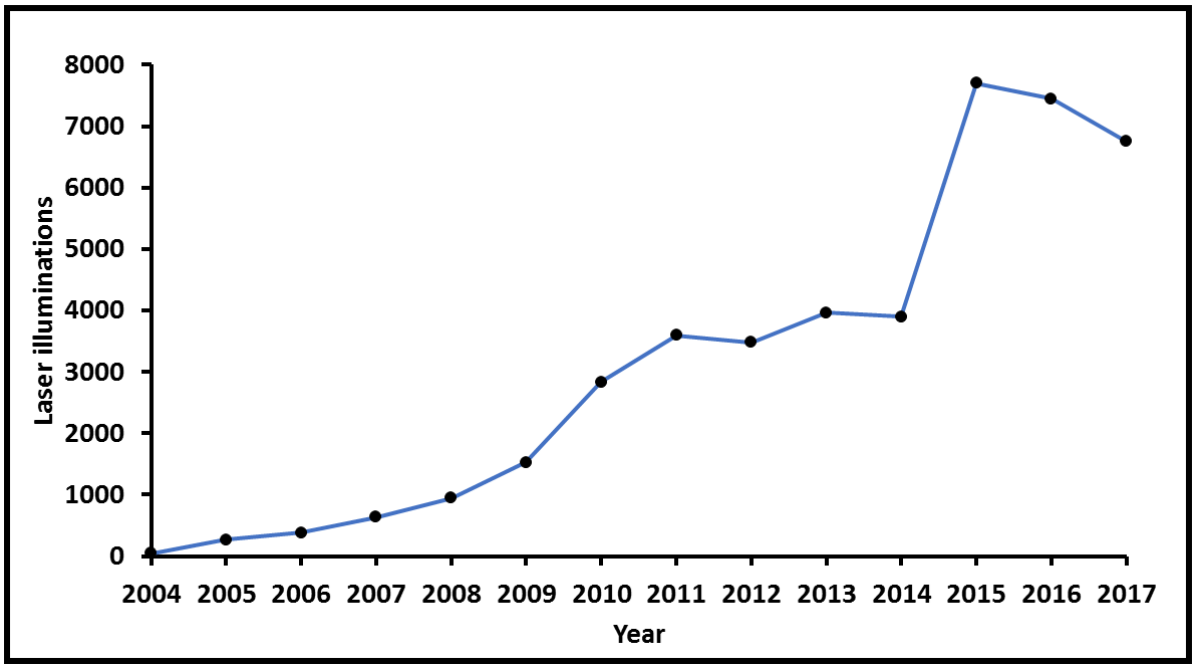

Figure 1.26: Statistical graph of aviation safety-related laser incidents that occurred in the United States and were reported between 2004–2017 [210].

Optical limiting (OL) is an important NLO phenomenon that is used to protect sensitive instruments including the human eye from being damaged by intense laser beams [208, 211]. Optical limiters are also used for other applications such as; laser power regulation and the restoration and/or stabilisation of signal levels in optical data transmission and logical systems [208, 211-213]. Over the past decade, there has been an increase in the need for optical limiting materials, since the number of reported laser incidents related to aviation safety has increased

drastically, **Figure 1.26**, from there only being 43 reported cases in 2004 to over 7 000 cases being reported in 2017.

The typical transmission response of a material scales linearly with the increase in incident light intensity [214, 215]. However, at higher light intensities the optical properties of the material can change rapidly resulting in nonlinear effects (**Figure 1.27**). Optical limiting materials are designed to decrease the amount of light transmittance upon exposure to high light intensity such as laser beams [211, 215, 216]. These materials should strongly attenuate intense light by only allowing a beam of "safe" intensity to pass through while still maintaining a relatively high output fluence (**Figure 1.28**) [213, 216].

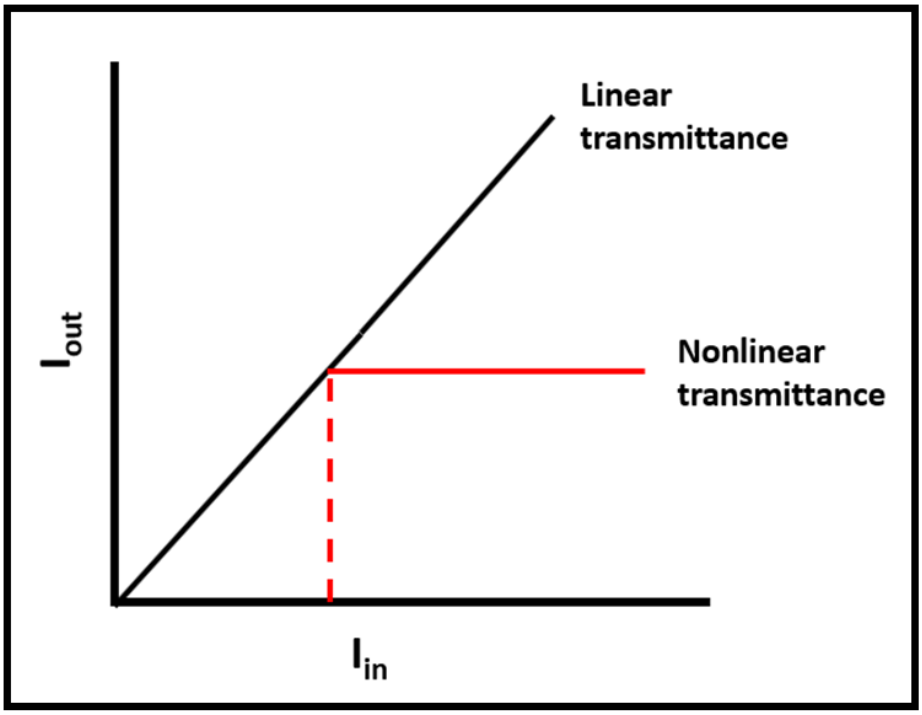

Figure 1.27: Representation of the ideal response of an optical limiter.

An ideal optical limiter should have the following properties:

- High linear transmittance at low intensity.
- A low limiting threshold fluence for the nonlinear response.
- A fast response time (nano or picosecond).
- Low optical scattering.
- A broadband response (within the visible region).

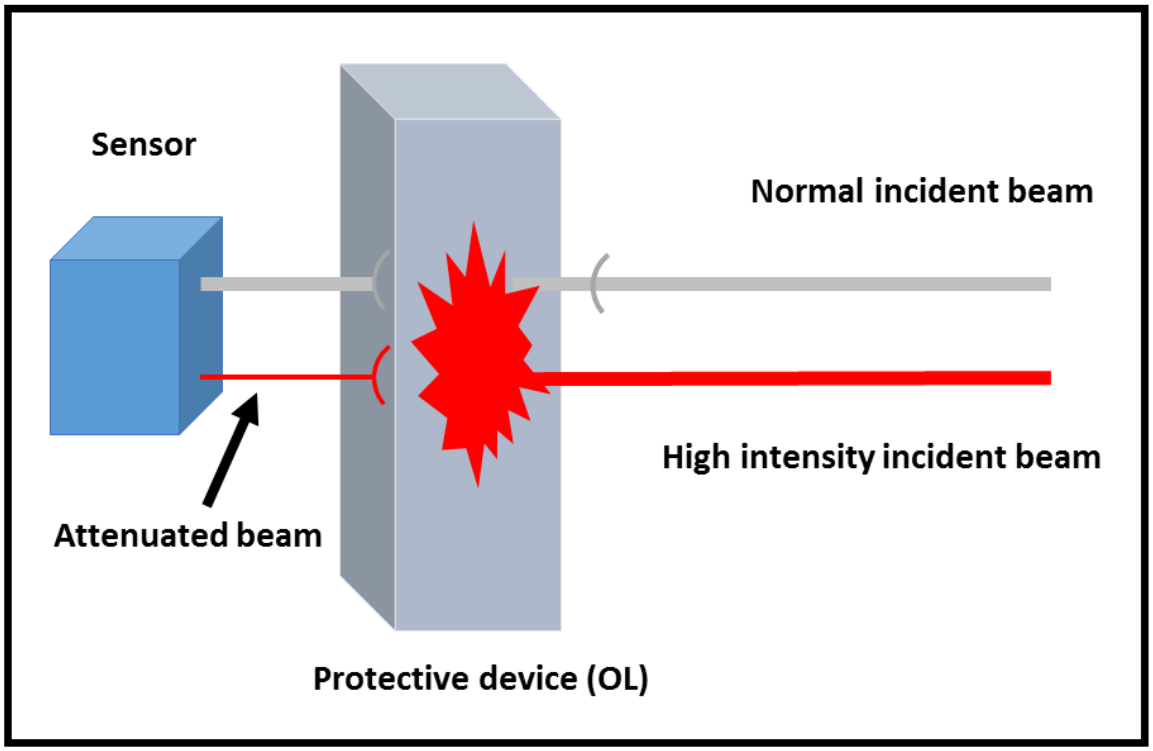

Figure 1.28: Representation of the ideal functioning of an optical limiter.

1.7.1. Optical limiting mechanisms

There are two main optical limiting mechanisms; dynamic (active) and passive optical limiting. Dynamic optical limiting uses an active-internal feedback mechanism [209, 211]. Dynamic

systems use a device that controls or restricts the light intensity that is transmitted. An example of a dynamic OL is a photosensor that controls an iris that restricts the intensity of light incident on an optical system [211]. Dynamic systems only work when components such as a sensor, a processor and an actuation module are connected. These systems rely on a change in the sensor occurring when a signal is communicated to the processor for the light intensity to be decreased. Dynamic OL devices have relatively slow response times, due to the signal communication that is required. They are highly complex since multiple components are required for their functionality and for their accurate and reliable connection. Communication amongst these components makes the systems difficult to operate by unskilled individuals [209, 211].

Passive optical limiting uses nonlinear optical materials, which are also sometimes referred to as smart materials. The sensing, processing and actuation processes of the system are inherent within the smart materials [214]. There are no additional components required for the functionality of the passive OL device, since this functionality is a physical characteristic of the material [211]. Therefore, unlike dynamic OL, the response rate of a passive OL is not affected by the communication of various components making the response simpler and faster to achieve.

This study focuses on passive OL, which can be further subdivided into three distinct processes; i) nonlinear absorption (NLA), ii) nonlinear scattering (NLS) or induced scattering, and (iii) nonlinear refraction (NLR), the origins of which differ markedly (**Figure 1.29**) [211, 217, 218]. Nonlinear scattering (**A**) is induced by the interaction of light with small centres [218]. The NLS system disperses the intense laser beams into larger spatial dimensions. This, in turn, reduces

the intensity of the direct incident laser beam [211]. Thermally induced NLS is commonly used in nanomaterial systems [218]. The scattering can be either directional or uniform depending on the size of the scattering centres [211]. The principles of nonlinear refraction and absorption are based on transitions between discrete states. Nonlinear refraction (**C**) operates by refracting incident radiation (light intensity) away from the sensor and is thus based on defocusing. In contrast, the nonlinear absorption process (**B**) absorbs the incident light, therefore, utilising a self-focusing concept. NLA is the key phenomenon in nonlinear optical spectroscopy. This study makes use of the principles of NLA to determine the optical limiting activity of solutions and polymer thin films containing selected series of molecular dyes [211, 219]. The NLA mechanism is primarily associated with the combination of two optical limiting processes; reverse saturable absorption (RSA) and multi-photon absorption (MPA) [219, 220].

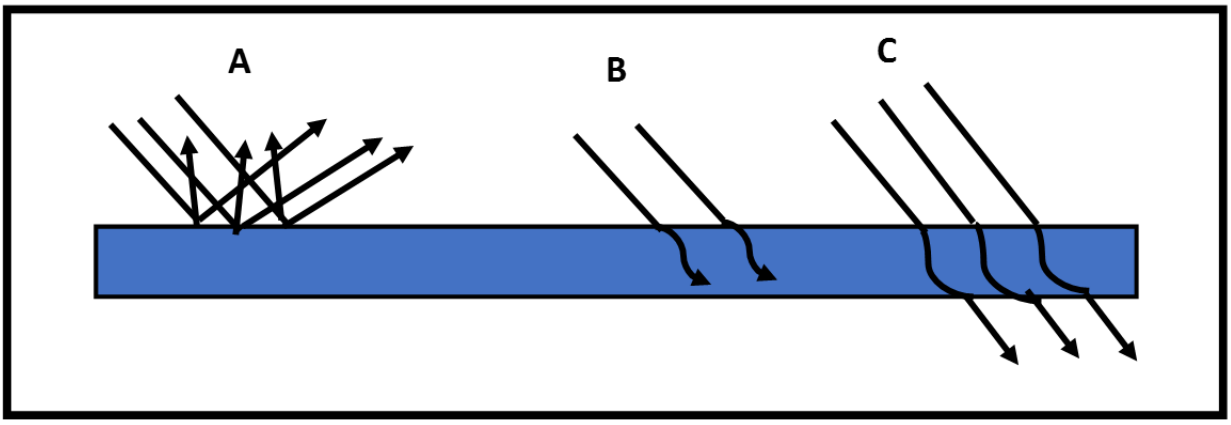

Figure 1.29: The differing responses associated with (A) nonlinear scattering, (B) nonlinear absorption and (C) nonlinear refraction.

The RSA process is generally observed when the excited state absorption (ESA) cross-section is larger than the ground state absorption cross section. In the context of molecular dyes that readily undergo ISC, such as porphyrins and phthalocyanines, this can be explained using a five vibrational band level model (**Figure 1.30**), which describes the absorption cross-sections (σ_n) and lifetimes (τ_n) of the states involved. A three-level model mechanism (**Figure 1.31**) can also be used for dyes that typically do not undergo ISC, such as most non-halogenated BODIPY dyes.

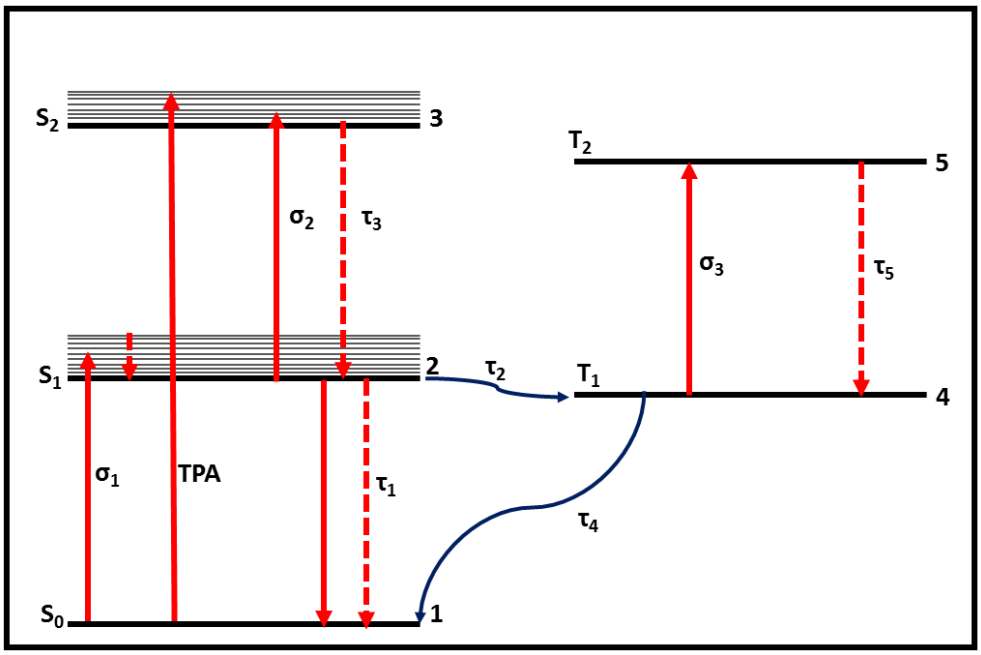

Figure 1.30: A five-level model for the RSA mechanism. The solid red lines represent the absorption and emission processes, while the dotted lines represent internal conversion and non-radiative decay. The blue wavy lines represent intersystem crossing and phosphorescence.

The optical limiting dye typically starts in the ground state, where it is irradiated by intense laser light, which ultimately populates a singlet excited state through either linear one photon or non-linear multiphoton absorption. Multiphoton absorption occurs as a result of the simultaneous absorption of two or more photons via the formation of virtual states. Two-photon absorption (TPA) is the most common MPA process. TPA occurs via the absorption of a photon that excites a molecule from the ground state to a virtual excited state followed by the simultaneous absorption of a second photon. On a femtosecond timescale, MPA is required to generate a nonlinear response. On the nanosecond timescale that was investigated in this study, however, this is not necessarily the case, since the longer timescale enables additional processes to occur that populate other excited states where ESA can subsequently also occur. The dye undergoes internal conversion, where necessary, from higher singlet excited state and relaxes back to populate the S_1 state. Especially when there is a heavy atom present, some of the dye molecules undergo intersystem crossing from the S_1 state to T_1 where they can undergo further excitation to a higher excited triplet state (T_n) as well as undergoing phosphorescence from the T_1 state to the ground state.

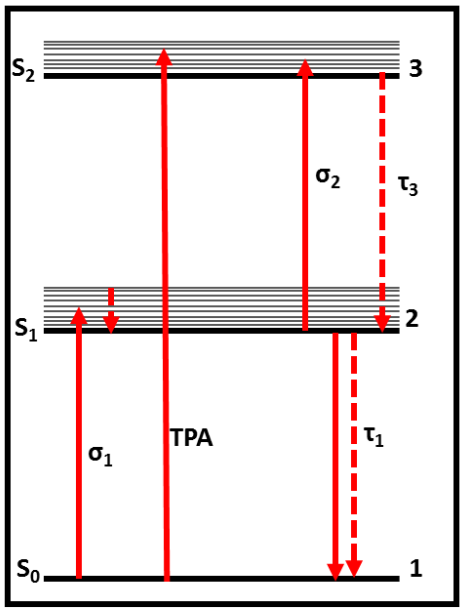

Figure 1.31: A three-level model for the RSA mechanism. The solid red lines represent the absorption and emission processes, while the dotted lines represent internal conversion and non-radiative decay.

On the nanosecond timescale in the context of this study, the nonlinear transmission of light usually originates primarily from non-saturable ESA at high incident light intensities. If the absorption cross-sections of the S_1 and/or T_1 excited states (σ_2 or σ_3) are smaller than that of the ground state (σ_1), saturable absorption is observed due to an increase in transmission with increasing incident light intensities. In contrast, if the absorption cross-section of the excited states is larger than in the ground state, RSA behaviour is observed, which involves a decrease in transmission as the incident intensity increases.

Various organic and inorganic materials have been studied for use as optical limiting materials. Optical limiting can occur in either solid or liquid media. Metal nanoclusters and carbon-related

nanomaterials have been extensively studied as possible OL materials [221, 222]. Carbon nanotubes have been shown to exhibit very strong NLO responses at 532 and 1064 nm [223, 224], largely due to NLS, particularly through a thermally induced mechanism. Recently, organic dyes such as phthalocyanines (Pcs) and porphyrins have been found to possess favourable optical limiting properties due primarily to NLA [225-228]. Porphyrin related macrocycles are studied for nonlinear optics mainly because of their extensively delocalised π-electron systems, which yield excellent third-order nonlinear optical limiting properties. Pc structures can be easily modified without compromising the stability of the structure or altering its key properties. The insertion of a heavy metal ion in the central cavity of the ligand yielding metallophthalocyanines (MPcs) and metalloporphyrins [227] increases the population in the T_1 excited state via ISC (**Figure 1.30**). Pcs have a high absorption cross-section in the T_1 excited state compared to the ground state at 532 nm, so this provides a strong RSA response. In a similar manner, porphyrins have great potential as optical limiters due to their photochemical and photophysical stability and facile structural modification. In this study, the OL properties of a series of Sn(IV) thienylporphyrins (**Figure 1.33**) that are known to have unusually high singlet oxygen and hence triplet state quantum yields were studied to assess their suitability for use in OL applications [229].

Since the literature on the optical limiting properties of Pcs [225-227] suggests that molecules with low symmetry that generate a significant ground state dipole moment tend to provide enhanced optical limiting responses, the boronic-acid-functionalised 3,5-distyrylBODIPY dyes that were prepared for glucose sensing applications (**Figure 1.33**) were also studied to assess their suitability for optical limiting, along with a 3,5,7-tristyrylBODIPY dye. BODIPY dyes have

C_{2v} symmetry, which is lower than the D_{4h} and C_{4v} symmetry of Pcs and most MPcs, respectively [230]. The structures of BODIPY dyes can be modified to make them more suitable for use in NLO. Typical 1,3,5,7-tetramethylBODIPY core dyes have a main absorption band at ca. 500 nm in the heart of the visible region and because of this BODIPY dyes are usually not studied as optical limiters for visible region lasers, such as the second harmonic of Nd:YAG lasers at 532 nm. However, upon structural modification through styrylation at the 3,5-positions, the main absorption band red-shifts into the near infrared region and there is only limited absorbance across most of the visible region under ambient light conditions [2, 3, 11].

1.7.2. Optical limiting parameters

The Z-scan method is considered to be the best approach for determining optical limiting parameters [231, 232]. The technique can be used to analyse the nonlinear absorption and refraction properties of molecular dyes and the nonlinear properties of a wide range of optical materials in liquids, solids or solutions [233]. The Z-scan method is commonly used to measure nonlinear changes because it is highly sensitive, and it is easy to measure and interpret the data [231-233]. The measurements are analysed using a method described by Sheik-Bahae [234]and can involve either the open-aperture or closed-aperture setups. In this study, the open aperture Z-scan technique was used because it is better suited for measuring nonlinear absorption coefficients (β) in a sample, whereas the closed aperture technique examines nonlinear refraction responses and the parameters depend primarily on the thickness of the material.

In this study, the NLO properties of BODIPY and porphyrin dyes were determined in solution and in polymer thin films to determine their suitability for practical applications. To prevent nonlinear scattering and aggregation, the studies in solution were conducted within the Beer-Lambert linear range.

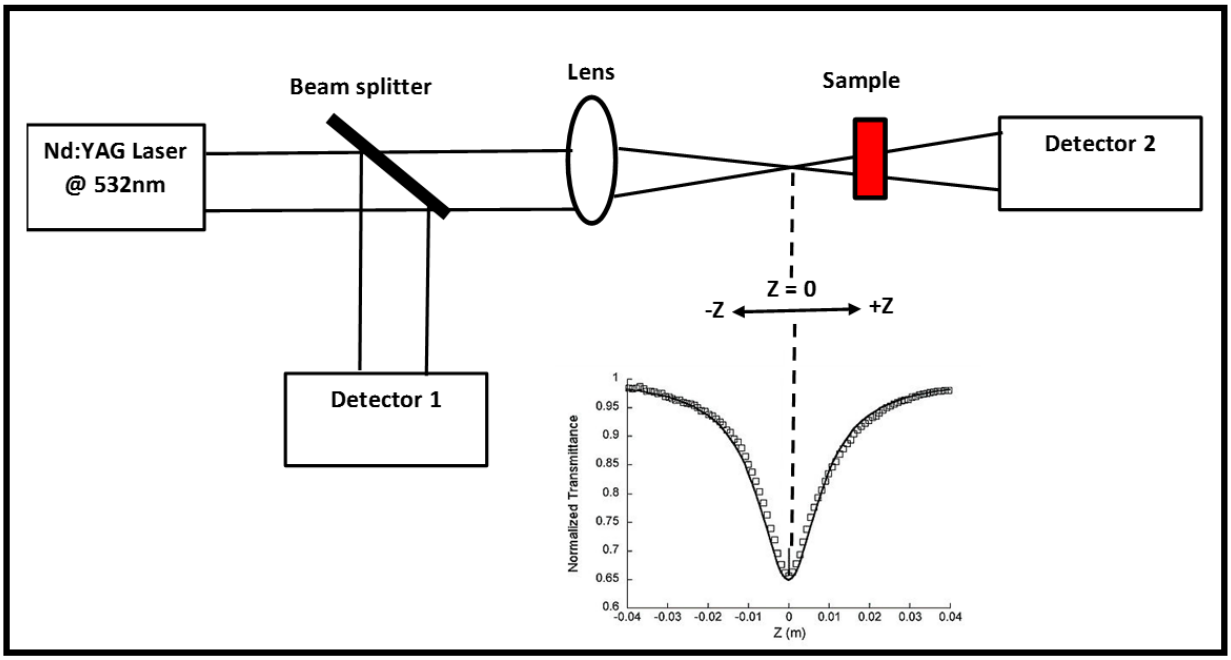

Figure 1.32: Z-scan experimental setup.

Figure 1.32 illustrates a typical single beam Z-scan open aperture instrumental setup. The polarised Gaussian laser beam is orientated perpendicular to the plane of the sample, which is moved along the z-direction (laser beam propagation direction) so that it lies both in and out of the laser focal point. The transmitted signal goes directly to the detector. The magnitude of the detected signal is plotted as a function of the sample position. The Z-scan plots for nonlinear

absorption are typically convex-shaped curves, due to a decrease or increase in transmission along the z-axis. A downward dip in the plots indicates RSA behaviour.

The normalised transmittance of the open aperture measurement for a Gaussian laser pulse time profile can be derived from **Equation 4** [234].

$$T(z) = \frac{1}{\sqrt{\pi} q_0(z)} \int_{-\infty}^{\infty} \ln[1 + q_0(z) e^{-\tau^2}] d\tau \quad (4)$$

where $q_0(z)$ provides an indication of the extent of the nonlinear response. The $q_0(z)$ value for circular-shaped beams is given by **Equation 5**:

$$q_0(z) = \frac{2\beta_{eff} P_0 l_{eff}}{\pi \omega(z)^2} \quad (5)$$

where β_{eff} is the effective nonlinear absorption coefficient of the material, P_0 is the peak power of the laser pulse, and l_{eff} is the effective pathlength, given by **Equation 6**:

$$l_{eff} = \frac{1 - e^{(-\alpha L)}}{\alpha} \quad (6)$$

where α is the linear absorption coefficient, and L is the pathlength of the material. When femtosecond laser pulses are used the β value depends only on the two-photon absorption (TPA) and the other possible multiphoton processes. However, when nanosecond pulses are used, as is the case in this study, an RSA response can arise, if the ESA from the S_1 and/or T_1 states is more

intense than absorption by the ground state. Therefore, the intrinsic value for β that is associated with TPA alone cannot be determined, and only an effective β (β_{eff}) value can be derived instead.

The beam width as a function of sample position w(z) in Equation 2 can be obtained from **Equation 7**:

$$\omega(z)=\omega_0\sqrt{1+\left(\frac{z}{z_0}\right)^2} \quad (7)$$

where z and z_0 are the translation distance of the sample relative to the focus, and Rayleigh length (z_0). The Rayleigh length, is defined as $\pi\omega_0^2/\lambda$ (λ is the wavelength of the laser), and ω_0 is the beam waist at the focus (z = 0), which is the distance from the centre of the incident laser beam to a point at which the intensity reduces to $1/e^2$ of its on-axis value.

The effective nonlinear absorption coefficient, β_{eff}, can be extracted from the experimentally measured transmittance using **Equations 4-7**. An analytical version of this formula (**Equation 8**) can be used to derive $q_0(z)$ directly from the normalised transmittance [8, 235]:

$$T(z) = 0.363e^{\left(\frac{-q_0(z)}{5.60}\right)} + 0.286e^{\left(\frac{-q_0(z)}{1.21}\right)} + 0.213e^{\left(\frac{-q_0(z)}{24.62}\right)} + 0.096e^{\left(\frac{-q_0(z)}{115.95}\right)} + 0.038e^{\left(\frac{-q_0(z)}{965.08}\right)} \quad (5)$$

If **Equation 4** is substituted into **Equation 5**, the $q_0(z)$ value can be defined as:

$$q_0(z) = \frac{Q_0}{1+\frac{z^2}{z_0^2}} \quad (9)$$

where Q_0 is given as:

$$Q_0 = \frac{2\beta_{eff} P_0 l_{eff}}{\pi \omega_0^2} \quad (\mathbf{10})$$

The peak value and FWHM of the Gaussian-shaped curve defined by **Equation 8** provide the Q_0 and z_0 values that are defined in **Equations 9** and **10**, respectively. The β_{eff} value can be determined using **Equation 11**, and this provides a measure for how suitable materials are for use as optical limiting:

$$\beta_{eff} = \frac{\lambda z_0 Q_0}{2 P_0 l_{eff}} \quad (\mathbf{11})$$

Optical limiting materials have positive nonlinear absorption coefficients, since there is markedly lower transmittance as the focal point of the laser light in the Z-scan measurement is approached. For molecules that have zero linear absorption at the laser wavelength of 532 nm, all of the observed absorption at that wavelength is initially due to a multi-photon absorption process. RSA responses consistent with TPA-assisted ESA have been reported previously for an azaBODIPY, due to its relatively long-lived S_1 excited states and an α value of zero [236]. In contrast, linear absorption is likely to be a significant factor in populating the S_1 and T_1 excited states of 3,5-distyryl and 3,5-divinyleneBODIPYs that have also recently been reported to have promising OL properties by Mack and co-workers, since they have significant non-zero α values [8, 235, 237, 238].

The third-order nonlinear susceptibility has an imaginary component, $Im[\chi^{(3)}]$, that provides a measure of how rapidly OL materials respond to the perturbation initiated by an intense incident laser pulse. The third-order susceptibility value has a direct relationship with the β_{eff} value that is described by **Equation 12** [232, 234]:

$$Im\left[\chi^{(3)}\right] = \frac{n^2 \varepsilon_0 c \lambda \beta_{eff}}{2\pi} \quad (\mathbf{12})$$

where n and c are the linear refractive index and speed of light, respectively, and ε_0 is the permittivity of free space. Values that lie in the 10^{-12}–10^{-10} esu range have been reported to provide an indication that compounds are promising candidates for use as OL materials [215, 221, 239].

The interaction of the permanent dipole of the molecules with intense laser radiation causes a bias in the average orientation of the molecules, which results in induced hyperpolarizability. The second-order hyperpolarizability value is directly related to the $Im[\chi^{(3)}]$ value as shown in **Equation 13** [232, 234]:

$$\gamma = \frac{Im\left[\chi^{(3)}\right]}{f^4 C_{mol} N_A} \quad (\mathbf{13})$$

where N_A is Avogadro's constant, C_{mol} is the concentration of the active species in the excited state per mole, and f is the Lorentz local field factor, $f = (n^2+2)/3$. In 2003, the optimal range of

hyperpolarizability values for an effective OL material was reported to be as low as the 10^{-34}–10^{-29} esu range for organic dyes in solution [215, 221].

1.7.3. Thin films

For practical applications, it is important that the optical limiters also be studied in the solid state rather than in solution only. This can be achieved by embedding the compounds into polymer thin films. Dyes **1b**, **2b** and **6** (**Figure 24**) were embedded in polystyrene thin films. Polystyrene is a transparent synthetic aromatic hydrocarbon polymer that has been extensively used for protective packaging [240].

1.7.4. BODIPY dyes and porphyrins studied for optical limiting applications

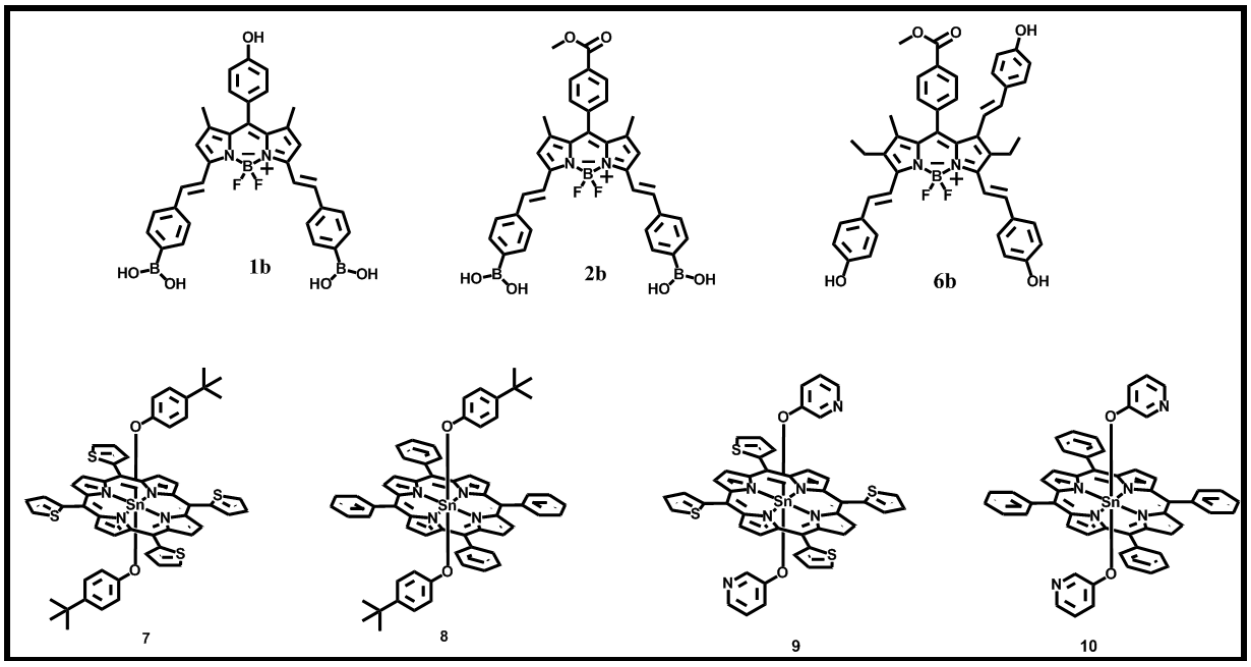

Figure 1.33: BODIPY dyes and porphyrins studied for optical limiting.

1.8. Summary of aims

The aims of this thesis were to:

1. Synthesise and characterise a series of BODIPY dyes with phenylboronic acid groups attached to styryls at the 3,5-positions.
2. Study their ability to detect glucose via electrochemical, fluorescence and colourimetric sensing.
3. Synthesise and characterise a series of *meso*-thienylporphyrins and a tristyryl BODIPY dye with hydroxyl substituted styryls at the 3,5,7-positions.
4. Study the nonlinear optical behaviour of both the BODIPY and porphyrin dyes.
5. Conduct molecular modelling to elucidate trends in the electronic structures and optical properties of all the dyes that were synthesised.

Publications

The results discussed in chapter 5 have recently been published in a peer reviewed journal [241].

N. Ndebele, J. Mack, and T. Nyokong, “A 3, 5 - DistyrylBODIPY Dye Functionalized with Boronic Acid Groups for Direct Electrochemical Glucose Sensing,” *Electroanalysis* **2019**, 31, 137-145.

Chapter 2

Experimental

2.1. Materials

Reagents were used without further purification unless otherwise noted.

2,4-Dimethylpyrrole was obtained from Achemo Chemicals. 4-Hydroxybenzaldehyde, 4-bromobenzaldehyde, 4-dimethylaminobenzaldehyde, 4-formylphenylboronic acid, methyl-4-formylbenzoate, 4-pyridinecarboxyaldehyde, trifluoroacetic acid (TFA), tetrachloro-1,4-benzoquinone (*p*-chloranil), triethylamine (TEA), 4-*tert*-butylphenol, 3-hydroxypyridine, tin(IV) chloride dihydrate, boron trifluoride diethyl etherate ($BF_3{\cdot}OEt_2$), piperidine, D-(+)-glucose (180.16 g/mol), sucrose (342.30 g/mol), deuterated chloroform and methanol, potassium hexacyanoferrate (II), potassium hexacyanoferrate (III), polystyrene (Mw 192.00 g/mol), tetrabutylammonium tetrafluoroborate ($TBABF_4$) and Rhodamine 6G were purchased from Sigma-Aldrich.

Acetic acid (glacial), petroleum ether, ethyl acetate, dichloromethane (CH_2Cl_2) and D-(−)-fructose (180.16 g/mol) were purchased from Merck. D-Lactose monohydrate (360.31 g/mol) was purchased from Meggle. Dimethylformamide (DMF) and dimethylsulfoxide (DMSO) were purchased repeatedly from various chemical enterprises. Sodium acetate anhydrous was purchased from Saarchem, while benzene, potassium chloride, glacial acetic acid (99%) and hydrochloric acid 32% (HCl) were purchased from Minema. Sodium hydroxide (NaOH) and sodium chloride (NaCl) were obtained from B&M Scientific. Sodium tetraborate-decahydrate ($NaB_4O_7{\cdot}10H_2O$), sodium phosphate dibasic (Na_2HPO_4) and potassium dihydrogen orthophosphate (KH_2PO_4) were obtained from Riedel-de Haen. Silica gel 60 was used to purify

the BODIPY dye products through column chromatography. Aqueous solutions were prepared with Millipore water from a Milli-Q-Water Systems (Millipore Corp., Bedford, MA, USA).

2.2. Instrumentation

I. Ultraviolet-visible (UV-vis) absorption spectroscopy

The UV-visible absorption spectra were obtained using a Shimadzu UV-2550 spectrophotometer at room temperature. The solution measurements were carried out in a 1 cm quartz cuvette cell, while the thin film measurements were measured with the film mounted on a glass slide.

II. Nuclear magnetic resonance (NMR) spectroscopy

The ^{1}H-NMR spectra were recorded on a Bruker AMX 600 NMR spectrometer in methanol-d_4 and chloroform-d_3 at room temperature.

III. Fluorescence emission spectroscopy

The fluorescence emission and excitation spectra were measured with a Varian Cary Eclipse fluorescence spectrophotometer in a fluorescent cell of 1 cm path length.

IV. Fluorescence lifetimes

Luminescence lifetimes were measured using a PicoQuant FluoTime 200 time-correlated single photon counting setup. A diode laser (LDH-P_670 with PDL 800-B, 670 nm, 20 MHz repetition rate, 44 ps pulse width, Picoquant GmbH) was utilised as the excitation source. Fluorescence was detected under the magic angle with a Peltier cooled photomultiplier tube (PMT) (PMA-C 192-N-M, Picoquant) and integrated electronics (PicoHarp 300E, Picoquant GmbH). A monochromator with a 4 nm spectral width was used to select the required emission wavelength. The response function of the system was measured using a scattering Ludox solution (DuPont), with a full width at half-maximum (FWHM) of ca. 300 ps. All luminescence decay curves were measured at the maximum of the emission peak and the lifetime data were obtained by deconvolution of the

decay curves using the FluoFit Software program (Pico Quant GmbH, Germany) [242]. **Figure 2.1** illustrates the instrumental setup.

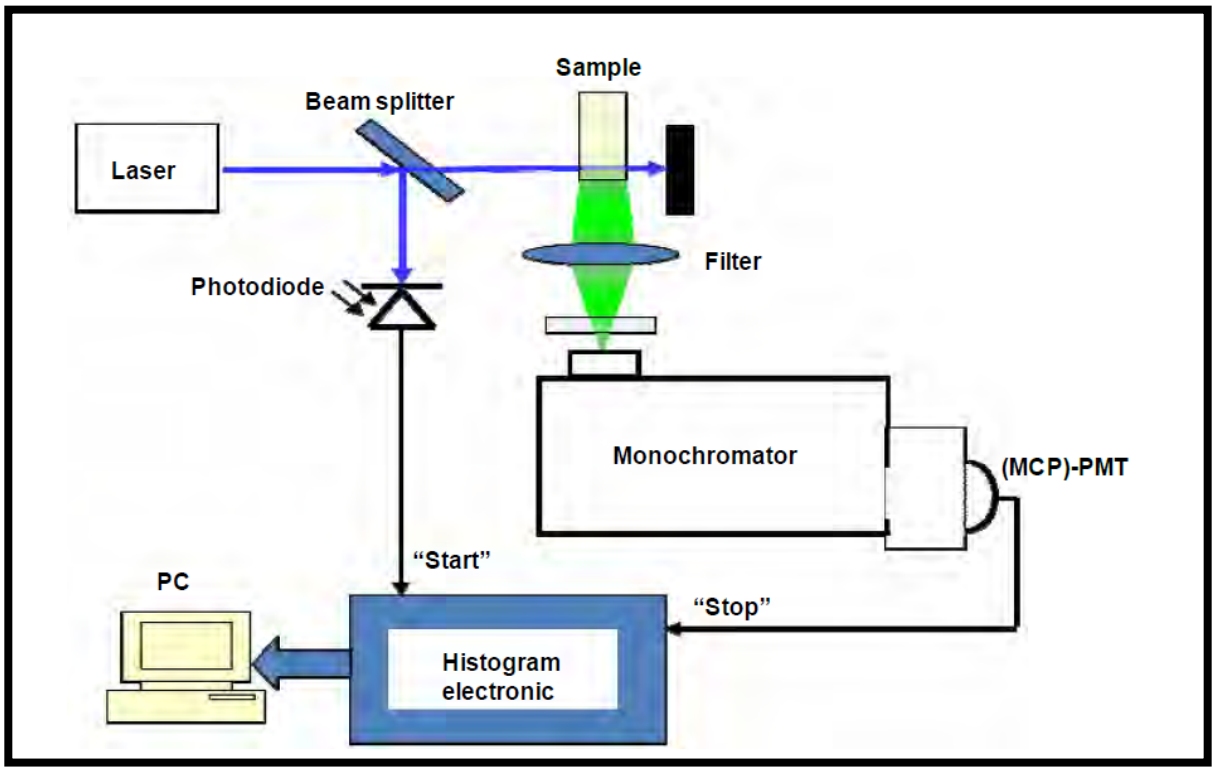

Figure 2.1: Schematic diagram of the time-correlated single photon counting (TCSPC) setup. (MCP)-PMT = Microchannel plate photomultiplier tube, and PC = Personal computer.

V. Mass spectrometry

The mass spectral data were measured using a Bruker AutoFLEX III Smart Beam TOF/TOF mass spectrometer. The instrument was operated in a positive ion mode over an m/z range from 500–3000 amu. The voltages of ion sources 1 and 2 were set at 19.0 and 16.7 kV, respectively. The lens was set at 8.50 kV. The reflector 1 and 2 voltages were set at 21 and 9.7 kV, respectively. α-

Cyano-4-hydroxycinnamic acid was used as the MALDI matrix, and a 355 nm Nd:YAG laser was used as the ionising source.

VI. Fourier-Transform Infrared (FT-IR) spectroscopy

Infrared spectra were recorded using a Perkin Elmer Spectrum 100 FT-IR spectrometer.

VII. Time-dependent density function theory (TD-DFT) Calculations

The Gaussian 09 software package running on the Lengau cluster based in the Centre for High-Performance Computing in Cape Town was used for the TD-DFT calculations. The geometry optimisations were carried out at the B3LYP/6-31G(d) level of theory. The TD-DFT calculations were carried out by using the CAM-B3LYP functional with 6-31G(d) basis set. Avogadro was used to generate molecular orbital images [243].

VIII. Scanning electron microscopy (SEM)

The thickness and morphology of the thin films were determined with SEM images from a TESCAN Vega TS 5136LM instrument.

IX. Z-scan experiments

All Z-scan analyses were performed with frequency-doubled Nd:YAG lasers (Quanta-Ray, 1.5 J/ 7 and 10 ns FWHM pulse duration) as the source of excitation. The laser was operated in a near Gaussian transverse mode at 532 nm (second harmonic), with 10 ns pulses and a repetition rate of 10 Hz and an energy range of 0.1 μJ–0.1 mJ, limited by the energy detectors (Coherent J5-09). The low repetition rate of the laser prevents cumulative thermal nonlinearities. The beam was spatially filtered to remove the higher order modes and tightly focused with a 15 cm focal length

lens. No damage was detected between runs after the samples were moved or replaced. The Z-scan data in solution were obtained using a 2 mm quartz cuvette. The Z-scan instrumental setup is illustrated in **Figure 2.2**

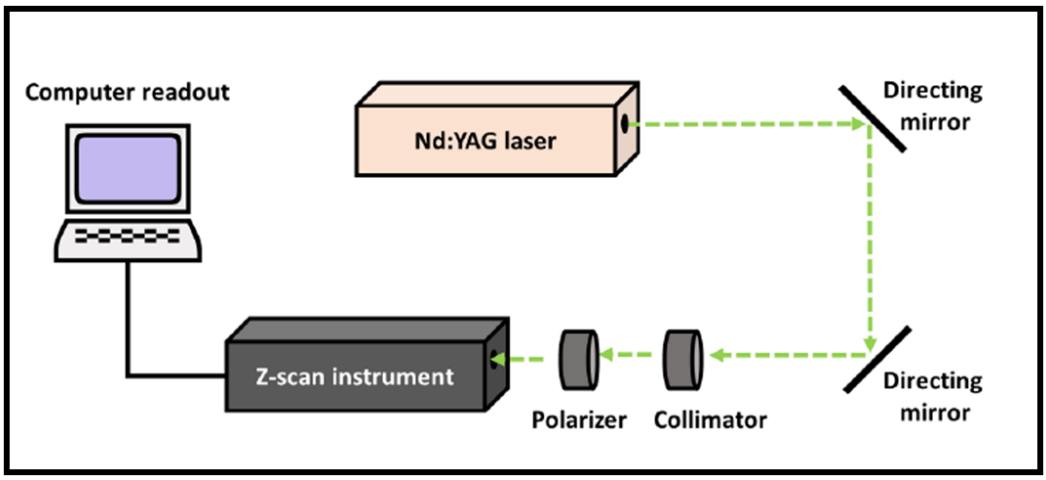

Figure 2.2: The Z-scan instrumental laser setup.

X. Electrochemistry

All electrochemical experiments (cyclic voltammetry, dispersive pulse voltammetry and chronoamperometry) were performed by using an Autolab Potentiostat PGSTAT 302 electrochemical workstation (Eco Chemie, Utrecht, The Netherlands) driven by the general-purpose electrochemical system data processing software (GPES, software version 4.9). A three-electrode electrochemical cell comprising a glassy carbon electrode (GCE, geometric area = 0.071 cm^2) as the working electrode, a platinum wire counter electrode and an Ag|AgCl and 3 M KCl reference electrode, was used. The GCE surfaces were polished on a Buehler-felt pad with alumina (10; 1; 0.3; 0.05 |μm). For all electrodes, following the polishing step, sonication was carried out for 5 min in Millipore water to remove any impurities.

XI. Scanning electrochemical microscopy (SECM)

Scanning electrochemical microscopy (SECM) experiments were carried out with a Uniscan Model 370 instrument that had a 10 µm Pt microelectrode (Uniscan) as the tip. SECM approach curves were obtained using the Pt microelectrode with a Pt counter electrode and Ag|AgCl wire as the pseudo-reference electrode. Measurements were obtained by monitoring changes in the steady-state current of $K_3[Fe(CN)_6]$ oxidation at −0.1 V *vs* Ag|AgCl as the tip travels. Glassy carbon plates (Goodfellow, UK) of 1 × 1 cm and 2 mm thickness were also used as substrates for SECM (**Figure 2.3**).

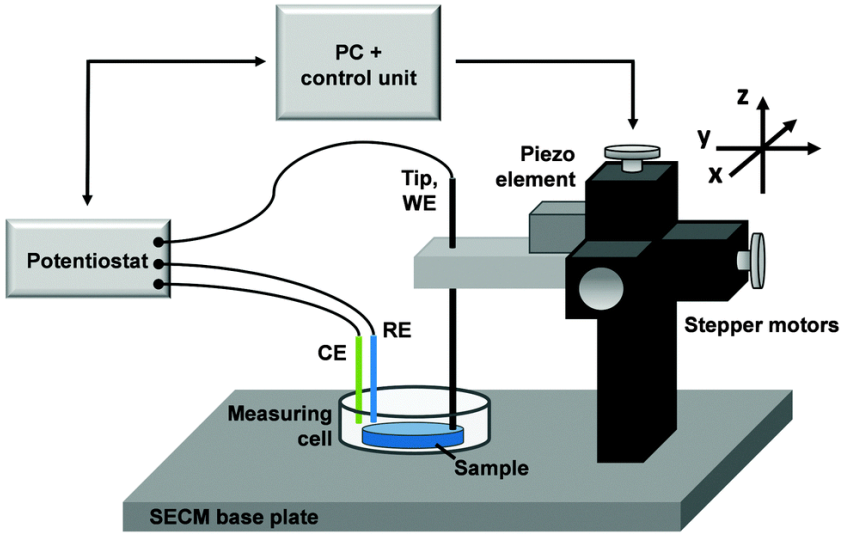

Figure 2.3: Schematic diagram of the SECM setup [181]. WE = Working electrode, RE = Reference electrode, CE = Counter electrode, x,y = the horizontal directions of the positioning system attached to the UME and z = the vertical direction of the positioning system attached to the UME.

2.3. Synthesis and Characterisation of BODIPY dyes and porphyrins

*2.3.1. Synthesis of BODIPY core series **a***

BODIPY dye **1-5a** were prepared by using a method described by Loudet and Burgess [2] with minor modifications (**Scheme 2.1**). All of these dyes have been reported previously [2, 29, 244]

A mixture of 2,4-dimethylpyrrole (1.248 g, 13.50 mmol) and the appropriate benzaldehyde (6.749 mmol) was dissolved in dry DCM (40 ml) under argon. TFA (0.4 ml) was added to the mixture and stirred at room temperature. The consumption of the aldehyde was monitored by TLC. When the aldehyde was consumed, a solution of *p*-chloranil (4.125 g, 8.099 mmol) in dry DCM was added at 0°C with a syringe and stirred for 30 min at room temperature. TEA (1.284 g, 40.50 mmol) was added at 0°C and stirred for a further 30 min. Thereafter $BF_3{\cdot}OEt_2$ (9.580 g, 67.49 mmol) was added dropwise, and the reaction was stirred for 12 h at room temperature. The mixture was washed with water and eluted with DCM. The solvent was dried on a rotary evaporator. The residue was purified via silica column chromatography with 4:1 petroleum ether, ethyl acetate as the eluent to yield the pure orange crystalline solid compound **(Figure 2.4)**.

Figure 2.4: BODIPY core crystals

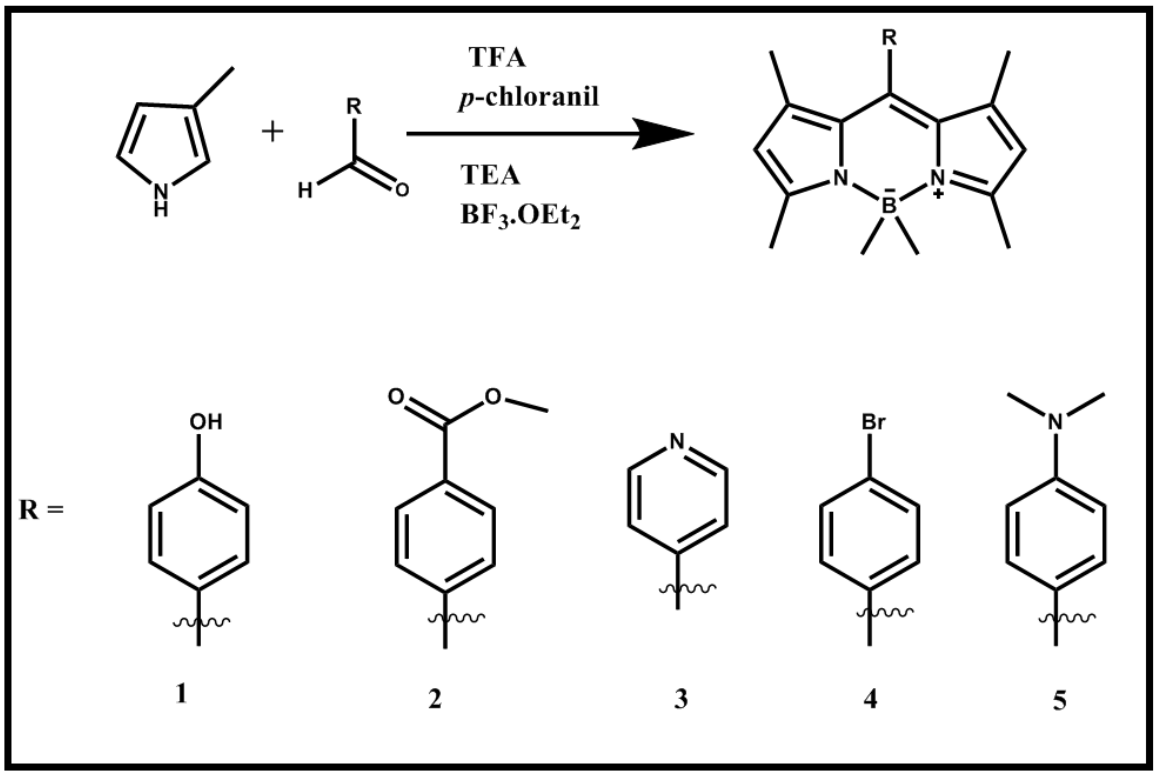

Scheme 2.1: Synthesis of BODIPY dye **1-5a**. TFA = trifluoracetic acid, DCM = dichloromethane, *p*-chloranil = tetrachloro-1,4-benzoquinone and $BF_3{\cdot}OEt_2$ = boron trifluoride diethyl etherate.

1a: Yield: 59%. ^{1}H NMR (600 MHz, $CDCl_3$) δ 7.17–7.14 (m, 2H), 6.99–6.96 (m, 2H), 6.00 (s, 2H), 5.20–5.05 (m, 1H), 2.57 (s, 6H), 1.46 (s, 6H). FT-IR (ν_{max}/cm^{-1}): OH stretch (3550–3000), aromatic C-H (2930–2790) and aliphatic C-H (1470).

2a: Yield: 42%. ^{1}H NMR (600 MHz, $CDCl_3$) δ 8.20 (s, 2H), 7.42 (s, 2H), 6.01 (s, 2H), 4.00 (s, 3H), 2.58 (s, 6H), 1.38 (s, 6H). FT-IR (ν_{max}/cm^{-1}): C=O (1742), O-C (1042), aromatic C-H (2930–2790) and aliphatic C-H (1480).

3a: Yield: 55%. ^{1}H NMR (600 MHz, $CDCl_3$) δ 8.82 (s, 2H), 7.34 (d, *J* = 5.8 Hz, 2H), 6.03 (s, 2H), 2.59 (s, 6H), 1.43 (s, 6H). FT-IR: (ν_{max}/cm^{-1}): aromatic C-H (2930) and aliphatic (1470).

4a: Yield: 52%. ^{1}H NMR (600 MHz, $CDCl_3$) δ 7.67 (d, *J* = 8.3 Hz, 2H), 7.20 (d, *J* = 8.3 Hz, 2H), 6.02 (s, 2H), 2.58 (s, 6H), 1.48–1.39 (s, 6H). FT-IR (ν_{max}/cm^{-1}): aromatic C-H (2930–2790) and aliphatic (1550).

5a: Yield: 41%. ^{1}H NMR (600 MHz, $CDCl_3$) δ 7.08 (d, *J* = 8.7 Hz, 2H), 6.79 (d, *J* = 8.6 Hz, 2H), 5.99 (s, 2H), 3.04 (s, 6H), 2.57 (s, 6H), 1.50 (s, 6H). FT-IR (ν_{max}/cm^{-1}): aromatic C-H (2930–2970) and aliphatic C-H (1550).

*2.3.2. Synthesis of styrylated BODIPY series **b***

The boronic-acid-functionalised dyes **1-5b** were synthesised by following a modified version (**Scheme 2.2**) of the Knoevenagel condensation method [2, 24].

4-Formylphenylboronic acid (0.4 g, 2.668 mmol), and glacial acetic acid (1 ml) and piperidine (1.5 ml) were added to a solution of BODIPY **1-5a** (0.8892 mmol) in dry C_6H_6 (50 ml) in a round bottom flask fitted with a Dean-Stark trap. The reaction mixture was heated with constant stirring. The consumption of the BODIPY was monitored by TLC and UV-visible absorption spectroscopy. The resultant product was washed with water and eluted with ethyl acetate, and the solvent was evaporated on a rotary evaporator. The residue was purified by silica column chromatography yielding blue dyes **1-5b**.

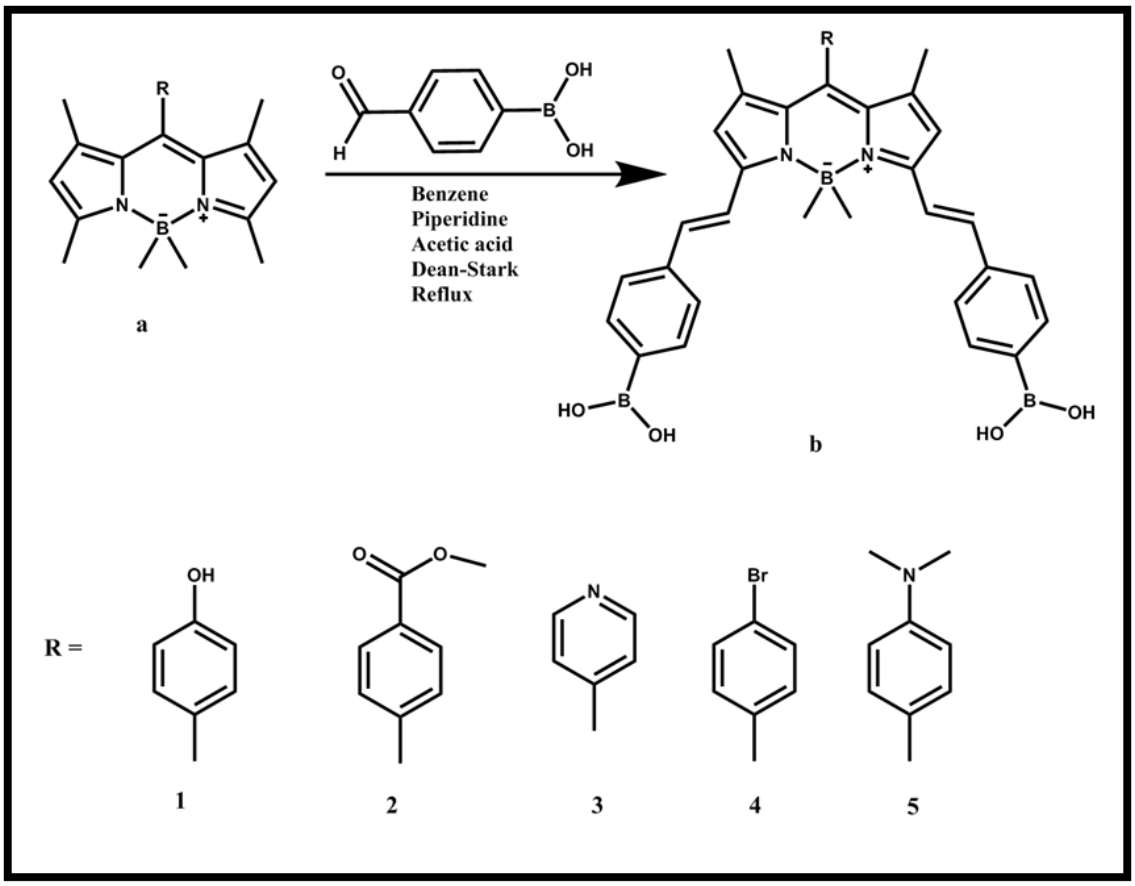

Scheme 2.2: Synthesis of styrylated BODIPYs **1-5b**.

1b: Yield: 44%. ^{1}H NMR (600 MHz, methanol-d_4) δ 8.24 (s, 2H), 7.75–7.65 (m, 2H), 7.57–7.45 (m, 4H), 7.19 (s, 4H), 7.00 (s, 2H), 6.83 (s, 2H), 6.73 (s, 2H), 2.07 (s, 6H). FT-IR (ν_{max}/cm^{-1}): OH (3500–3000), aromatic C-H (2930–2790) and aliphatic C-H (1470). MALDI TOF-MS calc. 604.23 amu; Found 602.8 m/z.

2b: Yield: 40%. ^{1}H NMR (600 MHz, methanol-d_4) δ 8.22 (s, 2H), 7.71 (s, 4H), 7.65–7.58 (m, 4H), 7.56- 7.51 (m, 4H), 7.19 (s, 2H), 6.86 (s, 2H), 3.39 (s, 3H), 2.10 (s, 6H). FT-IR (ν_{max}/cm^{-1}): OH (3500–3000), aromatic C-H (2930–2790), aliphatic C-H (1477), C=O (1740) and C-O (19040). MALDI TOF-MS calc. 646.24 amu; Found 645. 21 m/z.

3b: Yield: 52%. ^{1}H NMR (600 MHz, methanol-d_4) δ 8.22 (s, 2H), 7.78–7.66 (m, 2H), 7.56–7.43 (m, 4H), 7.24 (s, 4H), 7.02 (s, 2H), 6.80 (s, 2H), 6.70 (s, 2H), 2.07 (s, 6H). FT-IR (ν_{max}/cm^{-1}): OH (3500–3000), aromatic C-H (2930–2790) and aliphatic C-H (1470). MALDI TOF-MS calc. 589.23 amu; Found 590.2 m/z.

4b: Yield: 42%. ^{1}H NMR (600 MHz, methanol-d_4) δ 8.10–8.01 (m, 2H), 7.94 (s, 2H), 7.78 (s, 4H), 7.69–7.61 (m, 2H), 7.49 (s, 4H), 7.28 (s, 2H), 7.04–6.73 (m, 2H), 2.10–2.04 (m, 6H). FT-IR (ν_{max}/cm^{-1}): OH (3500–3000), aromatic C-H (2930–2790) and aliphatic C-H (1550). MALDI TOF-MS calc. 666.15 amu; Found 666.54 m/z.

5b: Yield: 55%. ^{1}H NMR (600 MHz, methanol-d_4) δ 8.10–8.01 (m, 2H), 7.94 (s, 2H), 7.78 (s, 4H), 7.69–7.61 (m, 2H), 7.49 (s, 4H), 7.28 (s, 2H), 7.04–6.73 (s, 2H), 3.33 (s, 6H), 2.18 (s, 6H). FT-IR (ν_{max}/cm^{-1}): OH (3500–3000), aromatic C–H (2930–2790) and aliphatic C–H (1550). MALDI TOF-MS calc. 631.28 amu; Found 631.88 m/z.

*2.3.3. Synthesis of BODIPY **6***

BODIPY **6** was synthesised using the same procedure used to prepare BODIPYs **1-5b**. However, the only noteworthy change was the use of a 3-ethyl-2,4-dimethylpyrrole and not the 2,4-dimethylpyrrole that was used in the synthesis of the other dyes. **Scheme 2.3** illustrates the synthetic route followed when synthesising BODIPY **6**

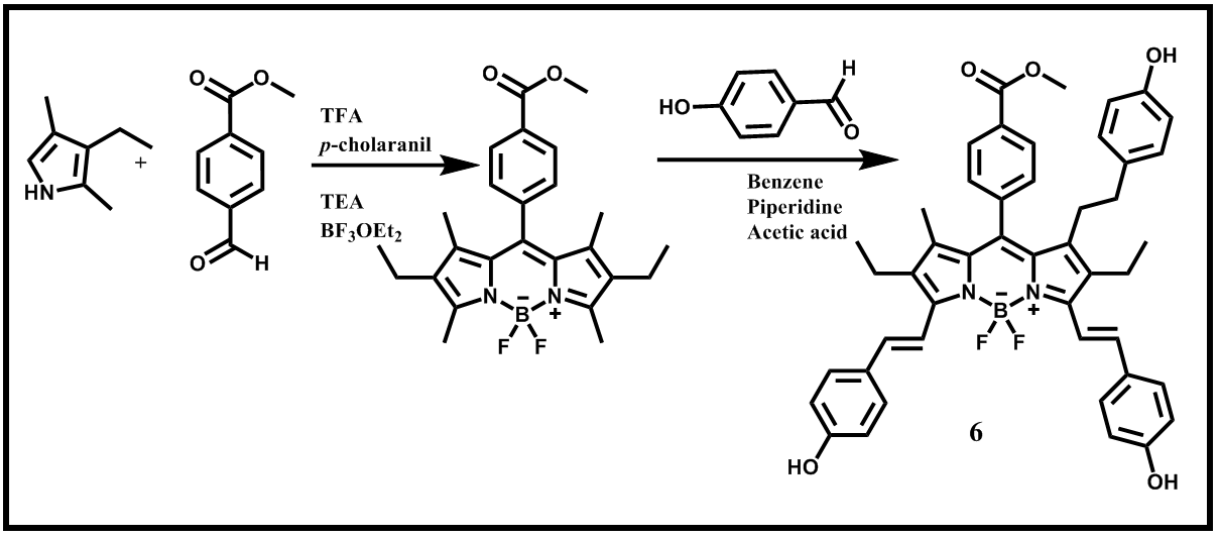

Scheme 2.3: Synthetic route used to synthesise BODIPY **6**.

6: ^{1}H NMR (600 MHz, methanol-d_4) δ 8.30–8.16 (m, 2H), 8.07 (s, 1H), 7.75–7.61 (m, 4H), 7.57 (s, 2H), 7.48 (s, 2H), 7.35 (s, 4H), 7.06 (s, 1H), 6.99 (s, 1H), 6.96 (s, 2H), 6.93 (s, 1H), 6.84 (s, 1H), 6.81 (s, 1H), 3.98 (s, 3H), 2.68 (s, 4H), 1.43 (s, 3H), 1.19–1.15 (m, 6H) ppm. MALDI TOF-MS calc. 750.31 amu; Found 750.77 m/z.

2.3.4. Synthesis of porphyrins 7 and 8

Free base porphyrins were synthesised following a modified synthetic procedure reported [245].

Scheme 2.4.

A mixture of 5 mmol of the appropriate aldehyde and freshly distilled pyrrole (5 mmol, 0.35 mL) was dissolved in propionic acid (200 mL) and refluxed for 5 h. Thereafter, the reaction mixture was cooled, filtered and washed with cold methanol. The products obtained were purified by silica column chromatography yielding green crystals. The free base porphyrins were then

metallated with Sn(IV) ions without further characterization by using a previously reported method [245, 246].

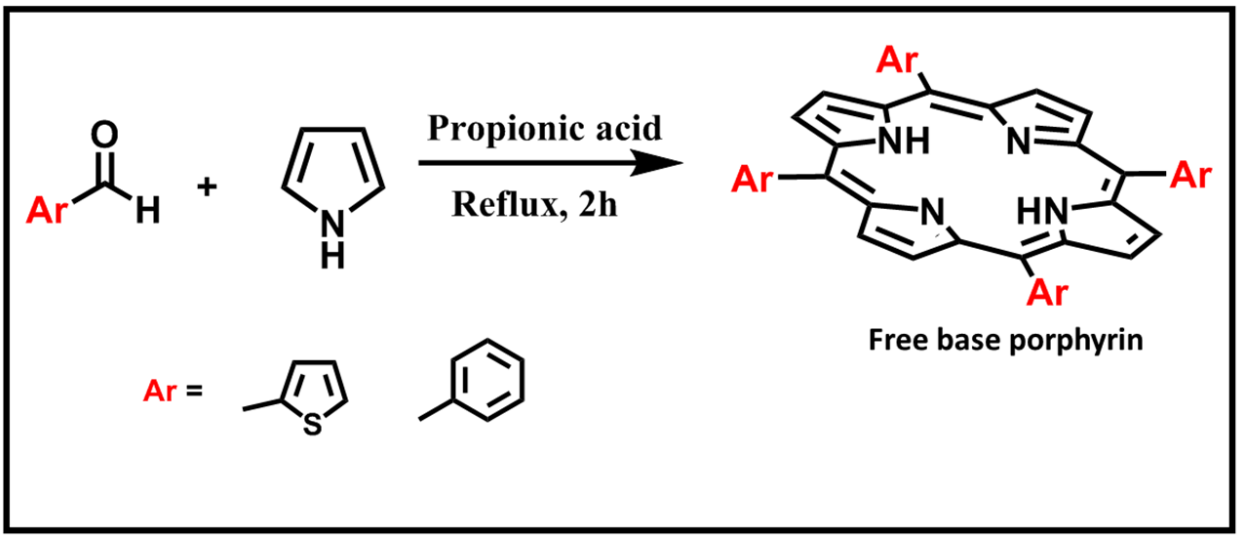

Scheme 2.4: Synthesis of free base **7** and **8** porphyrins.

A mixture of the appropriate free base porphyrin (5 mmol) and $SnCl_2 \cdot 2H_20$ (2 mmol, 0.45g) was dissolved in dry pyridine (50 mL) and refluxed for 12 h. The reaction mixture was cooled, and an ammonia solution (20 mL) was slowly added to the mixture and refluxed for another hour. The reaction mixture was then cooled, and 100 mL of water was added. A green precipitate was formed for **7**, while a purple precipitate was obtained for **8**. The precipitates were washed and filtered with water. The filter cake was dissolved in chloroform and dried to provide the free base porphyrins. Axial ligands were then added to the porphyrins by using the following method (**Scheme 2.5**):

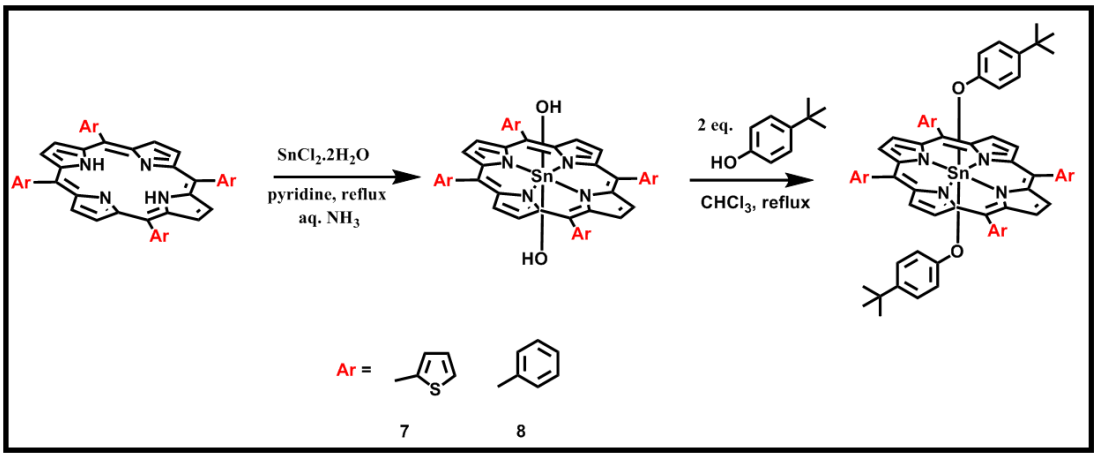

Scheme 2.5: Synthetic route followed for the metalation and the addition of axial ligands of porphyrins **7** and **8**.

1 equiv. of the appropriate porphyrin was dissolved in a minimal volume of dry chloroform, and an excess of 4-(*tert*-butyl)phenol was added. The mixture was refluxed for 4 h, and the completion of the reaction was monitored by UV-visible absorption spectroscopy by following the red-shift of the B band. The solvent was evaporated, and the resulting residue was purified on a neutral alumina column by using 9:1 chloroform/methanol (v/v) as the eluent to give the target compounds **7** and **8** as green and purple solids, respectively.

7: Yield: 68%. ^{1}H NMR (600 MHz, $CDCl_3$) δ 9.22 (s, 8H), 8.00–7.89 (m, 8H), 7.55–7.52 (m, 4H), 5.65 (d, J = 8.5 Hz, 4H), 1.83 (d, J = 8.5 Hz, 4H), 1.26 (s, 18H). MALDI TOF-MS: calc. for M−L 905.06 amu; found 906.10 m/z.

8: Yield: 74%. ^{1}H NMR (600 MHz, $CDCl_3$) δ 9.00 (s, 8H), 8.06–8.04 (m, 8H), 7.76 (d, J = 7.7 Hz, 12H), 5.65 (d, J = 8.6 Hz, 4H), 1.89 (d, J = 8.6 Hz, 4H), 1.29 (s, 18H). MALDI TOF-MS: calc. for M−L 881.23 amu; found 882.24 m/z.

Porphyrins **9** and **10** were synthesised and characterised as reported previously by Babu *et al.* [229].

9: ^{1}H NMR ($CDCl_3$, 600 MHz): δ 2.20 (2H, d), 3.25 (2H, d), 5.62 (2H, m), 7.06 (2H, d), 7.56 (4H, m), 7.95 (8H, d), 9.31 (8H, s). MS (MALDI-TOF): calc. for $[M\text{-}3PyO]^+$ 849.99 amu; found 850.27 m/z. $[M\text{-}(3PyO)_2]^+$ 755.96 amu; found 756.19 m/z.

10: ^{1}H NMR ($CDCl_3$, 600 MHz): δ 2.20 (2H, d), 3.24 (2H, d), 5.61 (2H, m), 7.03 (2H, d), 7.82 (12H, m), 8.21 (8H, d), 9.16 (8H, s). MS (MALDI-TOF): calc. for $[M]^+$ 920.19 amu; found 920.72 m/z.

2.4. Preparation of thin films

Polystyrene (200 mg) was dispersed in chloroform (4 ml) and sonicated for 30 min. Thereafter BODIPY dyes **1b, 2b** and **6** (0.00497 mmol) in chloroform (1 ml) were each added to a polystyrene solution and the three solutions were stirred for 24 h. The homogenous mixtures were coated on thin glass slides by using the drop-dry method (**Figure 2.5**). The resultant thin films were air dried to remove the solvent. The average thickness of the thin films was determined by scanning electron microscopy to be ca. 12.5, 13 and 15 µm for dyes **1b**, **2b** and **6b**, respectively.

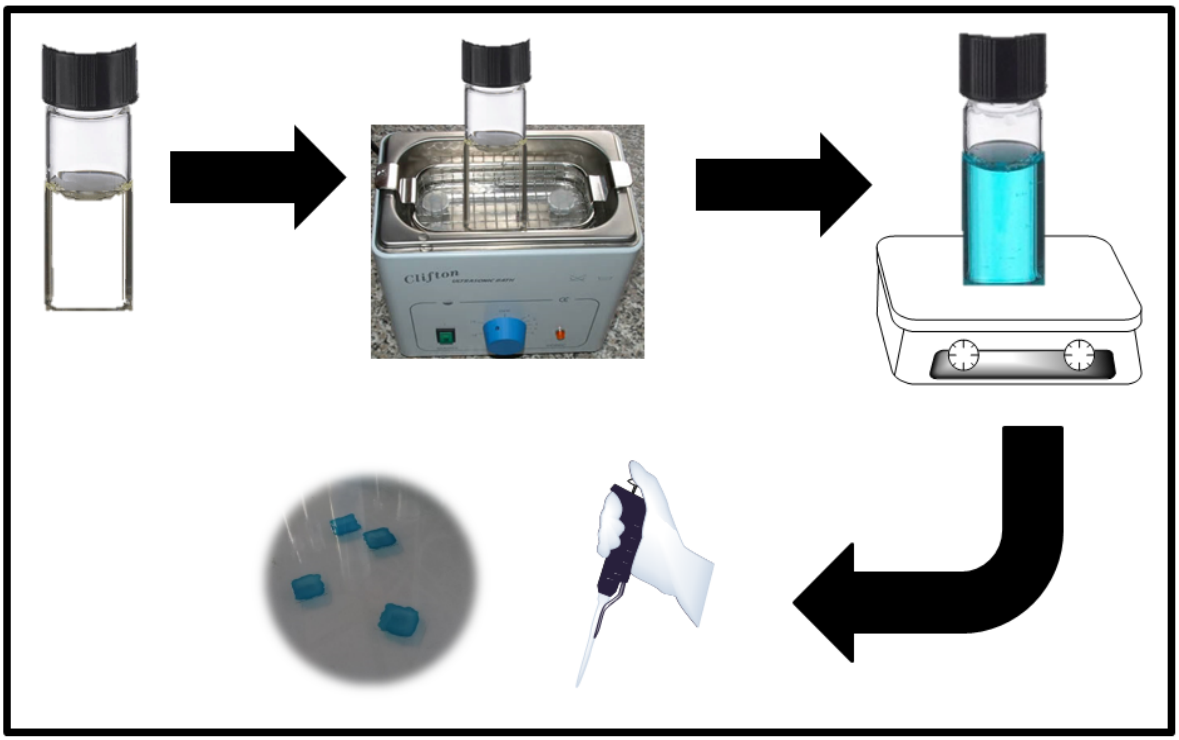

Figure 2.5: Preparation of the polymer thin films for NLO studies.

2.5. Modifying the working electrode surface

The working electrode surface used in the glucose sensing studies was modified by using the drop dry method [247].

A glassy carbon electrode (GCE) was used as the working electrode. The electrode surface was polished on a Buehler-felt pad using alumina (0.05 µm), then rinsed with Millipore water to remove any impurities, and dried at 60°C. 1 µL of the 1 mg/1mL (DMF) solutions of **1b** and **2b** were separately dropped onto the polished electrode surfaces and the modified electrodes were then dried in an oven at 60°C for 5 min and allowed to cool at room temperature before use. The electrode is described throughout as GCE-**1b** and GCE-**2b**.

2.6. Theoretical calculations

The DFT method was used to carry out geometry optimisations for BODIPYs **1a, 1b, 2a, 2b, 3a, 3b, 4a, 4b, 5a, 5b, 6** and the corresponding BODIPY core (**6-core**) as well as for porphyrins **7-10** and the two free base tetraphenyl- (**H_2TPP**) and tetrathienyl- (**H_2TTP**) porphyrins used to synthesise **7-10**. Where appropriate methyl groups replace *tert*-butyls in the structures to simplify the calculations. The molecular modelling was conducted using the B3LYP functional of the Gaussian 09 program package with 6-31G(d) basis sets [248]. A similar approach was used to calculate electronic absorption spectra by using the TD-DFT method with the CAM-B3LYP functional, which includes a long-range correction of the exchange potential and incorporates an increasing fraction of Hartree-Fock exchange as the interelectronic separation increases [249].

Chapter 3

Synthesis and characterisation

This chapter reports on the synthesis and characterisation of the series of BODIPY dyes and porphyrins synthesised for the various applications investigated in this study. The dyes were characterised by using ^{1}H-NMR, UV-Visible absorption spectroscopy, fluorescence emission and FT-IR spectroscopy, and MALDI-TOF mass spectrometry.

3.1. Synthesis

3.1.1. Synthesis of BODIPY cores

BODIPY dyes **1-5a** have been reported previously [2, 29, 244] and differ from each other only at the *meso*-positions. These dyes were synthesised using an acid-catalysed one-pot, three-step method with commercially available 2,4-dimethylpyrrole and appropriate aldehyde derivatives by using dry DCM as a solvent [1, 45]. The reaction was carried out under inert argon at room temperature. TFA was used as the Lewis acid catalyst. Protonation of the carbonyl oxygen results in a partial positive charge, so the pyrrole unit can easily undergo nucleophilic substitution. This yielded the dipyrromethane intermediates. The methyl groups on the pyrrole are important for this study, since they block the 2,4-position carbons from reacting and polymerising, thus improving the yields obtained. The same principles were followed when synthesising **6**. However, a 3-ethyl-2,4-dimethyl pyrrole was used as the pyrrole precursor.

Dipyrromethanes are highly unstable and are therefore immediately oxidised with *p*-chloranil to form relatively stable dipyrromethenes. The third step in the BODIPY core dye synthesis involves the complexation of the dipyrromethene with BF_2 under basic conditions, by using excess $BF_3{\cdot}OEt_2$. Target compounds **1-5a** were purified by silica gel chromatography.

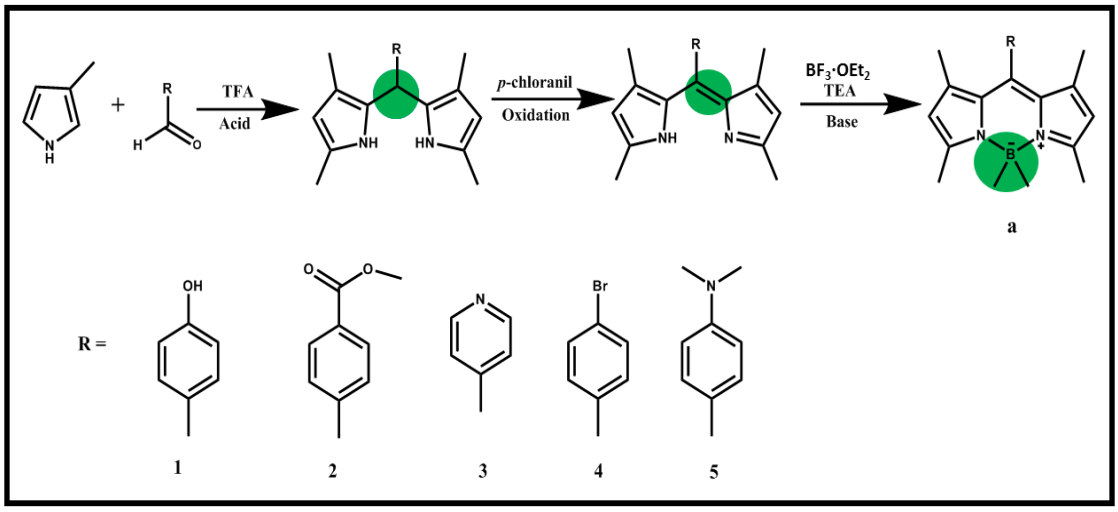

Scheme 3.1: Acid-catalysed condensation synthesis of BODIPY cores **1-5a**. The green circles highlight the changes that occur upon every step in the reaction.

3.1.2. Synthesis of styrylated BODIPY dyes

The **1-5a** series of BODIPY dyes were structurally modified through further reactions to make the dyes suitable for use in various applications. The **1-5b** series of dyes were synthesised using a modified Knoevenagel condensation reaction method which involves the condensation of the aldehyde derivative (phenylboronic acid for **1-5** and phenylhydroxyl for **6**) with the active 3,5-position or 1,3,5-position methyl carbons. The addition of the reactive aldehyde derivatives enables the main spectral bands to be shifted to longer wavelengths and extends the π-conjugation system of the dye.

3.1.3. Synthesis of Porphyrins

Porphyrins **7-10** were synthesised by treating the appropriate free base porphyrins with $SnCl_2 \cdot H_2O$, to insert Sn (IV) into the central cavity. The porphyrins were further modified through

the addition of axial ligands by hydrolysing the *trans*-dihydroxyl axial ligands in *tert*-butylphenol (**7** and **8**) or pyridine (**9** and **10**) in the presence of excess ammonia.

3.2. Characterisation

3.2.1. Structural analysis

In addition to the meticulous use of optical spectroscopy and thin layer chromatography to confirm the presence and absence of spectral bands in well-separated column chromatography fractions that are consistent with the major transitions of different types of BODIPY structure, the synthesised dyes were also characterised by ^{1}H-NMR spectroscopy. This technique is used to confirm that the observed spectrum is consistent with the structure of the target dye based on the observed chemical shifts and integrated number of proton signals for each peak. FT-IR spectroscopy was used to confirm the presence of various functional groups in the dye structures, and MALDI-TOF mass spectroscopy was used to confirm the molecular weights.

*3.2.1.1 Structural analysis of BODIPY **1a** and **1b***

BODIPY **1a** has 19 protons in total, all of which were identified in the ^{1}H-NMR spectrum (**Figure 3.1**). A singlet observed at 1.46 ppm integrated to six protons and was attributed to the 3,5-position methyl groups, while a similar singlet at 2.57 ppm can be attributed to the 1,7-position methyls. The 3,5-position protons lie upfield due to being shielded by the pyrrolic nitrogen atoms. The four protons in the *meso*-aryl rings are observed as two doublets at 7.14 and 6.98 ppm. The two protons at the 2,6-positions of the core are observed as a singlet at 6.00 ppm. The BODIPY dye has a hydroxyl group on the *meso*-aryl ring that lies at 5.12 ppm. The spectrum was run in $CDCl_3$, so the solvent residual peak was observed at 7.28 ppm, while the H_2O peak lies at 1.63 ppm.

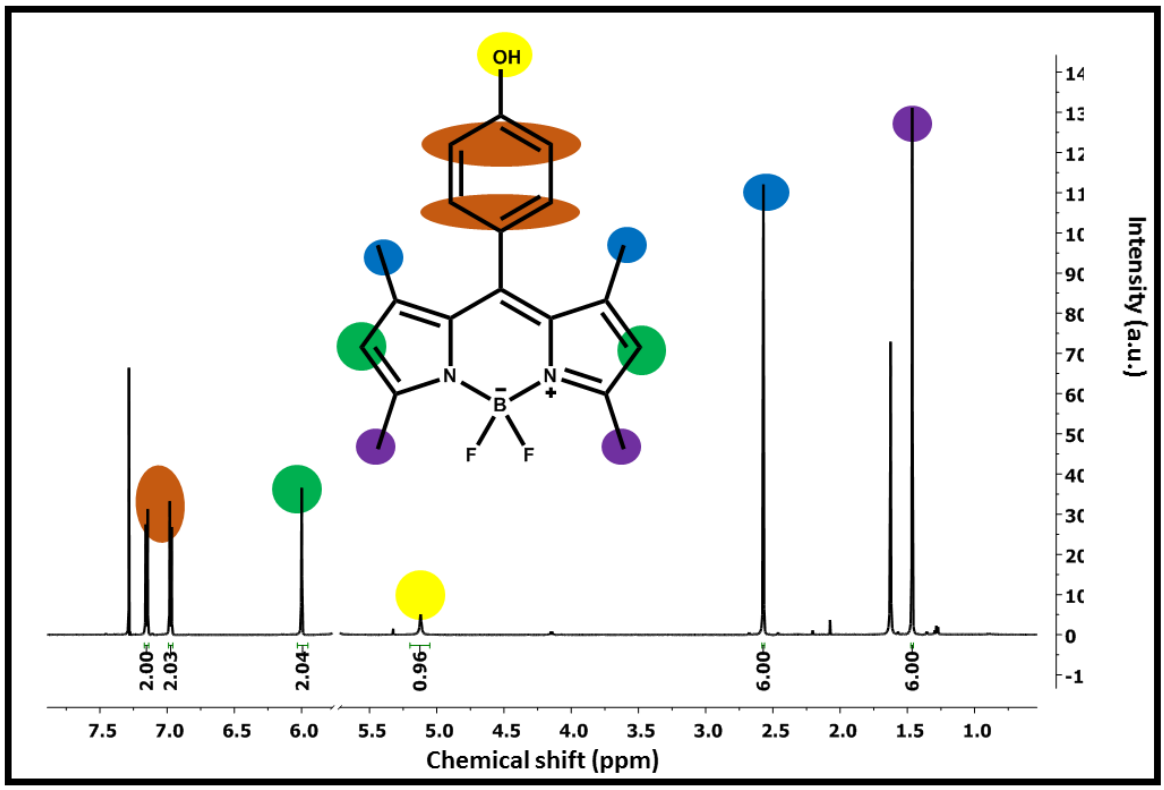

Figure 3.1: ^{1}H-NMR spectra of BODIPY **1a** in $CDCl_3$.

BODIPY **1b**, which was prepared from **1a**, has twenty-nine protons. However, only twenty-four of those protons can be identified using ^{1}H-NMR spectroscopy, since hydroxyl groups are subject to solvent exchange when methanol-d_4 is used. The use of this solvent was required for solubility reasons. Six protons were observed as a singlet at 2.07 ppm which were attributed to the 1,7-position methyls of the core structure, in a similar manner to the ^{1}H-NMR spectrum of **1a**. A singlet integrating to two protons was observed at 6.73 ppm, which was attributed to the protons at the 2,6-positions of the core structure shifted downfield due to the presence of the styryls at the 3,5-positions. Two sets of singlets each integrating to two protons at 6.83 and 7.00 ppm can be attributed to the styryl ethenes. A complex series of multiplets and singlets were observed

between 8.24–7.19 ppm integrating to a total of twelve protons, which were attributed to the protons on the three aromatic phenyl rings.

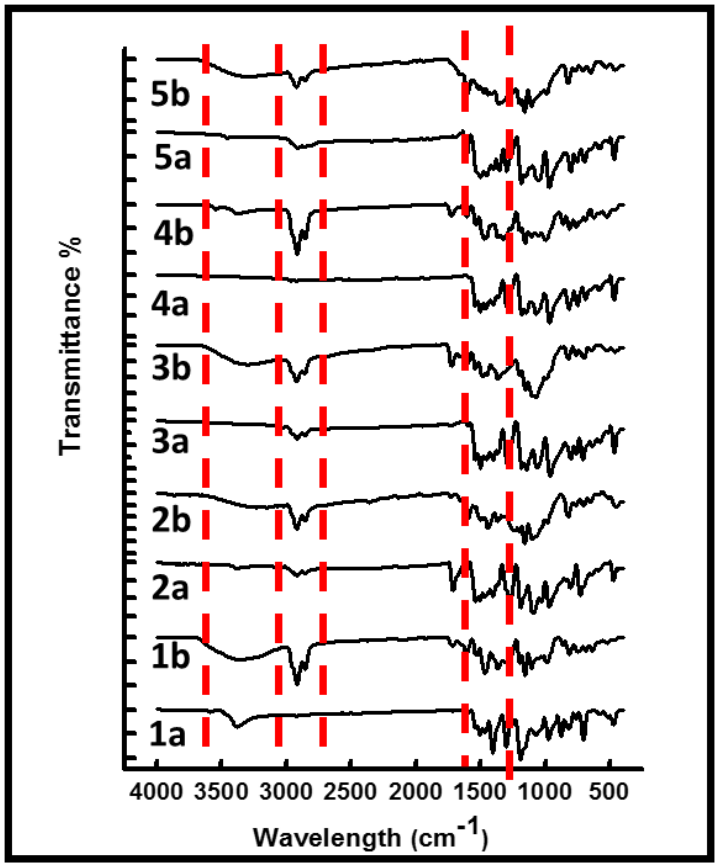

Figure 3.2: FT-IR spectra of BODIPY dyes **1-5(a**,**b**). Pairs of dashed red lines highlight from left to right, the OH-stretches, the aromatic C-H stretches, and the aliphatic C-H stretches, respectively.

The FT-IR analysis spectra of BODIPY dye **1a** and **1b** (**Figure 3.2**) further confirmed the structures of both dyes as the characteristic vibrations and peaks were observed. The OH stretch attributed to the hydroxyl group of the *meso*-aryl rings of both dyes and the four other hydroxyls in the boronic acid moieties of **1b** lie between 3550–3000 cm^{-1}. A broader and relatively more intense band is observed in the spectrum of **1b** (**Figure 3.2**) as would be anticipated due to the presence

of five hydroxyls in this structure. The aromatic C-H stretch is observed between 2930–2790 cm^{-1}, while the aliphatic C-H stretch lies at 1470 cm^{-1}. The molecular mass BODIPY of **1b** was calculated to be 604.23 amu. MALDI-TOF mass spectrometry analysis confirmed that a parent peak was observed at 602.8 m/z.

*3.2.1.2. Structural analysis of BODIPY **2a** and **2b***

^{1}H-NMR (**Figure 3.3**) confirmed the presence of all 21 protons of BODIPY **2a**. Two doublets at 8.20 and 7.40 ppm were again attributed to the *meso*-aryl ring, while a singlet integrating to two protons at 6.01 ppm can be attributed to the 2,6-position protons, and six proton singlets at 2.58 and 1.38 ppm were attributed to the methyl groups on the pyrrole at the 1,3,5,7-positions. The peak for the methyl group of the ester aldehyde at the *meso*-position lies at 4.00 ppm. BODIPY **2b**, which was prepared from **2a**, has thirty-one protons in total, but only twenty-seven protons could be identified due to the use of methanol-d_4. Singlets for the six protons from the 1,7-position methyls, the three protons of the ester methyl and the 2,6-position protons of the core can again be readily identified at 2.10, 3.98 and 6.71 ppm, along with singlets integrating to two protons each at 6.86 and 7.19 ppm which are attributed to the styryl ethenes. Signals totalling to twelve protons that lie between 7.71–7.58 ppm are again attributed to the protons of the three phenyl rings.

The FT-IR spectrum of **2b** (**Figure 3.2**) contains the anticipated hydroxyl stretch after **2a** is styrylated. A C=O stretch is observed at 1742 cm^{-1}, along with an O–C stretch at 1042 cm^{-1}, that can be attributed to the phenylacetyl moiety on the *meso*-aryl rings in the spectra for both dyes.

The molecular mass of **2b** was calculated to be 644.07 amu. MALDI-TOF MS confirmed the presence of a parent peak at 645.21 m/z.

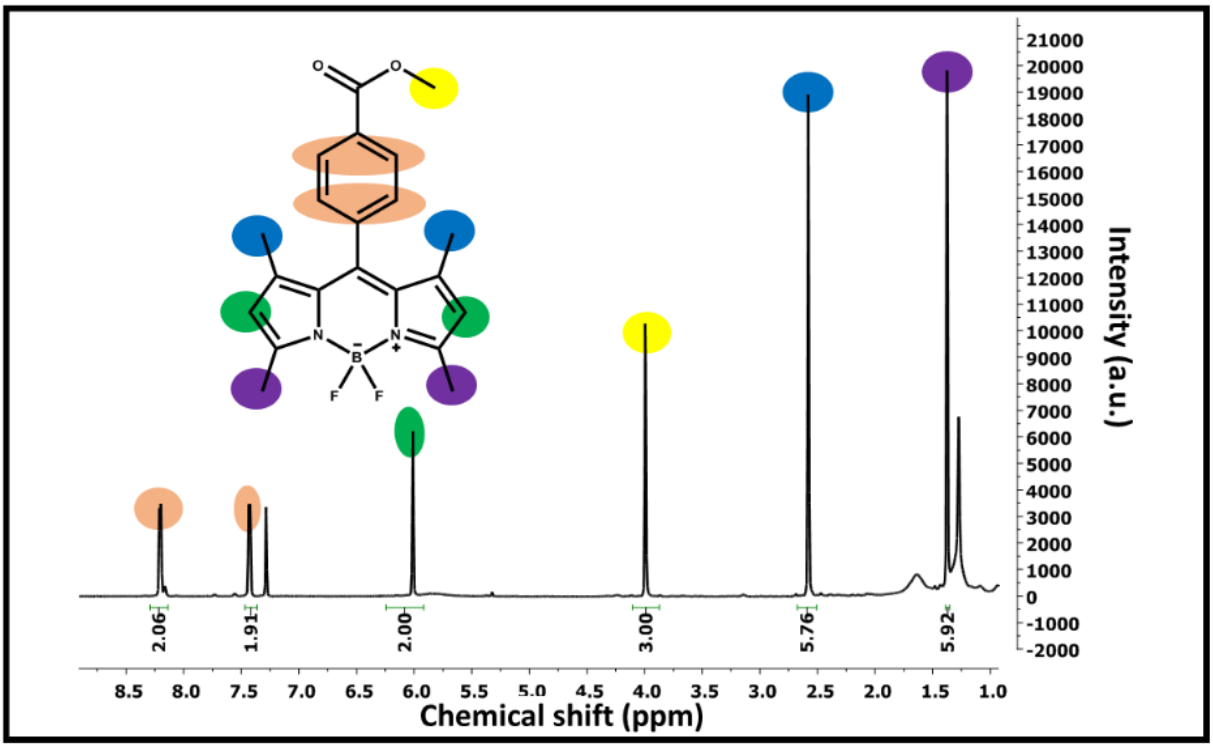

Figure 3.3: ^{1}H-NMR spectra of BODIPY **2a** in $CDCl_3$.

*3.2.1.3. Structural analysis of BODIPY **3a** and **3b***

The ^{1}H NMR spectrum of BODIPY **3a** has the anticipated 18 proton signals (**Figure 3.4**). Two six proton singlets at 1.32 and 2.59 ppm can again be attributed to the four methyl groups on the BODIPY core, while a two proton singlet at 6.03 ppm is attributed to the 2,6-position protons. Two proton doublets at 7.34 and 8.81 ppm can be attributed to the four protons on the *meso*-aryl ring. BODIPY **3b**, which was prepared from **3a**, has twenty-eight protons. However, only twenty-four of those protons can be identified due to solvent exchange. A six proton singlet at

2.07 ppm can be attributed to the 1,7-position methyls, a two proton singlet at 6.70 ppm can be attributed to the 2,6-position protons, and two singlets integrating to two protons each at 6.80 and 7.02 ppm can be attributed to the styryl ethenes. Multiplets and singlets observed between 8.22–7.24 ppm again integrate to twelve protons and can be attributed to the three phenyl rings.

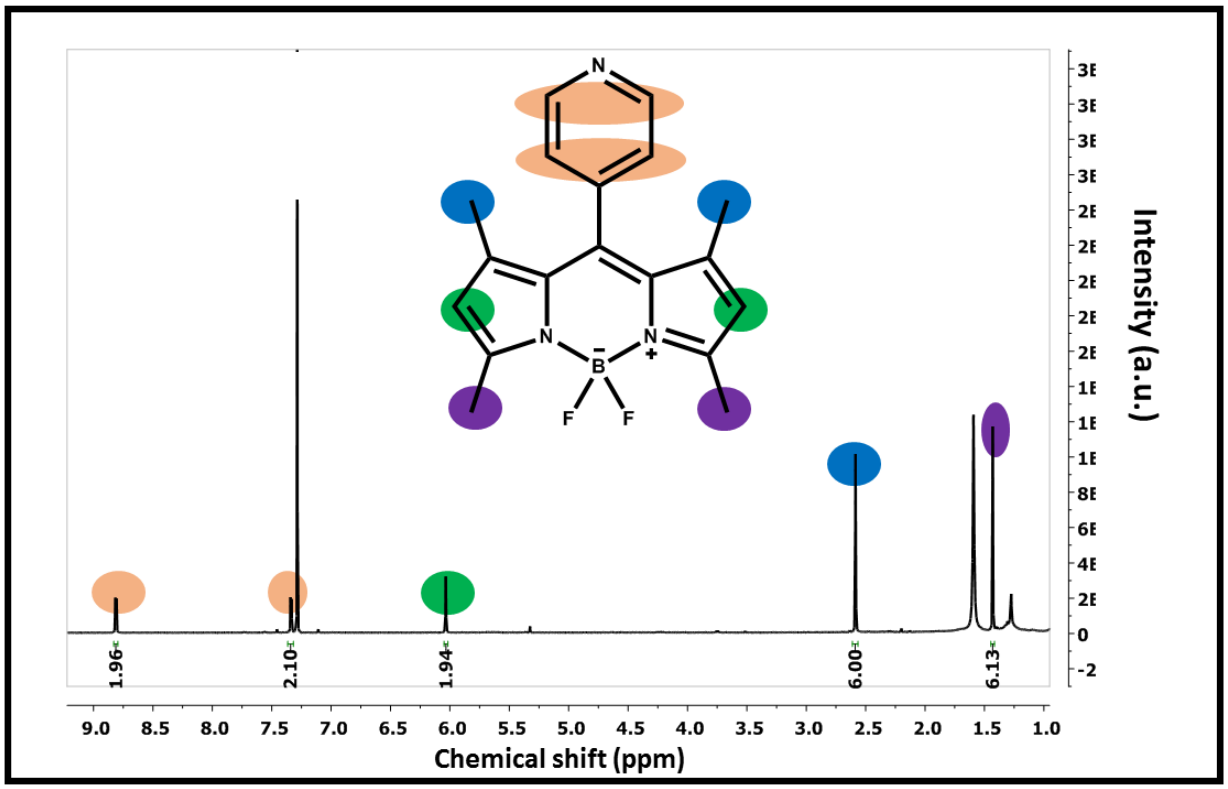

Figure 3.4: ^{1}H-NMR spectra of BODIPY **3a** in $CDCl_3$.

The FT-IR spectrum of **3b** (**Figure 3.2**) contains a hydroxyl stretch between 3550–3000 cm^{-1} after **3a** is styrylated. The molecular mass of **3b** was calculated to be 589.23 amu. MALDI-TOF mass spectrometry confirmed that a parent peak was obtained at 590.2 m/z.

*3.2.1.4. Structural analysis of BODIPY **4a** and **4b***

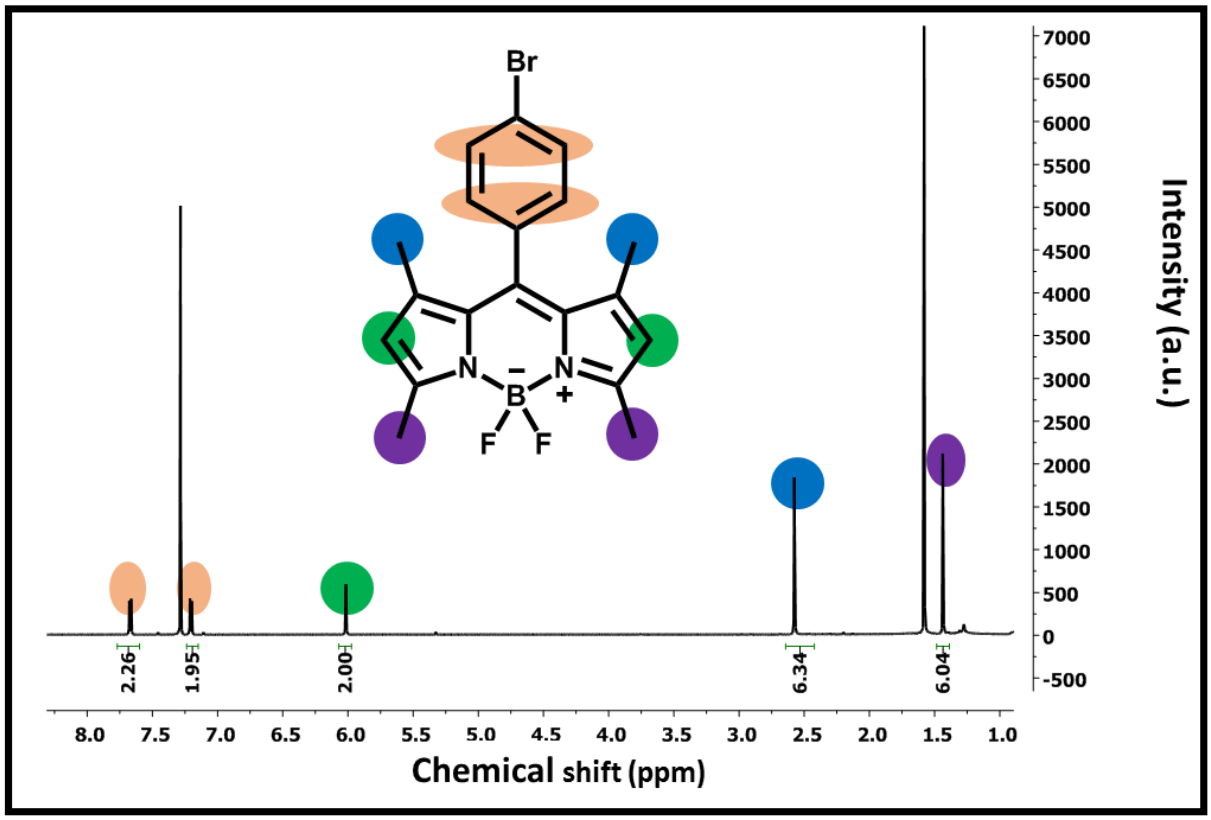

Figure 3.5: ^{1}H-NMR spectra of BODIPY **4a** in $CDCl_3$

Figure 3.5 contains the ^{1}H-NMR spectrum of **4a**. All 18 protons can be readily assigned. Two doublets at 7.64 and 7.27 ppm integrating to two protons each can again be assigned to the *meso*-aryl ring protons, while the singlet at 6.02 ppm can be attributed to 2,6-position protons, and the six proton singlets at 2.58 and 1.44 ppm can be attributed to the four methyl groups on the BODIPY core. BODIPY **4b**, which was prepared from **4a**, has twenty-eight protons, but only twenty-four were successfully identified by using ^{1}H-NMR spectroscopy due to solvent exchange. A multiplet integrating to six protons between 2.10–2.04 ppm was attributed to the 1,7-position

methyls, while a two proton singlet at 6.73 ppm was attributed to the 2,6-position protons, and two proton singlets at 7.28 and 7.61 ppm were attributed to the styryl ethene bridges. A four proton singlet at 7.49 ppm, and multiplets and singlets that lie between 7.61–8.10 ppm that integrate eight protons were attributed to the three phenyl rings.

The FT-IR spectrum of **4b** (**Figure 3.2**) contains a 3550–3000 cm^{-1} hydroxyl stretch after **4a** is styrylated. The molecular mass of **4b** was calculated to be 666.15 amu. MALDI-TOF mass spectrometry confirmed that a parent peak was obtained at 666.54 m/z.

*3.2.1.5. Structural analysis of BODIPY **5a** and **5b***

BODIPY **5a** has twenty-four protons, which can all be readily identified in the ^{1}H-NMR spectrum (**Figure 3.6**). Two six proton singlets at 1.50 and 2.57 ppm can again be attributed to the four methyl groups on the core, while two doublets integrating to two protons each at 7.08 and 6.80 ppm can be attributed to the *meso*-aryl ring, and a two proton singlet at 5.99 ppm can be attributed to the 2,6-position protons. A six proton singlet at 3.04 ppm can be assigned to the dimethylamino group methyls. BODIPY **5b**, which was prepared from **5a**, has thirty-four protons. However, only thirty protons could be identified by ^{1}H-NMR spectroscopy due to solvent exchange. The six protons from the 1,7-position methyls can be assigned to a peak at 2.18 ppm, while those for the dimethylamino group lie at 3.33 ppm. A two proton singlet at 7.28 ppm is attributed to the 2,6-position protons. Singlets and multiplets totalling to twelve protons associated with the phenyl ring protons lie between 8.10–7.49 ppm.

The FT-IR spectrum of **5b** (**Figure 3.2**) contains an OH-stretch at 3550–3000 cm^{-1}, due to the styrylation of **5a**. The molecular mass of **5a** was calculated to be 631.28 amu. MALDI-TOF mass spectrometry confirmed that a parent peak was obtained at 631.80 m/z.

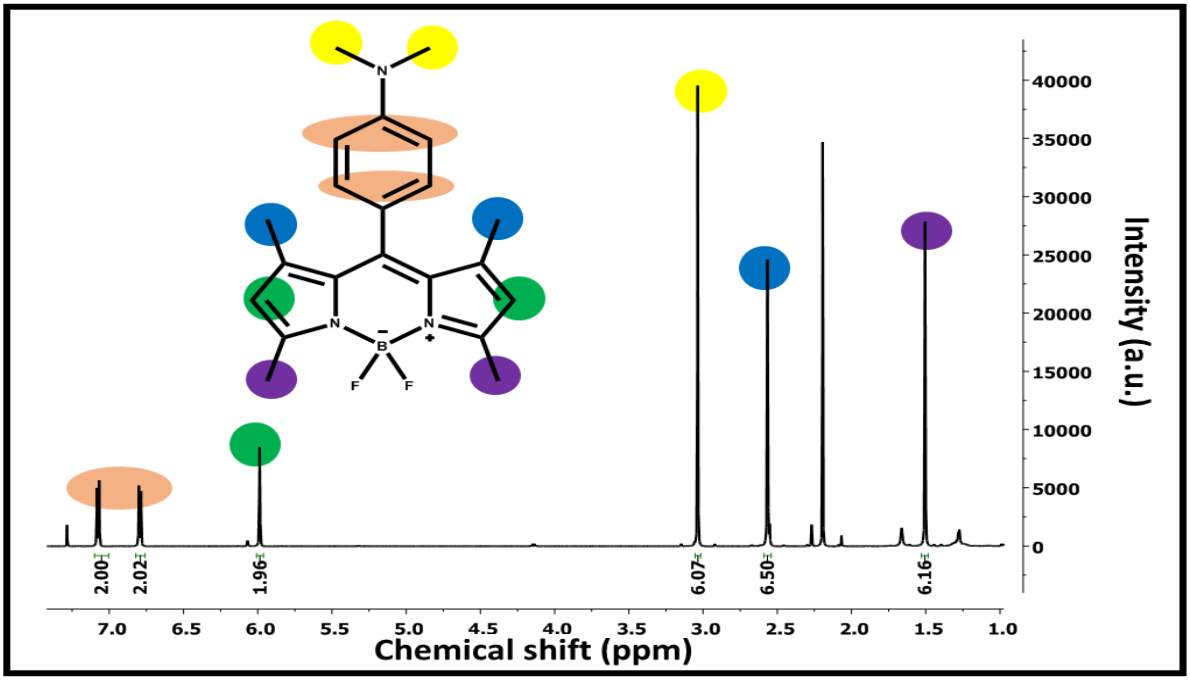

Figure 3.6: ^{1}H-NMR spectra of BODIPY **5a** in $CDCl_3$.

*3.2.1.6. Structural analysis of BODIPY **6***

BODIPY **6** has forty-one protons in its skeletal structure, but only thirty-eight were identified in the ^{1}H-NMR spectrum due to solvent exchange. A six proton multiplet between 1.19–1.15 ppm was attributed to the terminal methyl groups of the 2,6-position ethyls. A singlet was observed at 2.68 ppm, which integrates to four protons and can be attributed to the other four protons on the ethyls. A three proton peak associated with the methyl at the 1-position of the BODIPY core lies at 1.43 ppm, and a three proton singlet at 3.98 ppm can be attributed to the methyl group

on the *meso*-aryl ring in a similar manner to that in the spectrum of core dye **2a** (**Figure 3.3**). Singlets and multiplets observed between 6.99–6.81 ppm integrating to six protons can be attributed to three styryl ethenes. A series of multiplets that lie between 8.16–7.06 ppm integrate to sixteen protons and can be assigned to the protons of the four phenyl rings. The molecular mass of **6** was calculated to be 750.21 amu. MALDI-TOF mass spectrometry confirmed that a parent peak was obtained at 750.77 m/z (**Figure 3.7**).

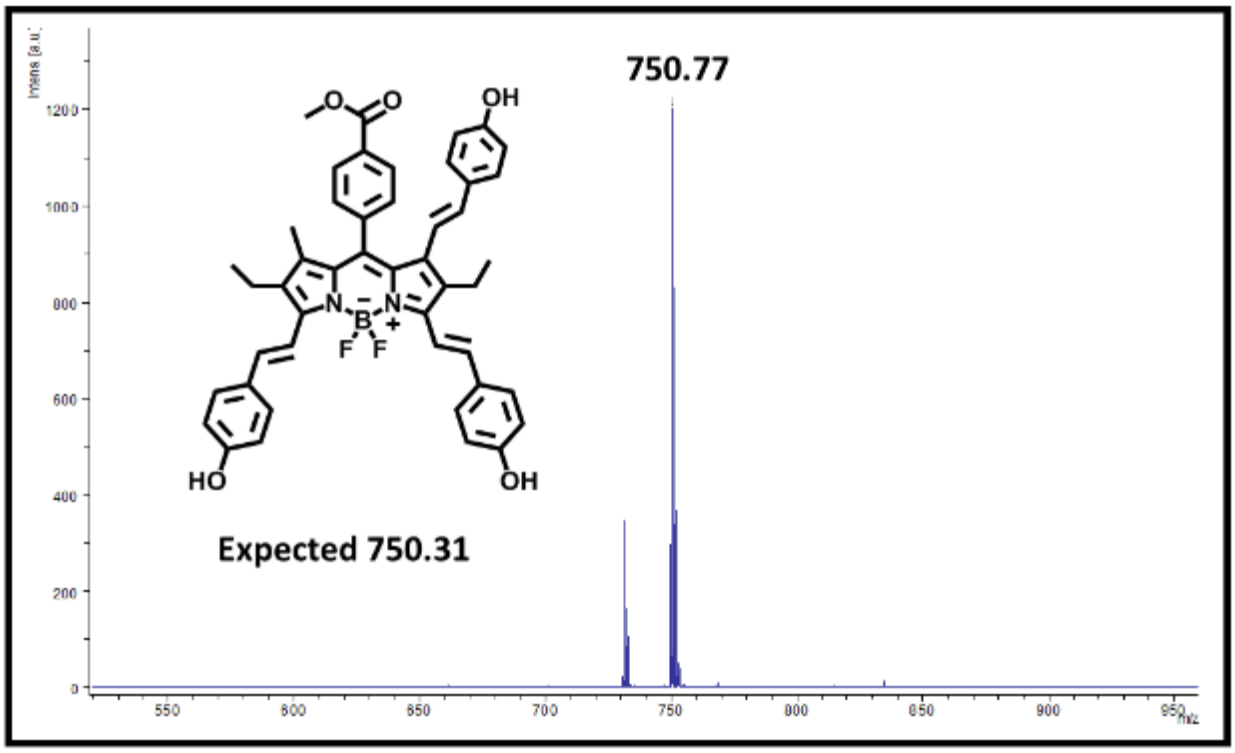

Figure 3.7: The mass spectrum of BODIPY **6** provides a typical example of those obtained.

3.2.1.7. Structural analysis of Porphyrin 7

Porphyrin **7** was characterised in a similar manner to what was reported previously by Balaji *et al*. [229] for porphyrin **9**, which was prepared by metal insertion of the same free base porphyrin

sample and differs only in terms of the axial ligation. All 46 protons were identified in the ^{1}H NMR spectrum. An eight proton singlet at 9.22 ppm was attributed to the β-position protons of the porphyrin ligand. The *meso*-thienyl substituents have 12 protons. Eight appear as doublets between 8.00–7.89 ppm, while the peak for the other four protons lies at 7.54 ppm. A multiplet observed at 5.65 ppm integrated to four protons and was attributed to the four protons at the *meta*-positions of the *tert*-butylphenols, since the porphyrin ring current has a shielding effect [229]. Two doublets observed at 1.83 ppm integrate to four protons and were attributed to the *ortho*-position protons, since they lie upfield compared to the *meta*-position protons due to the stronger porphyrin ring current effect [250-252]. Eighteen protons observed as a singlet at 1.26 ppm were attributed to the methyls on the *tert*-butylphenol axial ligands.

Axial ligands are often not observed in mass spectra due to ionisation caused by the matrix [251, 252]. A peak observed at 906.10 amu was attributed to the mass of **7** with one axial ligand attached and the mass was calculated to be 905.6 m/z.

*3.2.1.8. Structural analysis of porphyrin **8***

Porphyrin **8** was characterised in a similar manner to what was reported previously by Balaji *et al*. [229] for porphyrin **10**, which was prepared by metal insertion of the same free base porphyrin sample and differs only in terms of the axial ligation. All 54 protons were readily identified by ^{1}H-NMR spectroscopy. An eight proton singlet observed at 9.00 ppm and was attributed to the protons at the β-positions of the porphyrin ring. Twenty protons from the *meso*-phenyl ring substituents appear as two peaks. A multiplet that integrated to eight protons between 8.06–

8.04 ppm was attributed to the *ortho*-position protons, while a second peak that was observed as a multiplet at 7.76 ppm and integrated to 12 protons was attributed to the *meta*- and *para*-position protons. A doublet at 5.65 ppm, which integrated to four protons, was attributed to the four protons at the *meta*-positions of the *tert*-butylphenols. The protons lie out of the aromatic downfield region due to the shielding effect of the porphyrin ring current [229]. Another doublet was observed at 1.83 ppm that integrated to four protons, and was attributed to the protons at the *ortho*-positions of the *tert*-butylphenols. This signal lies upfield compared to the *meta*-position protons since the porphyrin ring current has an even stronger effect [250-252]. Eighteen protons observed as singlets at 1.26 ppm were attributed to the methyl groups associated with the *tert*-butyls of the axial ligands.

The ionisation limitations experienced in obtaining the mass spectrum of porphyrin **7** was also encountered with porphyrin **8**. A peak at 882.24 amu for **8** with only one of the original axial ligands corresponds to the calculated mass of 881.23 m/z.

3.3. Optical spectroscopy

The UV-visible absorption spectra of the BODIPY core series **1-5a** are typical of those obtained for BODIPY cores with aromatic substituents at the *meso*-position. The absorption spectra of a BODIPY core dye typically contains a main absorption band at ca. 500 nm due to the the $S_0 \longrightarrow S_1$ transition, a shoulder of intensity that is attributed to a 0-1 vibrational overtone, and in the UV region weaker bands that involve transitions to higher energy states (S_2 and above) [9, 48]. **Figure 3.8** shows the UV-visible absorption spectrum of BODIPY **1a**. To avoid redundant explanations, only selected spectra are shown in this manner when similar trends are observed. Details are summarised in **Table 3.2**.

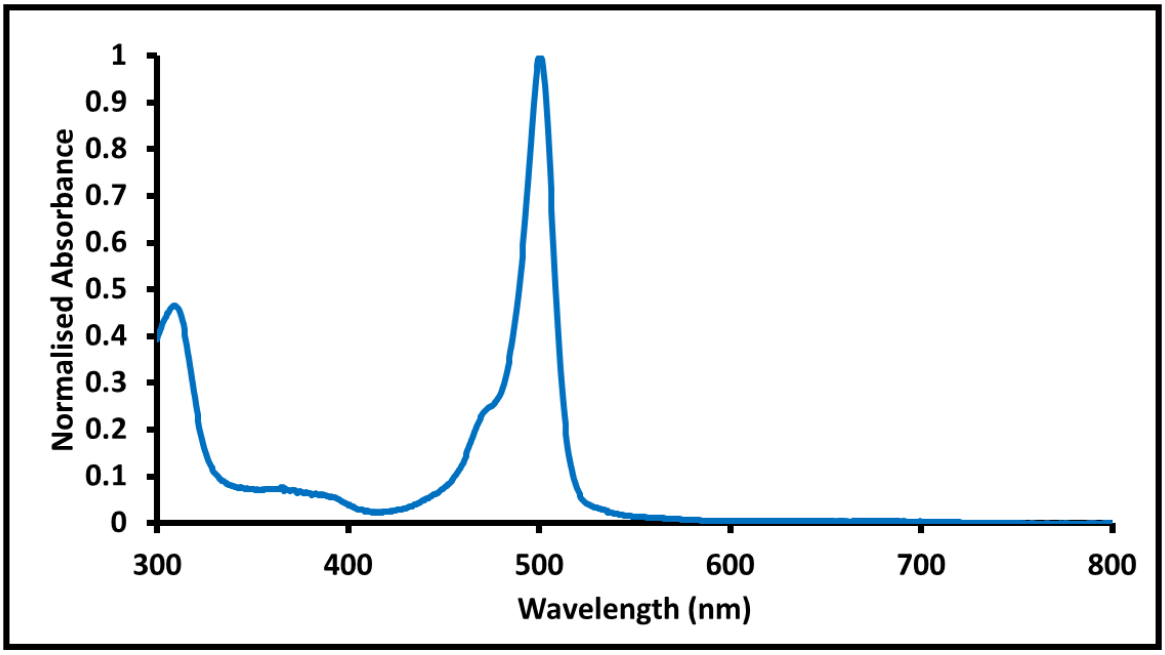

Figure 3.8: Normalised UV-visible absorption spectra of BODIPY **1a** in ethanol.

The BODIPY dyes in the **1-5a** series all have a single intense absorption band that lies between 500−505 nm. No evidence of aggregation was observed in various solvents. Upon styrylation at the 3,5-positions the main spectral band red-shifts significantly by ca. 130 nm, **Figure 3.9**, for reasons that will be explored in depth in Chapter 7.

The effect of solvent polarity was investigated on the **b** series BODIPY dyes. The absorption and emission spectra of the dye were studied in DMSO, ethanol and THF (**Table 3.2**). It was observed that the main absorption band of the dyes was more red-shifted in DMSO compared to THF and ethanol. There was no obvious trend in terms of the effect of solvent polarity on the absorption spectra of the dyes.

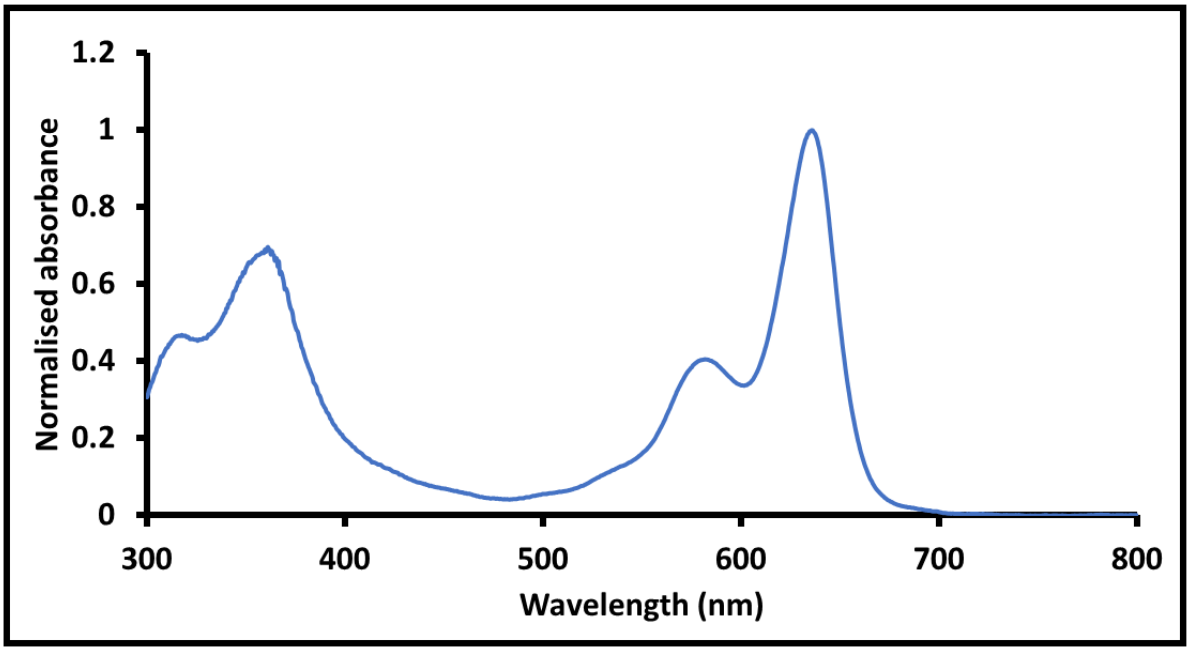

Figure 3.9: Normalised absorption spectra of BODIPY **1b** in ethanol.

The UV-visible spectra of the free base porphyrins and porphyrins **7** and **8** are shown in **Figures 3.10** and **3.11**, respectively. The free base porphyrins have an intense B band and four weak Q bands, and this can be readily explained using Gouterman's 4-orbital model (**Figure 1.13**). It can be observed that the absorption bands of compounds with *meso*-thienyl rings are red-shifted compared to those with *meso*-phenyl rings (**Table 3.1)**. The reasons for the red-shift are explained in Chapter 7. The insertion of the Sn(IV) ion in the central cavity leads to there only being two Q rather than four Q bands, as is typically observed for metalloporphyrins due to their four-fold symmetry [66, 70]. The addition of different axial ligands did not result in significant changes in the absorption spectra.

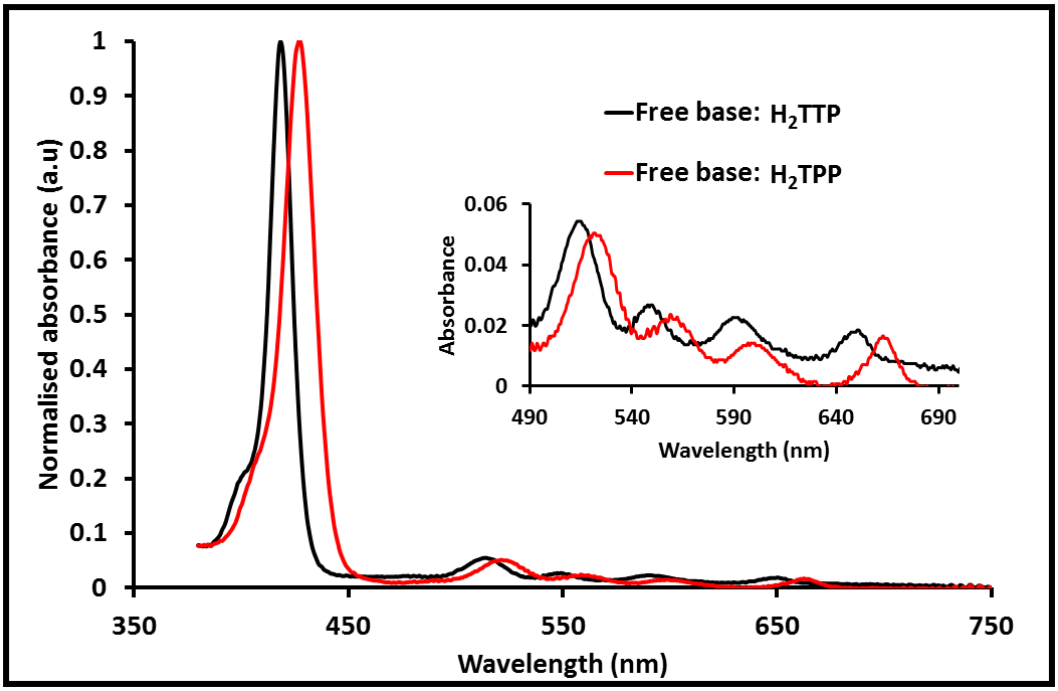

Figure 3.10: Normalised absorption spectra of the free base porphyrins in benzene. Red = **H_2TTP** and black = **H_2TPP**.

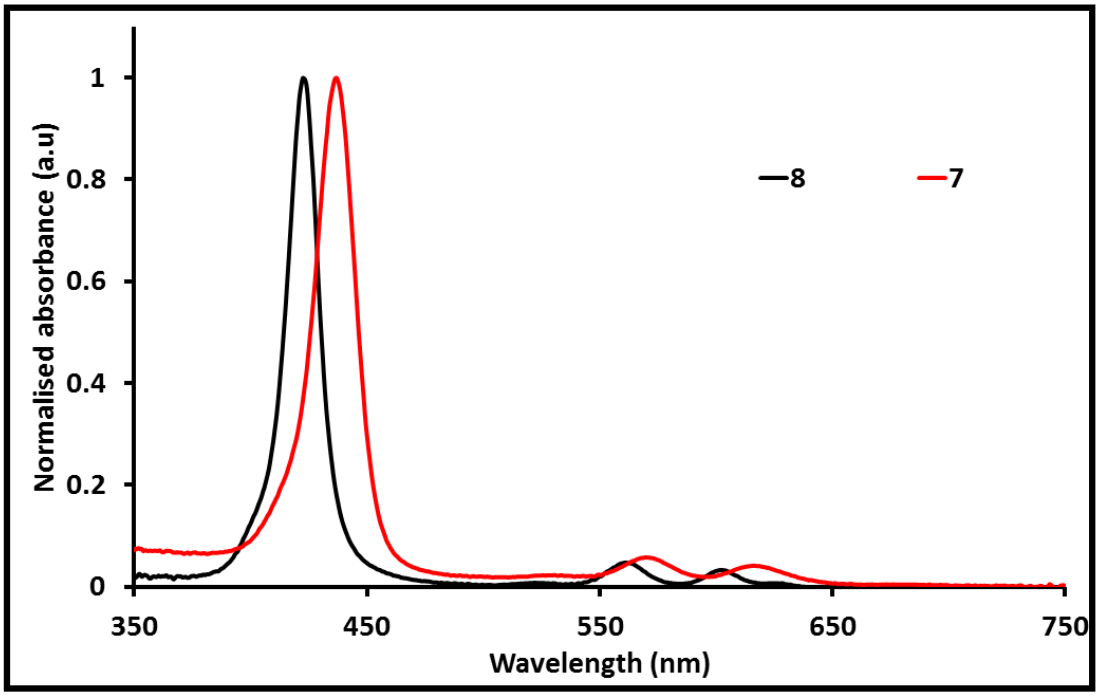

Figure 3.11: Normalised absorption spectra of porphyrin **7** and **8** in benzene. Red = 7 and black = 8.

The molar extinction coefficients (log ε) of the dyes synthesised in this study were calculated by plotting the absorbance of the main spectral band against varying concentrations of the individual dyes according to the Beer-Lambert law (**Equation 14**).

$$A = \varepsilon \cdot c \cdot l \qquad (\mathbf{14})$$

where A is the absorbance, ε the molar extinction, and c and l are the concentration and pathlength of the cell, respectively. The concentrations were kept below 1 x 10^{-5} mol. L^{-1} and no evidence of aggregation was observed. **Tables 3.1** and **3.2** summaries the Log ε values obtained for the porphyrins and BODIPY dyes, respectively.

3.4. Physicochemical properties

3.4.1. Fluorescence quantum yields

Figure 3.12 A and **B** show the absorption, emission and excitation fluorescence spectra of BODIPY **1a**, **1b**. The fluorescence excitation spectra of the BODIPY dyes and porphyrins synthesised in this study are very similar to the absorption spectra. The fluorescence emission spectra are a near mirror image of that of the absorption spectra as is expected given the rigid structures of the dyes when Kasha's rule is followed, and emission occurs out of the lowest vibrational level of the singlet excited state.

BODIPY dyes are known to have high fluorescence quantum yields (ϕ_F) compared to porphyrins and phthalocyanines. **Tables 3.1** and **3.2** show the ϕ_F values calculated for the porphyrins and BODIPY dyes, respectively; the ϕ_F values are calculated using a comparative method described in **Equation 2.** Series **1-5a** dyes were excited at *ca.* 470 nm, whereas the **b** series was excited at 610 nm, with Rhodamine and ZnPc being used as the standards for the **1-5a** and **b** dye series, respectively. The effect of solvent polarity on dyes **1b**, **2b, 4b** and **5b** was investigated by measuring absorption and emission spectra and calculating fluorescence quantum yields in ethanol, DMSO and THF (**Table 3.2**). There was no clear solvent polarity related trend observed. Comparatively high Φ_F values were obtained for **1-3b**. The lower values for **4b** and **5b** are related to the presence of bromine atom and dimethylamino moiety on the *meso*-aryl rings.

The porphyrins were excited at 429 nm, and Rhodamine was used as the standard. The fluorescence quantum yields were calculated to be below 0.01 due to the heavy atom effect related to the presence of a Sn (IV) metal ion.

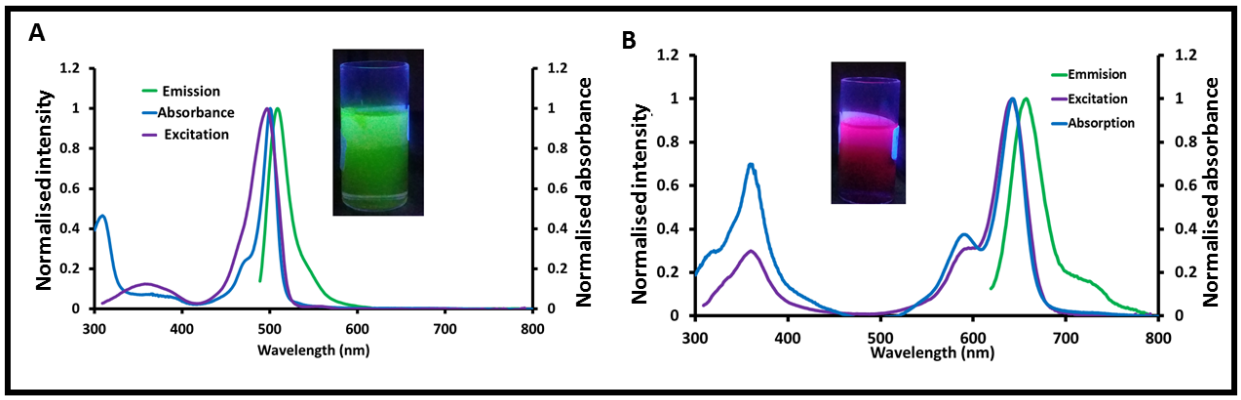

Figure 3.12: Normalised emission, excitation and absorption spectra of BODIPYs **1a** (A) and **1b** (B) in ethanol. The insets show images of solutions of the dyes under ambient light.

3.4.2. Fluorescence lifetimes

The fluorescence lifetime (τ_F) is the time taken for the fluorescence emission intensity to decay by 1/e. The τ_F values for the dyes synthesised in this study were determined using the TCSPC technique. The τ_F value of a molecule is independent of the excitation and emission wavelengths when Kasha's rule applies. The dyes studied exhibited mono-exponential fluorescence decay curves. **Figure 3.13** provides the exponential decay curve and residual curve obtained for **1b**, and is used to illustrate typical fluorescence decay and residual curves. The τ_F values of the dyes studied are summarised in **Tables 3.1** and **3.2** for the porphyrins and BODIPY dyes, respectively**.** The τ_F values for **1-5b** lie in the 4−5 ns range, while a greater variation was observed in the presence of different *meso*-aryl rings for the porphyrins, since there is scope for free rotation.

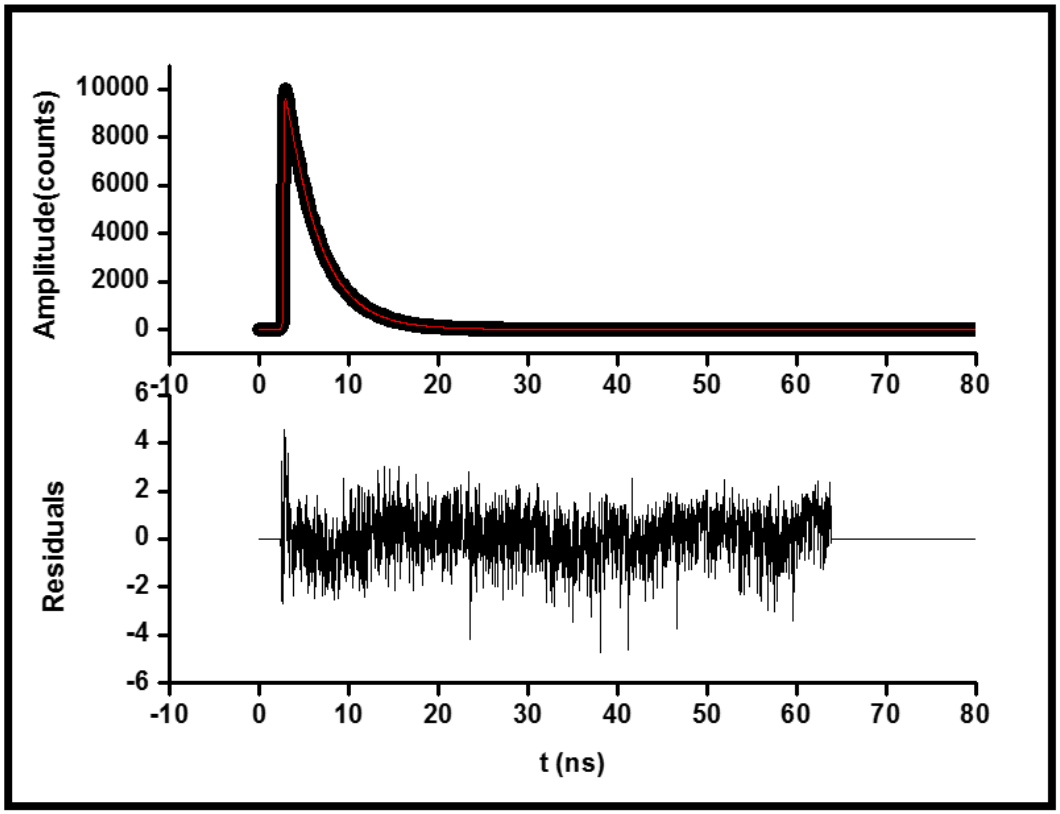

Figure 3.13: The fluorescence decay and residual curves for BODIPY **1b** in DCM.

Table 3.1: Summary of the photophysical properties of the porphyrins.

	λ_{max} (nm)					
	B band	**Q bands**	λ_{em}	ϕ_F	τ_F (ns)	**Log ε**
***H_2TTP**	428	532, 562, 597, 660	670, 728	0.002	1.26	---
***H_2TPP**	418	513, 548, 589, 644	652, 715	0.13	11.5	---
7	438	570, 617	---	<0.01	---	5.1
8	422	561, 602	---	<0.01	---	5.3
***9**	441	568, 613	637, 694	<0.01	1.76	5.0
***10**	426	559, 598	607, 660	0.04	5.42	5.3

*Values obtained from the literature [229]. All log ε values were determined in DMF, while other parameters were calculated in DMF.

Table 3.2: Summary of the photophysical properties of the BODIPY dyes.

	Solvent	λ_{max} (nm)		ΔStokes (cm^{-1})	ϕ_F	τ_F (ns)	Log ε
		λ_{Abs}	λ_{em}				
1a	Ethanol	502	514	465	0.28[a]	3.35	4.23
	Ethanol	633	654	507	0.50	3.61	4.55
1b	DMSO	643	666	537	0.42	3.39	---
	THF	637	656	454	0.47	3.71	---
2a	Ethanol	502	511	351	0.56[b]	3.26	4.80[b]
	Ethanol	635	658	550	0.48	3.59	4.61
2b	DMSO	641	666	558	0.37	3.51	---
	THF	635	651	387	0.49	3.72	---
3a	Ethanol	501	515	543	0.58[c]	5.4[c]	4.46
3b	Ethanol	635	660	597	0.52	1.62	4.51
4a	Ethanol	501	512	429	0.84[b]	4.44	4.84
	Ethanol	633	655	531	0.25	3.83	4.41
4b	DMSO	638	661	545	0.27	4.48	---
	THF	633	651	437	0.31	4.51	---
5a	Ethanol	504	508	156	0.3	3.54	3.84
	Ethanol	632	649	414	0.23	3.28	4.11
5b	DMSO	636	660	571	0.11	2.91	---
	THF	628	651	562	0.18	3.12	---
6	Ethanol	658	683	556	0.2	3.73	4.55
	DCM	655	682	604	---	---	4.85

a- [2], b - [29], c - [244], --- not studied.

3.5. Summary

The **1-5a** series of BODIPY dyes was successfully synthesised using the acid-catalysed condensation method in one pot and characterised using ^{1}H-NMR, UV-visible absorption and FT-IR spectroscopy. The main absorption bands of the dyes were consistently observed to lie between 500−505 nm which is typical of 1,3,5,7-tetratmethylBODIPY core dyes [2, 253]. Substitution at the 3,5-(and 7)-positions yielded the **1-5b** series of dyes. FT-IR spectroscopy was used to confirm the presence of various functional groups characteristic of the respective dyes.

The UV-visible absorption spectra of these dyes were highly red-shifted relative to those of the **1-5a** series. The main absorption band of the dyes lie between 630–660 nm, with the main spectral band of the 3,5,7-tristyrl dye **6** being the furthest red-shifted. The red-shift in the main absorption bands was attributed to the extension of the π-conjugation system due to the addition of the styryl groups.

Porphyrins **7** and **8** were synthesised from the free base porphyrins by inserting Sn(IV) in the central cavity along with appropriate axial ligands. The synthesis of the dyes was confirmed through ^{1}H-NMR and UV-visible absorption spectroscopy and mass spectrometry. That addition of the central metal resulted in the red-shifting of the B bands and disappearance of two of four of the free base B bands.

Chapter 4

Fluorescence and colourimetric detection of glucose

4.1. BODIPY dyes in glucose detection

In this chapter, the fluorescence and colourimetric sensing abilities of the BODIPYs **1-5b** upon reaction with glucose is described. The dyes were functionalised with boronic-acid-substituted styryl groups at the 3,5-positions, to provide boronic acid moieties as receptors because of their high affinity towards saccharides [138, 142, 254]. A *bis*-boronic acid system was designed through the addition of two phenylboronic acids to the BODIPY core yielding a distyryl dye. The aim behind this was to enhance the selectivity of the dyes towards glucose over other prevalent saccharides such as fructose. Previous studies have indicated that mono-boronic acid systems have a high binding affinity towards fructose [147, 149]. In contrast, *bis*-boronic acid systems have been reported to be relatively selective towards glucose [131, 147, 149]. Hence, a *bis*-boronic acid dye structure was conceptualised and characterised in this study.

4.2. Fluorescence Glucose detection

Glucose detection studies were conducted using fluorimetry. Due to solubility limitations of the BODIPY dyes studied, phosphate saline buffer (PBS) could not be used. A 52% v/v PBS (pH 7.4) / methanol solution mixture was used instead. The dyes were analysed for glucose detection at pH values of ca. 7.4 because this is the optimal physiological pH that is preferred for diabetes-related sensors.

The fluorescence emission (**Figures 4.1**, **4.2** and **4.3**) of the respective dyes were studied with 5 µM of the dye being used. The fluorescence emission spectra of the dyes were initially measured in PBS/methanol solution. Thereafter, an aliquot of buffered 0.1 M glucose solution was added, and after 2 min of mixing, the fluorescence emission spectrum was measured. More aliquots were added in a similar manner until a final glucose concentration of 100 mM was obtained.

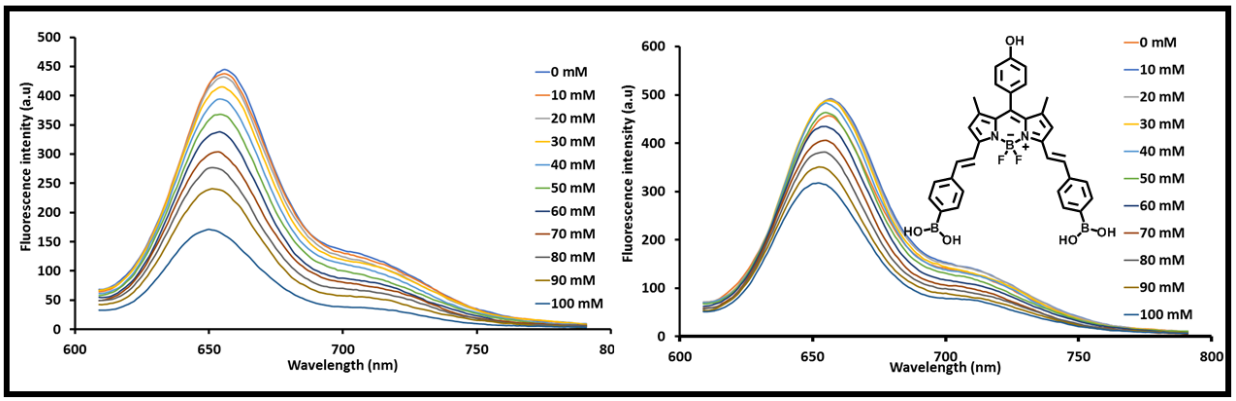

Figure 4.1: Fluorescence emission (λ_{em} = 590 nm) spectra of **1b** (5 µM) at varying (A) glucose and (B) fructose concentrations (0−100 mM) in methanol-PBS at pH 7.5.

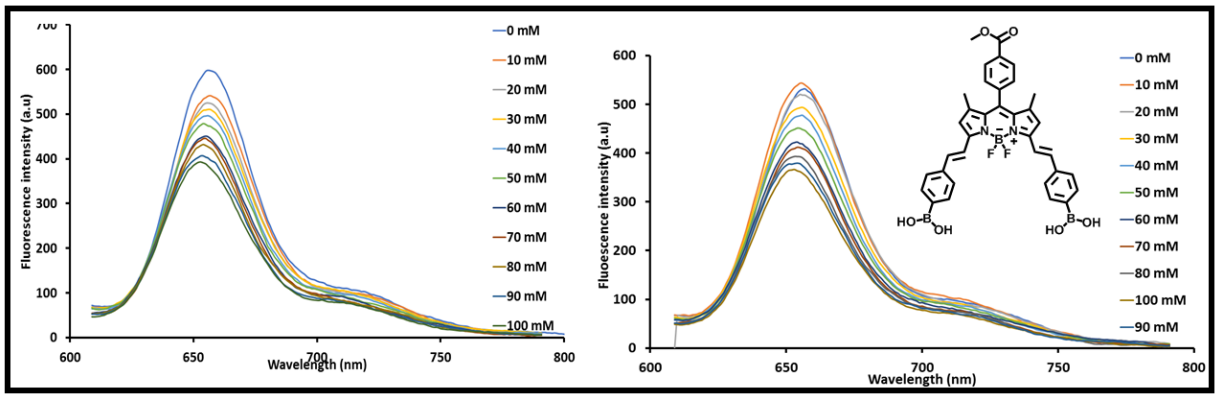

Figure 4.2: Fluorescence emission (λ_{em} = 590 nm) spectra of **2b** (5 µM) in varying (A) glucose and (B) fructose concentrations (0−100 mM) in methanol-PBS at pH 7.5.

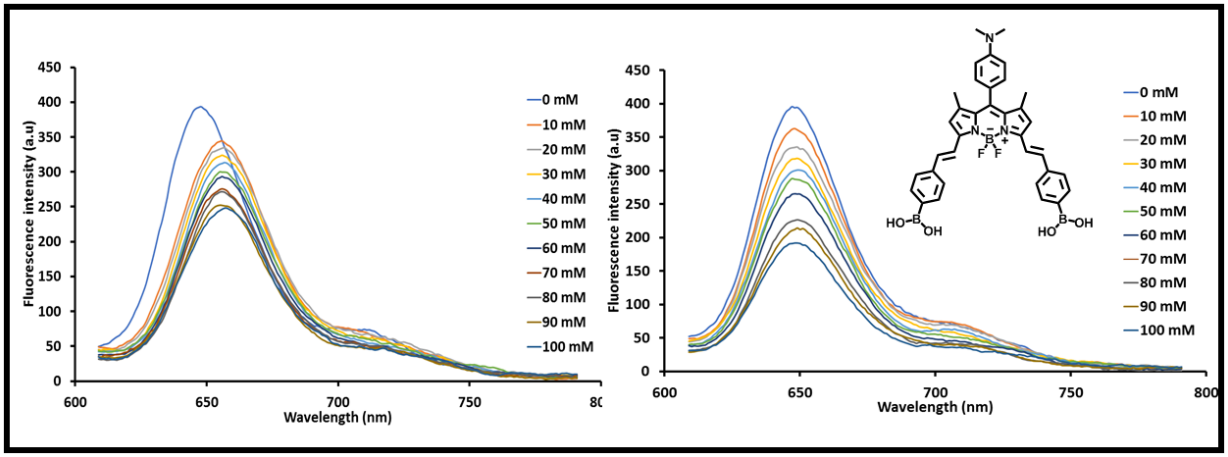

Figure 4.3: Fluorescence emission (λ_{em} = 590 nm) spectra of **5b** (5 µM) in varying (A) glucose and (B) fructose concentrations (0−100 mM) in methanol-PBS at pH 7.5.

It was observed from the figures above that upon the addition of glucose there was a decrease in the fluorescence intensity. However, an increase in the fluorescence intensity was expected due to a “turn-on” fluorescence effect related to an ICT quenching mechanism of the

fluorescence in the absence of the analyte (glucose or fructose). The decrease in fluorescence observed can be attributed to systematic changes in the optical density of the solutions at the excitation due to the titration of the dyes with glucose or fructose. **Figure 4.3A** indicates that there was a minor shift in the wavelength of the emission band of BODIPY **5b** after the addition of 10 mM glucose. Changes of this type were consistently observed throughout the titrations of the dyes with glucose. The shifts in emission wavelength provides evidence that an interaction took place upon addition of glucose. The absence of a "turn on" fluorescence response is investigated further in Chapter 7 with molecular modelling calculations.

4.3. pH studies

Boronic acid interactions are well known to be pH dependent. Therefore, it was of paramount importance that pH studies be conducted in order to determine the stability of the dye at various pH values in the presence and absence of glucose. Since BODIPY dyes **1-5b** did not provide the anticipated fluorescence sensor response for glucose at physiological pH, pH studies were carried out to examine what happens at acidic and basic pH. **Figures 4.4**, **4.5**, and **4.6** provide the fluorescence emission spectra of the **1b**, **2b** and **5b** in the presence of glucose at various pH values ranging from pH 3–12. 50 µM of glucose and fructose were added to the 5 µM dye solution, and the fluorescence emission of the dyes was studied.

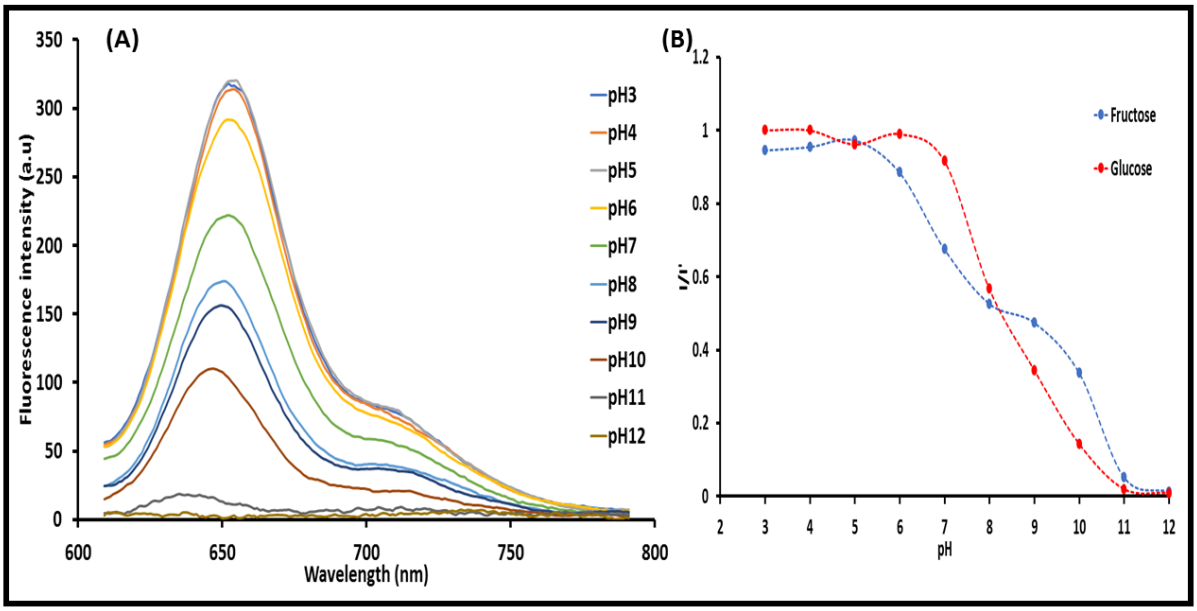

Figure 4.4: (A) Fluorescence emission (λ_{em} = 590 nm) of **1b** with 50 mM glucose, (B) normalised intensity spectra of 50 mM glucose (red) and fructose (blue) in varying pH buffer media.

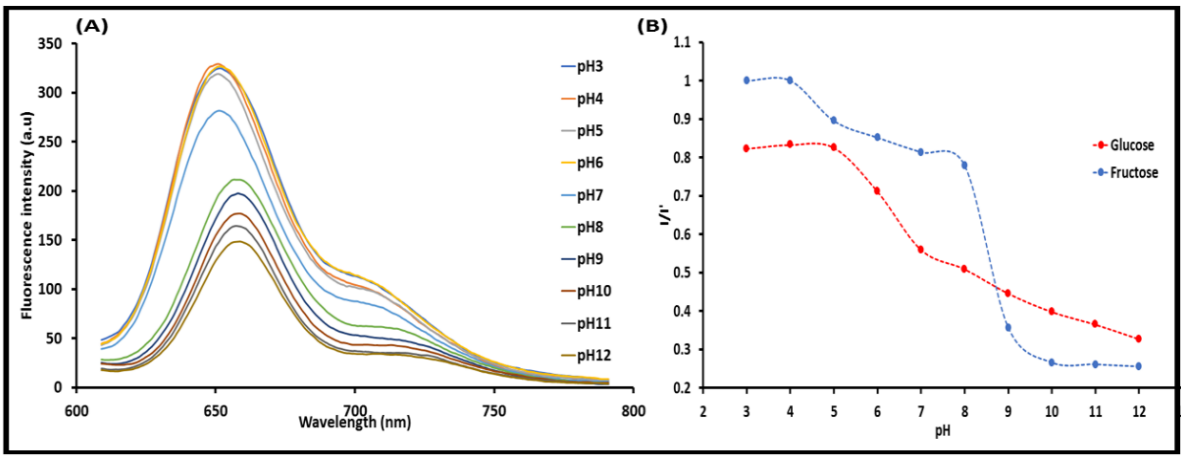

Figure 4.5: Fluorescence emission spectra (λ_{em} = 590 nm) of **2b** with 50 mM glucose (A), normalised intensity spectra of 50 mM glucose (red) and fructose (blue) in buffer media of varying pH (B).

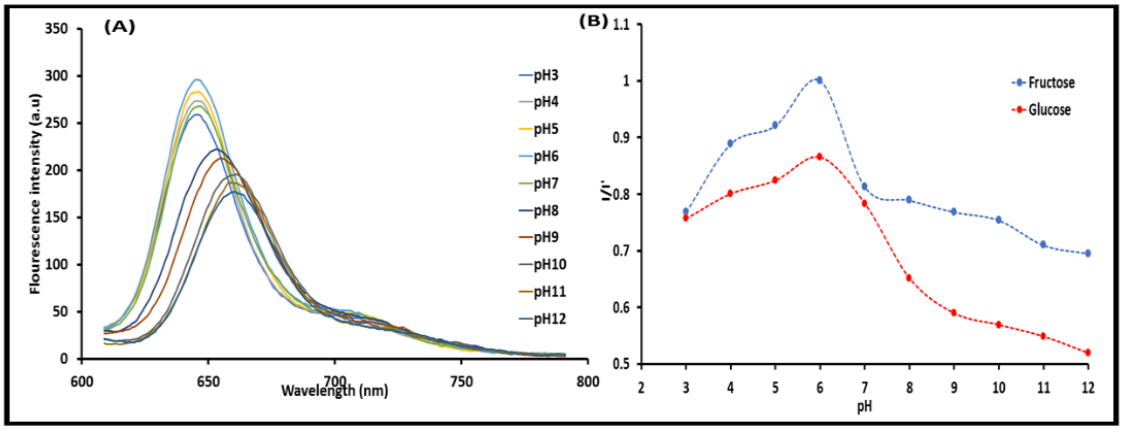

Figure 4.6: (A) Fluorescence emission (λ_{em} = 590 nm) of **5b** with 50 mM glucose, (B) normalised intensity spectra of 50 mM glucose (red) and fructose (blue) in buffer media of varying pH.

It was observed (**Figures 4.4 – 4.6**) that there was a drastic decrease in the fluorescence intensity between pH 8–12 upon the addition of glucose and fructose, a shift in the emission wavelength was also observed at these pH values. In contrast, the fluorescence spectra of the dyes remained largely the same in the acidic and physiological regions. Phenylboronic acid molecules generally have *p*K_a ranges of 8–9 [255]. Under basic conditions the *p*K_a of the boronic acid molecules decreases to *ca.* 7 as it reacts with the water (environment) and becomes anionic (**Scheme 1.6**) in its anionic form it can readily bind to the diols. According to the literature when the surrounding environment has a pH either equal to or greater than the *p*K_a value, the boronic acid molecules can easily form tetrahedral boronate complexes with diols in solution [255]. The *p*K_a values of the dyes used in this study were determined using **Figures 4.4–4.6B**. The values were estimated to be ca. 8.0, 7.5 and 7.5 for BODIPYs **1b**, **2b** and **5b**, respectively, with glucose, and

ca. 7.2, 8.3 and 7.0 with fructose. The optimal pH range for binding between the analyte and the boronic acid moiety usually lies above the *p*K_a value of the molecule [134, 256, 257].

4.4. Colourimetry

BODIPY dyes **1-5b** generally provide blue solutions in organic solvents (**Figure 4.7**) as their main absorption band lies between 630–635 nm (reflecting blue light). Colourimetric studies were conducted to investigate if any colour changes are observed that are clearly visible to the naked eye when the probes are reacted with the analytes in various pH media due to reactions between glucose as the analyte and the boronic acid receptor.

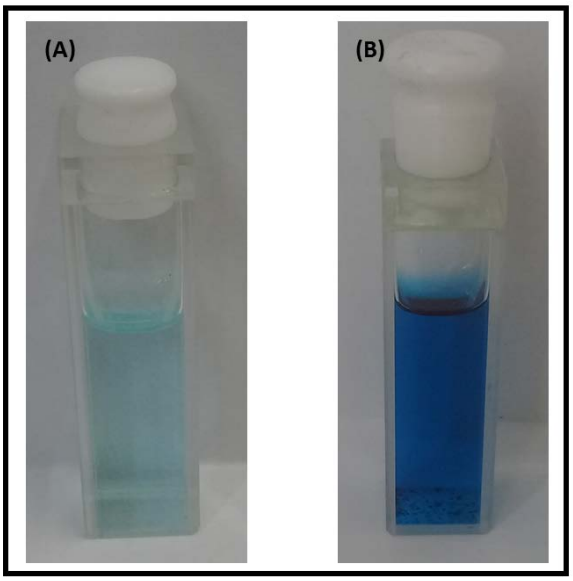

Figure 4.7: 5 µM (A) and 10 M (B) solutions of BODIPY dye **2b** in methanol.

Figures 4.8 and **4.9** provide images of BODIPY **2b** dissolved in different pH buffers with 50 mM glucose. For ease of visualization, images are provided using higher probe and analyte concentrations. No colour changes visible to the naked eye were observed when studies were conducted between pH 3−7, **Figure 4.8**. A slight red-shift in the main absorption band of the dyes is observed in the UV-visible absorption spectra (**Figure 4.10**), however.

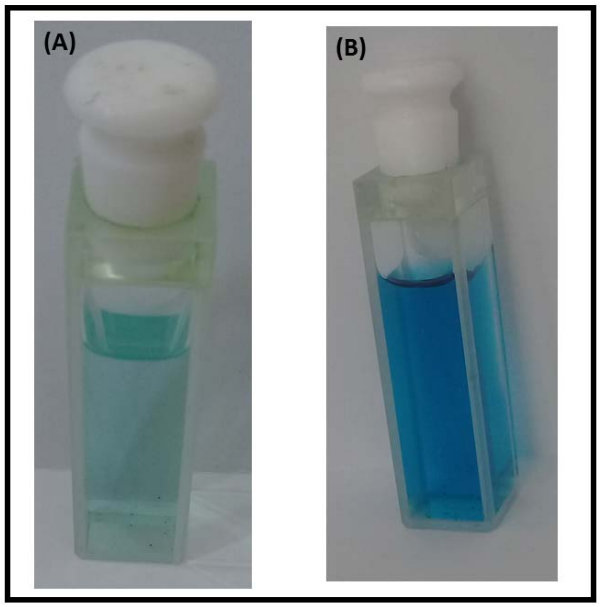

Figure 4.8: 5 µM BODIPY **2b** with 50 mM glucose (A), and 10 M BODIPY **2b** with 0.1 M glucose (B) in pH 3 buffer media.

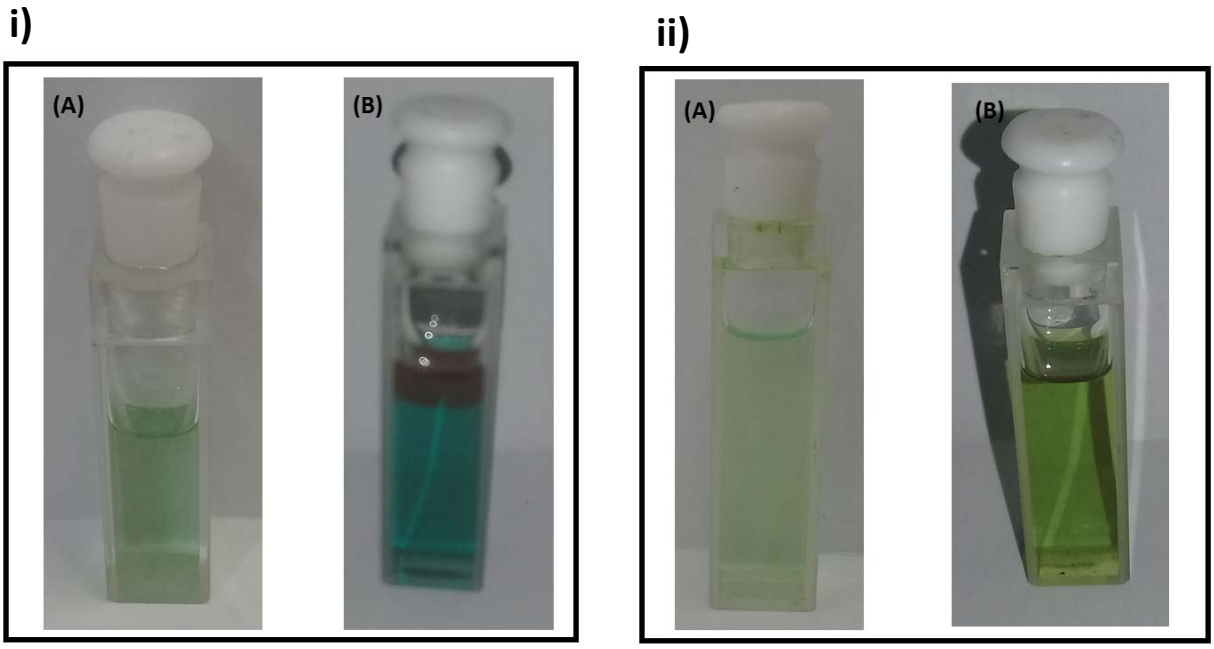

Figure 4.9: (i) BODIPY **2b** (A) 5 µM with 50 mM glucose, (B) 10 M with 0.1 M glucose in pH 9 buffer media, and (ii) BODIPY **2b** (A) 5 µM with 50 mM glucose (B) 10 M with 0.1 M glucose in pH 12 buffer media.

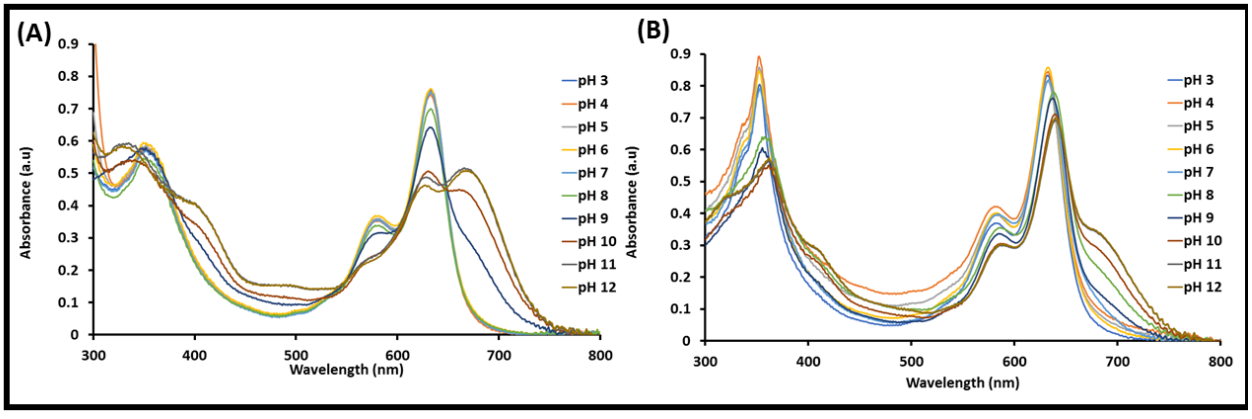

Figure 4.10: UV-visible absorption spectra of 5 µM **1b** (A) and **2b** (B) solutions with 50 mM glucose in buffer media of varying pH buffer media

In contrast, colour changes were observed at basic pH range after the addition of the glucose analyte. Between pH 8−9, the solutions turn slightly greenish-blue (**Figure 4.9i**), while there is a pronounced green colour at pH 10−12 (**Figure 4.9ii**). These colour changes are unlikely to provide the basis of a sensor system that is selective for glucose, however, since similar spectral changes are also observed in the presence of fructose (**Figures 4.4**, **4.5**, and **4.6**).

4.5 Summary

BODIPY dyes **1-5b** did not exhibit the fluorescence "turn-on" mechanism upon reaction with glucose and fructose at physiological pH that has been described for BODIPY dyes that are substituted with boronic acid moieties at the *meso*-aryl position [258-262]. The probable reasons for the absence of a PET or ICT type quenching mechanism have been investigated by molecular modelling and will be described in Chapter 7. At basic pH, a marked shift in the emission and absorption band maxima is observed along with colourimetric changes in the solutions that are clearly visible to the naked eye when glucose interacts with the dyes. Since fluorescence sensing at physiological pH did not work in the manner envisaged, the selectivity, binding efficiency and limits of detection for glucose and fructose could not be determined nor compared in this context. Chapter 5 will describe the electrochemical glucose sensing of BODIPY dyes **1b** and **2b**.

Chapter 5

Direct electrochemical detection of Glucose

5.1. BODIPY dyes used for electrochemical sensing

Novel BODIPY dyes functionalised with boronic acid moieties in the 3,5-positions of the BODIPY core structure were synthesised (**Figure 5.1**) and studied for direct glucose sensing using fluorescence and electrochemistry. A great number of the previously studied glucose biosensors use enzymes such as GOx for the detection of glucose. This chapter describes the direct, enzymeless detection of glucose using BODIPYs **1b** and **2b**. Phenylboronic acid was conjugated to the BODIPYs because it has a high affinity towards saccharides. In this study, it is used as a bioreceptor to bind directly to glucose molecules. Selectivity was addressed through the use of a *bis*-boronic acid system and tested by the addition of sucrose and fructose into the sample matrix. The boronic-acid-substituted 3,5-distyrylBODIPY dyes that were studied were immobilised onto the working electrode, and the glucose detection properties were analysed using various electrochemical techniques. The results described in this chapter have recently been published in a peer reviewed journal [241].

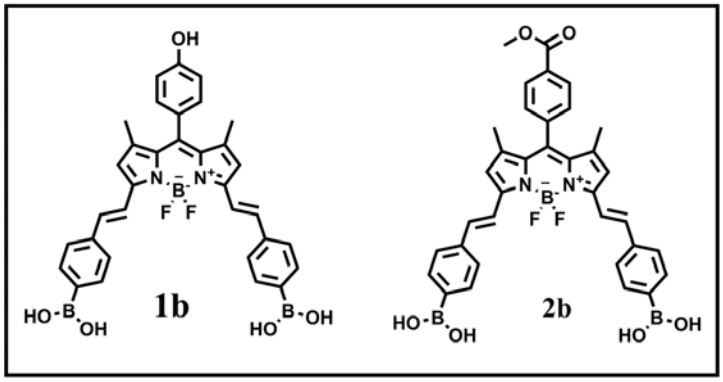

Figure 5.1: The molecular structures of the dyes used to detect glucose electrochemically

5.2. Electrochemical characterisation

The electrochemical properties of BODIPY dyes have not been studied in depth because relatively little work has been carried out in this field. However, it is recognised that their electrochemical properties depend on the nature of the α, β and *meso*-position substituents [123]. The redox properties of BODIPY dyes are well documented by Nepomnyashchii and Bard, who explain that BODIPY dyes exhibit reduction and oxidation waves mainly due to the addition or removal of electrons to or from the π-system [123]. This study represents the first time that BODIPY dyes have been used for the direct electrochemical detection of glucose.

The redox activity of **1b** and **2b** were investigated using cyclic and differential pulse voltammetry. **Figure 5.2** illustrates two voltammograms obtained for **1b**. The DPV technique is typically more sensitive than CV [189, 190]. The peaks obtained indicate that **1b** has three reduction reactions, two of which are reversible, and two reversible oxidation reactions, while **2b** has three reversible reduction and three oxidation steps, only two of which are reversible. The peak potentials for reduction reactions for **1b** occurred at −1.89, −1.55 and −0.40 V for R1, R2, R3, respectively, and the oxidation reactions lie at 0.00 and 0.33 V for O1 and O2, respectively, **Figure 5.2.** The peak potentials for the reduction reaction processes of **2b** were observed at −1.83, −1.33 and −0.73 V, while the oxidation processes lie at 0.12, 0.36 and 1.37 V.

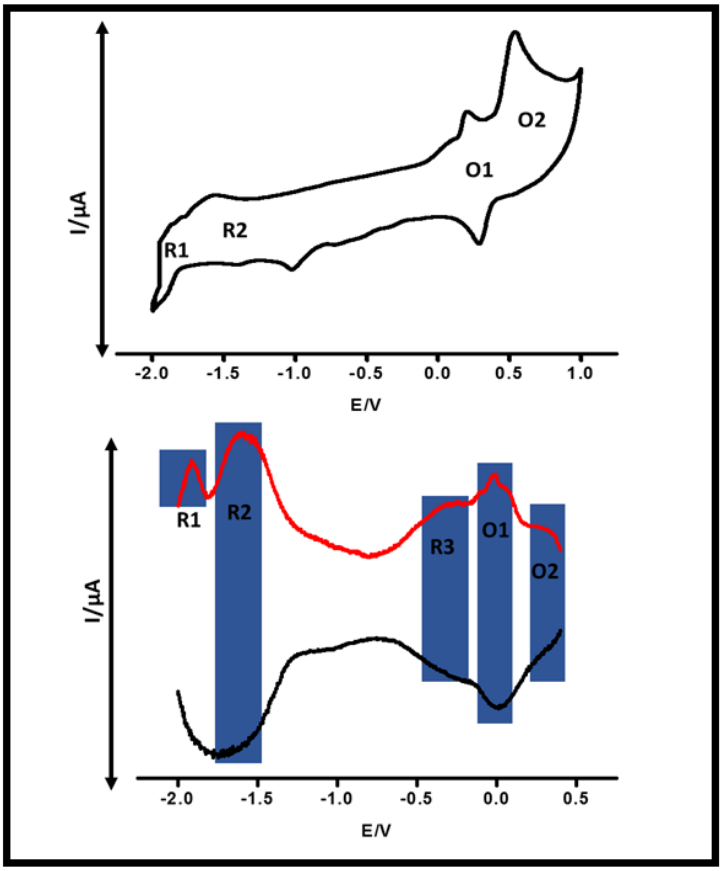

Figure 5.2: (A) Cyclic and (B) differential pulse voltammograms for **1b** obtained at 0.3 mM in DMF using $TBABF_4$ as the supporting electrolyte.

5.3. Characterisation of the modified electrodes

Glassy carbon electrodes were used as the working electrode of choice. The bare glassy carbon electrodes (GCE-**bare**) were modified using **1b** and **2b** following the drop-coating procedure described in Chapter 2 forming GCE-**1b** and GCE-**2b** [247]. BODIPY dyes **1b** and **2b** were used to modify the bare electrode in order to enhance the transfer of electrons and increase the selectivity of the electrode towards the detection of glucose. BODIPY dyes have a near planar π-conjugation system due to the two pyrrole units being held in a co-planar position by the tetrahedral geometry of the boron atom. This geometry enables the dyes to easily adsorb onto the electrode surface through π-π stacking as has been reported for other porphyrin-related dyes such as phthalocyanines [177, 263, 264]. The modified electrodes were characterised by using the CV and SECM techniques.

5.3.1. Cyclic voltammetry

The electron transfer behaviour of the bare and modified electrodes was characterised by using cyclic voltammetry to study the use of the electrodes in a redox couple solution comprised of $[Fe(CN)_6]^{3/4-}$ in a 1 mM solution using 0.1 M KCl as the supporting electrolyte (**Figure 5.3**). The electrodes produced peak potential (ΔE_p) values that are indicative of their electron transfer abilities [265]. The ΔE_p value for GCE-**bare** was calculated to be 73 mV, while the ΔE_p values of GCE-**1b** and GCE-**1b** could not be determined due to the absence of peaks in the redox couple solution utilised.

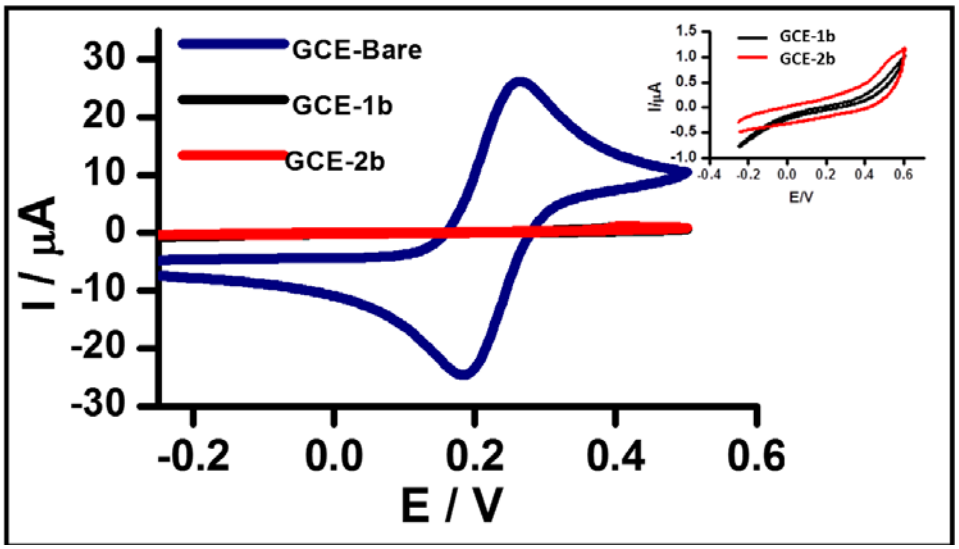

Figure 5.3: Cyclic Voltammograms of GCE-**Bare**, GCE-**1a** and (C) GCE-**2b** in 1 mM $[Fe(CN)_6]^{3/4-}$ with 0.1 M KCl at a scan rate of 100 mV/s.

Although these results indicate that the transfer of electrons was blocked, it does not mean that the electrodes cannot transfer electrons and detect the desired analyte [266]. SECM was used to investigate further why the ΔE_p could not be determined for the two modified electrodes.

5.3.2. Scanning electron microscopy

SECM was also used to characterise all three electrodes. The approach curves (**Figure 5.4**) were obtained in 5 mM $[Fe\ (CN)_6]^{3/4-}$ by using 0.1 M KCl as the supporting electrolyte. The curves illustrate the changes in the tip current of the UME as it is approached by the substrate using the Fe^{3+}/Fe^{2+} couple as a redox mediator. The UME has a hemispherical diffusion layer in solution [185-187, 263]. As the electrode is moved closer to the surface and the UME is approached, the hemispherical layer changes into a "convection style" redox reaction which results in an increase in current, if the surface is conductive [185-187, 263]. In contrast, if the surface is insulating, the

diffusion is hindered resulting in a decrease in current as is observed in **Figure 5.4** for a Teflon surface. It can be observed that the current increases as the tip approaches the GCE-**bare** electrode and hence this demonstrates that the electrode is a conductor, while in contrast GCE-**1b** and GCE-**2b** are both insulative since their current decreases. This is fully consistent with the CV results obtained in section 5.3.1.

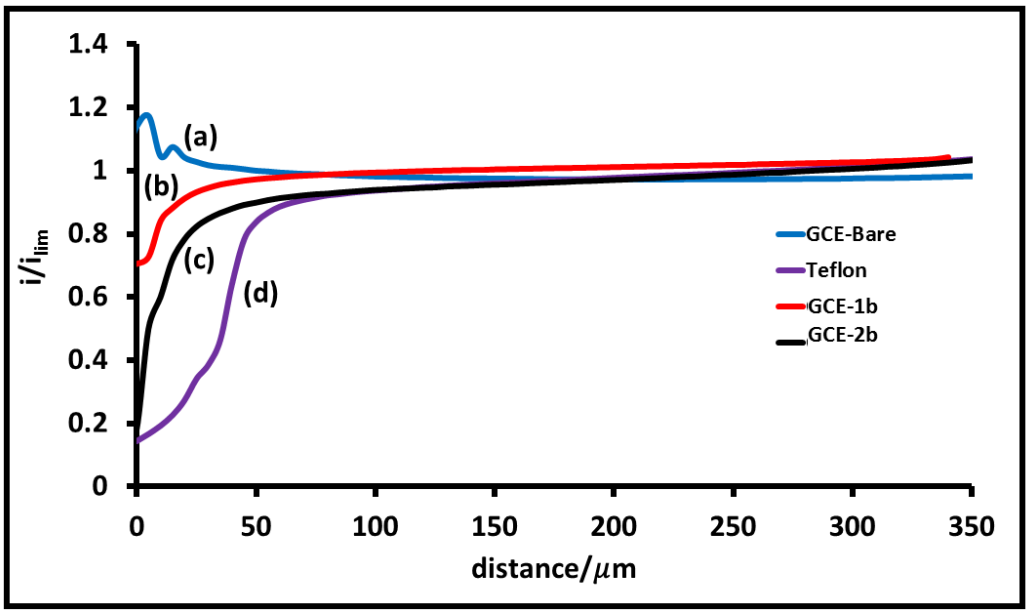

Figure 5.4: SECM approach curves for (a) GCE-**bare**, (b) GCE-**1b**, (c) GCE-**2b** and (d) non-conducting Teflon in 5 mM $[Fe(CN)_6]^{3/4-}$ in 0.1 M KCl.

5.4. Glucose detection

In this study, glucose was detected directly without the use of an enzyme. **Scheme 1.6** illustrates the binding mechanism between glucose and the boronic acid moieties. That principle is used in this study to quantify the detection of glucose using electrochemical techniques.

5.4.1. Differential pulse voltammetry

Differential pulse voltammetry is a highly sensitive electrochemical technique that can be used to analyse and detect analytes at very low concentrations. **Figure 5.5** contains the DPV scans obtained in 0.5 mM glucose solutions. It was observed that GCE-**bare** electrode did not show any response to the presence of glucose at the studied concentrations. However, the modified GCE-**1b** and GCE-**2b** electrodes were both able to detect glucose at a potential of ca. 0.22 V (**Table 5.1**). This indicates that the modification served its purpose and that the BODIPY dyes enhance the ability of the electrodes to detect glucose.

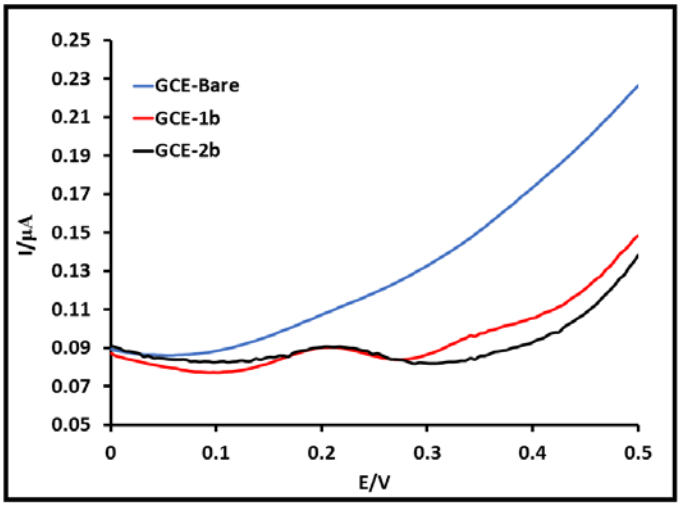

Figure 5.5: Differential pulse voltammograms of (blue) GCE-**bare**, (red) GCE-**1b** and (black) GCE-**2b** in a 0.5 mM glucose solution in pH 7.4 PBS with 0.1 M KCl as the supporting electrolyte.

5.4.2. Stability studies

Stability studies were conducted to determine the stability and reproducibility of the electrocatalysts analysed in this study, and to determine if there are any chemical changes that may occur in the reaction process and subsequently affect the accuracy of the results obtained. The reproducibility of the probes was investigated with 0.5 mM glucose solutions. A series of DPV scans were run. **Figure 5.6** shows the various scans obtained for (A) GCE-**1b** and (B) GCE-**2b**. It was observed that the GCE-**2b** response stabilised directly after the first scan, whereas with GCE-**2a** the peak only stabilised after the fourth scan. This means that **2b** is more suitable for repeated use as an electrocatalyst in quantitative sensor applications.

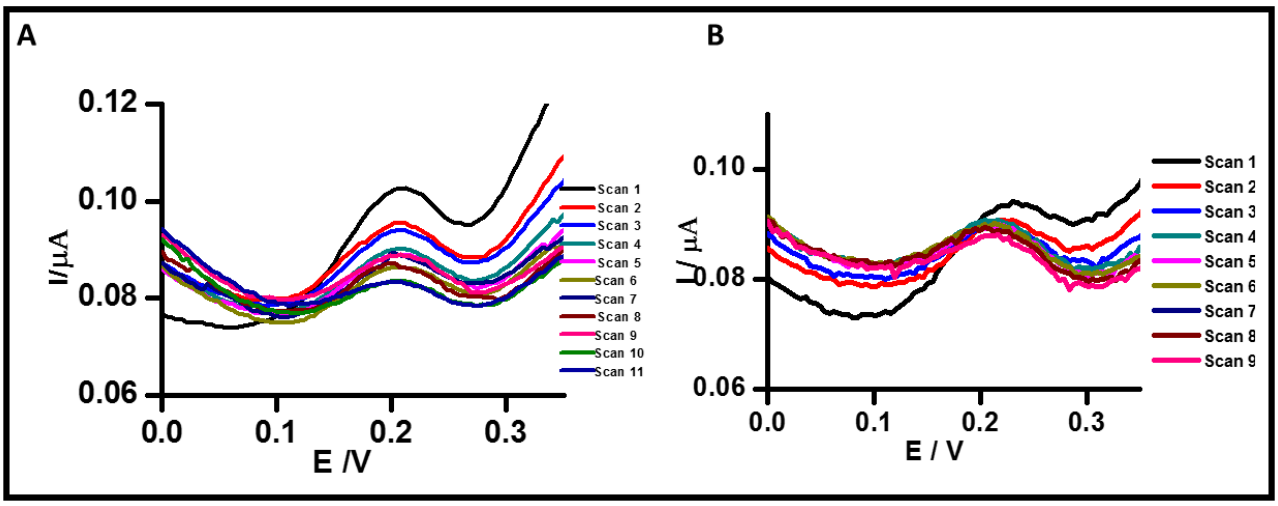

Figure 5.6: DPV scans for (A) GCE-**1b** and (B) GCE-**2b** in 0.5 mM glucose solutions in pH 7.4 PBS using 0.1 M KCl as the supporting electrolyte.

The relative standard deviation (RSD) for the potential peak currents was calculated in order to determine the level of precision in this study, since this provides a crucial factor in determining

the suitability of sensors for practical use, particularly in a biological context. The RSD value is defined as the ratio of the standard deviation (δ) to the mean (μ) as defined in **Equation 15**.

$$RSD = \frac{\delta}{\mu} \times 100 \quad (\mathbf{15})$$

The RSD values were calculated to be 3.2% and 2.5% for GCE-**1b a**nd GCE-**2b**, respectively.

5.4.3. Chronoamperometry

Figure 5.7 shows the chronoamperometric evolutions at various glucose concentration for GCE-**1b**. The first scan shown for GCE-**1b** is in the buffer solution alone (0 mM). Thereafter, an equivalent of 0.2 mM glucose was added and a run using the chronoamperometric technique on AutoLab. This was carried out consistently until a final concentration of 1 mM was reached. An increase in current was observed with increasing glucose concentration as would be expected. Chronoamperometry studies were conducted to determine the LoD of the electrocatalyst. This was achieved by plotting the various currents obtained from each scan against glucose concentration (inset). **Equation 16** was used to calculate the LoD.

$$LoD = \frac{3\delta}{S} \quad (\mathbf{16})$$

where δ, is the standard deviation derived from the chronoamperometry curve and S is the slope (selectivity) of the linear plot.

The calculated LoD values were determined to be 4.83 and 1.13 μM for GCE-**1b** and GCE-**2b**, respectively. These LoD values are comparable to those previously reported in the literature with phthalocyanine and graphene-coated electrodes as shown in **Table 5.1** [267, 268].

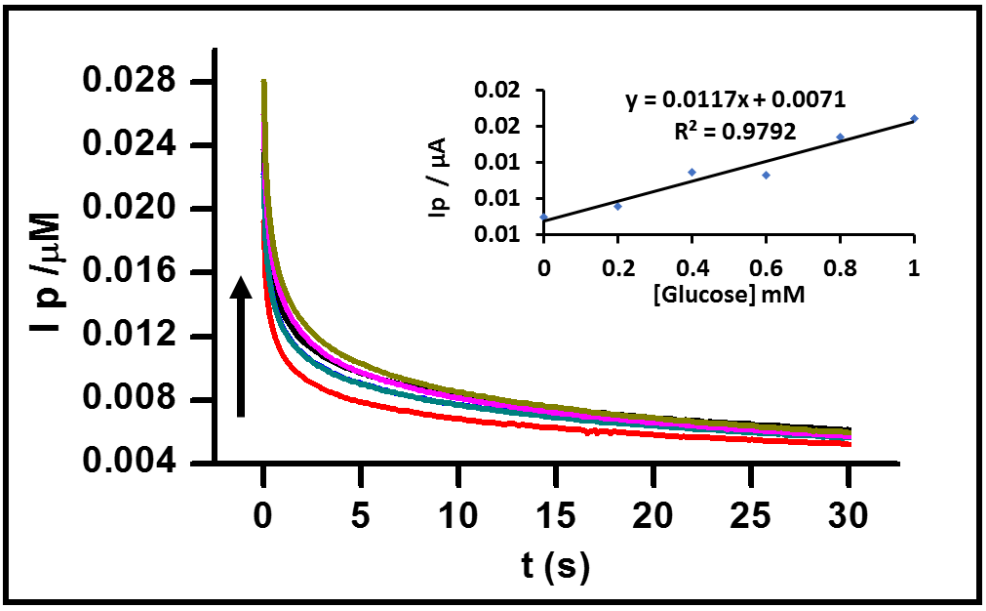

Figure 5.7: Chronoamperometric scans of GCE-**1b** at various glucose concentrations (0.0 mM – 1.0 mM), inset = current vs. glucose concentrations.

Table 5.1: A summary of the electrochemical data derived for different surfaces in a 0.5 mM glucose solution in 7.4 pH PBS with 0.1 M KCl as the supporting electrolyte.

Electrode [a]	Potential (V)	LoD (μM)	Linear range (mM)	Sensitivity	Reference
GCE-**bare**	---	---	---	---	This study
GCE-**1b**	0.22	4.83	0.1 – 1	0.0117 μA mM^{-1}	This study
GCE-**2b**	0.22	1.13	0.1 – 1	0.0013 μA mM^{-1}	This study
GCE-CoPc-$(CoTPP)_4$	---	10	up to 11	0.0242 μA mM^{-1}	[267]
Cu_2O/GNs	0.6	3.3	0.3 – 3.3	200 μA mM^{-1} cm^{-2}	[268]
Cu_2O nanocubes	0.6	5.9	0.3 – 3.3	285 μA mM^{-1} cm^{-2}	[268]
NiO HHS-Nafion/GCE	0.49	1.2	0.5 – 4.5	1052.8 μM mM^{-1} cm^{-2}	[269]
FAD-PABA	0.5	240	1.0 – 17	5.94 μA mM^{-1}	[270]
ABBA/PSA/PSSA electrospun fibers	--	750	0.75 – 14	--	[271]
Poly(aniline boronic acid)	--	--	3.4 – 20.4	--	[272]
MPBA/AuNPs/pDA/Au–PB/Au	--	0.05	0.0001 – 0.0135	--	[273]

[a] The nomenclature used for the electrodes is described in more detail in references [267-273].

5.4.4. Interference studies

Boronic acid has an affinity for carbohydrates. Most boronic acid applications depend upon the ability of boronic acid to bind to carbohydrate (1,2 and 1,3 *cis*-diols). There are numerous carbohydrates and other molecules that are found in biological systems that might potentially interfere with the detection of glucose and thus affect the results obtained from the detection of glucose in the whole blood. Therefore, it is of great importance to determine the influence that these molecules have when detecting for glucose. In this study, we determined the impact of fructose and sucrose (**Figure 5.8**). The DPV scans indicate that very little change in the peak potential separation of glucose in the presence of studied interferences was observed. The ΔE_p value obtained was still suitable for the detection of glucose. The sensor system maintained a high sensitivity towards glucose as the interferences exhibited negligible oxidation currents and no extra peaks were observed.

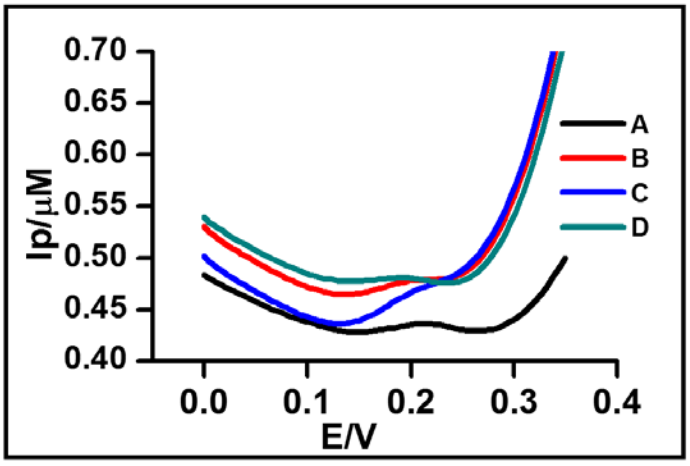

Figure 5.8: DPV scans for the GCE-**2b** electrode with (A) 0.5 mM glucose, (B) 0.5 mM glucose and 1 mM fructose, (C) 0.5 mM glucose and 1 mM sucrose and (D) 0.5 mM glucose, 1 mM fructose and 1 mM sucrose solutions in 7.4 pH PBS with 0.1 M KCl as a supporting electrolyte.

5.5. Summary

The synthesis of novel BODIPY dyes functionalised with boronic acid substituted styryls at the 3,5-positions was successful, and the compounds were characterised by UV-visible absorption, FT-IR and ^{1}H NMR spectroscopy and mass spectrometry. The dyes were used as electrocatalytic probes for the direct detection of glucose. The modification of the electrodes with the synthesised dyes was analysed by cyclic voltammetry and SECM. The detection ability of the electrodes was determined using DPV and chronoamperometry. The dyes were found to be suitable for use in the determination of glucose, since the detection limits obtained were 1.13 and 4.83 µM for **2a** and **2b**, respectively, and the dyes were found to be selective for glucose as potential interferences were found to have negligible effects on the detection.

Chapter 6

Nonlinear optical parameters of BODIPY dyes and porphyrins

6.1. BODIPY dyes and porphyrins in NLO

Molecular dyes with extended π-conjugated systems characteristically possess large electronic polarizabilities. Thus, conjugated molecules are expected to have substantial hyperpolarizability values, particularly second-order hyperpolarizabilities. According to the literature, molecules with donor and acceptor separated by a π-conjugation system exhibit unusually large third-order susceptibility, which increases the rate of response of the materials [215, 274, 275]. Structural modification of BODIPY dyes particularly at the 1,3,5,7-positions through the addition of styryls results in the extension of the π-conjugation system can form dyes of this type. The red-shift of the main absorption band of BODIPY dyes **1b** and **2b**, results in weaker absorbance in the visible region, thus making the dyes potentially suitable for use as optical limiters. The large energy gap between the S_1 and S_2 states of the dyes (**Chapter** 7) also favours the use of the dyes in optical limiting, since this means that there is relatively weak absorbance across most of the visible region under ambient light conditions. A significant RSA response is anticipated on the nanosecond timescale, if the cross-sections of the S_1 and/or T_1 excited states are greater than that of the ground state.

Structural modifications to porphyrin ligands, such as substitution at the peripheral positions and the addition of a central metal ion, can enhance their suitability for study as optical limiting materials [226, 276]. The porphyrins in this study have B bands that lie between 418–430 nm. The highest energy of the four Q bands of free base porphyrins **H_2TTP** and **H_2TPP** lie at 532 and 513 nm, respectively. Further modification of the free bases yielding Sn(IV) porphyrins **7-10**

resulted in a shift of the Q bands, thus little or no absorption was observed in the visible region and most especially at 532 nm, which is the second harmonic of the Nd:YAG laser.

In this study, the NLO properties of 3,5-distyrylBODIPY dyes **1b** and **2b** with phenylboronic acid groups attached to the styryls at the 3,5-positions and tristyryl-BODIPY **6** with hydroxyl groups introduced in a similar manner at the 3,5,7-positions were studied in solution (DCM and Benzene) and in the solid state when embedded in polystyrene thin films. A series of four Sn(IV) porphyrins **7-10** were also synthesised with varying *meso*-substituents (thienyl or phenyl), and axial ligands (*tert*-butylphenyl or pyridine) and these dyes were studied in benzene. These dyes were all studied as possible optical limiters by using the second harmonic of Nd/YAG laser at 532 nm.

6.2. BODIPY dyes embedded in thin films

BODIPY dyes **1b**, **2b** and **6** were studied in solution and polymer thin films. The dyes were mixed with polystyrene (the method is explained in Chapter 2, section 2.5) and drop coated to form thin films. The ground state absorption spectra of the dyes are provided in **Figure 6.1**. The main absorption bands of the dyes remain largely unchanged, especially in the spectrum of **6**. However, there is evidence of some band broadening related to aggregation, and a redshift of the main absorption bands is also observed.

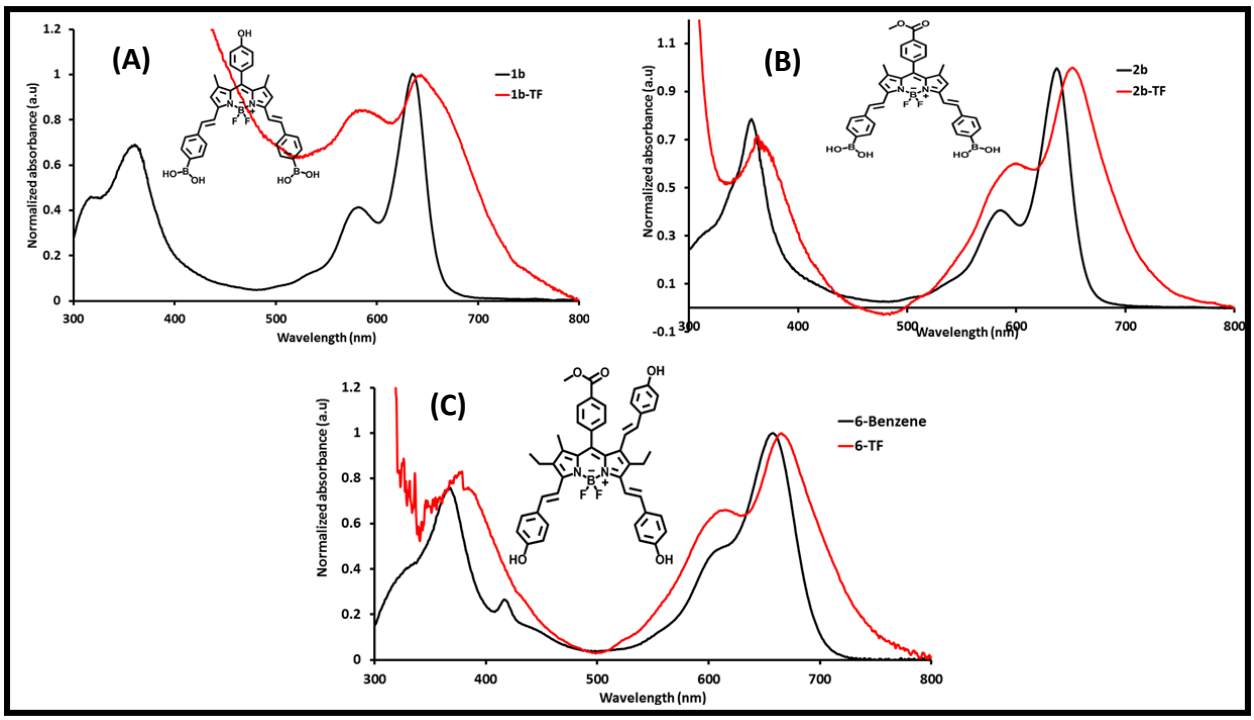

Figure 6.1: UV-visible absorption spectra of (A) **1b**, (B) **2b** and (C) **6**. The spectra were recorded in benzene solution (black) and when embedded in thin films (red).

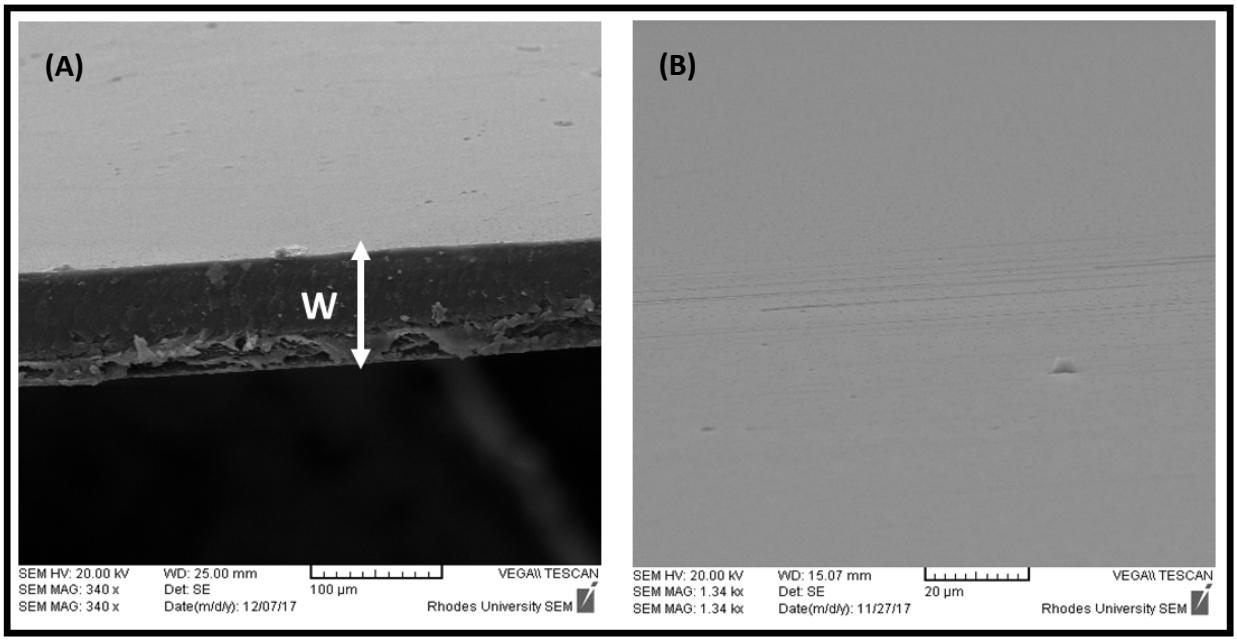

Figure 6.2: SEM images of the thin films embedded with BODIPY dyes illustrating (A) where the width of the film is measured, and (B) the surface of the thin film.

The surfaces of the polymer thin films were studied **(Figure 6.2)** by using scanning electron microscopy; the technique was used to determine the width (thickness) of the films which is required for the optical limiting parameter calculations. The surface and texture of the thin films were found to be smooth (**Figure 6.2B**). The thickness of the film embedded with **1b** was determined to be *ca.* 12.5 µm on average, while those with **2b** and **6** had thicknesses of ca. 13 and 15 µm, respectively.

6.3. Nonlinear optical parameters

In this study, the nonlinear optical parameters were determined using the open aperture Z-scan technique and the setup described in Chapter 2, with 10 and 7 ns excitation pulses used for the BODIPY dyes and porphyrins, respectively, at a wavelength of 532 nm. Most measurements were carried out in solution and the optical limiting properties of BODIPY dyes **1b**, **2b** and **6** were also studied in the solid state. The efficiency of the studied samples was described using four key parameters; i) the effective nonlinear absorption coefficient, β_{eff}, ii) the imaginary third-order susceptibility, $Im[\chi^{(3)}]$, iii) the second order hyperpolarizability, γ, and iv) the limiting intensity, I_{lim}, and these parameters were calculated using the method described by Sheik-Bahae [231, 232, 234]. The values obtained are summarised in Table 6.1.

6.3.1. Nonlinear absorption coefficients and reversible saturable absorption mechanism

The nonlinear absorption coefficient is an important parameter that is used to determine whether materials have the potential to be used as nonlinear absorbers for optical limiting. It provides a measure of the nonlinear absorptivity of molecules, which on the nanosecond timescale is usually observed due to the population of an excited state that absorbs more strongly than the ground state [231, 277]. The β_{eff} values are obtained on the basis of the calculations that would normally be used for two-photon absorption on the femtosecond timescale. The presence of an RSA profile during open aperture Z-scan measurements is used to determine if materials have the potential to be utilised as optical limiters, due to the transfer of electronic molecules from the ground state to strongly absorbing S_1 and/or T_1 excited state [211, 227, 278]. For

materials with positive nonlinear absorption, an RSA profile results in their transmittance decreasing as they approach the zero position in the Z-scan instrument [279, 280].

Figures 6.3-6.6 show the open aperture Z-scan signals of the dyes that were studied. The curves obtained show a convex structure which is due to the decrease in transmission along the z-axis. The Z-scan results were used to calculate β_{eff} values (**Table 6.1**), by fitting the data to Equations 4–11. β_{eff} is calculated using Equation 11. No obvious trend was observed in the comparison of the two solvents used with regards to BODIPYs **1b** and **2b**. However, the β_{eff} values obtained in thin films are higher than those obtained in solution. This is important for practical applications and is probably related primarily to there being higher concentrations of the dye in the thin films. The samples in thin films were slightly aggregated as observed in **Figure 6.4**.

Unlike other molecules analysed in this study, porphyrin **8** did not show a reversible saturable absorption profile but also exhibited saturable absorption at lower input fluence values. The saturable absorption may be associated with aggregation of the dye and nonlinear scattering [211, 218], and merits further in-depth investigation. Despite having a lower percentage transmittance, the porphyrins studied had higher β_{eff} values than the BODIPY dyes. The β_{eff} values obtained in solution in this study lie in the range reported for previously studied BODIPY dyes and porphyrins [8, 208, 277]. For compounds to be characterised as good optical limiters, they must reduce the transmittance by a minimum of 50% [277]. It is noteworthy that several of the dyes studied reduced transmittance by far more than 50%.

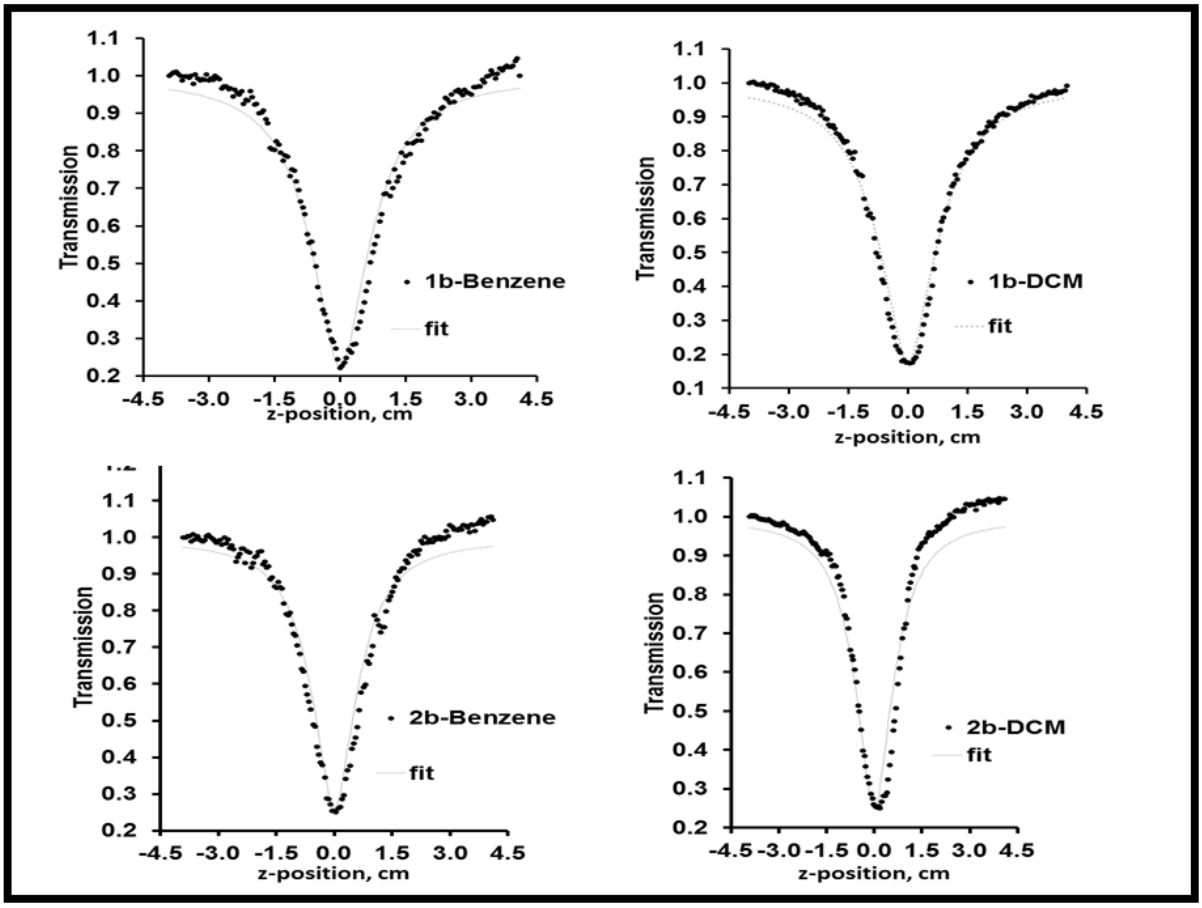

Figure 6.3: Open aperture Z-scan profiles of BODIPYs **1b** and **2b** in benzene and DCM.

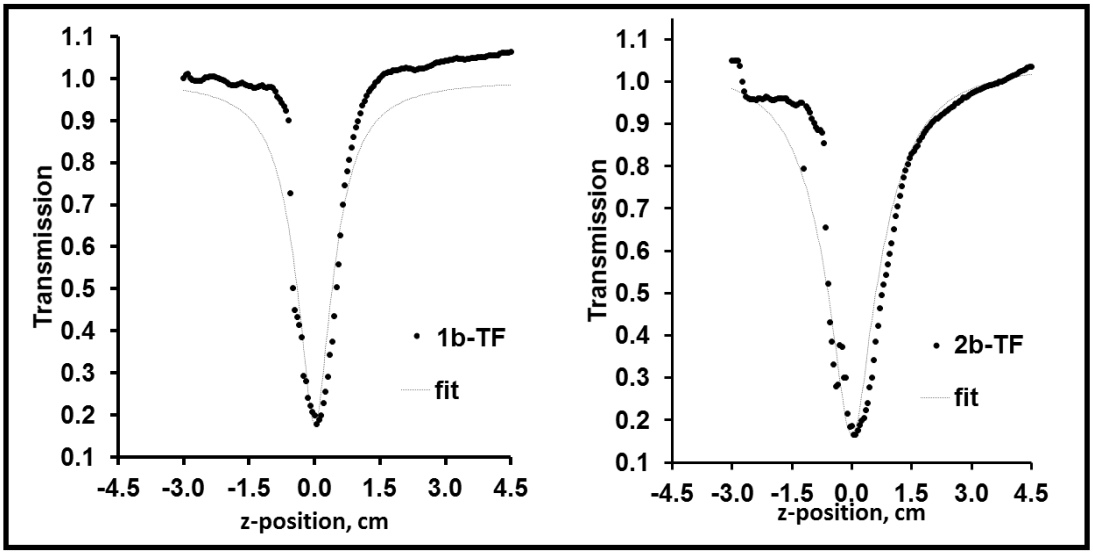

Figure 6.4 Open aperture Z-scan profiles of BODIPYs **1b** and **2b** in thin films.

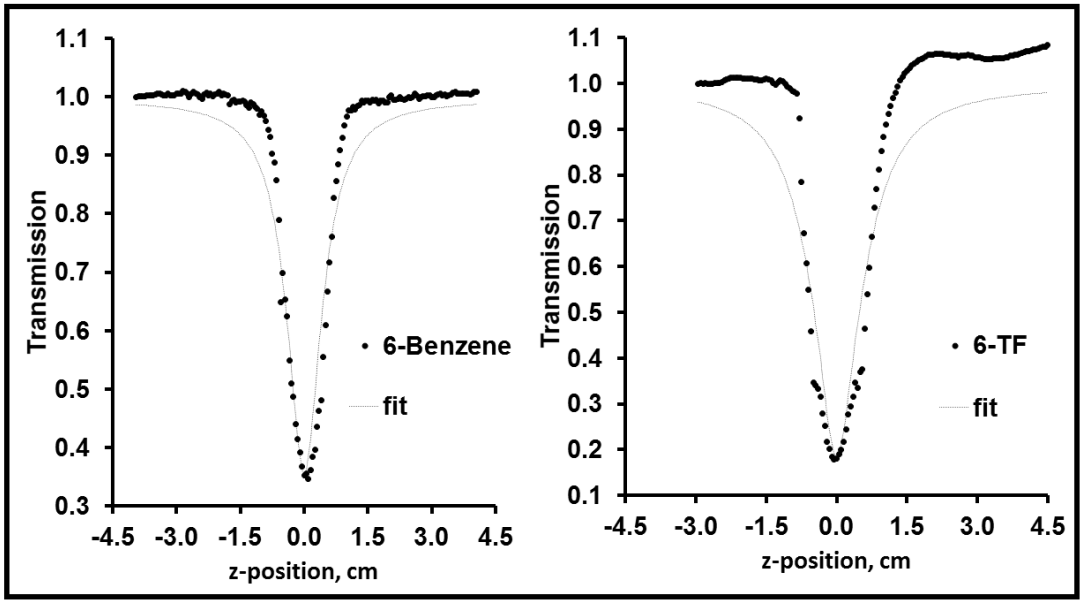

Figure 6.5: Open aperture Z-scan profiles of BODIPY **6** in benzene and thin film.

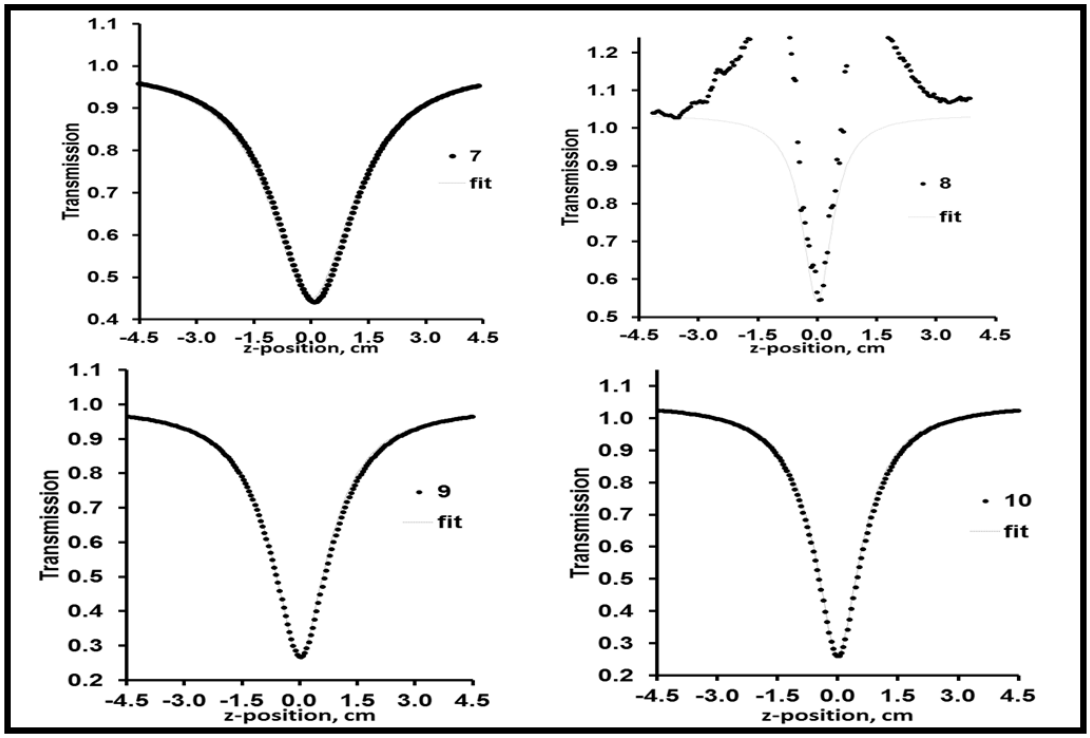

Figure 6.6: Open aperture Z-scan profiles of porphyrins **7-10** in benzene.

6.3.2. Second-order hyperpolarizability and third-order nonlinear susceptibility

The second order hyperpolarizability value is associated with the interaction of the permanent dipole of optical limiting material and the incident light [277, 278]. The γ values are summarised in **Table 6.1**. The values calculated for the samples in solution are well within the reported optimal range, 10^{-34}–10^{-29} esu [8]. An increase in the γ value results in an increase in the optical limiting behaviour of a material. The third-order susceptibility, is described as the measure of the rate of response of the material to the perturbation by an intense laser [277]. The calculated $Im[\chi^{(3)}]$ values for the dyes studied in this study are provided in **Table 6.1**. The values obtained lie within the reported range (10^{-8} to 10^{-15} esu) for optical limiting material [8, 277]. The values

obtained from the solid-state samples are higher than those of the samples in solution. This indicates that the solid-state samples are better optical limiters as they have a better, rapid, response. The γ and $l_m[\chi^{(3)}]$ values obtained for most of the dyes studied indicate that they could potentially be used as optical limiting materials.

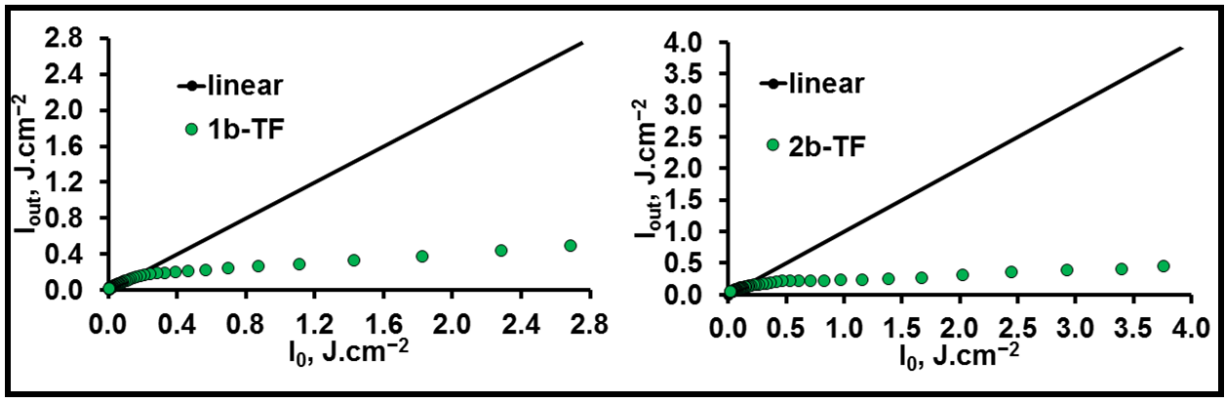

Figure 6.7: Input *vs* output fluence plots for BODIPYs **1b** and **2b** in polymer thin films.

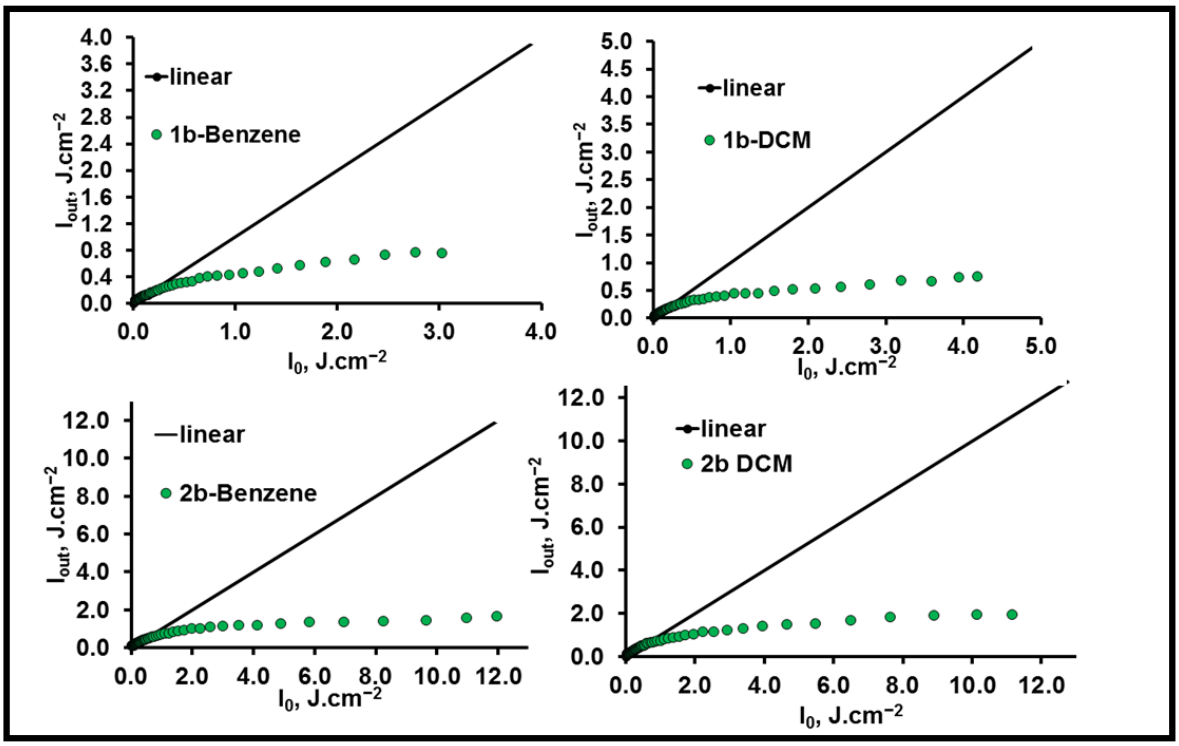

Figure 6.8: Input *vs* output fluence plots for BODIPYs **1b** and **2b** in benzene and DCM.

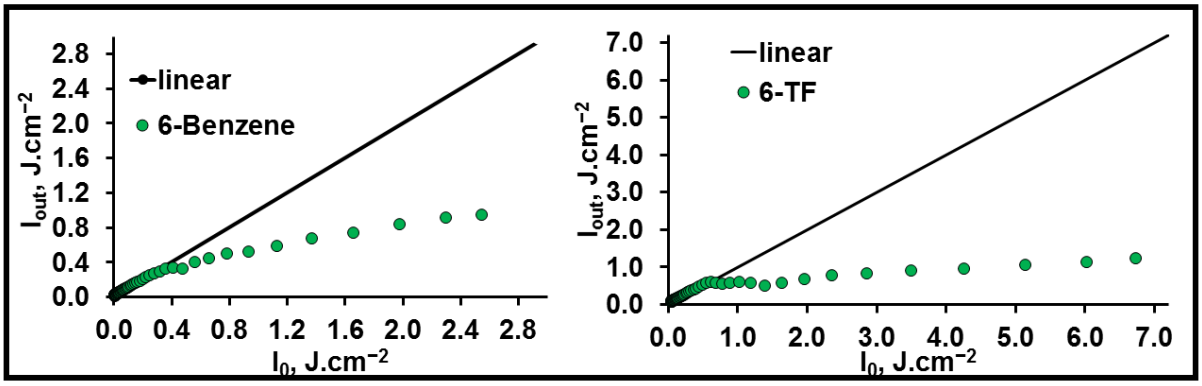

Figure 6.9: Input *vs* output fluence plots for BODIPY **6** in benzene and a polymer thin film.

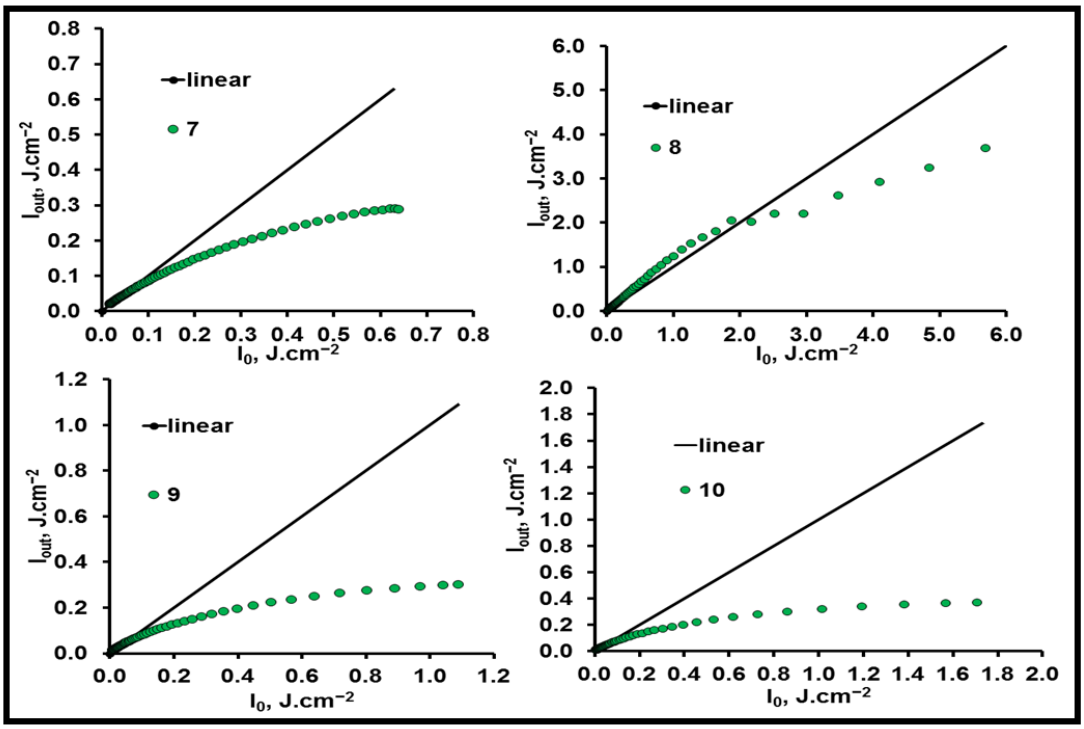

Figure 6.10: Input *vs* output fluence plots for porphyrins **7 – 10** in benzene.

6.3.3. Optical limiting threshold

The limiting threshold fluence, is defined as the input fluence at which the nonlinear transmittance is at 50% of the linear transmittance [239, 281]. Generally, nonlinear optical limiting materials should exhibit strong nonlinear behaviour at low I_{lim} values to respond effectively to incident laser pulses [239, 281]. The highest limiting threshold that is said to prevent significant harm to the human eye has been reported to be 0.95 J cm^{-2} [230]. Therefore, I_{lim} values obtained below a 0.95 J cm^{-1} input fluence provide a good indication of the ability of the material to function as an optical limiter [239, 282]. I_{lim} values are determined by plotting input fluence *vs.* output fluence (**Figures 6.7-6.10**) or transmission *vs.* fluence (**Figures 6.11-6.14**). The I_{lim} values

are summarised in **Table 6.1**. Porphyrin **8** showed very little nonlinear behaviour, since the dye remained close to the linear response line until ca. 2 J.cm^{-2} (**Figure 6.10**) and its transmittance did not decrease by at least 50%, so an I_{lim} value could not be calculated. BODIPYs **2b** and **6** showed the least favourable optical limiting behaviour in solution with regards to I_{lim} as the values obtained were above 0.95 J cm^{-1}. However, **2b** performed better in the solid state. Although **6** performed better in the polystyrene thin film, the I_{lim} value obtained was still above this target threshold value. The dyes possess stronger optical limiting properties in the solid-state due primarily to the higher concentration of the dyes in this context (**Table 6.1**).

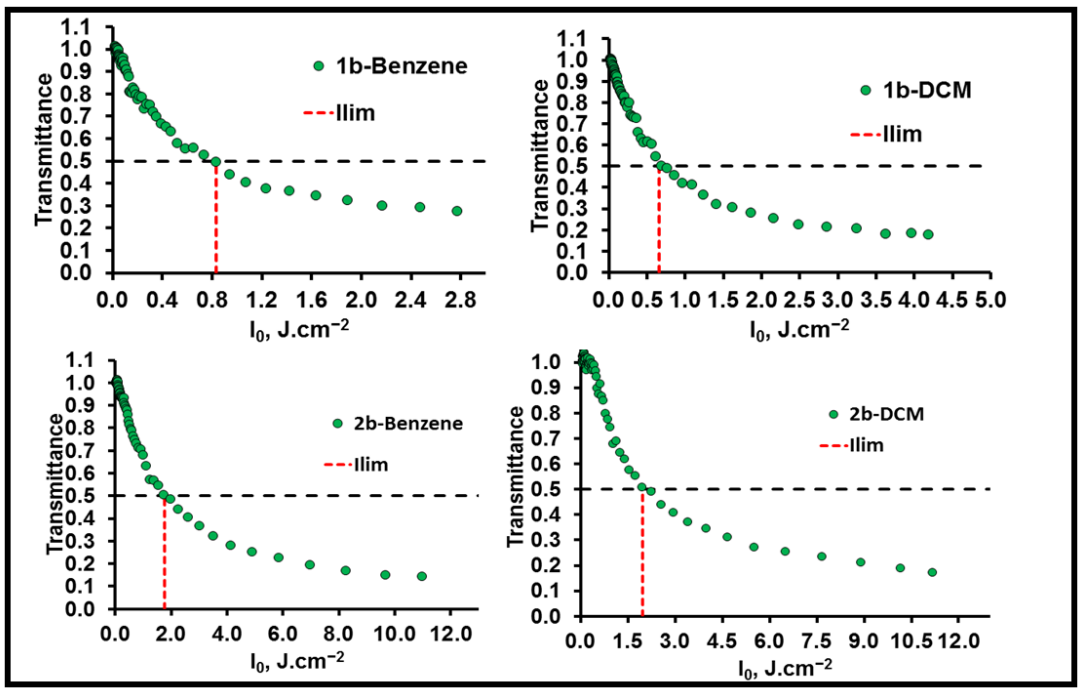

Figure 6.11: Normalised transmittance *vs* output intensity plot of BODIPYs **1b** and **2b** in benzene and DCM. The calculation of the I_{lim} values is illustrated with horizontal black and vertical red lines.

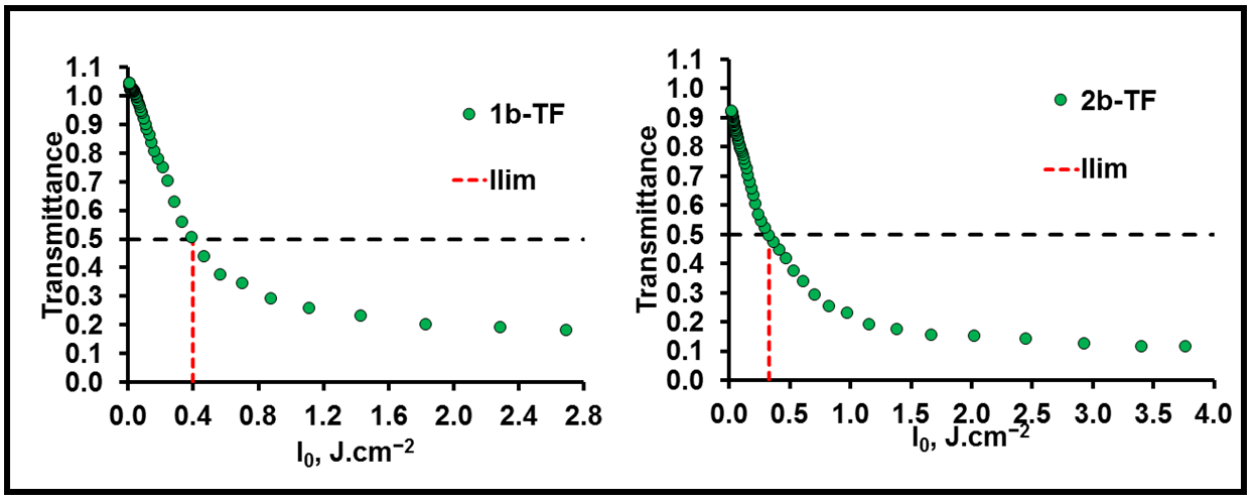

Figure 6.12: Normalised transmittance *vs* output intensity plot of BODIPYs **1b** and **2b** in polymer thin films. The calculation of the I_{lim} values is illustrated with horizontal black and vertical red lines.

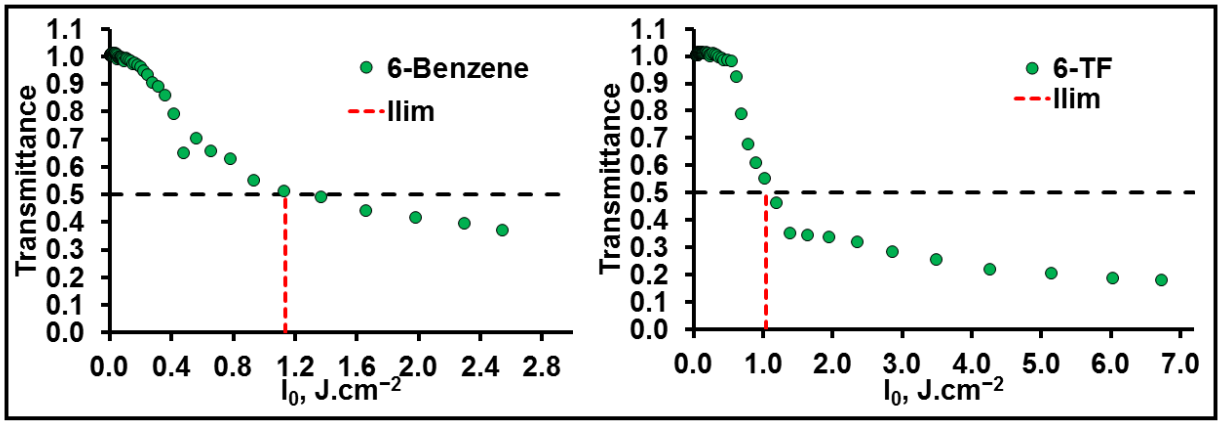

Figure 6.13: Normalised transmittance *vs* output intensity plot of BODIPY **6** in benzene. The calculation of the I_{lim} values is illustrated with horizontal black and vertical red lines.

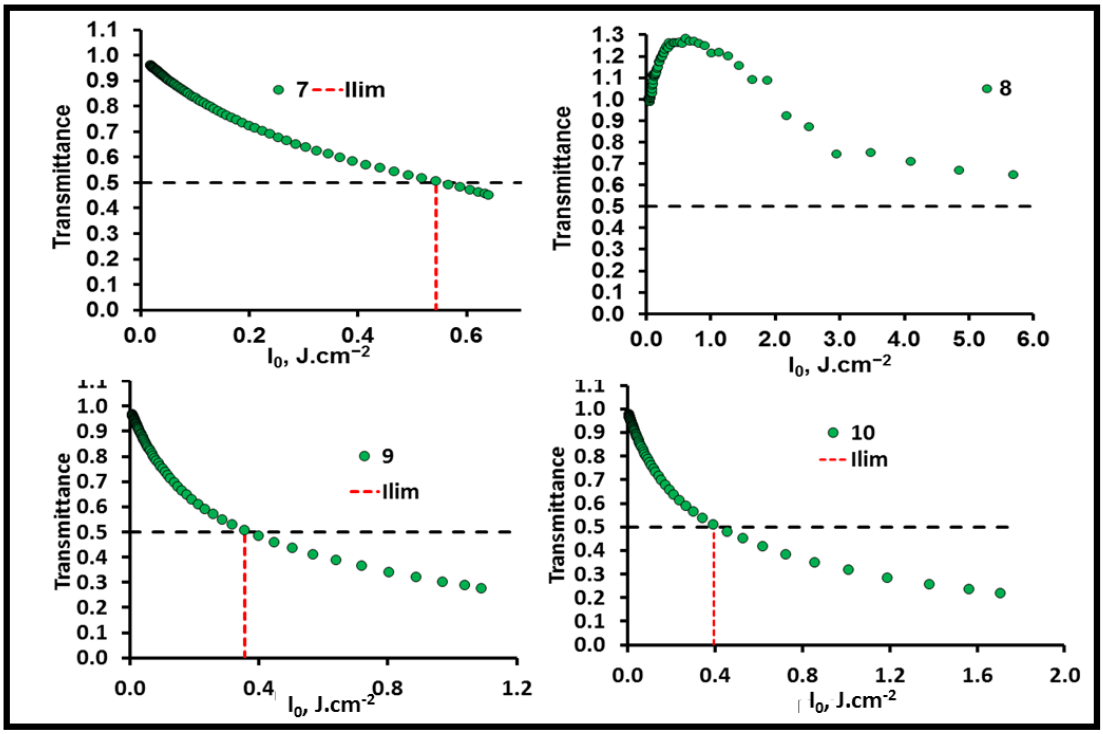

Figure 6.14: Normalised transmittance *vs* output intensity plot of porphyrins **7-10** in benzene. The calculation of the I_{lim} values is illustrated with horizontal black and vertical red lines.

Table 6.1: Nonlinear optical parameters of dyes studied

	Solvent	Conc. (M)	α (cm^{-1})	β_{eff} ($cm.GW^{-1}$)	$Im[\chi^{(3)}]$ (esu)	γ (esu)	I_{lim} ($J.cm^{-2}$)
1b	DCM	2.8×10^{-5}	5.18	331	7.2×10^{-10}	1.3×10^{-29}	0.66
	Benzene	3.0×10^{-5}	1.66	240	5.2×10^{-10}	8.9×10^{-30}	0.95
1b-TF	Thin Film	$\approx 2.3 \times 10^{-3}$	217	15000	1.9×10^{-8}	$\approx 2.6 \times 10^{-30}$	0.40
2b	DCM	2.6×10^{-5}	3.2	129	2.8×10^{-10}	5.5×10^{-30}	1.9
	Benzene	2.7×10^{-5}	2.28	130	2.9×10^{-10}	4.2×10^{-30}	1.8
2b-TF	Thin Film	$\approx 2.7 \times 10^{-3}$	112	8130	2.2×10^{-8}	$\approx 2.9 \times 10^{-30}$	0.33
6	Benzene	3.4×10^{-5}	0.806	144	3.5×10^{-10}	4.3×10^{-30}	1.1
	Thin Film	$\approx 4.2 \times 10^{-4}$	41	1000	1.9×10^{-9}	$\approx 2.9 \times 10^{-30}$	1.0
7	Benzene	6.5×10^{-5}	2.98	467	1.1×10^{-9}	2.0×10^{-30}	0.54
8	Benzene	9.0×10^{-5}	4.15	1.14	2.7×10^{-12}	5.0×10^{-33}	-
9	Benzene	1.1×10^{-5}	3.97	700	1.7×10^{-9}	6.5×10^{-30}	0.35
10	Benzene	4.7×10^{-5}	4.00	590	1.4×10^{-9}	1.3×10^{-29}	0.40

6.4. Summary

Extending the π-conjugation system of the BODIPY dyes by adding styryl substituents at the 3,5-positions for **1b** and **2b** and at the 3,5,7-positions for **6** shifted the main absorption band to the red decreasing the absorbance at 532 nm significantly hence enabling the dyes to the studied as possible optical limiters through the use of an open-aperture Z-scan instrument. The addition of appropriate aryl substituents to the *meso*-carbons to the porphyrin structure also red-shifted the Q-bands of the porphyrin, decreasing absorbance at 532 nm in a similar manner. The dyes were successfully studied at 532 nm using 10 and 7 ns pulsed Nd/YAG lasers. All dyes studied with the exception of **6** and **8** were found to have significant and favourable optical limiting activity. The dyes studied in polystyrene thin films exhibited more favourable nonlinear optical properties, which can be attributed to the higher concentrations present when the dyes were studied in the solid state, since the γ values obtained in solution and thin films are comparable. Further research is merited especially with regards to the use of thin films for the porphyrins studied.

CHAPTER 7

MOLECULAR MODELLING

7.1. Geometry optimisations and TD-DFT calculations

Molecular modelling studies were conducted to investigate the structure-property relationships, and spectral trends of the series of BODIPY dyes and porphyrins studied throughout this study using an approach described previously [9, 15]. The Gaussian 09 software package was used to conduct the calculations. Density functional theory (DFT) calculations were used to conduct the geometry optimisations by combining the Becke – 3-Parameter, Lee Yang and Parr (B3LYP) functional with the default SDD basis sets of the Gaussian program. The SDD basis sets provide a reasonable approximation for all atoms. In the context of the time-dependent density functional theory (TD-DFT) calculations, the B3LYP functional underestimates the energies of excitations with long-range change transfer character that frequently occur in the case of π-extended BODIPY dyes [283]. TD-DFT calculations were therefore carried out with the Coulomb-attenuated B3LYP (CAM-B3LYP) functional in order to accurately determine the main trends in the electronic absorption spectra of the dyes synthesised and characterised in this study. The CAM-B3LYP function has a long-range correction for the exchange potential. This is achieved by combining the hybrid B3LYP function with increasing a Hartree-Fock (HF) fraction as the interelectronic separation increases [283, 284].

7.2. Molecular modelling of the BODIPY dyes

This section explores trends in the electronic absorption spectra of the BODIPY dyes studied and the effect of the different types of structural modification on the properties of these dyes.

The HOMO→LUMO one-electron transition provides the dominant contribution to the main absorption bands of the **1-5a** and **1-5b** series of BODIPY dyes (**Table 7.1**). The trends predicted in the TD–DFT calculations for the main spectral bands of the dyes were hence found to be associated with changes in the energies of the HOMO and LUMO. In **Table 7.1**, it can be observed that changes in the *meso*-phenyl rings of the BODIPY core do not have a significant effect on the HOMO–LUMO band gap or on the spectral properties of the dyes. Consequently, the wavefunction, the band energies and oscillator strengths of the main spectral bands are similar for all of the dyes studied in the **1-5a** series. The trends observed in the calculated HOMO–LUMO gaps of the dyes were consistent with the experimental observations. Substitution at the *meso*-position has very little effect on the properties of the respective dyes because the *meso*-aryl rings lie orthogonal to the plane of the BODIPY core due to the steric hindrance caused by the methyl groups at the 1,7-positions. This results in relatively poor π-conjugation, so changes in the structure of the *meso*-phenyl substituent have little or no impact on the MO energies, since there is only an inductive rather than a mesomeric interaction.

Figure 7.1 provides the angular nodal patterns of the HOMO and LUMO of the BODIPY dyes studied. The frontier MOs of all of the dyes in the **1-5a** series are similar in this regard. BODIPY dyes have rigid planar conformations after complexation with BF_2. The HOMO and LUMO of the

dyes are well separated from the other MOs (**Figure 7.2**).

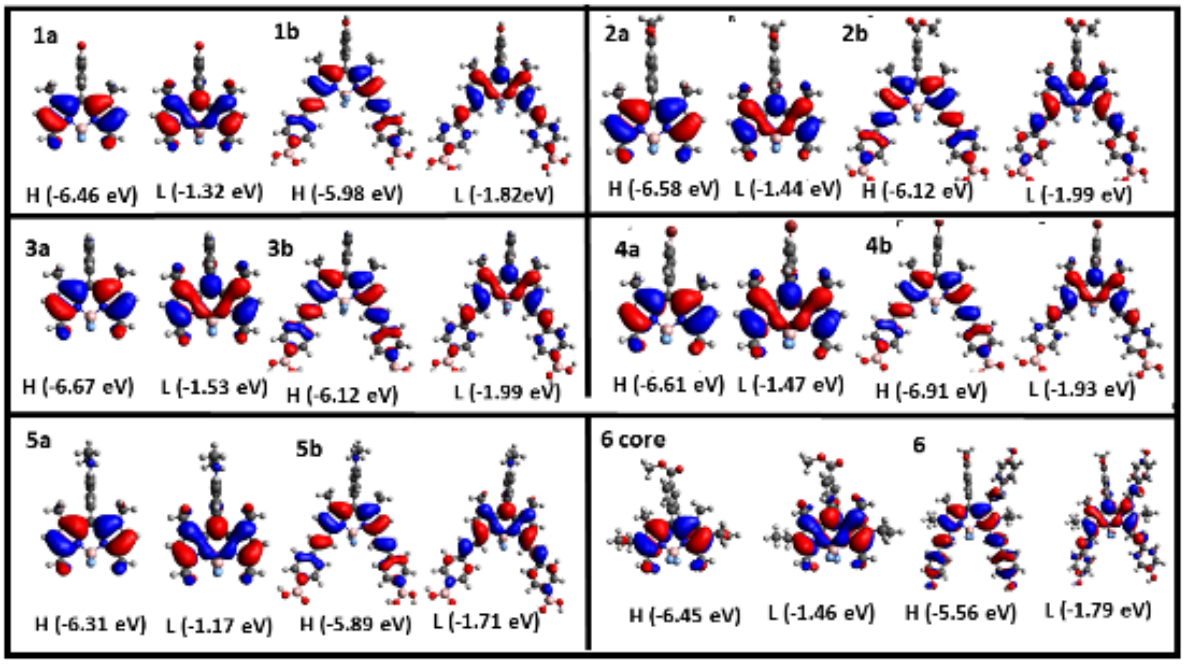

Figure 7.1: Angular nodal patterns at an isosurface value of 0.02 a.u. and MO energies of the LUMO and LUMO of the BODIPY dyes at the CAM-B3LYP/SDD level of theory.

BODIPY core dyes **1-5a** were structurally modified through the addition of styryls at the 3,5-positions to form the **1-5b** series of BODIPY dyes and at the 3,5,7-positions to form **6**. Upon styrylation of the BODIPY cores, a red-shift of the main absorption and emission bands is observed (**Figure 7.3**). The addition of styryls has a greater effect on the HOMO than on the LUMO. The HOMO undergoes a relative destabilisation due to the mesomeric effect of the electron donating styryl groups, since it has larger MO coefficients at the 3,5-positions than the LUMO (**Figures 7.1** and **7.2**). The relative destabilisation of the HOMO results in a narrowing of the

HOMO–LUMO band gap and thus in the observed red-shift in the main absorption bands. The experimental data are consistent with the theoretical calculations in this regard (**Table 7.1**).

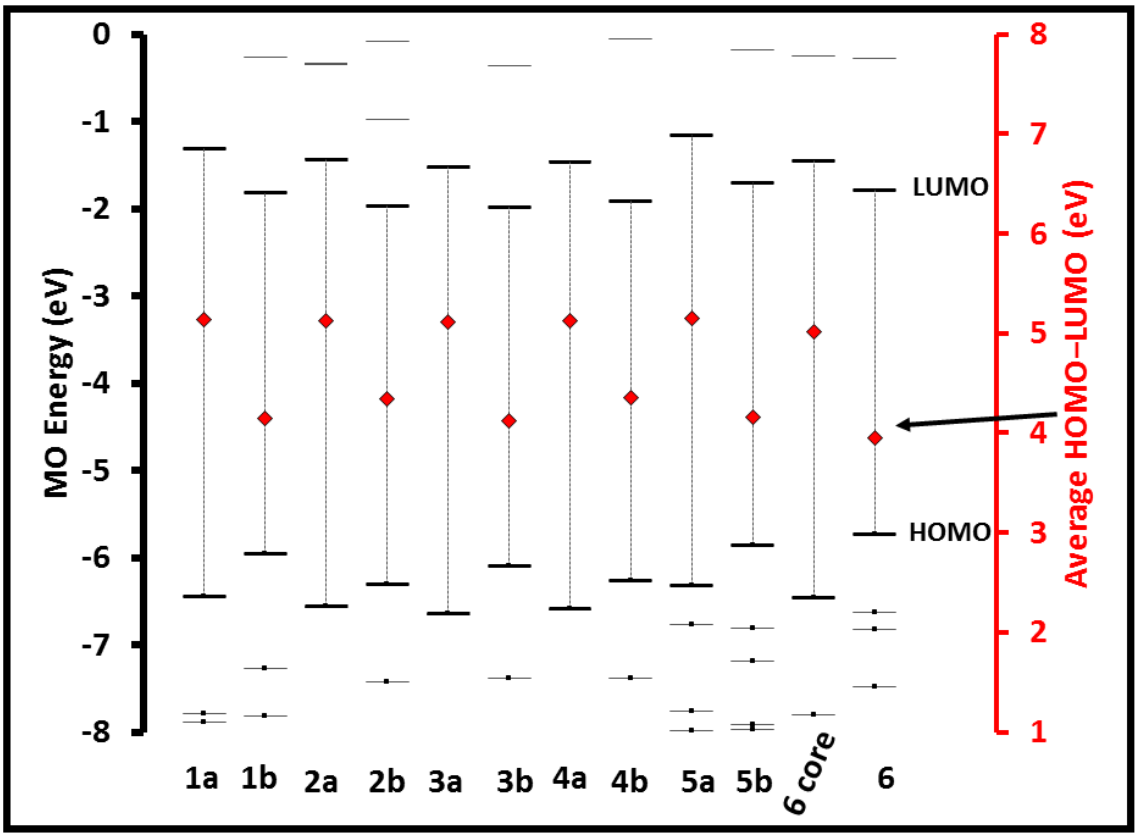

Figure 7.2: Frontier MO energies and HOMO–LUMO gaps of the BODIPY dyes at the CAM-B3LYP/SDD level of theory. The HOMO and LUMO are highlighted with darker lines. The red diamonds denote the HOMO–LUMO band gaps, and are plotted against the secondary axis. Occupied MOs are highlighted with small black squares.

The absence of MOs that are localised on the boronic-acid-substituted styryl moieties close in energy to the HOMO and LUMO of the ***b*** series of dyes in **Figure 7.2** accounts for there being no fluorescence "turn-on" mechanism related to the binding of a glucose molecule in Chapter 4.The research of Shen and co-workers [284] on a fluorescence probe for hypoxic cell imaging provides a recent example of how an ICT effect associated with a nitro substituted styryl group at the 3-position can occur when there is an MO localised on the styryl group that lies close in energy to the HOMO or LUMO of the BODIPY core. This consequently results in a fluorescence "turn-on" after an amino substituted styryl group is formed at acidic pH. It was initially hoped that something similar would occur with dyes **1-5b**. The addition of styryls on the ***a*** series of dyes results in a large red-shift of the main absorption bands of the dyes (**Figure 7.3**), which decreases the absorption of the dyes in the visible region, and particularly at 532 nm, since there are no excited states close in energy to the S_1 state. The large energy gap (**Figure 7.2**) between the S_1 and S_2 states of the **1-5b** series makes the dyes suitable for use as optical limiters, since there is relatively weak absorbance across most of the visible region under ambient light conditions

Table 7.1: Calculated and observed electronic excitation wavelengths of BODIPYs **1-5a**, **1-5b** and **6**, and their respective calculated oscillator strengths and wavefunction.

BODIPY	#[a]	E (eV)[b]	$\lambda_{(exp)}$[c]	$\lambda_{(calc)}$[d]	$\nu_{(calc)}$[e]	f[f]	Wavefunction[g]
1a	$S_0 \rightarrow S_1$	3.01	502	411	24.3	0.54	97% H → L; …
1b	$S_0 \rightarrow S_1$	2.32	633	533	18.7	1.04	97 % H → L; …
2a	$S_0 \rightarrow S_1$	3.01	503	412	24.3	0.54	97 % H → L; …
2b	$S_0 \rightarrow S_1$	2.31	635	536	18.7	1.04	97 % H → L; …
3a	$S_0 \rightarrow S_1$	3.00	501	413	24.2	0.54	97 % H → L; …
3b	$S_0 \rightarrow S_1$	2.31	645	536	18.7	1.04	97 % H → L; …
4a	$S_0 \rightarrow S_1$	3.00	501	412	24.3	0.54	97 % H → L; …
4b	$S_0 \rightarrow S_1$	2.32	633	536	18.7	1.07	97 %H → L; …
5a	$S_0 \rightarrow S_1$	3.02	504	411	24.4	0.53	97 %H → L; …
5b	$S_0 \rightarrow S_1$	2.33	632	532	18.8	1.03	97 %H → L; …
6 core	$S_0 \rightarrow S_1$	2.87	---	430	23.3	0.59	97 %H → L; …
6	$S_0 \rightarrow S_1$	2.19	658	565	17.7	1.04	96 %H → L; …

[a] – Number of the excitation state in ascending energy. [b] – Calculated band energies reported in eV. [c] – Experimental wavelengths obtained in DCM and recorded in nm. [d] – Theoretically calculated wavelengths in nm. [e] – Calculated band energies (10^3 cm^{-1}). [f] – Theoretically calculated oscillator strengths. [g] – MO wavefunctions based on eigenvectors predicted by TD-DFT calculation for the B3LYP geometries optimised using 6-31G(d) basis set. H and L = HOMO and LUMO, respectively.

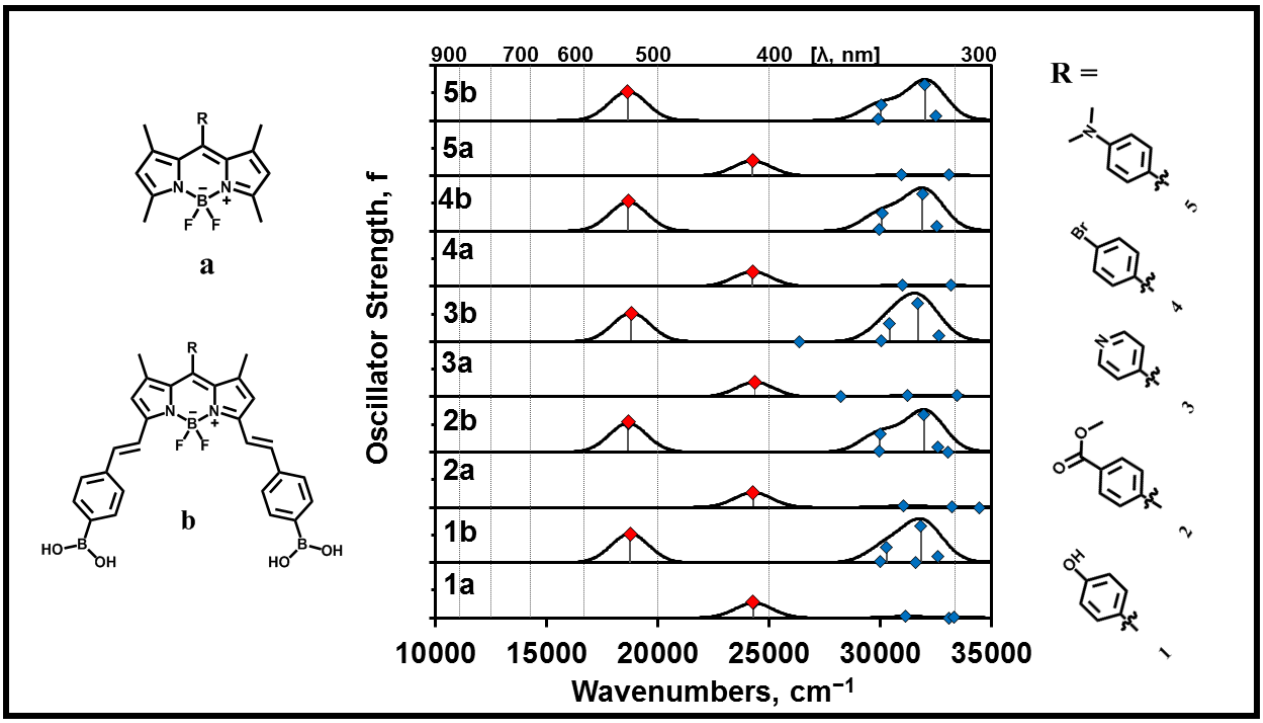

Figure 7.3: Calculated TD-DFT spectra for B3LYP optimised geometries for BODIPY dyes **1-5a** and **1-5b** at the CAM-B3LYP/SDD level of theory. The red diamonds highlight the main visible region absorption bands. The simulated spectra were generated using the Chemcraft program with a fixed bandwidth of 2000 cm^{-1} [285].

7.3. Molecular modelling of the porphyrins studied

The electronic structures and optical properties of porphyrins can be understood through an application of Gouterman's 4-orbital model (Chapter 1, section 1.2.2) [66, 70]. In this context, the π-system MOs are associated primarily with the 16 atom 18 π-electron inner ligand perimeter and can be viewed as being comparable to the MOs of a parent $C_{16}H_{16}^{2-}$ hydrocarbon perimeter. The MOs are arranged in an ascending energy order of M_L = 0, ±1, ±2, ±3, ±4, ±5, ±6, ±7, and 8, due to the destabilising effect of adding extra angular nodal planes. The HOMO and LUMO of the porphyrin ligand have M_L = ±4 and ±5 angular nodal properties, respectively. Excitation of electrons from the HOMO to the LUMO results in ΔM_L = ±1 and ±9 transitions, and hence in the intense allowed B bands and weaker forbidden Q bands at higher and lower energy, respectively (**Figure 7.4**). The calculated wavelengths and oscillator strengths of the major bands in the porphyrin spectra are summarised in **Table 7.2**.

In the context of Michl's perimeter model, the four frontier π-MOs derived from the HOMO and LUMO of the parent 16 atom 18 π-electron hydrocarbon are referred to as **a**, **s**, **-a**, and **-s** MOs (**Figure 7.5** and **7.6**), respectively [16, 286], since this simplifies the comparison of trends in the energies of MOs of dyes with differing symmetries. The **a** and **-a** MOs are aligned with a nodal plane along the y-axis, and the **s** and **-s** MOs have large MO coefficients at these positions (**Figure 7.5** and **7.6**). Substitution at the *meso*-positions of the porphyrin ligand has a direct effect on the spectral properties of a porphyrin, since this can affect the relative energies of the **a**, **s**, **-a**, and **-s** MOs. Tetrathienylporphyrins **7** and **9** have narrower average HOMO–LUMO band gaps than the analogous tetraphenylporphyrins (**Figure 7.7**) when all four of the MOs derived from the HOMO

and LUMO of the parent $C_{16}H_{16}^{2-}$ hydrocarbon perimeter are taken into account. This is due to the **s, -a**, and **-s** MOs of the *meso*-thienylporphyrins being more stabilised than the **a** MOs because of the larger MO coefficients at the *meso*-positions. This is consistent with the red-shift observed in the Q and B bands of the porphyrins with the thienyl rings in the *meso*-positions (**Figure 7.5**). The electronic properties of the porphyrins studied are summarised in **Table 7.2**.

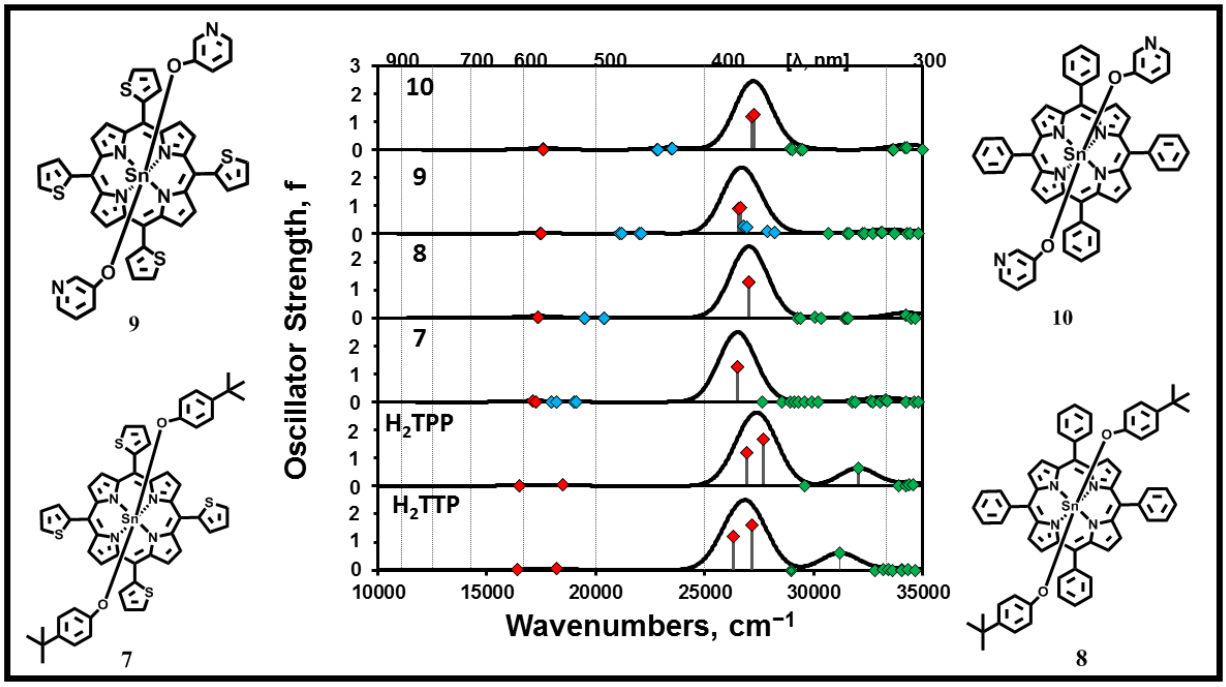

Figure 7.4: Calculated TD-DFT spectra for B3LYP optimised geometries for porphyrins **7-10** and their respective free bases at the CAM-B3LYP/SDD level of theory. Red diamonds highlight the Q and B bands of Gouterman's 4-orbital model [66, 70]. Blue diamonds highlight transitions from MOs localised on the axial ligands that lie close in energy to the **a** and **s** MOs in **Figure 7.7** into the **-a** and **-s** MOs. The simulated spectra were generated using the Chemcraft program with a fixed bandwidth of 2000 cm^{-1} [285].

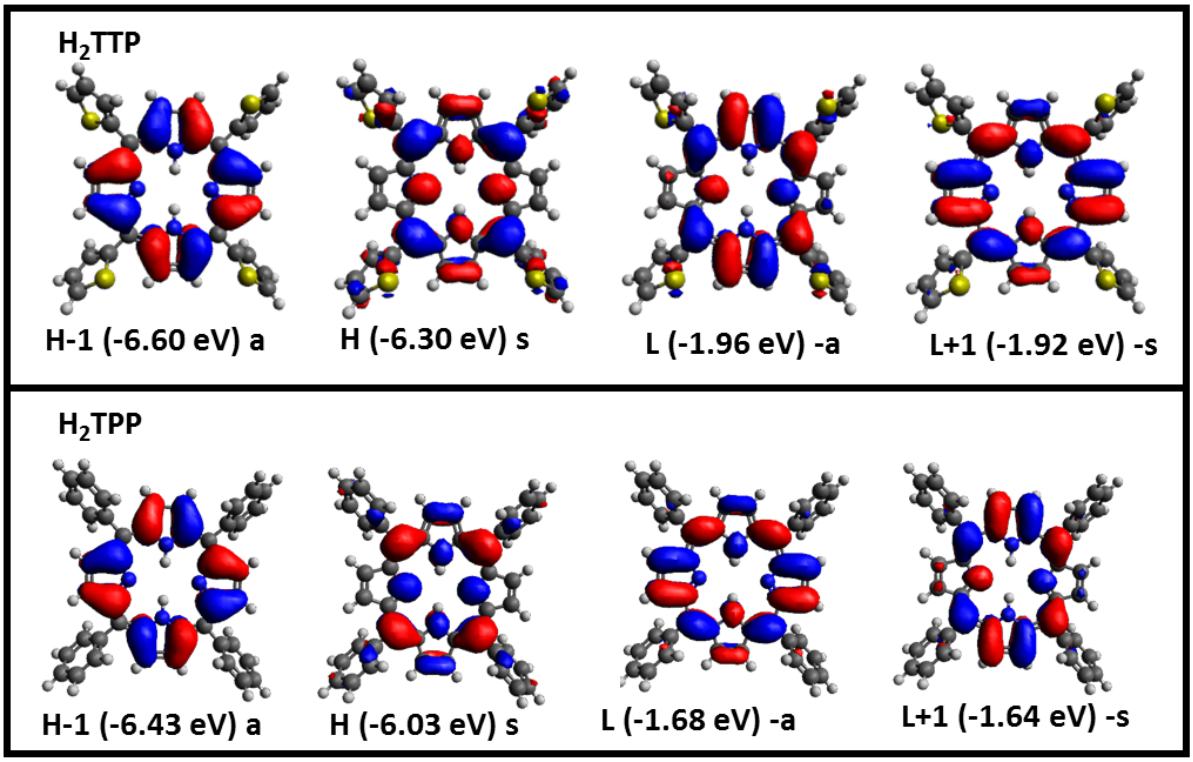

Figure 7.5: Angular nodal patterns at an isosurface value of 0.02 a.u. and MO energies of the **a**, **s**, **-s**, and **-s** MOs for free base porphyrins, **H_2TTP** and **H_2TPP**, at the CAM-B3LYP/SDD level of theory.

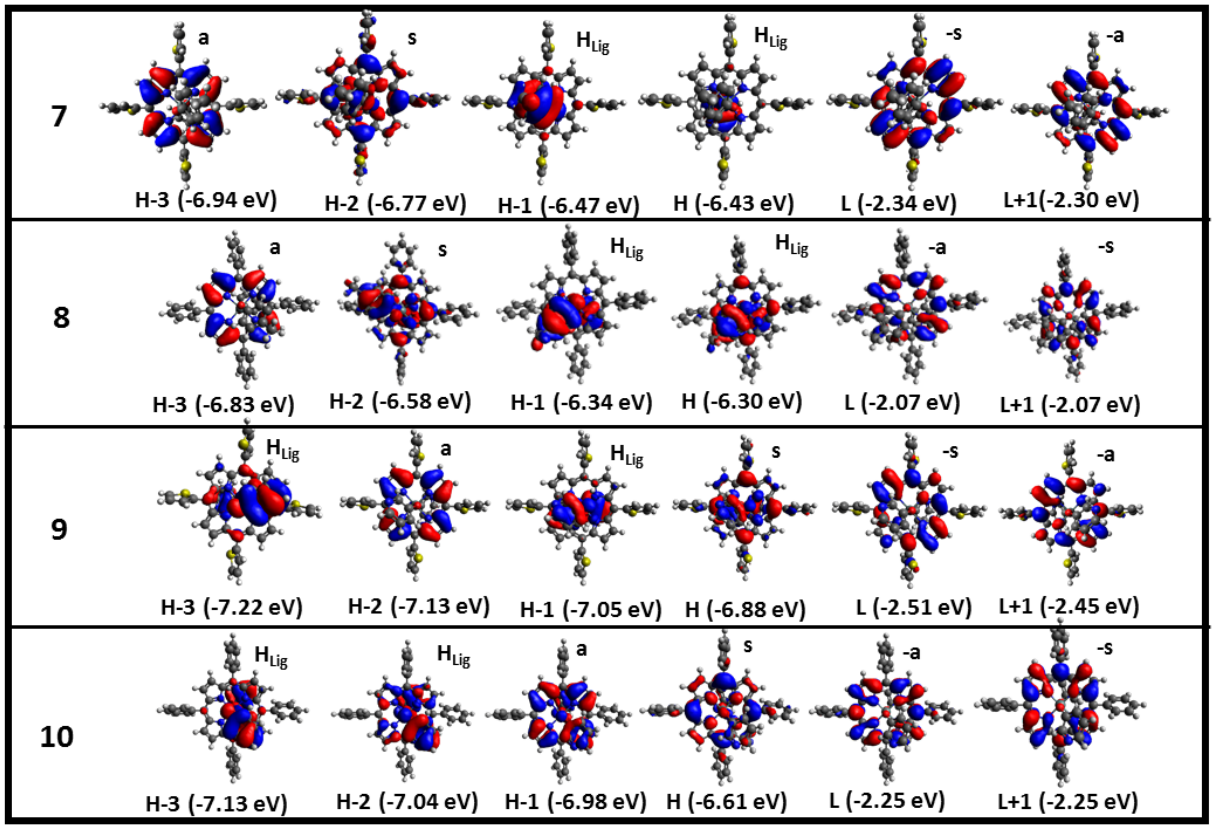

Figure 7.6: Angular nodal patterns at an isosurface value of 0.02 a.u. and MO energies of the **a**, **s**, **-s**, and **-s** MOs for porphyrins **7-10** at the CAM-B3LYP/SDD level of theory. L and H are used to denote the LUMO and HOMO MOs, respectively, and lig as a subscript denotes an MO that is localised on the axial ligands.

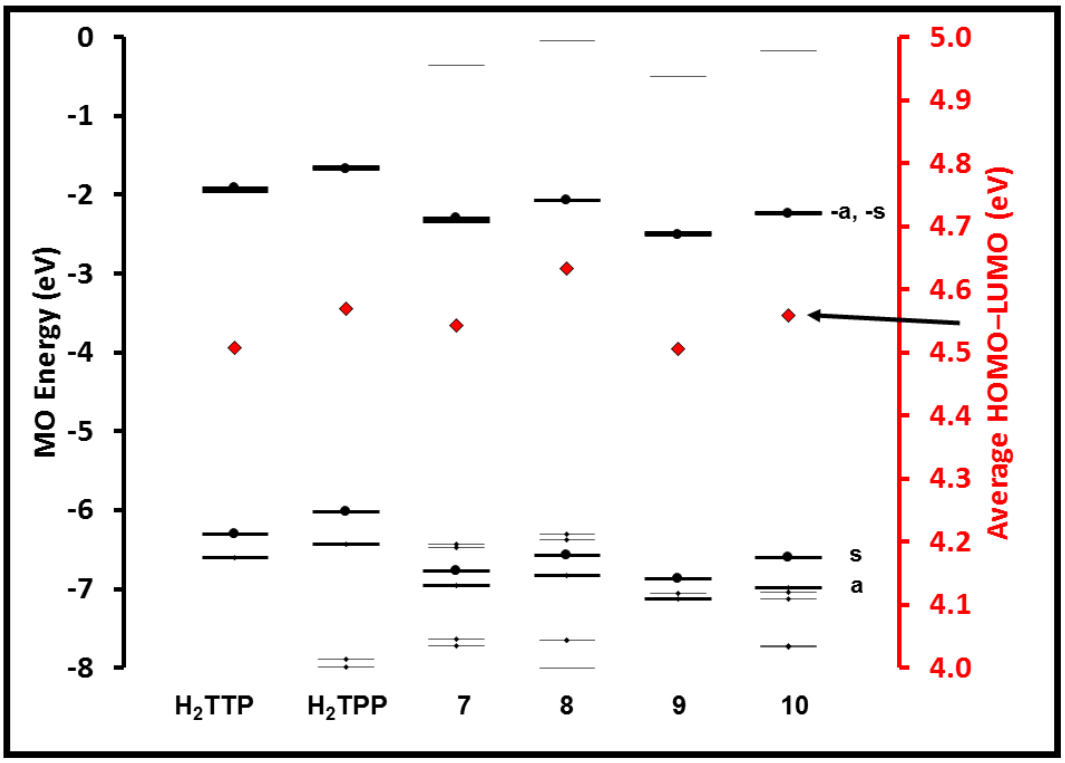

Figure 7.7: Frontier MO energies and HOMO–LUMO gap values for porphyrins **7-10** and their respective free base porphyrins (**H_2TTP** and **H_2TPP**) at the CAM-B3LYP/SDD level of theory. The **a**, **s**, **-a** and **-s** MOs are highlighted with solid black lines. The **s** and **-s** MOs are highlighted with black circles. Red diamonds denote the average HOMO–LUMO band gaps when the **a**, **s**, **-a** and **-s** MOs that are derived from the HOMO and LUMO of the $C_{16}H_{16}^{2-}$ parent hydrocarbon perimeter are all taken into account. The average HOMO−LUMO gap values are plotted against a secondary axis. Occupied MOs are highlighted with small black squares.

Table 7.2: Calculated and observed electronic excitation wavelengths of the free base tetraphenylporphyrin (**H_2TPP**) and tetrathienylporphyrin (**H_2TTP**) model compounds and porphyrins **7**-**10** and their calculated wavelengths, oscillator strengths and wavefunctions.

		#[a]	E (eV)[b]	$\lambda_{(exp)}$[c]	$\lambda_{(calc)}$[d]	$\nu_{(calc)}$[e]	f[f]	Wavefunction[g] =
H_2TTP	Q	1	2.03	660	610	16.4	0.015	59% **s**→**-s**; 40% **a**→**-a**; …
	Q	2	2.26	562	548	18.2	0.044	60% **s**→**-a**; 39% **a**→**-s**; …
	B	3	3.26	428	380	26.3	1.21	55% **a**→**-a**; 33% **s**→**-s**; …
	B	4	3.37		368	27.2	1.63	60% **a**→**-s**; 40% **s**→**-a**; …
H_2TPP	Q	1	2.05	644	606	16.5	0.029	65% **s**→**-s**; 35% **a**→**-a**; …
	Q	2	2.29	548	540	18.5	0.039	61% **s**→**-a**; 39% **a**→**-s**; …
	B	3	3.34	418	371	26.9	1.21	60% **a**→**-a**; 29% **s**→**-s**; …
	B	4	3.43		361	27.7	1.68	61% **a**→**-s**; 40% **s**→**--a**; …
7	Q	1	2.12	617	584	17.1	0.024	29% **s**→**-s**; 24% **a**→**-a**; 24% **H^{Lig}**→**-a**; 23% **H^{Lig}**→**-a**; …
	Q	2	2.14		580	17.2	0.017	34% **s**→**-a**; 26% **a**→**-s**; 19% **H^{Lig}**→**s**; 18% **H^{Lig}**→**-s**; …
	B	7	3.29	437	377	26.5	1.24	52% **s**→**-s**; 36% **a**→**-a**; …
	B	8	3.29		377	26.5	2.25	50% **s**→**-a**; 39% **a**→**-s**; …
8	Q	1	2.15	602	577	17.3	0.035	31% **a**→**-s**; 13% **s**→**-a**; 53% **H^{Lig}** →**-a**; …
	Q	2	2.15		577	17.3	0.034	31% **a**→**-a**; 13% **s**→**-s**; 53% **H^{Lig}**→**-s**; …
	B	7	3.35	422	370	27.0	1.28	52% **a**→**-a**; 26% **s**→**-s**; …
	B	8	3.63		342	39.3	1.28	52% **a**→**-s**; 26% **s**→**-a**; …
9	Q	1	2.16	613	573	17.4	0.020	52% **a**→**-s**; 36% **a**→**-a**; …
	Q	2	2.16		572	17.5	0.015	50% **a**→**-a**; 37% **a**→**-s**; …
	B	7	3.29	441	376	26.6	0.885	30% **a**→**-a**; 17% **H^{Lig}**→**-a**; 13% **H^{Lig}**→**-s**; 13% **a**→**-s** ;10% **a**→**-s;** …

	B	8	3.31		375	26.7	0.946	29% **a**→**-s**; 14% **a**→**-a**; 13% $\mathbf{H^{Lig}}$→**-s**; 12% $\mathbf{H^{Lig}}$→**-s**; 10% **a**→**-a**; …
10	Q	1	2.18	598	569	17.6	0.034	63% **s**→**-s**; 29% **a**→**-a**; …
	Q	2	2.18		568	17.6	0.026	62% **s**→**-a** ;29% **a**→**-s;** …
	B	7	3.37	426	368	27.2	1.18	39% **a**→**-s**; 28% **s**→**-a**; 16% $\mathbf{H^{lig}}$→**-a**; 14% $\mathbf{H^{Lig}}$→**-s**; …
	B	8	3.38		366	27.3	1.28	40% **a**→**-a**; 28% **s**→-s; 16% $\mathbf{H^{Lig}}$→**-a**; 15% $\mathbf{H^{Lig}}$→**-s**; …

[a] – Number of the excitation state in ascending energy. [b] – Calculated band energies reported in eV. [c] – Experimental wavelengths obtained in DCM and recorded in nm. [d] – Theoretically calculated wavelengths in nm. [e] – Calculated band energies (10^3 cm^{-1}). [f] – Theoretically calculated oscillator strengths. [g] – MO wavefunctions based on eigenvectors predicted by TD-DFT calculation for the B3LYP geometries optimised using 6-31G(d) basis set. **a**, **s**, **-s**, and -**a** are the respective energies of the MOs. H is used to denote the HOMO and lig as a superscript denotes an MO that is localised on the axial ligands.

7.4. Summary

DFT and TD-DFT calculations were successfully carried out and were used to establish the structure property relationships of the series of related BODIPY dyes and porphyrins that were studied. Trends identified in the calculations assisted in understanding the spectroscopic properties that were observed experimentally. The visualisation of the optimised geometries, MO energies and the nodal patterns provided explanations of the spectral phenomena observed, especially with regard to the effects of structural modifications to the BODIPY core and at the *meso*-positions of the porphyrin ligand. TD-DFT calculations can be used as a guide for the rational design of dyes for the various applications explored in this study and other dyes to be prepared and characterised in future.

Chapter 8

Conclusions and future work

8. 1 Conclusions

A series of BODIPY core dyes **1-5a** with different *meso*-substituents was successfully synthesised using a modified one-pot synthesis method. These BODIPY dyes were functionalised with boronic-acid-substituted styryl groups at the 3,5-positions by using a modified version of the Knoevenagel condensation reaction yielding a series of novel dyes **1-5b**. A series of novel axially ligated tetrathienyl- and tetraphenylporphyrins (**7-10**) was also prepared by inserting Sn(IV) ion into the central cavity. The addition of axial ligands above and below the ring through the insertion of a high valent metal ion, such as Sn(IV), hinders aggregation in solution making the dyes more suitable for applications. The successful syntheses of these dyes were confirmed by ^{1}H-NMR, FT-IR, and UV-visible spectroscopy, mass spectrometry and fluorimetry.

BODIPY dyes **1-5b** were functionalised with boronic acid moieties to make the dyes suitable for use as glucose biosensors. Boronic acid moieties have a high affinity towards saccharides and can hence be used as receptors in the molecular recognition of glucose [131, 137]. *Bis*-boronic acid dyes were prepared since it was hoped that this would enhance the selectivity of the biosensor towards glucose over other saccharides [131]. The sensor was investigated for glucose detection using fluorescence, colourimetric and electrochemical sensing techniques.

The fluorescence sensing did not work as anticipated since the dyes **1-5b** did not effectively detect glucose at physiological pH. An increase in the fluorescence intensity was expected upon the addition of glucose, and the intensity was expected to continue increasing with the concentration of glucose added to the sample. However, a decrease in the fluorescence intensity was instead observed, which can be attributed in part to systematic changes in the optical density

of the dyes upon interaction with glucose, since significant shifts were observed in the absorption and emission band wavelengths in this context. When pH and colourimetric studies were conducted, the results indicated that the dyes interacted with glucose at basic pH in a manner suitable for sensor applications based on optical spectroscopy, since a significant colour change was observed after the addition of glucose at pH 8.5–11. Since similar shifts are also observed in the presence of fructose, however, it is unlikely that a selective glucose sensor can be formed on this basis.

Electrochemistry was also used to investigate the sensing abilities of dyes **1b** and **2b**. The data obtained from the sensing experiments demonstrated that it was possible to detect glucose electrochemically at pH 7.4 when dye molecules were immobilised onto modified glassy carbon working electrodes. The LoD values were calculated to be 4.83 and 1.13 μM for **1b** and **2b**, respectively. Interference studies were conducted whereby sucrose and fructose were added into the sample matrix. It was found that their presence did not significantly affect the ability of the sensor dyes to detect glucose. Further research on this type of glucose sensor is clearly merited.

The addition of boronic-acid-substituted styryl groups leads to a red-shift of the main absorption band of the dyes and decreases the absorbance values for the dyes in the green region of the visible. This enables the dyes to be studied as potential optical limiters for the second harmonic of Nd:YAG lasers at 532 nm. Four important nonlinear optical parameters (second-order

hyperpolarizabilities, third-order susceptibilities, optical limiting thresholds and the nonlinear absorption coefficients) of BODIPYs **1b**, **2b** and **6** were studied in DCM and benzene. The dyes were mixed with polystyrene and embedded in thin films to investigate the feasibility of using the dyes in practical applications. The nonlinear optical parameters of the porphyrin molecules (**7**-**10**) were also studied in benzene. A red-shift of the Q-bands of tetrathienylporphyrins resulted in a decrease in the absorption relative to the analogous tetraphenylporphyrins under ambient light conditions at 532 nm, so the optical limiting properties of these dyes were also investigated at this wavelength. All of the dyes studied besides **8** showed favourable optical limiting behaviour. Generally, the dyes performed better in thin films, since the concentration of the dyes was significantly higher in this context. The results obtained demonstrate that the BODIPY and porphyrin dyes studied merit further in depth study for this application.

8.2. Future work

Suggestions for future work include:

(i) Design new BODIPY dyes through molecular modelling studies that have MOs localised on the boronic acid functionalised moieties that lie in close proximity to the HOMO or LUMO in energy terms in order to obtain an ICT or PET quenching mechanism, so that “turn-on” fluorescent sensing of glucose can be utilized to form a sensor.

(ii) The direct electrochemical study of similar saccharides (such as sucrose and fructose) and other possible molecules (such as uric acid and ascorbic acid) that might affect the selectivity and accurate detection of glucose. This would determine if dyes **1a** and **1b** are selective towards glucose.

(iii) The study of the nonlinear optical properties of Sn(IV) tetraarylporphyrins in thin films to investigate their practicality for applications and whether the porphyrins offer improved responses when embedded in polymer thin films.

(iv) Design new BODIPY dyes with push-pull structures in a rational manner and investigate their nonlinear optical behaviour.

References

[1] A. Treibs, and F. H. Kreuzer, "Difluorboryl-Komplexe von Di-und Tripyrrylmethenen," *Justus Liebigs Annalen der Chemie* **1968**, vol. 718, no. 1, pp. 208-223.

[2] A. Loudet, and K. Burgess, "BODIPY dyes and their derivatives: syntheses and spectroscopic properties," *Chemical Reviews* **2007**, vol. 107, no. 11, pp. 4891-4932.

[3] G. Ulrich, R. Ziessel, and A. Harriman, "The chemistry of fluorescent bodipy dyes: versatility unsurpassed," *Angewandte Chemie International Edition* **2008**, vol. 47, no. 7, pp. 1184-1201.

[4] Y. Ni, and J. Wu, "Far-red and near infrared BODIPY dyes: synthesis and applications for fluorescent pH probes and bio-imaging," *Organic & Biomolecular Chemistry* **2014**, vol. 12, no. 23, pp. 3774-3791.

[5] F. J. Monsma Jr, A. C. Barton, H. Chol Kang D.L. Brassard, R.P. Haugland, and D.R. Sibley., "Characterization of novel fluorescent ligands with high affinity for D_1 and D_2 dopaminergic receptors," *Journal of Neurochemistry* **1989**, vol. 52, no. 5, pp. 1641-1644.

[6] T. G. Pavlopoulos, M. Shah, and J. H. Boyer, "Laser action from a tetramethylpyrromethene-BF_2 complex," *Applied Optics* **1988**, vol. 27, no. 24, pp. 4998-4999.

[7] N. Molupe, B. Babu, D. O. Oluwole, E. Prinsloo, J. Mack, and T. Nyokong, "The investigation of in vitro dark cytotoxicity and photodynamic therapy effect of a 2, 6-dibromo-3, 5-

distyryl BODIPY dye encapsulated in Pluronic® F-127 micelles," accepted for publication in *Journal of Coordination Chemistry* in 2019. [288].

[8] G. Kubheka, J. Mack, N. Kobayashi, M. Kimura, and T. Nyokong,, "Optical limiting properties of 2, 6-dibromo-3, 5-distyrylBODIPY dyes at 532 nm," *Journal of Porphyrins and Phthalocyanines* **2017***,* vol. 21, no. 07n08, pp. 523-531.

[9] H. Lu, J. Mack, Y. Yang, and Z. Shen, "Structural modification strategies for the rational design of red/NIR region BODIPYs," *Chemical Society Reviews* **2014***,* vol. 43, no. 13, pp. 4778-4823.

[10] R. P. Haugland, *Handbook of fluorescent probes and research chemicals*, Molecular Probes, Eugene Oregon, United States 1992.

[11] O. Buyukcakir, O. A. Bozdemir, S. Kolemen, S. Erbas, and E.U. Akkaya., "Tetrastyryl-Bodipy dyes: convenient synthesis and characterization of elusive near IR fluorophores," *Organic Letters* **2009***,* vol. 11, no. 20, pp. 4644-4647.

[12] T. E. Wood, and A. Thompson, "Advances in the chemistry of dipyrrins and their complexes," *Chemical Reviews* **2007***,* vol. 107, no. 5, pp. 1831-1861.

[13] A. Schmitt, B. Hinkeldey, M. Wild G. Jung., "Synthesis of the Core Compound of the BODIPY Dye Class: 4,4'-Difluoro-4-bora-(3a,4a)-diaza-*s*-indacene," *Journal of Fluorescence* **2009***,* vol. 19, no. 4, pp. 755-758.

[14] Y. W. Wang, A. B. Descalzo, Z. Shen X. Z. You, and K. Rurack., "Dihydronaphthalene-Fused Boron–Dipyrromethene (BODIPY) Dyes: Insight into the Electronic and Conformational

Tuning Modes of BODIPY Fluorophores," *Chemistry–A European Journal* **2010***,* vol. 16, no. 9, pp. 2887-2903.

[15] L. Gai, J. Mack, H. Lu H, H. Yamada, D. Kuzuhara, G. Lai, Z. Li, and Z. Shen, "New 2, 6-Distyryl-Substituted BODIPY Isomers: Synthesis, Photophysical Properties, and Theoretical Calculations," *Chemistry–A European Journal* **2014***,* vol. 20, no. 4, pp. 1091-1102.

[16] J. Michl, "Magnetic circular dichroism of cyclic. pi.-electron systems. 1. Algebraic solution of the perimeter model for the A and B terms of high-symmetry systems with a (4N+ 2)-electron [n] annulene perimeter," *Journal of the American Chemical Society* **1978***,* vol. 100, no. 22, pp. 6801-6811.

[17] N. Boens, V. Leen, and W. Dehaen, "Fluorescent indicators based on BODIPY," *Chemical Society Reviews* **2012***,* vol. 41, no. 3, pp. 1130-1172.

[18] M. Zhang, E. Hao, Y. Xu S. Zhang, H. Zhu, Q. Wang, C. Yu, and L. Jiao, "One-pot efficient synthesis of pyrrolylBODIPY dyes from pyrrole and acyl chloride," *RSC Advances* **2012***,* vol. 2, no. 30, pp. 11215-11218.

[19] L. Wu, and K. Burgess, "A new synthesis of symmetric boraindacene (BODIPY) dyes," *Chemical Communications* **2008**, no. 40, pp. 4933-4935.

[20] K. Tram, H. Yan, H. A. Jenkins S. Vassiliev, and D. Bruce, "The synthesis and crystal structure of unsubstituted 4, 4-difluoro-4-bora-3a, 4a-diaza-*s*-indacene (BODIPY)," *Dyes and Pigments* **2009***,* vol. 82, no. 3, pp. 392-395.

[21] V. P. Yakubovskyi, M. P. Shandura, and Y. P. Kovtun, "Boradipyrromethenecyanines," *European Journal of Organic Chemistry* **2009**, vol. 2009, no. 19, pp. 3237-3243.

[22] Z. Li, E. Mintzer, and R. Bittman, "First Synthesis of Free Cholesterol− BODIPY Conjugates," *The Journal of Organic Chemistry* **2006**, vol. 71, no. 4, pp. 1718-1721.

[23] J. H. Boyer, A. M. Haag, G. Sathyamoorthi M.L. Soong, K. Thangaraj, and T.G. Pavlopoulos., "Pyrromethene–BF_2 complexes as laser dyes: 2," *Heteroatom Chemistry* **1993**, vol. 4, no. 1, pp. 39-49.

[24] K. Rurack, M. Kollmannsberger, and J. Daub, "Molecular switching in the near infrared (NIR) with a functionalized boron–dipyrromethene dye," *Angewandte Chemie International Edition* **2001**, vol. 40, no. 2, pp. 385-387.

[25] G. Ulrich, C. Goze, M. Guardigli, A. Roda, and R. Ziessel, "Pyrromethene dialkynyl borane complexes for "Cascatelle" energy transfer and protein labeling," *Angewandte Chemie International Edition* **2005**, vol. 117, no. 24, pp. 3760-3764.

[26] G. Ulrich, S. B. Goeb, A. De Nicola, P. Retailleau, and R. Ziessel, "Chemistry at boron: synthesis and properties of red to near-IR fluorescent dyes based on boron-substituted diisoindolomethene frameworks," *The Journal of Organic Chemistry* **2011**, vol. 76, no. 11, pp. 4489-4505.

[27] Y. Ni, W. Zeng, K.-W. Huang, and J. Wu, "Benzene-fused BODIPYs: synthesis and the impact of fusion mode," *Chemical Communications* **2013**, vol. 49, no. 12, pp. 1217-1219.

[28] L. Jiao, C. Yu, J. Li, and M. Wu, "β-Formyl-BODIPYs from the Vilsmeier− Haack reaction," *The Journal of Organic Chemistry* **2009**, vol. 74, no. 19, pp. 7525-7528.

[29] J. H. Gibbs, L. T. Robins, Z. Zhou, P. Bobadova-Parvanova, M. Cottam, G.T. McCandless, F.R. Fronczek, and M.G.H. Vicente, "Spectroscopic, computational modeling and cytotoxicity of a series of *meso*-phenyl and *meso*-thienyl-BODIPYs," *Bioorganic & Medicinal Chemistry* **2013***,* vol. 21, no. 18, pp. 5770-5781.

[30] L. Li, B. Nguyen, and K. Burgess, "Functionalization of the 4, 4-difluoro-4-bora-3a, 4a-diaza-*s*-indacene (BODIPY) core," *Bioorganic & Medicinal Chemistry Letters* **2008***,* vol. 18, no. 10, pp. 3112-3116.

[31] Y.-H. Yu, Z. Shen, H.-Y. Xu, Y.-W. Wang, T. Okujima, N. Ono, Y.-Z. Li, and X.Z. You, "Synthesis, crystal structures and spectroscopic characterizations of two difluoroboradiaza-*s*-indacene dyes," *Journal of Molecular Structure* **2007***,* vol. 827, no. 1, pp. 130-136.

[32] S. K. Kim, and J. L. Sessler, "Ion pair receptors," *Chemical Society Reviews* **2010***,* vol. 39, no. 10, pp. 3784-3809.

[33] S. O. McDonnell, and D. F. O'Shea, "Near-infrared sensing properties of dimethylamino-substituted BF_2– azadipyrromethenes," *Organic Letters* **2006***,* vol. 8, no. 16, pp. 3493-3496.

[34] V. F. Donyagina, S. Shimizu, N. Kobayashi, and E.A. Lukyanets, "Synthesis of N, N-difluoroboryl complexes of 3,3'-diarylazadiisoindolylmethenes," *Tetrahedron Letters* **2008***,* vol. 49, no. 42, pp. 6152-6154.

[35] J. Bañuelos, F. L. Arbeloa, T. Arbeloa, V. Martinez, and I.L. Arbeloa, "BODIPY laser dyes applied in sensing and monitoring environmental properties,". In *Chronic Materials,*

Phenomena and their Technological Applications, P. R. Somani (Ed), Applied Science *Innovations Pvt. Ltd*, Maharashtra, India 2012, pp. 641-677.

[36] W. Zhao, and E. M. Carreira, "Conformationally restricted aza-bodipy: a highly fluorescent, stable, near-infrared-absorbing dye," *Angewandte Chemie International Edition* **2005***,* vol. 117, no. 11, pp. 1705-1707.

[37] T. Yogo, Y. Urano, Y. Ishitsuka, F. Maniwa, and T. Nagano, "Highly efficient and photostable photosensitizer based on BODIPY chromophore," *Journal of the American Chemical Society* **2005***,* vol. 127, no. 35, pp. 12162-12163.

[38] A. Kamkaew, S. H. Lim, H. B. Lee, L.V. Kiew, L.Y. Chung, and K. Burgess, "BODIPY dyes in photodynamic therapy," *Chemical Society Reviews* **2013***,* vol. 42, no. 1, pp. 77-88.

[39] C. Goze, G. Ulrich, L. J. Mallon, B.D. Allen, A. Harriman, and R. Ziessel, "Synthesis and photophysical properties of borondipyrromethene dyes bearing aryl substituents at the boron center," *Journal of the American Chemical Society* **2006***,* vol. 128, no. 31, pp. 10231-10239.

[40] A. Harriman, G. Izzet, and R. Ziessel, "Rapid energy transfer in cascade-type bodipy dyes," *Journal of the American Chemical Society,* **2006**, vol. 128, no. 33, pp. 10868-10875.

[41] K. Rurack, M. Kollmannsberger, and J. Daub, "A highly efficient sensor molecule emitting in the near infrared (NIR): 3,5-distyryl-8-(p-dimethylaminophenyl) difluoroboradiaza-*s*-indacene," *New Journal of Chemistry* **2001***,* vol. 25, no. 2, pp. 289-292.

[42] A. Coskun, and E. U. Akkaya, "Difluorobora-s-diazaindacene dyes as highly selective dosimetric reagents for fluoride anions," *Tetrahedron Letters* **2004***,* vol. 45, no. 25, pp. 4947-4949.

[43] Z. Dost, S. Atilgan, and E. U. Akkaya, "Distyryl-boradiazaindacenes: facile synthesis of novel near IR emitting fluorophores," *Tetrahedron* **2006***,* vol. 62, no. 36, pp. 8484-8488.

[44] J. S. Hayes, "Synthesis, Characterization, and Evaluation of Novel BODIPY Dyes With Theranostic Applications," PhD thesis, Louisiana State University, United States, 2014.

[45] V. Leen, "Synthesis and application of reactive BODIPY dyes," PhD thesis, Katholieke Universiteit Leuven, Belgium, 2010.

[46] R. Ziessel, G. Ulrich, and A. Harriman, "The chemistry of Bodipy: a new El Dorado for fluorescence tools," *New Journal of Chemistry* **2007***,* vol. 31, no. 4, pp. 496-501.

[47] X. F. Zhang, and N. Feng, "Photoinduced Electron Transfer–based Halogen–free Photosensitizers: Covalent *meso*–Aryl (Phenyl, Naphthyl, Anthryl, and Pyrenyl) as Electron Donors to Effectively Induce the Formation of the Excited Triplet State and Singlet Oxygen for BODIPY Compounds," *Chemistry–An Asian Journal* **2017***,* vol. 12, no. 18, pp. 2447-2456.

[48] F. L. Arbeloa, J. Banuelos, V. Martínez, T. Arbeloa, and I. López Arbeloa, "Structural, photophysical and lasing properties of pyrromethene dyes," *International Reviews in Physical Chemistry* **2005***,* vol. 24, no. 2, pp. 339-374.

[49] F. L. Arbeloa, T. L. Arbeloa, I. L. Arbeloa, I. Garcia-Moreno, A. Costela, R. Sastre, and F. Amat-Guerri, "Photophysical and lasing properties of pyrromethene 567 dye in liquid solution.: Environment effects," *Chemical Physics* **1998**, vol. 236, no. 1-3, pp. 331-341.

[50] S. Fery-Forgues, and D. Lavabre, "Are fluorescence quantum yields so tricky to measure? A demonstration using familiar stationery products," *Journal of Chemical Education* **1999**, vol. 76, no. 9, pp. 1260.

[51] C. Würth, M. Grabolle, J. Pauli, M. Spieles, and U. Resch-Genger, "Relative and absolute determination of fluorescence quantum yields of transparent samples," *Nature Protocols* **2013**, vol. 8, no. 8, pp. 1535.

[52] A. M. Brouwer, "Standards for photoluminescence quantum yield measurements in solution (IUPAC Technical Report)," *Pure and Applied Chemistry* **2011**, vol. 83, no. 12, pp. 2213-2228.

[53] R. F. Kubin, and A. N. Fletcher, "Fluorescence quantum yields of some rhodamine dyes," *Journal of Luminescence* **1982**, vol. 27, no. 4, pp. 455-462.

[54] A. Ogunsipe, J.-Y. Chen, and T. Nyokong, "Photophysical and photochemical studies of zinc (II) phthalocyanine derivatives—effects of substituents and solvents," *New Journal of Chemistry* **2004**, vol. 28, no. 7, pp. 822-827, 2004.

[55] M. Hof, V. Fidler, and R. Hutterer, "Basics of fluorescence spectroscopy in biosciences". In *Fluorescence Spectroscopy in Biology*, M. Hof, V. Fidler, and R. Hutterer (Eds), Springer, Berlin, Germany, vol. 3, pp. 3-29, 2005.

[56] D. V. O'Connor, and D. Phillips, *Time-correlated single photon counting*, Academic Press, Cambridge, Massachusetts, 2012.

[57] K. M. Kadish, *Porphyrin Science: With Applications to Chemistry, Physics, Materials Science, Engineering, Biology and Medicine*, World Scientific, Singapore, 2010.

[58] J. H. Chou, M. E. Kosal, H. S. Nalwa, N. A. Rakow, and K. S. Suslick, "Applications of porphyrins and metalloporphyrins to materials chemistry,". In *Urbana, The Porphyrin Handbook,* K. M. Kadish, K. Smith, and R. Guilard (Eds), Academic Press, Cambridge, Massachusetts, vol. 6, pp. 43-131, 2000.

[59] A. Semeikin, O. Golubchikov, and O. Koifman, "Synthesis and Applications of Porphyrins," *ChemInform,* vol. 37, no. 3, pp. no-no, 2006.

[60] W. Kuster, and P. Deihle, "Beiträge zur Kenntnis des Bilirubins und Hämins," *Hoppe Seyler's Zeitschrift fur Physiologische Chemie* **1912***,* vol. 82, p. 463-483.

[61] H. Fischer, and K. Zeile, "Syntheses of hematoporphyrin,protoprophyrin and hemin" *Justus Liebigs Annalen der Chemie*, **1929***,* vol. 468, pp. 98-116.

[62] M. K. Cyrañski, T. M. Krygowski, M. Wisiorowski, N. Jr. van Eikema Hommes, and P. R. Schleyer, "Global and Local Aromaticity in Porphyrins: An Analysis Based on Molecular Geometries and Nucleus-Independent Chemical Shifts," *Angewandte Chemie International Edition* **1998***,* vol. 37, no. 1-2, pp. 177-180.

[63] K. M. Smith, "General and synthetic aspects". In *Porphyrins and metalloporphyrins*, K. M. Smith, Elsevier, Amsterdam, Netherlands, pp. 1-55, 1975.

[64] E. Vogel, “The porphyrins from the'annulene chemist's' perspective,” *Pure and Applied Chemistry,* **1993**, vol. 65, no. 1, pp. 143-152.

[65] P. Spellane, M. Gouterman, A. Antipas, S. Kim, and Y. C. Liu, “Porphyrins. 40. Electronic spectra and four-orbital energies of free-base, zinc, copper, and palladium tetrakis (perfluorophenyl) porphyrins,” *Inorganic Chemistry* **1980***,* vol. 19, no. 2, pp. 386-391.

[66] M. Gouterman, “Optical spectra and electronic structure of porphyrins and related rings”. In *The Porphyrins,* D. Dolphin (Eds), Academic Press, Cambridge, Massachusetts, vol. 3, pp. 1-156, 1978.

[67] A. Ghosh, T. Wondimagegn, and H. J. Nilsen, “Molecular structures, tautomerism, and carbon nucleophilicity of free-base inverted porphyrins and carbaporphyrins: A density functional theoretical study,” *The Journal of Physical Chemistry B* **1998***,* vol. 102, no. 50, pp. 10459-10467.

[68] M. R. Moore, "An historical introduction to porphyrin and chlorophyll synthesis," In *Tetrapyrroles*, M. J. Warren, and A. G. Smith (Eds), Springer, Berlin, Germany, pp. 1-28, 2009.

[69] F. Li, S. I. Yang, Y. Ciringh, J. Seth, C. H. Martin, D. L, Singh, D. Kim, R. R. Birge, D. F. Bocian, and D. Holten, “Design, synthesis, and photodynamics of light-harvesting arrays comprised of a porphyrin and one, two, or eight boron-dipyrrin accessory pigments,” *Journal of the American Chemical Society* **1998***,* vol. 120, no. 39, pp. 10001-10017.

[70] M. Gouterman, “Spectra of porphyrins,” *Journal of Molecular Spectroscopy* **1961***,* vol. 6, pp. 138-163.

[71] J. Mack, Y. Asano, N. Kobayashi, and M. J. Stillman, "Application of MCD spectroscopy and TD-DFT to a highly non-planar porphyrinoid ring system. New insights on red− shifted porphyrinoid spectral bands," *Journal of the American Chemical Society* **2005***,* vol. 127, no. 50, pp. 17697-17711.

[72] Z.-C. Sun, Y.-B. She, Y. Zhou, X.-F. Song, and K. Li, "Synthesis, characterization and spectral properties of substituted tetraphenylporphyrin iron chloride complexes," *Molecules* **2011***,* vol. 16, no. 4, pp. 2960-2970.

[73] P. Rothemund, "A new porphyrin synthesis. The synthesis of porphin1," *Journal of the American Chemical Society* **1936***,* vol. 58, no. 4, pp. 625-627.

[74] A. D. Adler, F. R. Longo, J. D. Finarelli, Goldmacher, J. Assour, and L. Korsakoff, "A simplified synthesis for *meso*-tetraphenylporphine," *The Journal of Organic Chemistry* **1967***,* vol. 32, no. 2, pp. 476-476, 1967.

[75] L. T. Nguyen, M. O. Senge, and K. M. Smith, "Simple methodology for syntheses of porphyrins possessing multiple peripheral substituents with an element of symmetry," *The Journal of Organic Chemistry* **1996***,* vol. 61, no. 3, pp. 998-1003.

[76] J. S. Lindsey, I. C. Schreiman, H. C. Hsu, P.C. Kearney, and A.M. Marguerettaz, "Rothemund and Adler-Longo reactions revisited: synthesis of tetraphenylporphyrins under equilibrium conditions," *The Journal of Organic Chemistry* **1987***,* vol. 52, no. 5, pp. 827-836.

[77] F. Longo, J. Finarelli, and J. Kim, "The synthesis and some physical properties of *ms*-tetra(pentafluorophenyl)-porphyrin and *ms*-tetra(pentachlorophenyl)porphyrin", *Journal of Heterocyclic Chemistry* **1969**, vol. 6, pp. 927-931.

[78] A. D. Adler, F. R. Longo, and W. Shergalis, "Mechanistic investigations of porphyrin syntheses. I. Preliminary studies on ms-tetraphenylporphin," *Journal of the American Chemical Society* **1964***,* vol. 86, no. 15, pp. 3145-3149.

[79] J. E. Falk, *Porphyrins and metalloporphyrins*, vol. 2, Elsevier, Amsterdam, Netherlands, 1964.

[80] A. D. Adler, F. R. Longo, F. Kampas, and J. Kim, "On the preparation of metalloporphyrins," *Journal of Inorganic and Nuclear Chemistry* **1970***,* vol. 32, no. 7, pp. 2443-2445.

[81] J. Buchler, "Synthesis and properties of metalloporphyrins,". In *The Porphyrins*, D. Dolphin, Academic Press, Cambridge, Massachusetts, vol. 1, pp. 389-483, 1978.

[82] J. Hoard, "Stereochemistry of porphyrins and metalloporphyrins". In *Porphyrins and Metalloporphyrins*," K. M. Smith (Ed.)*,* Elsevier, Amsterdam, Netherlands, pp. 317-380, 1975.

[83] National Diabetes Data Group, "Classification and diagnosis of diabetes mellitus and other categories of glucose intolerance," *Diabetes* **1979***,* vol. 28, no. 12, pp. 1039-1057.

[84] A. D. Association, "Diagnosis and classification of diabetes mellitus," *Diabetes Care* **2014***,* vol. 37, no. Supplement 1, pp. S81-S90.

[85] World Health Organization, "Definition, diagnosis and classification of diabetes mellitus and its complications", World Health Organization, Geneva, 1999.

[86] The Diabetes Control and Complications Trial Research Group, "Lifetime benefits and costs of intensive therapy as practiced in the diabetes control and complications trial", *Journal of the American Medical Association,* **1996***,* vol. 276, no.17, pp. 1409-1415.

[87] R. Badugu, J. R. Lakowicz, and C. D. Geddes, "Boronic acid fluorescent sensors for monosaccharide signaling based on the 6-methoxyquinolinium heterocyclic nucleus: progress toward noninvasive and continuous glucose monitoring," *Bioorganic & Medicinal Chemistry* **2005***,* vol. 13, no. 1, pp. 113-119.

[88] D. C. Klonoff, "Continuous glucose monitoring: roadmap for 21st century diabetes therapy," *Diabetes Care* **2005***,* vol. 28, no. 5, pp. 1231-1239.

[89] World Health Organization, *Global report on diabetes*, World Health Organization, 2016.

[90] The Diabetes Control and Complications Trial Research Group, "The effect of intensive treatment of Diabetes on the development and progression of long-term complications in insulin-dependent diabetes mellitus", *The New England Journal of Medicine* **1993**, vol. 329, no. 14, pp. 977-986.

[91] UK Prospective Diabetes Study Group, "Intensive blood-glucose control with sulphonylureas or insulin compared with conventional treatment and risk of complications in patients with type 2 diabetes (UKPDS 33)," *The Lancet* **1998***,* vol. 352, pp. 837-853.

[92] L. C. Clark Jr, and C. Lyons, "Electrode systems for continuous monitoring in cardiovascular surgery," *Annals of the New York Academy of Sciences* **1962***,* vol. 102, no. 1, pp. 29-45.

[93] S. Park, H. Boo, and T. D. Chung, "Electrochemical non-enzymatic glucose sensors," *Analytica Chimica Acta* **2006**, vol. 556, no. 1, pp. 46-57.

[94] J. Wang, "Electrochemical glucose biosensors," *Chemical Reviews* **2008**, vol. 108, no. 2, pp. 814-825.

[95] T. Kulkarni, and G. Slaughter, "Application of semipermeable membranes in glucose biosensing," *Membranes* **2016**, vol. 6, no. 4, pp. 55.

[96] J. Wang, "Glucose biosensors: 40 years of advances and challenges," *Electroanalysis* **2001**, vol. 13, no. 12, pp. 983-988.

[97] G. Wang, X. He, L. Wang, A. Gu, Y. Huang, B. Fang, B. Geng, and X. Zhang, "Non-enzymatic electrochemical sensing of glucose," *Microchimica Acta* **2013**, vol. 180, no. 3-4, pp. 161-186.

[98] J. P. Lowry, K. McAteer, S. S. El Atrash, A. Duff, and R. D. O'Neil, "Characterization of glucose oxidase-modified poly (phenylenediamine)-coated electrodes in vitro and in vivo: homogeneous interference by ascorbic acid in hydrogen peroxide detection," *Analytical Chemistry* **1994**, vol. 66, no. 10, pp. 1754-1761.

[99] F. Tang, X. Meng, D. Chen, J. Ran, and C. Zheng, "Glucose biosensor enhanced by nanoparticles," *Science in China Series B: Chemistry* **2000**, vol. 43, no. 3, pp. 268-274.

[100] J. Liu, and J. Wang, "A novel improved design for the first-generation glucose biosensor," *Food Technology and Biotechnology* **2001**, vol. 39, no. 1, pp. 55-58.

[101] J. Wang, N. Naser, and M. Ozsoz, "Plant tissue-based amperometric electrode for eliminating ascorbic acid interferences," *Analytica Chimica Acta* **1990***,* vol. 234, pp. 315-320.

[102] A. E. Cass, G. Davis, G. D. Francis, H. A. O. Hill, W. J. Aston, I. J. Higgins, E. V. Plotkin, L. D. Scott, and A. P. Turner, "Ferrocene-mediated enzyme electrode for amperometric determination of glucose," *Analytical Chemistry* **1984***,* vol. 56, no. 4, pp. 667-671.

[103] J. Liu, A. Chou, W. Rahmat, M.N. Paddon-Row, and J.J. Gooding, "Achieving direct electrical connection to glucose oxidase using aligned single walled carbon nanotube arrays," *Electroanalysis* **2005***,* vol. 17, no. 1, pp. 38-46.

[104] G. F. Khan, M. Ohwa, and W. Wernet, "Design of a stable charge transfer complex electrode for a third-generation amperometric glucose sensor," *Analytical Chemistry* **1996***,* vol. 68, no. 17, pp. 2939-2945.

[105] S. B. Murugaiyan, R. Ramasamy, N. Gopal, and V. Kuzhandaivelu, "Biosensors in clinical chemistry: an overview," *Advanced Biomedical Research,* **2014**,vol. 3, pp. 1-23.

[106] R. Wilson, and A. Turner, "Glucose oxidase: an ideal enzyme," *Biosensors and Bioelectronics* **1992***,* vol. 7, no. 3, pp. 165-185.

[107] M. Shaolin, X. Huaiguo, and Q. Bidong, "Bioelectrochemical responses of the polyaniline glucose oxidase electrode," *Journal of Electroanalytical Chemistry and Interfacial Electrochemistry* **1991***,* vol. 304, no. 1-2, pp. 7-16.

[108] X. Kang, Z. Mai, X. Zou, P. Cai, and J. Mo, "A sensitive nonenzymatic glucose sensor in alkaline media with a copper nanocluster/multiwall carbon nanotube-modified glassy carbon electrode," *Analytical Biochemistry* **2007***,* vol. 363, no. 1, pp. 143-150.

[109] S. Cherevko, and C.-H. Chung, "Gold nanowire array electrode for non-enzymatic voltammetric and amperometric glucose detection," *Sensors and Actuators B: Chemical* **2009***,* vol. 142, no. 1, pp. 216-223.

[[110] Y. B. Vassilyev, O. Khazova, and N. Nikolaeva, "Kinetics and mechanism of glucose electrooxidation on different electrode-catalysts: Part I. Adsorption and oxidation on platinum," *Journal of Electroanalytical Chemistry and Interfacial Electrochemistry* **1985***,* vol. 196, no. 1, pp. 105-125.

[111] X. Cao, N. Wang, S. Jia, and Y. Shao, "Detection of glucose based on bimetallic PtCu nanochains modified electrodes," *Analytical Chemistry* **2013***,* vol. 85, no. 10, pp. 5040-5046.

[112] D. R. Thévenot, K. Toth, R. A. Durst, and G.S. Wilson, "Electrochemical biosensors: recommended definitions and classification," *Analytical Letters* **1992***,* vol. 34, no. 5, pp. 635-659, 2001.

[113] M. Byfield, and R. Abuknesha, "Biochemical aspects of biosensors," *Biosensors and Bioelectronics* **1994***,* vol. 9, no. 4-5, pp. 373-399.

[114] S. H. North, E. H. Lock, C. R. Taitt, and S.G. Walton, "Critical aspects of biointerface design and their impact on biosensor development," *Analytical and Bioanalytical Chemistry* **2010***,* vol. 397, no. 3, pp. 925-933.

[115] K. Rogers, "Recent advances in biosensor techniques for environmental monitoring," *Analytica Chimica Acta* **2006**, vol. 568, no. 1-2, pp. 222-231.

[116] I. E. Tothill, "Biosensors developments and potential applications in the agricultural diagnosis sector," *Computers and Electronics in Agriculture* **2001**, vol. 30, no. 1-3, pp. 205-218.

[117] G.-P. Nikoleli, S. Karapetis, S. Bratakou, D. P. Nikolelis, N. Tzamtzis, V. N. Psychoyios, and N. Psaroudakis, "Biosensors for security and bioterrorism: definitions, history, types of agents, new trends and applications". In *Biosensors for security and bioterrorism applications*, D.P. Nikolelis, and G.-P. Nikoleli (Eds), Springer, Berlin, Germany, pp. 1-13, 2016.

[118] T. Vo-Dinh, and B. Cullum, "Biosensors and biochips: advances in biological and medical diagnostics," *Fresenius' Journal of Analytical Chemistry* **2000**, vol. 366, no. 6-7, pp. 540-551.

[119] P. Mehrotra, "Biosensors and their applications–A review," *Journal of Oral Biology and Craniofacial Research* **2016**, vol. 6, no. 2, pp. 153-159.

[120] S. Malhotra, A. Verma, N. Tyagi, and V. Kumar, "Biosensors: Principle, Types And Applications," *International Journal Of Advance Research And Innovative Ideas In Education* **2017**, vol. 3, no. 2, pp. 3639-3644.

[121] N. J. Ronkainen, H. B. Halsall, and W. R. Heineman, "Electrochemical biosensors," *Chemical Society Reviews* **2010**, vol. 39, no. 5, pp. 1747-1763.

[122] W. Nawrot, K. Drzozga, S. Baluta, J. Cabaj, and K. Malecha, "A Fluorescent Biosensors for Detection Vital Body Fluids' Agents," *Sensors* **2018***,* vol. 18, no. 8, pp. 2357.

[123] A. B. Nepomnyashchii, and A. J. Bard, "Electrochemistry and electrogenerated chemiluminescence of BODIPY dyes," *Accounts of Chemical Research* **2012***,* vol. 45, no. 11, pp. 1844-1853.

[124] M. A. Cooper, "Optical biosensors in drug discovery," *Nature Reviews Drug Discovery* **2002***,* vol. 1, no. 7, pp. 515-528.

[125] K. Narsaiah, S. N. Jha, R. Bhardwaj, R. Sharma, and R. Kumar, "Optical biosensors for food quality and safety assurance—a review," *Journal of Food Science and Technology* **2012***,* vol. 49, no. 4, pp. 383-406.

[126] S. M. Borisov, and O. S. Wolfbeis, "Optical biosensors," *Chemical Reviews* **2008***,* vol. 108, no. 2, pp. 423-461.

[127] A. V. S. Piriya, P. Joseph, D. S. C. G. Daniel, L. Susithra, T. Kinoshita, and S. Muthusamy, "Colorimetric sensors for rapid detection of various analytes," *Materials Science and Engineering C* **2017***,* vol. 78, pp. 1231-1245.

[128] K. Tian, M. Prestgard, and A. Tiwari, "A review of recent advances in nonenzymatic glucose sensors," *Materials Science and Engineering: C* **2014***,* vol. 41, pp. 100-118.

[129] N. Bhalla, P. Jolly, N. Formisano, and P. Estrela, "Introduction to biosensors," *Essays in Biochemistry* **2016***,* vol. 60, no. 1, pp. 1-8.

[130] J. S. Hansen, J. B. Christensen, J. F. Petersen, T. Hoeg-Jensen, and J. C. Norrid, "Arylboronic acids: A diabetic eye on glucose sensing," *Sensors and Actuators B: Chemical* **2012***,* vol. 161, no. 1, pp. 45-79.

[131] K. Lacina, P. Skládal, and T. D. James, "Boronic acids for sensing and other applications-a mini-review of papers published in 2013," *Chemistry Central Journal* **2014***,* vol. 8, no. 1, pp. 60-77.

[132] W. Yang, X. Gao, and B. Wang, "Boronic acid compounds as potential pharmaceutical agents," *Medicinal Research Reviews* **2003***,* vol. 23, no. 3, pp. 346-368.

[133] W. Yang, H. He, and D. G. Drueckhammer, "Computer-guided design in molecular recognition: Design and synthesis of a glucopyranose receptor," *Angewandte Chemie International Edition* **2001***,* vol. 40, no. 9, pp. 1714-1718.

[134] G. F. Whyte, R. Vilar, and R. Woscholski, "Molecular recognition with boronic acids—applications in chemical biology," *Journal of Chemical Biology* **2013***,* vol. 6, no. 4, pp. 161-174.

[135] C. A. McClary, and M. S. Taylor, "Applications of organoboron compounds in carbohydrate chemistry and glycobiology: analysis, separation, protection, and activation," *Carbohydrate Research* **2013***,* vol. 381, pp. 112-122.

[136] R. Nishiyabu, Y. Kubo, T. D. James, and J.S. Fossey, "Boronic acid building blocks: tools for sensing and separation," *Chemical Communications* **2011***,* vol. 47, no. 4, pp. 1106-1123.

[137] T. D. James, K. S. Sandanayake, and S. Shinkai, “Saccharide sensing with molecular receptors based on boronic acid,” *Angewandte Chemie International Edition* **1996**, vol. 35, no. 17, pp. 1910-1922.

[138] J. Yan, G. Springsteen, S. Deeter, and B. Wang, “The relationship among pK_a, pH, and binding constants in the interactions between boronic acids and diols—it is not as simple as it appears,” *Tetrahedron* **2004**, vol. 60, no. 49, pp. 11205-11209.

[139] J. P. Lorand, and J. O. Edwards, “Polyol complexes and structure of the benzeneboronate ion,” *The Journal of Organic Chemistry* **1959**, vol. 24, no. 6, pp. 769-774, 1959.

[140] H. S. Mader, and O. S. Wolfbeis, “Boronic acid based probes for microdetermination of saccharides and glycosylated biomolecules,” *Microchimica Acta* **2008**, vol. 162, no. 1-2, pp. 1-34.

[141] J. Böeseken, "The use of boric acid for the determination of the configuration of carbohydrates," *Advances in Carbohydrate Chemistry*, **1949**, vol. 4, pp. 189-210.

[142] G. Springsteen, and B. Wang, “A detailed examination of boronic acid–diol complexation,” *Tetrahedron* **2002**, vol. 58, no. 26, pp. 5291-5300.

[143] N. DiCesare, and J. R. Lakowicz, “Evaluation of two synthetic MESglucose probes for fluorescence-lifetime-based sensing,” *Analytical Biochemistry* **2001**, vol. 294, no. 2, pp. 154-160.

[144] W. Stumm, R. Kummert, and L. Sigg, “A ligand exchange model for the adsorption of inorganic and organic ligands at hydrous oxide interfaces,” *Croatica Chemica Acta* **1980**, vol. 53, no. 2, pp. 291-312.

[145] L. Bosch, T. Fyles, and T. D. James, “Binary and ternary phenylboronic acid complexes with saccharides and Lewis bases,” *Tetrahedron* **2004**, vol. 60, no. 49, pp. 11175-11190.

[146] T. D. James, "Saccharide-selective boronic acid based photoinduced electron transfer (PET) fluorescent sensors,". In *Creative Chemical Sensor Systems*, T. Schrader (Eds), Springer, Berlin, Germany, pp. 107-152, 2007.

[147] H. Fang, G. Kaur, and B. Wang, “Progress in boronic acid-based fluorescent glucose sensors,” *Journal of Fluorescence* **2004**, vol. 14, no. 5, pp. 481-489.

[148] Y.-J. Huang, W.-J. Ouyang, X. Wu, Z. Li, J.S. Fossey, T.D. James, and Y.B. Jiang, “Glucose sensing via aggregation and the use of “knock-out” binding to improve selectivity,” *Journal of the American Chemical Society* **2013**, vol. 135, no. 5, pp. 1700-1703.

[149] M. D. Phillips, and T. D. James, “Boronic acid based modular fluorescent sensors for glucose,” *Journal of Fluorescence* **2004**, vol. 14, no. 5, pp. 549-559.

[150] Y. Egawa, T. Seki, S. Takahashi, and J-I. Anzai, “Electrochemical and optical sugar sensors based on phenylboronic acid and its derivatives,” *Materials Science and Engineering C* **2011**, vol. 31, no. 7, pp. 1257-1264.

[151] A. O’Mullane, "Electrochemistry. Reference Module in Chemistry," *Molecular Sciences and Chemical Engineering*, pp. 1-3, 2013.

[152] B. Bhattacharyya, *Electrochemical micromachining for nanofabrication, MEMS and nanotechnology*, William Andrew, Norwich, United Kingdom, 2015.

[153] J. Wang, *Analytical electrochemistry*: John Wiley & Sons, Hoboken, New Jersey, 2006.

[154] L. Pujol, D. Evrard, K. Groenen-Serrano, M. Freyssinier, A. Ruffien-Cizsak, and P. Gros, "Electrochemical sensors and devices for heavy metals assay in water: the French groups' contribution," *Frontiers in Chemistry* **2014**, vol. 2, pp. 1-24.

[155] A. Bard, and L. Faulkner, *Electrochemical Methods Fundamentals and Applications* John Wiley & Sons, Hoboken, New Jersey, 2002.

[156] L. Cui, J. Wu, and H. Ju, "Electrochemical sensing of heavy metal ions with inorganic, organic and bio-materials," *Biosensors and Bioelectronics* **2015**, vol. 63, pp. 276-286.

[157] P. Vanýsek, H. Tavassol, and K.-L. Pilson, "The Role of the Reference and Counter Electrodes in Electrochemical Impedance Measurement." *Electrochemical Society,* 2013.

[158] B. Bansod, T. Kumar, R. Thakur, S. Rana, and I. Singh, "A review on various electrochemical techniques for heavy metal ions detection with different sensing platforms," *Biosensors and Bioelectronics* **2017**, vol. 94, pp. 443-455.

[159] A. A. N. EC08, "Basic overview of the working principle of a potentiostat/galvanostat (PGSTAT)–Electrochemical cell setup," *Metrohm Autolab. BV*, pp. 1-3, 2011.

[160] N. Priyantha, and H. Ekanayake, "Electrochemical characteristics and analytical applications of hexadecylmethanesulfonate-modified glassy carbon electrodes," *Journal of the National Science Foundation of Sri Lanka* **2002**, vol. 30, no. 1-2, pp. 43-53.

[161] L. Falat, and H. Cheng, "Voltammetric differentiation of ascorbic acid and dopamine at an electrochemically treated graphite/epoxy electrode," *Analytical Chemistry* **1982**, vol. 54, no. 12, pp. 2108-2111.

[162] Z. Bo, and X. Lu, "Poly (vinyl chloride) membrane electrode for the determination of verapamil," *Analytica Chimica Acta* **1990***,* vol. 235, pp. 461-464.

[163] G. Wallace, and Y. Lin, "Preparation and application of conducting polymers containing chemically active counterions for analytical purposes," *Journal of Electroanalytical Chemistry and Interfacial Electrochemistry* **1988***,* vol. 247, no. 1-2, pp. 145-156.

[164] J. Schreurs, "Surface modified electrodes: an exploration into preparation, characterization and possibilities," PhD thesis, Eindhoven University of Technology, Netherlands, 1983.

[165] P. Moses, L. Wier, and R. Murray, "Chemically modified tin oxide electrode," *Analytical Chemistry* **1975***,* vol. 47, no. 12, pp. 1882-1886.

[166] B. F. Watkins, J. R. Behling, E. Kariv, and L.L. Miller, "Chiral electrode," *Journal of the American Chemical Society* **1975***,* vol. 97, no. 12, pp. 3549-3550.

[167] A. J. Bard, and L. R. Faulkner, *Electrochemical Methods: Fundamentals and applications*, Willey & Sons, United States, 2001.

[168] L. Rotariu, C. Bala, and V. Magearu, "New potentiometric microbial biosensor for ethanol determination in alcoholic beverages," *Analytica Chimica Acta* **2004***,* vol. 513, no. 1, pp. 119-123.

[169] J. M. Zen, A. Senthil Kumar, and D. M. Tsai, "Recent updates of chemically modified electrodes in analytical chemistry," *Electroanalysis* **2003***,* vol. 15, no. 13, pp. 1073-1087.

[170] S. Cosnier, A. Le Pellec, R. S. Marks, K. Périé, and J.P. Lellouche, "A permselective biotinylated polydicarbazole film for the fabrication of amperometric enzyme electrodes," *Electrochemistry Communications* **2003**, vol. 5, no. 11, pp. 973-977.

[171] S. Cosnier, and A. Lepellec, "Poly (pyrrole–biotin): a new polymer for biomolecule grafting on electrode surfaces," *Electrochimica Acta* **1999**, vol. 44, no. 11, pp. 1833-1836.

[172] A. Fang, H. T. Ng, and S. F. Y. Li, "A high-performance glucose biosensor based on monomolecular layer of glucose oxidase covalently immobilised on indium–tin oxide surface," *Biosensors and Bioelectronics* **2003**, vol. 19, no. 1, pp. 43-49.

[173] D. Quan, and W. Shin, "Modification of electrode surface for covalent immobilization of laccase," *Materials Science and Engineering: C* **2004**, vol. 24, no. 1-2, pp. 113-115.

[174] M. Gerard, A. Chaubey, and B. Malhotra, "Application of conducting polymers to biosensors," *Biosensors and Bioelectronics* **2002**, vol. 17, no. 5, pp. 345-359.

[175] P. Mailley, E. A. Cummings, S. Mailley, S. Cosnier, B. R. Eggins, and E. McAdams, "Amperometric detection of phenolic compounds by polypyrrole-based composite carbon paste electrodes," *Bioelectrochemistry* **2004**, vol. 63, no. 1-2, pp. 291-296.

[176] K. Gong, Y. Dong, S. Xiong, Y. Chen, and L. Mao, "Novel electrochemical method for sensitive determination of homocysteine with carbon nanotube-based electrodes," *Biosensors and Bioelectronics* **2004**, vol. 20, no. 2, pp. 253-259.

[177] J. J. Gooding, and D. B. Hibbert, "The application of alkanethiol self-assembled monolayers to enzyme electrodes," *TrAC Trends in Analytical Chemistry* **1999**, vol. 18, no. 8, pp. 525-533.

[178] R. Moscoso, J. Carbajo, and J. Squella, "1, 3-Dioxolane: A green solvent for the preparation of carbon nanotube-modified electrodes," *Electrochemistry Communications* **2014**, vol. 48, pp. 69-72.

[179] E. Barsoukov, and J. R. Macdonald, *Impedance spectroscopy: theory, experiment, and applications*, John Wiley & Sons, Hoboken, New Jersey, 2018.

[180] J. F. Watts, and J. Wolstenholme, *An introduction to surface analysis by XPS and AES*, Willey & Sons, United States. 2003.

[181] E. Ventosa, and W. Schuhmann, "Scanning electrochemical microscopy of Li-ion batteries," *Physical Chemistry Chemical Physics* **2015**, vol. 17, no. 43, pp. 28441-28450.

[182] M. V. Mirkin, W. Nogala, J. Velmurugan, and Y. Wang, "Scanning electrochemical microscopy in the 21st century. Update 1: five years after," *Physical Chemistry Chemical Physics* **2011**, vol. 13, no. 48, pp. 21196-21212.

[183] K. Eckhard, X. Chen, F. Turcu, and W. Schuhmann, "Redox competition mode of scanning electrochemical microscopy (RC-SECM) for visualisation of local catalytic activity," *Physical Chemistry Chemical Physics* **2006**, vol. 8, no. 45, pp. 5359-5365.

[184] J. L. Fernández, D. A. Walsh, and A. J. Bard, "Thermodynamic guidelines for the design of bimetallic catalysts for oxygen electroreduction and rapid screening by scanning electrochemical microscopy. M− Co (M: Pd, Ag, Au)," *Journal of the American Chemical Society* **2005**, vol. 127, no. 1, pp. 357-365.

[185] F.-R. F. Fan, B. Liu, and J. Mauzeroll, "Scanning electrochemical microscopy," In *Handbook of Electrochemistry*, C. G. Zoski (Eds), Elsevier, Amsterdam, Netherlands, pp. 471-540, 2007.

[186] A. J. Bard, G. Denuault, C. Lee, D. Mandler, and D.O. Wipf, "Scanning electrochemical microscopy-a new technique for the characterization and modification of surfaces," *Accounts of Chemical Research* **1990**, vol. 23, no. 11, pp. 357-363.

[187] J. Kwak, and A. J. Bard, "Scanning electrochemical microscopy. Theory of the feedback mode," *Analytical Chemistry* **1989**, vol. 61, no. 11, pp. 1221-1227.

[188] A. J. Bard, F.-R. F. Fan, D. T. Pierce, P.R. Unwin, D.O. Wipf, and F. Zhou, "Chemical imaging of surfaces with the scanning electrochemical microscope," *Science* **1991**, vol. 254, no. 5028, pp. 68-74.

[189] P. Kissinger, and W. R. Heineman, *Laboratory Techniques in Electroanalytical Chemistry, revised and expanded*, Marel Dekker, New York, New York, 1996.

[190] A. J. Bard, L. R. Faulkner, J. Leddy, and C.G. Zoski, *Electrochemical methods: fundamentals and applications*, Wiley and Sons, Hoboken, New Jersey, 1980.

[191] J. H. Zagal, "Metallophthalocyanines as catalysts in electrochemical reactions," *Coordination Chemistry Reviews* **1992**, vol. 119, pp. 89-136.

[[192] D. A. Geraldo, C. A. Togo, J. Limson, and T. Nyokong, "Electrooxidation of hydrazine catalyzed by noncovalently functionalized single-walled carbon nanotubes with CoPc," *Electrochimica Acta* **2008**, vol. 53, no. 27, pp. 8051-8057.

[193] D. C. Klonoff, "Overview of fluorescence glucose sensing: a technology with a bright future,"*Journal of Diabetes Science and Technology* **2012**, vol 6, pp 1242-1250.

[194] S. A. Hussain, D. Dey, S. Chakraborty, J. Saha, A. D. Roy, S. Chakraborty, P. Debnath, and D. Bhattacharjee, "Fluorescence Resonance Energy Transfer (FRET) sensor," *Journal of Spectroscopy and Dynamics,* **2015**, vol. 5, pp. 7-23.

[195] J. R. Lakowicz, "Emerging biomedical applications of time-resolved fluorescence spectroscopy."In *Probe Design and Chemical Sensing; Topics in Fluorescence Spectroscopy*, J. R. Lackowicz (Ed.), Plenum Press, New York, United States of America, vol. 4, pp. 178-193, 1994.

[196] J. C. Pickup, F. Hussain, N. D. Evans, and N. Sachedina, "In vivo glucose monitoring: the clinical reality and the promise," *Biosensors and Bioelectronics* **2005***,* vol. 20, no. 10, pp. 1897-1902.

[197] K. S. Suslick, N. A. Rakow, and A. Sen, "Colorimetric sensor arrays for molecular recognition," *Tetrahedron* **2004***,* vol. 60, no. 49, pp. 11133-11138.

[198] R. B. Dominguez, M. A. Orozco, G. Chávez, and A. Márquez-Lucero, "The Evaluation of a Low-Cost Colorimeter for Glucose Detection in Salivary Samples," *Sensors* **2017***,* vol. 17, no. 11, pp. 2495.

[199] H.-C. Wang, and A.-R. Lee, "Recent developments in blood glucose sensors," *Journal of Food and Drug Analysis* **2015***,* vol. 23, no. 2, pp. 191-200.

[200] B. Tang, L. Cao, K. Xu, L. Zhuo, J. Ge, Q. Li, and L. Yu, "A new nanobiosensor for glucose with high sensitivity and selectivity in serum based on fluorescence resonance energy

transfer (FRET) between CdTe quantum dots and Au nanoparticles," *Chemistry–A European Journal* **2008**, vol. 14, no. 12, pp. 3637-3644.

[201] A. P. De Silva, H. N. Gunaratne, T. Gunnlaugsson, A.J. Huxley, C.P. McCoy, J.T. Rademacher, and T.E Rice, "Signaling recognition events with fluorescent sensors and switches," *Chemical Reviews* **1997**, vol. 97, no. 5, pp. 1515-1566.

[202] E. U. Akkaya, M. E. Huston, and A. W. Czarnik, "Chelation-enhanced fluorescence of anthrylazamacrocycle conjugate probes in aqueous solution," *Journal of the American Chemical Society* **1990**, vol. 112, no. 9, pp. 3590-3593.

[203] S. L. Wiskur, H. Ait-Haddou, J. J. Lavigne, and E.V. Anslyn, "Teaching old indicators new tricks," *Accounts of Chemical Research* **2001**, vol. 34, no. 12, pp. 963-972.

[204] Y. Kubo, A. Kobayashi, T. Ishida, Y. Misawa, and T.D. James, "Detection of anions using a fluorescent alizarin–phenylboronic acid ensemble," *Chemical Communications* **2005**, no. 22, pp. 2846-2848.

[205] S.-y. Liu, Y.-b. He, G.-y. Qing, K.-x. Xu, and H.-j. Qin, "Fluorescent sensors for amino acid anions based on calix [4] arenes bearing two dansyl groups," *Tetrahedron: Asymmetry* **2005**, vol. 16, no. 8, pp. 1527-1534.

[206] J. Y. Lee, S. K. Kim, J. H. Jung, and J.S. Kim, "Bifunctional fluorescent calix[4]arene chemosensor for both a cation and an anion," *The Journal of Organic Chemistry* **2005**, vol. 70, no. 4, pp. 1463-1466.

[207] A. P. De Silva, T. S. Moody, and G. D. Wright, "Fluorescent PET (Photoinduced Electron Transfer) sensors as potent analytical tools," *Analyst* **2009**, vol. 134, no. 12, pp. 2385-2393.

[208] K. M. Kadish, "Properties and materials". In The *Porphyrin Handbook*, R. Guilard, K. Kadish and K. M. Smith (Eds), Academic Press, Cambridge, Massachusetts, pp. 1-36, 2003.

[209] J. Perry, K. Mansour, I.-Y. Lee, X.-L. Wu, P. Bedworth, C.-T. Chen, D. Ng, S. Marder, P. Miles, and T. Wada, "Organic optical limiter with a strong nonlinear absorptive response," *Science* **1996**, vol. 273, no. 5281, pp. 1533-1536.

[210] P. Murphy, "Laser pointer safety", 2008. http://www.laserpointersafety.com/news/news/othernews_files/d5fca5f3330bef52f1c5465b03502776-569.php#on

[211] L. W. Tutt, and T. F. Boggess, "A review of optical limiting mechanisms and devices using organics, fullerenes, semiconductors and other materials," *Progress in Quantum Electronics* **1993**, vol. 17, no. 4, pp. 299-338.

[212] G.-K. Lim, Z.-L. Chen, J. Clark, R. G. S. Goh, W.-H. Ng. H.-W. Tan, R. H. Friend, P. K. H. Ho, and L.-L, Chua, "Giant broadband nonlinear optical absorption response in dispersed graphene single sheets," *Nature Photonics* **2011**, vol. 5, no. 9, pp. 554.

[213] Y.-P. Sun, and J. E. Riggs, "Organic and inorganic optical limiting materials. From fullerenes to nanoparticles," *International Reviews in Physical Chemistry* **1999**, vol. 18, no. 1, pp. 43-90.

[214] J. Perry, "Organic and metal-containing reverse saturable absorbers for optical limiters". In *Nonlinear Optics of Organic Molecules and Polymers,* H. S. Nalwa, and S. Miyata (Eds), CRC Press, Boca Raton, United States, pp. 813-840, 1997.

[215] R. L. Sutherland, *Handbook of Nonlinear Optics*, Marcel Dekker, New York, New York, 2003.

[216] C. W. Spangler, "Recent development in the design of organic materials for optical power limiting," *Journal of Materials Chemistry* **1999***,* vol. 9, no. 9, pp. 2013-2020.

[217] J. Wang, Y. Chen, R. Li, H. Dong, L. Zhang, M. Lotya, J. N. Coleman, and W. J. Blau, "Nonlinear optical properties of graphene and carbon nanotube composites". In *Carbon Nanotubes,* S. Yellampalli (Eds), InTech Open, London, United Kingdom, pp. 395-425, 2011.

[218] J. Wang, and W. J. Blau, "Inorganic and hybrid nanostructures for optical limiting," *Journal of Optics A: Pure and Applied Optics* **2009***,* vol. 11, no. 2, 024001.

[219] R. Leite, S. Porto, and T. Damen,"The thermal lens effect as a power - limiting device," *Applied Physics Letters* **1967***,* vol. 10, no. 3, pp. 100-101.

[220] G. S. He, J. D. Bhawalkar, C. F. Zhao, and P.N. Prasad, "Optical limiting effect in a two-photon absorption dye doped solid matrix," *Applied Physics Letters* **1995***,* vol. 67, no. 17, pp. 2433-2435.

[221] D. Dini, M. J. Calvete, and M. Hanack, "Nonlinear optical materials for the smart filtering of optical radiation," *Chemical Reviews* **2016***,* vol. 116, no. 22, pp. 13043-13233.

.

[222] C. Zhang, Y. Song, and X. Wang, "Correlations between molecular structures and third-order non-linear optical functions of heterothiometallic clusters: a comparative study," *Coordination chemistry reviews,* vol. 251, no. 1-2, pp. 111-141, 2007.

[223] L. Vivien, P. Lancon, D. Riehl, F. Hache, and E. Anglaret, "Carbon nanotubes for optical limiting," *Carbon* **2002***,* vol. 40, no. 10, pp. 1789-1797.

[224] L. Vivien, E. Anglaret, D. Riehl, F. Hache, F. Bacou, M. Andrieux, F. Lafonta, C. Journet, C. Goze, and M. Brunet, "Optical limiting properties of singlewall carbon nanotubes," *Optics Communications* **2000***,* vol. 174, no. 1-4, pp. 271-275.

[225] D. Dini, M. Barthel, and M. Hanack, "Phthalocyanines as active materials for optical limiting," *European Journal of Organic Chemistry* **2001***,* vol. 2001, no. 20, pp. 3759-3769.

[226] M. Calvete, G. Y. Yang, and M. Hanack, "Porphyrins and phthalocyanines as materials for optical limiting," *Synthetic Metals* **2004***,* vol. 141, no. 3, pp. 231-243.

[227] G. De La Torre, P. Vazquez, F. Agullo-Lopez, and T. Torres, "Role of structural factors in the nonlinear optical properties of phthalocyanines and related compounds," *Chemical Reviews* **2004***,* vol. 104, no. 9, pp. 3723-3750.

[228] K. J. McEwan, G. Bourhill, J. M. Robertson, and H. L Anderson, "The nonlinear optical characterization of *meso*-substituted porphyrin dyes," *Journal of Nonlinear Optical Physics & Materials* **2000***,* vol. 9, no. 04, pp. 451-468.

[229] B. Babu, E. Amuhaya, D. Oluwole, E. Prinsloo, J. Mack, and T. Nyokong, "Preparation of NIR absorbing axial substituted tin (IV) porphyrins and their photocytotoxic properties," *Medicinal Chemistry Communication* **2019**, vol. 10, pp. 41-48.

[230] R. Matthes, C. P. Cain, D. Courant, D. A. Freund, B. A. Grossman, P. A. Kennedy, D. J. Lund, M. A. Mainster, A. A. Manekov, and W. J. Marshall, "Revision of guidelines on limits of exposure to laser radiation of wavelengths between 400 nm and 1.4 mu m," *Health Physics* **2000***,* vol. 79, no. 4, pp. 431-440.

[231] M. G. Kuzyk, and C. W. Dirk, *Characterization techniques and tabulations for organic nonlinear optical materials*: Marcel Dekker, 1998.

[232] R. Matthes, C. P. Cain, D. Courant, D. A. Freund, B. A. Grossman, P. A. Kennedy, D. J. Lund, M. A. Mainster, A. A. Manekov, and W. J. Marshall, "Revision of guidelines on limits of exposure to laser radiation of wavelengths between 400 nm and 1.4 mu m," *Health Physics* **2000***,* vol. 79, no. 4, pp. 431-440.

[233] R. DeSalvo, A. A. Said, D. J. Hagan, E.W. van Stryland, and M. Sheik-Bahae,"Infrared to ultraviolet measurements of two-photon absorption and n_2 in wide bandgap solids," *IEEE Journal of Quantum Electronics* **1996***,* vol. 32, no. 8, pp. 1324-1333.

[234] M. Sheik-Bahae, A. A. Said, T.-H. Wei, D. J. Hagan, and E. W. van Stryland, "Sensitive measurement of optical nonlinearities using a single beam," *IEEE Journal of Quantum Electronics* **1990***,* vol. 26, no. 4, pp. 760-769.

[235] J. Harris, L. Gai, G. Kubheka, J. Mack, T. Nyokong, and Z. Shen,"Optical Limiting Properties of 3,5-Dithienylenevinylene BODIPY Dyes at 532 nm, *Chemistry–A European Journal* **2017***,* vol. 23, no. 58, pp. 14507-14514.

[236] G. Kubheka, O. Achadu, J. Mack, and T. Nyokong, "Optical limiting properties of 3, 5-diphenyldibenzo-azaBODIPY at 532 nm," *New Journal of Chemistry* **2017***,* vol. 41, no. 20, pp. 12319-12325.

[237] B. P. Ngoy, Z. Hlatshwayo, N. Nwaji, G. Fomo, J. Mack, and T. Nyokong, "Photophysical and optical limiting properties at 532 nm of BODIPY dyes with p-benzyloxystyryl groups at the 3,5-positions," *Journal of Porphyrins and Phthalocyanines* **2018***,* vol. 22, no. 05, pp. 413-422.

[238] A. K. May, J. Stone, B. P. Ngoy, J. Mack, T. Nyokong, M. Kimura, and N. Kobayashi, "Photophysical and optical limiting properties of a novel distyryl-BODIPY with fused crown ether moieties," *Journal of Porphyrins and Phthalocyanines* **2017***,* vol. 21, no. 12, pp. 832-843.

[239] T. Pritchett, Models for saturable and reverse saturable absorption in materials for optical limiting, *Sensors and Electron Devices Directorate*,Army Research Laboratory, Adelphi, MD, pp. 1-2, 2002.

[240] J. Maul, B. G. Frushour, J. R. Kontoff, H. Eichenauer, K. H. Ott, and C. Schade, "Polystyrene and styrene copolymers," *Ullmann's Encyclopedia of Industrial Chemistry*, 2000.

[241] N. Ndebele, J. Mack, and T. Nyokong, "A 3, 5 - DistyrylBODIPY Dye Functionalized with Boronic Acid Groups for Direct Electrochemical Glucose Sensing," *Electroanalysis* **2019**, 31, 137-145.

[242] W. Becker, H. Hickl, C. Zander, K. H. Drexhage, M. Sauer, S. Siebert, and J. Wolfrum, "Time-resolved detection and identification of single analyte molecules in microcapillaries by time-correlated single-photon counting (TCSPC)," *Review of Scientific Instruments* **1999**, vol. 70, no. 3, pp. 1835-1841.

[243] M. D. Hanwell, D. E. Curtis, D. C. Lonie, T. Vandermeersch, E. Zurek, and G. R, Hutchison, "Avogadro: an advanced semantic chemical editor, visualization, and analysis platform," *Journal of Cheminformatics* **2012**, vol. 4, pp. 1-17.

[244] M. A. Alamiry, A. Harriman, L. J. Mallon, G. Ulrich, and R. Ziessel, "Energy-and Charge-Transfer Processes in a Perylene–BODIPY–Pyridine Tripartite Array," *European Journal of Organic Chemistry* **2008**, vol. 2008, no. 16, pp. 2774-2782.

[245] C. Brückner, P. C. Foss, J. O. Sullivan, R. Pelto, M. Zeller, R.R. Birge, and G. Crundwell, "Origin of the bathochromically shifted optical spectra of *meso*-tetrathien-2'0-and 3'0-ylporphyrins as compared to *meso*-tetraphenylporphyrin," *Physical Chemistry Chemical Physics* **2006**, vol. 8, no. 20, pp. 2402-2412.

[246] D. P. Arnold, "Aromatic ring currents illustrated-NMR spectra of tin (IV) porphyrin complexes: an advanced undergraduate experiment," *Journal of Chemical Education* **1988**, vol. 65, no. 12, pp. 1111-1112.

[247] K. Peeters, K. De Wael, L. Vincze, and A. Adriaens, "Comparison of different surface modification techniques for electrodes by means of electrochemistry and micro synchrotron radiation x-ray fluorescence. Dimerization of cobalt (ii) tetrasulfonated

phthalocyanine and its influence on the electrodeposition on gold surfaces," *Analytical Chemistry* **2005***,* vol. 77, no. 17, pp. 5512-5519.

[248] M. J. Frisch, G. W. Trucks, H. B. Schlegel, G. E. Scuseria, M. A. Robb, J. R. Cheeseman, G. Scalmani, V. Barone, B. Mennucci, G. A. Petersson,H. Nakatsuji, M. Caricato, X. Li, H. P. Hratchian, A. F. Izmaylov, J. Bloino, G. Zheng, J. L. Sonnenberg, M. Hada, M. Ehara, K. Toyota, R. Fukuda, J. Hasegawa, M. Ishida, T. Nakajima, Y. Honda, O. Kitao, H. Nakai, T. Vreven, J. A. Jr. Montgomery, J. E. Peralta, F. Ogliaro, M. Bearpark, J. J. Heyd, E. Brothers, K. N. Kudin, V. N. Staroverov, T. Keith, R. Kobayashi, J. Normand, K. Raghavachari, A. Rendell, J. C. Burant, S. S. Iyengar, J. Tomasi, M. Cossi, N. Rega, J. M. Millam, M. Klene, J. E. Knox, J. B. Cross, V. Bakken, C. Adamo, J. Jaramillo, R. Gomperts, R. E. Stratmann, O. Yazyev, A. J. Austin, R. Cammi, C. Pomelli, J. W. Ochterski, R. L. Martin, K. Morokuma, V. G. Zakrzewski, G. A. Voth, P. Salvador, J. J. Dannenberg, S. Dapprich, A. D. Daniels, O. Farkas, J. B. Foresman, J. V. Ortiz, J. Cioslowski, and D. J. Fox, "Gaussian 09, rev. D. 01," *Gaussian Inc., Wallingford*, 2009.

[249] M. Shi, J. Tian, C. Mkhize, G. Kubheka, J. Zhou, J. Mack, T. Nyokong, and Z. Shen, "Synthesis, characterization and photodynamic therapy properties of an octa-4-*tert*-butylphenoxy-substituted phosphorus (V) triazatetrabenzcorrole," *Journal of Porphyrins and Phthalocyanines* **2014***,* vol. 18, no. 08n09, pp. 698-707.

[250] Y. Tong, D. G. Hamilton, J.-C. Meillon, and J. K. M. Sanders, “Sn (IV) Porphyrins as NMR Shift Reagents and Supramolecular Protecting Groups: Preparation of a Carboxylate–Catenane Porphyrin Complex,” *Organic Letters* **1999**, vol. 1, no. 9, pp. 1343-1346.

[251] S. V. Bhosale, C. Chong, C. Forsyth, S. J. Langford, and C. P. Woodward, “Investigations of rotamers in diaxial Sn (IV) porphyrin phenolates—towards a molecular timepiece,” *Tetrahedron* **2008**, vol. 64, no. 36, pp. 8394-8401.

[252] G. D. Fallon, S. J. Langford, M. A.-P. Lee, and E. Lygris, “Self-assembling mixed porphyrin trimers–the use of diaxial Sn (IV) porphyrin phenolates as an organising precept,” *Inorganic Chemistry Communications* **2002**, vol. 5, no. 9, pp. 715-718.

[253] A. Loudet, and K. Burgess, "BODIPY® Dyes and Their Derivatives: Syntheses and Spectroscopic Properties," *Handbook of Porphyrin Science (Volume 8) With Applications to Chemistry, Physics, Materials Science, Engineering, Biology and Medicine*, pp. 1-164: World Scientific, 2010.

[254] T. D. James, K. Sandanayake, and S. Shinkai, “Saccharide sensing with molecular receptors based on boronic acid,” *Angewandte Chemie International Edition* **1996**, vol. 35, no. 17, pp. 1910-1922.

[255] Z. Liu, and H. He, “Synthesis and applications of boronate affinity materials: from class selectivity to biomimetic specificity,” *Accounts of Chemical Research* **2017**, vol. 50, no. 9, pp. 2185-2193.

[256] D. Li, Y. Chen, and Z. Liu, "Boronate affinity materials for separation and molecular recognition: structure, properties and applications," *Chemical Society Reviews* **2015***,* vol. 44, no. 22, pp. 8097-8123.

[257] S. Jin, Y. Cheng, S. Reid, M. Li, and B. Wang, "Carbohydrate recognition by boronolectins, small molecules, and lectins," *Medicinal Research Reviews* **2010***,* vol. 30, no. 2, pp. 171-257.

[258] J. Zhai, T. Pan, J. Zhu, Y. Xu. J. Chen, Y. Xie, and Y. Qin, "Boronic acid functionalized boron dipyrromethene fluorescent probes: preparation, characterization, and saccharides sensing applications," *Analytical Chemistry* **2012***,* vol. 84, no. 23, pp. 10214-10220.

[259] J. S. Hansen, T. Hoeg-Jensen, and J. B. Christensen, "Redemitting BODIPY boronic acid fluorescent sensors for detection of lactate," *Tetrahedron* **2017***,* vol. 73, no. 21, pp. 3010-3013.

[260] J. S. Hansen, J. Petersen, T. Hoeg-Jensen, and J. B. Christensen, "Buffer and sugar concentration dependent fluorescence response of a BODIPY-based aryl monoboronic acid sensor," *Tetrahedron Letters* **2012***,* vol. 53, no. 44, pp. 5852-5855.

[261] J. S. Hansen, M. Ficker, J. F. Petersen, J. B. Christensen, and T. Hoeg-Jensen, "*Ortho*-substituted fluorescent aryl monoboronic acid displays physiological binding of D-glucose," *Tetrahedron Letters* **2013***,* vol. 54, no. 14, pp. 1849-1852.

[262] P. Ashokkumar, J. Bell, M. Buurman, and K. Rurack, "Analytical platform for sugar sensing in commercial beverages using a fluorescent BODIPY "light-up" probe," *Sensors and Actuators B: Chemical* **2018***,* vol. 256, pp. 609-615.

[263] S. Centane, O. J. Achadu, and T. Nyokong, "Effects of Substituents on the Electrocatalytic Activity of Cobalt Phthalocyanines when Conjugated to Graphene Quantum Dots," *Electroanalysis* **2017***,* vol. 29, no. 11, pp. 2470-2482.

[264] S. Nyoni, T. Mugadza, and T. Nyokong, "Improved l-cysteine electrocatalysis through a sequential drop dry technique using multi-walled carbon nanotubes and cobalt tetraaminophthalocyanine conjugates," *Electrochimica Acta* **2014***,* vol. 128, pp. 32-40.

[265] N. M. Elgrishi, K. J. Rountree, B. D. McCarthy, E. S. Rountree, T. T. Eisenhart, and J. L. Dempsey, "A Practical Beginner's Guide to Cyclic Voltammetry," *Journal of Chemical Education*, **2017**, vol. 95, pp.197-206.

[266] L. S. Mpeta, G. Fomo, and T. Nyokong, "Click chemistry electrode modification using 4-ethynylbenzyl substituted cobalt phthalocyanine for applications in electrocatalysis," *Journal of Coordination Chemistry*, **2018**, vol. 70, pp. 1623-1638.

[267] K. I. Ozoemena, and T. Nyokong, "Novel amperometric glucose biosensor based on an ether-linked cobalt (II) phthalocyanine–cobalt (II) tetraphenylporphyrin pentamer as a redox mediator," *Electrochimica Acta* **2006***,* vol. 51, no. 24, pp. 5131-5136.

[268] M. Liu, R. Liu, and W. Chen, "Graphene wrapped Cu2O nanocubes: non-enzymatic electrochemical sensors for the detection of glucose and hydrogen peroxide with enhanced stability," *Biosensors and Bioelectronics* **2013***,* vol. 45, pp. 206-212.

[269] R. A. Soomro, Z. H. Ibupoto, M. I. Abro, M. and Willander, "Electrochemical sensing of glucose based on novel hedgehog-like NiO nanostructures," *Sensors and Actuators B: Chemical* **2015***,* vol. 209, pp. 966-974.

[270] M. Şenel, C. Nergiz, M. Dervisevic, and E. Cevik, "Development of Amperometric Glucose Biosensor Based on Reconstitution of Glucose Oxidase on Polymeric 3-Aminophenyl Boronic Acid Monolayer," *Electroanalysis* **2013***,* vol. 25, no. 5, pp. 1194-1200.

[271] A. Tiwari, D. Terada, C. Yoshikawa, and H. Kobayashi, "An enzyme-free highly glucose-specific assay using self-assembled aminobenzene boronic acid upon polyelectrolytes electrospun nanofibers-mat," *Talanta* **2010***,* vol. 82, no. 5, pp. 1725-1732.

[272] E. Shoji, and M. S. Freund, "Potentiometric saccharide detection based on the pK_a changes of poly (aniline boronic acid)," *Journal of the American Chemical Society* **2002***,* vol. 124, no. 42, pp. 12486-12493.

[273] J. Li, Z. Wang, P. Li, N. Zong, and F. Li, "A sensitive non-enzyme sensing platform for glucose based on boronic acid–diol binding," *Sensors and Actuators B: Chemical* **2012***,* vol. 161, no. 1, pp. 832-837.

[274] Y. Chen, M. Hanack, W. J. Blau, D. Dini, Y. Liu, Y. Lin, and J. Bai, "Soluble axially substituted phthalocyanines: synthesis and nonlinear optical response," *Journal of Materials Science* **2006***,* vol. 41, no. 8, pp. 2169-2185.

[275] K. Ogawa, T. Zhang, K. Yoshihara, and, Y. Kobuke, "Large third-order optical nonlinearity of self-assembled porphyrin oligomers," *Journal of the American Chemical Society* **2002***,* vol. 124, no. 1, pp. 22-23.

[276] G. De La Torre, P. Vazquez, F. Agullo-Lopez, and T. Torres, "Phthalocyanines and related compounds: organic targets for nonlinear optical applications," *Journal of Materials Chemistry* **1998***,* vol. 8, no. 8, pp. 1671-1683.

[277] M. Hanack, D. Dini, M. Barthel, and S. Vagin, "Conjugated macrocycles as active materials in nonlinear optical processes: Optical limiting effect with phthalocyanine and related compounds, *The Chemical Record* **2002***,* vol. 3, pp. 129-148.

[278] Y. Chen, M. Hanack, Y. Araki, and O. Ito, "Axially modified gallium phthalocyanines and naphthalocyanines for optical limiting," *Chemical Society Reviews* **2005***,* vol. 34, no. 6, pp. 517-529.

[279] B. E. Saleh, M. C. Teich, and B. E. Saleh, *Fundamentals of Photonics*, John Wiley & Sons, Hoboken, New Jersey, 1991.

[280] N. Nwaji, J. Mack, J. Britton, and T. Nyokong, "Synthesis, photophysical and nonlinear optical properties of a series of ball-type phthalocyanines in solution and thin films," *New Journal of Chemistry* **2017***,* vol. 41, no. 5, pp. 2020-2028.

[281] C. Singh, K. Bindra, B. Jain, S. Oak, "All-optical switching characteristics of metalloporphyrins," *Optics Communications* **2005***,* vol. 245, no. 1-6, pp. 407-414.

[282] M. Hanack, T. Schneider, M. Barthel, J. S. Shirk, S. R. Flom, and R. G. S. Pong, "Indium phthalocyanines and naphthalocyanines for optical limiting," *Coordination Chemistry Reviews* **2001***,* vol. 219, pp. 235-258.

[283] T. Yanai, D. P. Tew, and N. C. Handy, "A new hybrid exchange–correlation functional using the Coulomb-attenuating method (CAM-B3LYP)," *Chemical Physics Letters* **2004***,* vol. 393, no. 1-3, pp. 51-57.

[284] S. Wang, H. Liu, J. Mack, J. Tian, B. Zou, H. Lu, Z. Li, J. Jiang, and Z. Shen, "A BODIPY-based 'turn-on'fluorescent probe for hypoxic cell imaging," *Chemical Communications* **2015**, vol. 51, no. 69, pp. 13389-13392.

[285] G. Zhurko, and D. Zhurko, "ChemCraft, version 1.6," *URL: http://www. chemcraftprog. com*, 2009.

[286] J. Michl, "Magnetic circular dichroism of aromatic molecules," *Tetrahedron* **1984**, vol. 40, no. 19, pp. 3845-3934.